UNIVERSITY OF CALIFORNIA

Santa Barbara

Mitochondrial DNA Inheritance, Dynamics, and Quality Control: Insights from *Caenorhabditis elegans*

A Dissertation submitted in partial satisfaction of the

requirements for the degree of Doctor of Philosophy

in Molecular, Cellular, and Developmental Biology

by

Sagen Elizabeth Flowers

Committee in charge:

Professor Joel Rothman, Chair

Professor Kathy Foltz

Professor David Low

Professor Anthony De Tomaso

December 2019

The dissertation of Sagen Elizabeth Flowers is approved.

_____
Kathy Foltz

_____
David Low

_____
Anthony De Tomaso

_____
Joel Rothman, Committee Chair

December 2019

Mitochondrial DNA Inheritance, Dynamics, and Quality Control: Insights from *Caenorhabditis elegans*

ACKNOWLEDGEMENTS

I first want to thank all of my colleagues both in and out of the Rothman lab. My collaborator Dr. Siddhartha Goyal helped me immensely in the beginning stages of my project and provided the optimism that I so desperately needed when I was off to a rocky start. Sarah Abdul-Wajid provided invaluable help in getting me started with coding. Dr. Boris Shraiman and his graduate student Kevin Kuns were also incredibly helpful in analysis of high throughput sequencing analysis and provided great insights into the confusing results I were presented with.

Within the Rothman lab, there isn't a single person that did not contribute to my project. When I started in the lab as an undergraduate researcher, my mentor Dr. Julia Dey gave me the basis for being an academic researcher and her mentorship will always be something I greatly cherish. When I then took on the role of mentor, I had wonderful mentees, and want to extend my deepest gratitude to all of them, without whom I would have not come to where I am today. Aditi Trivedi, Clementine Fulbert, Jasmin Kwak, and Rushali Kothari: you were all truly exceptional in the lab and I am so proud of you all.

I want to extend my appreciation to graduate students past and present that have been instrumental in the development of my project: of particular note, Dr. Yamila Torres-Cleuren's assistance with large data analysis, Melissa Alcorn's help with stats questions and emotional support, and Geneva Alok's help with constructing necessary crosses for the project; without her construction of the *pink-1* null allele, my project would have never come to fruition. Erik Spickard, Tsung-Han Yeh, Caroline Ackley, and Ethan EI have all been instrumental in providing new ways of thinking about how to interpret my results and how to go forward with new experiments. Dr. Pan Young Jeong has always been an excellent source of knowledge. Dr. Pradeep Joshi, our "lab dad", has

played an enormous role in my development as a researcher. His availability, encyclopedic knowledge of all things "*C. elegans*", and help in construction of crosses, has been so deeply vital to the progress of my project and I couldn't have made it without him there. Past lab members, including Dr. Misty Riddle, Dr. Bilge Birsoy, Dr. Nate Dudley, and Dr. Davon Callendar, must almost be mentioned for their wonderful insights and instruction. Lastly, and most importantly, Dr. Joel Rothman has been the most wonderful PI I could have hoped for. His compassion, kindness, trust, and support have all allowed me to believe in myself and my project. When things seemed the darkest, he was always there to give a pep-talk which propelled me to continue forward. I also want to thank the members of my committee, Kathy Foltz, David Low, and Tony De Tomaso for their input and guidance.

My friends have been so great during the last 9 years, and their belief in my ability to get through this program meant the world to me. My parents have always been so proud of the work I do, and I want to thank them for not losing faith in me. In particular, my brother, Dr. Matthew Peterson, has been an excellent resource for getting through a PhD program in one piece. Lastly, I relied on my husband, the love of my life, greatly for moral support throughout this entire process, and his incredible level of understanding, support, and being that shoulder to cry on, has not gone unnoticed. I couldn't have done this without him, no question. He deserves an award (or perhaps his own PhD!) for being such a necessary part of my success in this program, and I can't wait to start the next phase of our lives together as a family moving forward.

VITA OF SAGEN ELIZABETH FLOWERS
December 2019

EDUCATION

Ph.D., Molecular, Cellular, and Developmental Biology *(Expected)* December 2019
University of California, Santa Barbara

B.S., Cellular and Developmental Biology June 2011
University of California, Santa Barbara

PROFESSIONAL EMPLOYMENT

Graduate Student Researcher September 2011-December 2019
Department of Molecular, Cellular, and Developmental Biology, UC Santa Barbara

Teaching Assistant September 2011-June 2019
Department of Molecular, Cellular, and Developmental Biology, UC Santa Barbara

Teaching Associate September 2016-December 2017
Department of Molecular, Cellular, and Developmental Biology, UC Santa Barbara

Undergraduate Researcher June 2010-September 2011
Department of Molecular, Cellular, and Developmental Biology, UC Santa Barbara

RESEARCH PUBLICATIONS

Flowers, SE, Joshi PM, Alok G, Torres-Cleuren Y, Alcorn M, Rothman JH. Identification of a genetic event that results in rapid curing of a mtDNA disease in *C. elegans*, In Preparation 2019.

HONORS AND AWARDS

MCDB Departmental Continuing Student Fellowship 2016
UC Santa Barbara MCDB

Burnand-Partridge Foundation Scholarship 2015
Santa Barbara Scholarship Foundation

Edica Mary Uccello Scholarship 2014
Santa Barbara Scholarship Foundation

Phillip & Aida Siff Foundation Graduate Fellowship 2014
UC Santa Barbara Graduate Division

MCDB Merit Fellowship 2014
UC Santa Barbara MCDB

Jake Gimbel Trust Scholarship 2013
Santa Barbara Scholarship Foundation

MCDB Department Fellowship 2013
UC Santa Barbara MCDB

C.A. Storke Fellowship 2012
UC Santa Barbara MCDB

Burnand-Partridge Foundation Scholarship 2011
Santa Barbara Scholarship Foundation

TALKS AND PRESENTATIONS

MCDB Departmental Symposium Poster Presentation February 2016
UC Santa Barbara
"Elucidating the mechanisms for purifying selection of mitochondrial DNA."

MCDB Seminar October 2015
UC Santa Barbara
"Elucidating the Mechanisms of mtDNA Maintenance and Transmission in C. elegans."

MCDB Seminar February 2015
UC Santa Barbara
"Elucidating the Mechanisms of mtDNA Maintenance and Transmission."

MCDB Departmental Symposium Poster Presentation February 2015
UC Santa Barbara
"The Immortal Germline: Analyzing Mitochondrial Maintenance and Transmission in C. elegans."

20th International *C. elegans* Meeting Poster Presentation June 2015
UC Los Angeles
"Elucidating the mechanisms for purifying selection of mitochondrial DNA."

MCDB Seminar May 2014
UC Santa Barbara
"mtDNA Maintenance and Transmission in C. elegans."

MCDB Departmental Symposium Poster Presentation February 2013
UC Santa Barbara
"The Immortal Germline: Analyzing Mitochondrial Maintenance and Transmission in C. elegans."

FIELDS OF STUDY
Major Field: Developmental Biology

***C. elegans* developmental genetics of mtDNA quality control** Sep 2011-Dec 2019
PI: Professor Joel Rothman
***C. elegans* developmental genetics of programmed cell death** June 2010-Sep 2011
PI: Professor Joel Rothman
Mentor: Dr. Julia Dey

SOFTWARE SKILLS
MS Word, MS Excel, MS PowerPoint, ImageJ, FIJI, ApE Plasmid Editor, NIS elements, R, Python, Quantasoft

ABSTRACT

Mitochondrial DNA Inheritance, Dynamics, and Quality Control: Insights from *Caenorhabditis elegans*

by

Sagen Elizabeth Flowers

The endosymbiotic theory explains the origin of eukaryotic cells, in which one bacterium engulfed another bacterium resulting in the creation of mitochondria. Over time the engulfed bacterium transferred parts of its genome to the genome of the engulfing cell, eventually resulting in a dependence of the host on the organelle, and vice versa. However, with this theory, one must consider the problem of selfish DNA. Mitochondria contain their own DNA, containing a small set of essential genes that are involved in the oxidative phosphorylation machinery. How the host cell keeps this mtDNA in check is a large area of research, since if the population of mtDNA accumulates mutations, it results in mitochondrial disease. The general process by which mutated mtDNA is removed is known as purifying selection, but the various mechanisms through which this process operates are largely unknown.

My project tested various levels at which purifying selection may be operating using the genetically tractable nematode *C. elegans* and the mtDNA deletion mutant *uaDf5*. In this thesis, I describe foundational work to characterize mitochondrial dynamics and maintenance of mtDNA over the lifespan of the animal, focused primarily on the germline. Our data shows that there are three mechanisms through which purifying selection is operating: asymmetric segregation in early embryonic divisions, PCD in the mature female germline, and insulin signaling. In addition to the discovery of these

mechanisms, I also characterized the dynamics of mtDNA selection during development and aging, as well as the dynamics of mitochondrial activity in response to the environment. Lastly, I discovered a potent epigenetically activated mtDNA quality control mechanism that is activated in response to an initiating genetic event, or "IGE". Altogether, my work shows how *C. elegans* is an extremely useful system for examining mtDNA dynamics and for the further elucidation of the various ways in which the mtDNA population is maintained.

TABLE OF CONTENTS

LIST OF FIGURES AND TABLES

Chapter 1:

Chapter 2:

Chapter 3:

Chapter 4:

Chapter One

Introduction

SUMMARY

Mitochondria perform a multitude of essential processes in cells and defects in mitochondrial function underlie aging and many diseases. Mitochondria contain their own DNA (mtDNA), which is replicated independently of the nuclear genome. Because a typical cell contains many mitochondria and thus many mtDNA copies, defective mtDNAs can accumulate, resulting in heteroplasmy. Defects in mitochondrial function underpin aging and mtDNA mutations may be associated with the aging process. Moreover, mutations in mtDNAs are associated with a range of mitochondrial diseases, serious illnesses that afflict up to 1 in every 4,300 people. The replicative advantage of truncated mtDNAs carrying deletions poses a particular danger as "selfish elements". Mechanisms therefore exist to eliminate such defective mtDNAs, a process known as purifying selection.

Thus far, mitochondrial dynamics (fission and fusion) and mitophagy (the autophagic removal of dysfunctional mitochondria) are the main cellular processes identified for removal of defective mtDNA, however it remains to be seen if there are additional mechanisms. Recently it was found that the mitochondrial unfolded protein response (UPR^{MT}) and the insulin-signaling pathway (IIS) are processes which surprisingly are required for protection of defective mtDNAs. A deeper understanding of all mechanisms that act on deleterious mtDNA, and why there are pathways which shield defective mtDNA from removal, will improve the prospects for the fields of mitochondrial disease and aging.

MITOCHONDRIAL BIOLOGY

Origin of Mitochondria

Mitochondria are the main power producing element of the eukaryotic cell [1]. They are a double-membraned organelle with an outer membrane that is permeable to most things under 10kDa and a highly convoluted inner membrane which contains the oxidative phosphorylation machinery that is responsible for energy (ATP) generation [2]. The innermost compartment of the mitochondrion is known as the matrix and it contains proteins, ribosomes, and the mitochondrial genome (mtDNA) [3]. In addition to oxidative phosphorylation, mitochondria are also involved in a wide array of cellular processes, including heme [4–6] and lipid metabolism [7–11], the Krebs/TCA cycle [1,12], the urea cycle [13], ion homeostasis [14–16], and apoptosis [17–22].

Mitochondria are thought to have arisen from an endosymbiotic event that took place about 2.1 billion years ago in which an archaebacterial host engulfed a proteobacteria, and the proteobacteria became what is known as today's mitochondria [23–25]. Over time, there was gene transfer from the mtDNA to the nuclear genome resulting in what is now an incredibly compact mitochondrial genome that only encodes highly hydrophobic essential subunits of the oxidative phosphorylation machinery (also known as the mitochondrial respiratory complex, MRC; [1]).

One of the questions that arises in mitochondrial biology regards the persistence of the genome. Before the endosymbiotic event, the two genomes of the host and "parasite" would have certainly had strategies to outcompete other genomes [26–28]. This is a general tenant of biology and is a cornerstone of immunity [29–32]. How is it, that once the mitochondria came to be, that the mitochondria did not take over the host cell? Assuming its DNA is selfish, how did it, over time, actually come to live

harmoniously inside the host cell and why did it ever transfer its own genes to the host cell genome? How did this mutually dependent relationship arise? And, now that the eukaryotic cell is entirely dependent on mitochondria to survive, how does the host cell keep the mtDNA in check, given its assumed selfish behavior of replication?

Mitochondrial DNA and the MRC

In mammals, mtDNA is almost always a circular piece of DNA and its length is usually on the range of 15-18kb long [25,33]. In humans it is 16,569 bp long and contains 37 total genes: 13 protein-coding genes, in addition to two rRNAs (16s and 12s) and 22tRNAs, all of which are needed for the transcription and translation of the mtDNA (Fig. 1.1A) [34]. All of the 13 mitochondrial-encoded proteins are necessary subunits of the MRC which is made up of a total of 5 complexes (Fig. 1.1B) [1]. Complexes 1-4 are electron carriers; they are involved in the electron transfer from succinate or fumarate to the final electron acceptor oxygen (to make water). The energy from that electron transfer is then coupled to the movement of protons from the matrix across the mitochondrial inner membrane to the intermembrane space [35,36]. The 5^{th} complex is the ATP synthase which then brings the protons back into the matrix, and the corresponding release of energy drives the production of ATP [37,38]. A single molecule of glucose can yield as many as 32 ATP molecules when catabolized via the aerobic oxidative phosphorylation pathway, as opposed to anaerobic catabolism (i.e., glycolysis and fermentation) which yields only 2 ATP molecules, signifying the importance of mitochondria for the high energy demands of the cell.

Of the 13 MRC subunits encoded on the mtDNA, seven of them are in complex 1 (NADH-ubiquinone oxidoreductase), one is in complex 3 (ubiquinol-cytochrome C

oxidoreductase), three are in complex 4 (cytochrome C oxidase), and two are in complex 5 (ATP synthase/F0F1 ATPase) (Fig. 1.1B) [1,34]. The only complex that does not contain any mitochondrial-encoded subunits is complex 2 (succinate-ubiquinone oxidoreductase) [39]. One common quality of all of the mitochondrial-encoded subunits is that they are highly hydrophobic, which might explain why these genes never transferred to the nucleus [40].

There is very little non-coding sequence within the mtDNA – the protein-coding genes contain no introns and there are few intergenic regions, and of those, they are only a few bases long [3]. The longest non-coding region is the displacement loop (D-loop) which is the main control region for replication and transcription [3]. It contains one of the origins of replication and two of the main promoters for transcription [41]. Unlike nuclear DNA (nDNA) replication, replication of mtDNA is not linked to the cell cycle [42–44] which allows for strong variation in the number of mtDNA molecules per cell (known as the copy number). Also unlike nuclear DNA, mtDNA is transmitted maternally in most species, except for rare occasions in which paternal inheritance has been shown [45–47].

It has been shown that mtDNA has a much higher mutation rate than nuclear DNA, perhaps by as much as a magnitude fold higher [33,48,49]. The possible reasons for this are that the mitochondrial DNA polymerase, DNA polymerase gamma (POLG), is more error prone than the nuclear DNA polymerase [50–52], and the proximity of the mtDNA to the oxidative phosphorylation machinery makes it more likely to be hit with highly damaging reactive oxygen species (ROS; [53]), although this theory has undergone increased scrutiny in recent years [54]. If a cell or organism contains only wildtype mtDNA (WT-mtDNA) it is said to be homoplasmic. However, if there is a

mixture of WT-mtDNA and mutated mtDNA then this results in a state known as heteroplasmy [55,56]. Given the high mutation rate of mtDNA, it has become evident that the state of heteroplasmy is extremely common but is generally not tolerated well by the cell [55,56]. In addition to this observation, the mtDNA substitution rate at the long-term phylogenetic scale is much lower than would be extrapolated from the short-term pedigree mutation rate [49], showing that there is a process in which mutations are removed from the population. This process is known as purifying selection [57,58] and is the main topic of this dissertation.

Mitochondrial disease

Mitochondrial diseases are a group of conditions that affect mitochondrial function and affect as many as 1 in 4,300 people [55,59–64]. They can be due to mutations in either the mtDNA or the nDNA. Generally, these diseases present as dysfunction in the tissues or organs that have the largest energy demands, most commonly in the muscle and nervous system. Pathogenic mtDNA mutations were first discovered in human patients in the late 1980s [65,66] and since then the body of literature identifying mtDNA-related disease has significantly grown [55]. Mitochondrial diseases also include those disorders in which there is a defect in mitochondrial dynamics, quality control, or communication between the mitochondria and ER [61,62].

In order to progress toward mitochondrial disease therapy, we must learn more about the mechanisms that cells employ to remove deleterious mtDNA. There is evidence that some processes regulate mtDNA maintenance, such as mitochondrial fission/fusion dynamics and mitophagy [67–73], the mitochondrial unfolded protein response (UPR^{MT}; [74–80]), and most recently the insulin signaling pathway (IIS; [81,82]). However, all of

these processes only seem to be part of the story in that their effects on mtDNA mutation levels are intermediate. *C. elegans,* a free-living nematode, is an extremely attractive model for the discovery of new mechanisms through which purifying selection operates. In addition to the ease with which one may study genetic questions with this organism, there are also various elements of *C. elegans* development, which show conservation across animals, that are attractive areas to examine for the potential of mitochondrial maintenance. These elements include selective segregation with the early embryo [83–86], endodermal cannibalism of a portion of the germline progenitor cells during mid-embryogenesis [87], and programmed cell death (PCD) in mature female germline [22,87–92] (described further below). Understanding how mtDNA mutations are removed is not only important for the treatment of the subset of mitochondrial diseases that are caused by mtDNA mutations but also for the prevention of aging (described next).

Mitochondria in aging

The problem of aging has been one that has confounded scientists over the years [93]. Many theories that try to give a molecular basis of aging have been proposed, but there has been limited experimental evidence. However, the most widely accepted idea in the field of aging, the "free radical theory", places mitochondria front and center [94–97].

The free radical theory of aging was first proposed by Denham Harman in 1956 [96]. This theory states that increased mitochondrial respiration will lead to an increase in reactive oxygen species (ROS) levels, which in turn results in an accumulation of oxidative damage to nucleic acids, proteins, and lipids. This oxidative damage is thought to be the driving force behind aging.

Evidence supporting this theory includes mutations that affect ROS levels, mitochondrial function, and metabolism shifts [51,53,54,98]. Mutations that increase lifespan are associated with decreased oxygen consumption (isp-1; Rieske iron sulfur protein of complex III in the electron transport chain [99]), a shift from respiration to other metabolic pathways that don't require mitochondria (the insulin/IGF-1 receptor (IGFR) homolog DAF-2 [100] and the leucyl-tRNA synthetase 2 (LARS2) homolog LARS-2 [101]), and loss of mitochondrial function (the mitochondrial hydroxylase (MCLK1) homolog CLK-1 [102]) [2] . If animals are treated with mitochondrial inhibitors, such as antimycin A, there is a notable increase in lifespan. Additionally, increased expression of ROS scavengers via treatment with superoxide dismutase mimetics such as EUK-8 and EUK-134 result in an increased lifespan [2]. Mutations that are associated with increased ROS levels (such as the succinate dehydrogenase complex subunit C (SDHC) homolog MEV-1 [103]), as well as sensitivity to oxidative damage and hyperoxia (such as the NADH:ubiquinone oxidoreductase core subunit S2 (NDUFS2) homolog GAS-1 [104]), are associated with decreased lifespan [2].

Given the likely central role that mitochondria play in the process of aging, examination of how deleterious mitochondrial mutations behave as the organism ages will give crucial insight for slowing the aging process. These dynamics will be examined in chapter 4.

Mitochondria in *C. elegans*

A somewhat surprising and fascinating observation is that there are many similarities between human and *C. elegans* mtDNA (Fig. 1.1). Human mtDNA has only one extra gene compared to the *C. elegans* counterpart: ATP8, a subunit of complex 5

[3]. There is a high level of homology for all of the genes between species, and the overall size of the mitochondrial genome is roughly equal, with the size of the *C. elegans* mtDNA being 13,794bp (compared to 16,569 bp in humans) [2]. The organization of the genes, however, is quite different between the two, which is somewhat surprising given all of the similarities mentioned above.

The life cycle of the worm includes embryogenesis within an eggshell, and once it hatches it is in the first larval stage, L1, where it has about 560 somatic cells. The worm then goes through 3 more larval stages, L2, L3, and L4, before going through its final molt to become an adult hermaphrodite which has 959 somatic cells and can make up to 300 self-progeny [105] (Fig. 1.2). The total time between fertilization and becoming a gravid adult takes about 3 days at 20° C. Estimates of the mtDNA copy number *in C. elegans* range from 25,000 [106] to 90,000 [107] in the single-cell embryo, which remains largely unchanged through the L3 stage of larval development, suggesting that the mitochondrial genomes are roughly equally divided amongst the cells up until the L3 stage. The copy number then undergoes two incremental increases, concurrent with the growth of the germline. The L3-L4 transition sees an increase to 130,000 (5x) - 250,000 (3x), followed by a secondary increase in the L4-adult transition, resulting in a total of 800,000 (6x) - 4,000,000 (16x) copies. This results in an overall 30-40 fold increase in mtDNA in the animal between the embryo and adult, and the majority of this replication is specific to the oocytes (Fig. 1.2) [106,107].

MITOCHONDRIAL QUALITY CONTROL

Mitochondrial dynamics in purifying selection

One of the key processes identified thus far in mtDNA purifying selection is that of mitochondrial dynamics. Mitochondria are incredibly dynamic organelles. Mitochondria make up a network within the cell, and this filamentous network is constantly undergoing division/fission (usually assumed to be small bits breaking off the main mitochondrion) and fusion (in which the smaller bits refuse with the main mitochondrial network) [68,70,108]. The main players involved in the fission process are the dynamin 1 like (DNML1) homolog DRP-1 [109] and the fission mitochondrial 1 (FIS1) homolog FIS-2 [110,111]. The main actors involved in fusion are the OPA1 mitochondrial dynamin like GTPase (MGM1/OPA1) homolog EAT-3 [112], and the mitofusin (MFN1/2) homolog FZO-1 [113,114] (Fig. 1.3A).

If there is a disruption in either fusion or fission, there is an immediate impairment of the cell's ability to remove mutated mtDNA [69]. It is believed that mitochondrial quality control is tightly linked to fission/fusion due to the necessity of separating the healthy genomes from the mutated genomes prior to mutant mtDNA removal. In order to selectively remove only mutated mtDNA, it makes sense that the mitochondria must fragment, so that you may end up with a mitochondrion with a single genome inside it. Thus, the role of fission is clear.

Once divided, the cell may target a dysfunctional mitochondrion for degradation via a specialized form of autophagy that is specific to mitochondria, known as mitophagy [73,115]. Mitophagy, which works hand in hand with fission and fusion, has been shown to be an important process for selection against deleterious mtDNA [116]. In healthy mitochondria, the PTEN induced kinase 1 (PINK1) homolog, PINK-1, a serine threonine

kinase, is imported into the mitochondria and is then cleaved from the mitochondrial surface. However, if the mitochondrion has diminished membrane potential, which is thought to be a general indicator of reduced function, PINK-1 is only imported through the outer membrane and accumulates on the surface. This accumulation of PINK-1 signals to several downstream players, most notably the parkin RBR E3 ubiquitin protein ligase (PARKIN) homolog PDR-1, which is then recruited to the mitochondrion to ubiquitinate proteins on its surface, tagging the organelle for degradation by the liposome (Fig. 1.3B) [71,72,117–122].

The genetic bottleneck and Muller's ratchet/mutational breakdown

The proportion of mutated mtDNA (i.e., the heteroplasmic load) can vary greatly between offspring from a common heteroplasmic mother [123,124]. The genetic bottleneck hypothesis, which is based on population genetic theory [125], explains this rapid change in allele frequency by saying that there is a small population of mtDNA molecules that are randomly sampled from in the production of oocytes. The mechanisms underlying the genetic bottleneck are largely unknown, as is its purpose [123], though there is speculation that it is a way to avoid mutational breakdown via Muller's ratchet [126–130]. The genetic bottleneck appears to be one of many mechanisms through which purifying selection acts on mtDNA mutations.

The mitochondrial UPR as a potent protector of mtDNA mutations

The mitochondrial UPR (UPR^{MT}) is a quality control mechanism that is activated in response to mitochondrial stress and has been extensively studied *in C. elegans* [75–77]. In the event of mitochondrial protein misfolding, the UPR^{MT} is activated in order to

restore mitochondrial proteostasis. In mammals there are four axes of the UPR^{MT}; the canonical axis involves the action of ATF4, ATF5, CHOP, chaperones, and proteases, the sirtuin axis involves SIRT3, FOXO3A, SOD2 and catalase, the UPRims/ERalpha axis involves AKT, ERalpha, NRF1, OMI1, the proteasome, and respiration, and lastly the translation axis involves the pre-RNA processing and translation machinery [76].

In *C. elegans* the focus of research has been on the canonical UPR^{MT} pathway involving Activating Transcription Factor associated with Stress-1 (ATFS-1, a transcriptional regulator [79]) (Fig. 1.4A). Studies show that accumulation of misfolded mitochondrial peptide fragments in the cytosol and the localization of ATFS-1 within the cell dictates the UPR^{MT} response. Upon protein misfolding, a mitochondrial protease breaks up the proteins into smaller fragments which are then exported to the cytoplasm via the ABC transporter HAF-1. These peptide fragments then activate various proteins and may even act directly on ATFS-1 to regulate its location with the cell. Additionally, healthy mitochondria with a strong membrane potential import ATFS-1, whereas dysfunctional mitochondria are unable to import ATFS-1 due to the lowered membrane potential. When ATFS-1 is not imported, it, along with other proteins such as chromatin remodelers and transcription factors (including DVE-1, UBL-5, LIN-65, and MET-2) translocates into the nucleus and activates transcription of chaperones (including HSP-60 and HSP-6) and proteases, thus resulting in an increased folding capacity in the mitochondria [74–77,79].

Although the purpose of the UPR^{MT} is to protect against dysfunctional mitochondria, it has an unintended consequence of protecting mtDNA mutations from being detected and cleaned up by the cellular machinery [78,80]. How the cell selected for a mechanism which results in decreased mitochondrial quality control is a question of

increasing significance. Perhaps it is a necessary consequence for the sake of protection under dire conditions.

The insulin/IGF-1 signaling (IIS) pathway in mitochondrial surveillance

The highly conserved insulin/IGF-1 (insulin-like growth factor-1) pathway (IIS) has been studied for years in regard to its central role in aging [131–133]. In *C. elegans*, the IIS pathway is regulated by the binding of insulin-like peptides (ILPs) to the insulin/IGF-1 receptor (IGFR) homolog DAF-2, which ultimately results in inhibition of DAF-16/FoxO (a member of the FoxO family of transcription factors) from entering the nucleus to activate transcription of a set of genes that fight various forms of cellular stress [82,100] (Fig. 1.4B). Once bound by ILPs, DAF-2/IGFR activates AGE-1/PI3K, a phosphoinositide 3-kinase [134], which in turn activates a set of serine/threonine kinases including PDK-1/PDK (phosphoinositide-dependent kinase [135]) and Akt/Protein Kinase B (PKB) family members AKT-1 and AKT-2 [136]. Their activation then causes phosphorylation of DAF-16/FoxO, which then interacts with PAR-5 and FTT-2, a set of 14-3-3 proteins, thus inhibiting DAF-16/FoxO from translocating to the nucleus to regulate transcription and interact with other nuclear factors including SIR-2.1/SIRT1 (in the sirtuin family of NAD^+-dependent deacetylases; [137]), HCF-1/HCFC2 (host cell factor; [138]), HSF-1 (a heat shock transcription factor; [139]) and SKN-1/Nrf (a Nrf family transcription factor; [140]). DAF-18/PTEN (phosphatase and tensin homolog, a lipid phosphatase; [141,142]) counteracts AGE-1/PI3K signaling, and PPTR-1/PP2A (a serine-threonine phosphatase; [143]) counteracts AKT-1 signaling, thus acting as inhibitors of DAF-2/IGFR [82].

The IIS pathway is not only associated with regulation of lifespan and aging but is also implicated in a large set of processes, including dauer arrest, L1 arrest, germline proliferation, stress resistance, fat metabolism, and neuronal/behavioral programs [82]. Given the part that mitochondria play in aging and metabolism, it may not be surprising that researchers recently discovered that the IIS pathway is a crucial regulator of mtDNA quality control; they found that inhibition of the IIS pathway results in a rescue of various fitness parameters in a mtDNA mutator strain [81]. I explore the role of the IIS pathway, and other non-IIS dependent lifespan-regulating genes (including the coenzyme Q7 hydroxylase (COQ7) homolog CLK-1/MCLK1 [144], the genotoxic stress response activator CEP-1/p53 [145], and the von Hippel-Lindau tumor suppressor (VHL) homolog VHL-1 [146]) on mtDNA maintenance in chapter 4.

CELLULAR PROCESSES WHICH MAY ACT ON MTDNA MUTATIONS

Embryonic segregation

When the *C. elegans* egg is fertilized by the sperm, an entire chain of invariant events is initiated. The establishment of cellular asymmetry is established rapidly, prior to the first cellular division, which is largely dependent on the action of the PAR proteins [147–150]. One of the consequences of this asymmetrical partitioning is the specific movement of P granules into the germline progenitor cell, P1, which undergoes several more divisions to give rise to the entire germline lineage (Fig. 1.5) [151,152]. P granules, also known as germ granules in other organisms, are RNA- and protein - rich spheres that form in the cytoplasm of the germline and are believed to be necessary for the specification of the germ cell fate. Following fertilization, these P granules are segregated into the posterior side of the one cell embryo, which after the first cell division, becomes

the P1 cell. The P1 cell then undergoes several more divisions, eventually creating the P4 cell, which gives rise to the entire germline. With each of these divisions, the P granules are segregated into one of the daughters, so that the P4 cell is the only cell in the embryo containing the granules.

Another interesting phenomenon of selective sorting occurs with an intracellular bacterium called *Wolbachia pipientis,* most commonly referred to simply as *Wolbachia*. *Wolbachia* are bacteria in the order Rickettsiales, which interestingly enough, is thought to be the closest living relative to the ancestor of today's eukaryotic mitochondria [153–156]. *Wolbachia* typically infect arthropods and some filarial nematodes, and most of the studies have been done on their relationship with *Drosophila melanogaster* [157–160]. *Wolbachia* must be passed through the fly's maternal germline in order to propagate, very similarly to mitochondria. *Wolbachia* have developed a suite of fascinating strategies for ensuring their transmission, perhaps the most interesting of which is known as "cytoplasmic incompatibility" (CI) which results in inviable embryos if the mother is uninfected. The selective movement of *Wolbachia* into the posterior pole of the mature oocyte (which gives rise to the germline) requires the plus end directed motor kinesin heavy chain, as well as movement along microtubules [157–159].

Perhaps in a mechanism similar to P granule and/or *Wolbachia* sorting, the healthiest mitochondria may be selectively moved to the posterior region of the early embryo. Presumably, mitochondria that contain mutated mtDNA will have impaired oxidative phosphorylation machinery, which will present as a reduced or absent membrane potential. Conversely, mitochondria that contain WT-mtDNA probably have a robust membrane potential. So perhaps the machinery for the selective movement of healthy mitochondria uses a combination of the PAR/P granule-associated proteins and

microtubule motor proteins, as well as some sort of membrane potential sensor protein. As mentioned previously, PINK-1 is a mitochondrial membrane potential sensor, so it is an attractive candidate for this role. The potential role of early embryonic segregation as a mechanism for germline mtDNA quality control is explored in chapter 2.

Germline-specific mitochondrial quiescence during embryonic development

C. elegans can enter different developmental programs under cases of extreme stress or starvation. The most studied of these alternate developmental programs is dauer formation, which occurs if L2 larvae experience crowding, starvation, pheromones, or other forms of stress; dauers are able to remain in the dauer stage for several months until conditions improve, upon which they can resume normal development [82,161,162]. This alternate developmental stage results in worms closing up their cuticle and reducing movement in order to conserve energy in the absence of food. The other alternative developmental program is known as L1 arrest/diapause and occurs if L1 larvae hatch in the absence of food, in which they can halt development for up to several weeks until food becomes available [163–165]. There are several genes that are shared between dauer and L1 arrest, all of which are involved in the IIS pathway; *daf-18, age-1, akt-1*, and (likely) *daf-2* [82]. However, unlike the dauer pathway, L1 arrest is not dependent on *daf-16* [165].

L1 arrest is characterized by a developmental arrest in which the germline cells are locked in the G2 phase, and in the absence of DAF-18/PTEN, this G2 arrest is not seen, resulting in inappropriate growth of the germline even in the absence of food [165]. This arrest does not have a requirement for the downstream dauer pathway gene *daf-16*. Thus, the L1 arrest program is actively maintained by *daf-18* by a pathway that differs

from longevity and the canonical dauer pathway. In addition to cell cycle arrest, this L1 arrest program may specifically shut down mitochondrial activity in the germline cells in order to preserve the germline DNA. Mitochondrial activity is associated with increased ROS, which are known to be damaging to DNA [53]. Thus, it would make sense that the immortal, sacrosanct germ cell lineage would have programs in place to limit ROS production during times when cell growth is not happening. I will examine this as a possible level of germline mitochondrial quality control in chapter 2.

Programmed cell death in the mature female germline

Programmed cell death (PCD), also known as cell suicide or apoptosis, is a process in which a cell undergoes a self-destruct program [166,167]. The conditions that influence a cell's decision to do this include excess stress [167,168], immunity [169], and developmentally programmed death of extra cells [91,170]. The process of developmental PCD has been extensively studied in *C. elegans*, where 131 somatic cells are programmed to die, and in fact, it was the work done with *C. elegans* that greatly moved the understanding of apoptosis to where it is today [91]. The core machinery is highly conserved across metazoans [170], which makes it an attractive universal mechanism for maintaining the health of mtDNA.

In *C. elegans*, the genes involved in the canonical cell death pathway are *egl-1*, *ced-9*, *ced-4*, and *ced-3* (Fig.6A) [91,92]. EGL-1, which is homologous to BH3-only (Bcl-1 homology 3) domain proteins, is the upstream activator which acts on the CED-9:CED-4 complex that is present on the mitochondrial surface [171]. When EGL-1/BH3 is activated, it binds to CED-9/BCL2, thereby releasing CED-4/APAF1 to the cytoplasm [172]. Once CED-4/APAF1 is in the cytoplasm, it is free to act on the main executioner

caspase CED-3, switching it from the inactive procaspase form (pro-CED-3) to the activated caspase form [173]. Once activated, CED-3 starts a cascade of cellular events which irreversibly result in death of the cell [91,174]. There are other caspase-like genes, including *csp-1*, *csp-2*, and *csp-3*, which seem to play somewhat minor roles in the execution of PCD [91,175]. It's possible that CSP-2 and CSP-3 work together to inhibit improper activation of the cell death pathway by keeping CED-3 from undergoing autocleavage [176,177]. CSP-1, on the other hand, has more direct caspase activity, and seems to act in parallel with CED-3, acting upon different substrates. Importantly, CSP-1 appears to act independently of the canonical pathway players CED-9/BCL2 and CED-4/APAF1 [91,178]. The processes that occur downstream of caspase execution include nuclear DNA fragmentation, elimination of mitochondria, the inhibition of survival signals, and phosphatidylserine (PS) externalization on the outer cell membrane as an "eat me" signal [21,89,91,92,167,170,174,179]. The PS exposure on the cell surface signals to neighboring cells activates an engulfment program which is controlled by multiple redundant pathways, all of which converge on CED-10/RAC [180–182].

In addition to developmental somatic PCD, there is PCD that occurs in the mature female germline, which kills off as many as >95% of the potential oocytes [89,170,179,183]. Germline PCD is of two types: physiological (thought to be stochastic, perhaps as a way of killing off nurse cells for the developing oocytes), and DNA damage-induced [184]. Physiological germline PCD shares many of the same regulators as somatic PCD, except for the lack of requirement on *egl-1* [184,185]. DNA damage-induced PCD requires all of the core PCD machinery and is regulated by CEP-1/p53 in response to DNA damage [186]. In the event of UV-induced DNA image, CEP-1/p53 upregulates EGL-1 and CED-13 (another BH3-only protein), which both then signal the

rest of the downstream core pathway [19,89,179,184–187]. The possible role of PCD in mtDNA quality control is investigated in chapter 3.

Endodermal cannibalism

Recently, a fascinating discovery was made in *C. elegans* embryos. Termed by the authors "endodermal cannibalism", the germline progenitor cells (PGCs) pinch off a lobe that is roughly half the size of the cell - notably composed majorly of mitochondria - and that lobe then undergoes scission and is degraded by the surrounding endodermal cells [87]. This endodermal cannibalism process happens about midway through embryogenesis, after the P4 cell has further divided to produce the 2 primordial germ cells (PGCs) Z2 and Z3. This cannibalism event is dependent on the dual actions of LST4/SNX9 and CED-10/RAC, which has been recognized largely as a major downstream player in cell corpse engulfment following apoptosis [92,180–182]. LST4 and CED10 regulate dynamin and actin dynamics for the successful constriction and scission of the lobe (Fig. 1.6B). There are several components in these excised lobes, including P granules, but the majority of the material is actually mitochondria. This could be a quality control step for the developing organism to remove any deleterious genomes from the germline, since it occurs right after the bottleneck, when there is a reduced population of mitochondria, and right before the massive uptick in replication that is due to happen. The possible role of endodermal cannibalism is included in the experiments presented in chapter 3.

CONCLUSIONS

This dissertation explores the various pathways and genes that might be involved in the process of mtDNA quality control. In chapter 2 the roles of embryonic segregation and germline mitochondrial quiescence are investigated. Chapter 3 focuses on the regulation of a mtDNA deletion mutant "*uaDf5*" and examines the synergistic effects of genes in the mitophagy and PCD pathways. Finally, in chapter 4, both the dynamics and genetic basis of mtDNA mutation accumulation during aging is studied.

FIGURES

Figure 1

A.

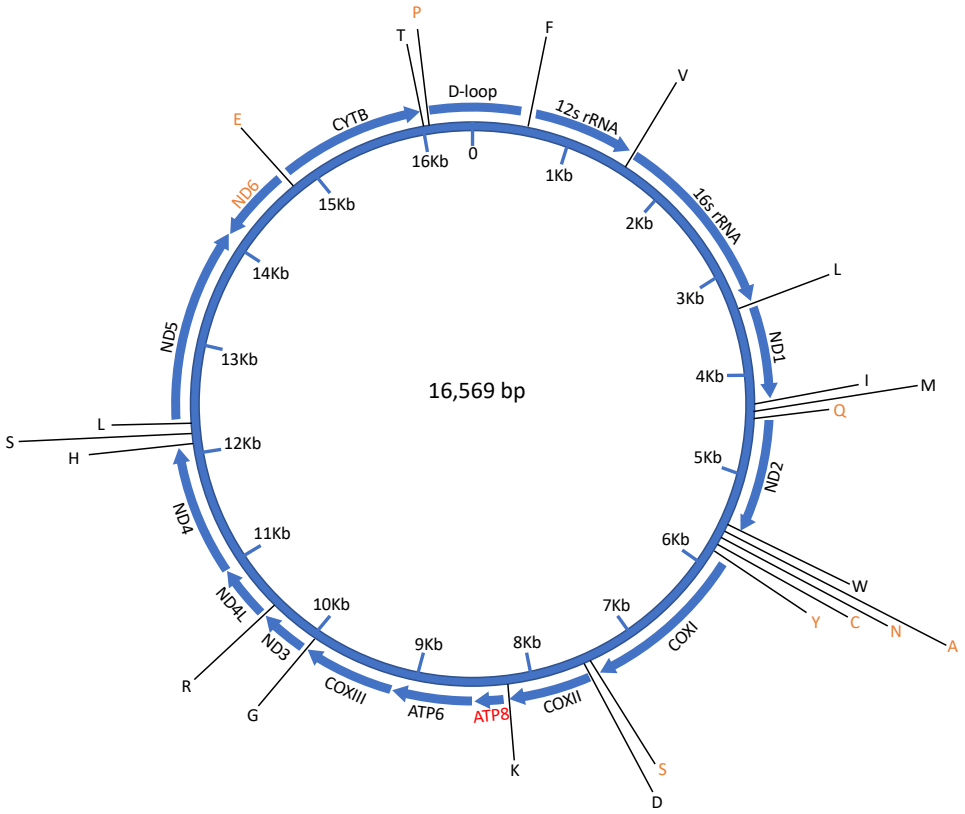

B.

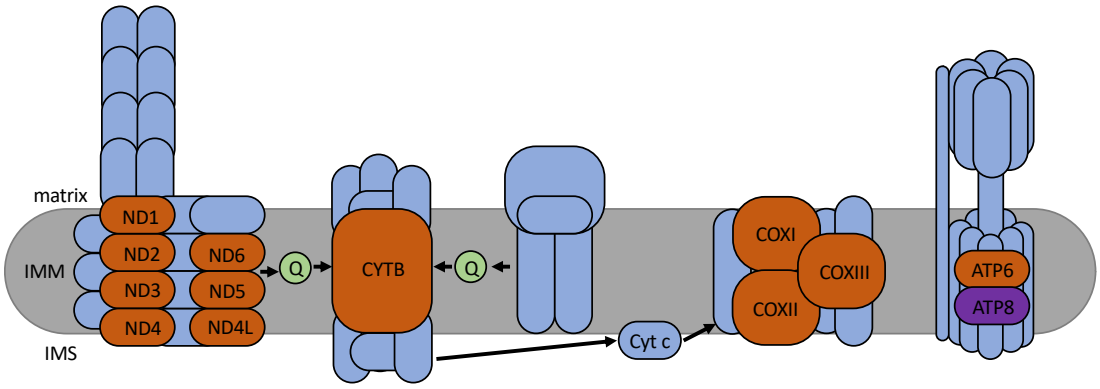

Complex:	I	III	II	IV	V
nDNA-encoded:	~39	10	4	10	~14
mtDNA-encoded:	7	1	0	3	2

C.

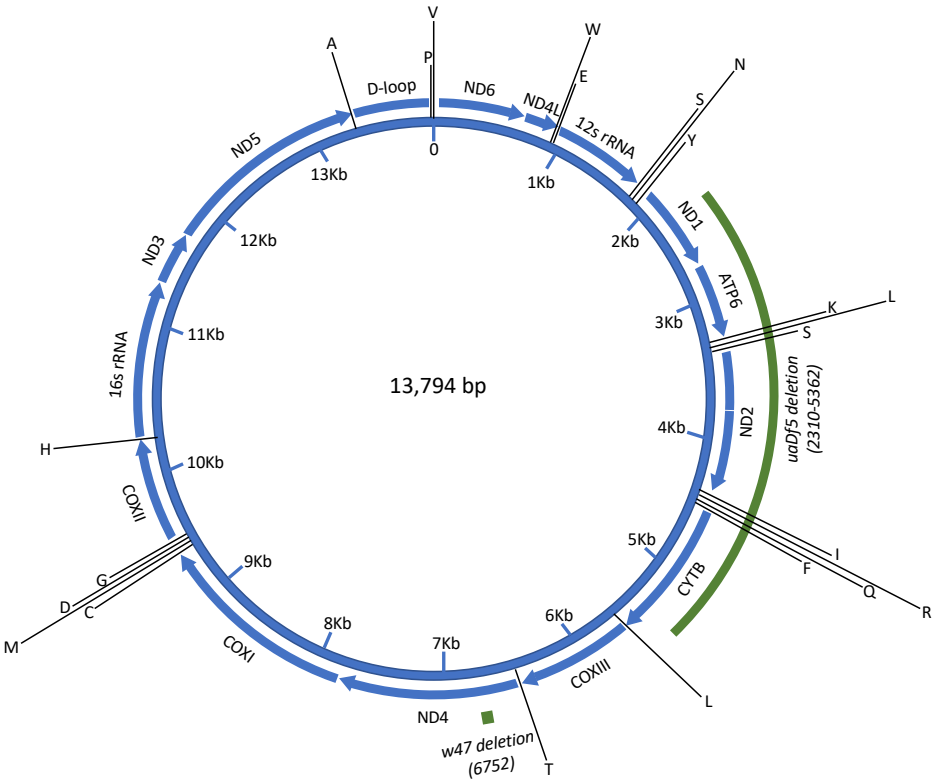

D.

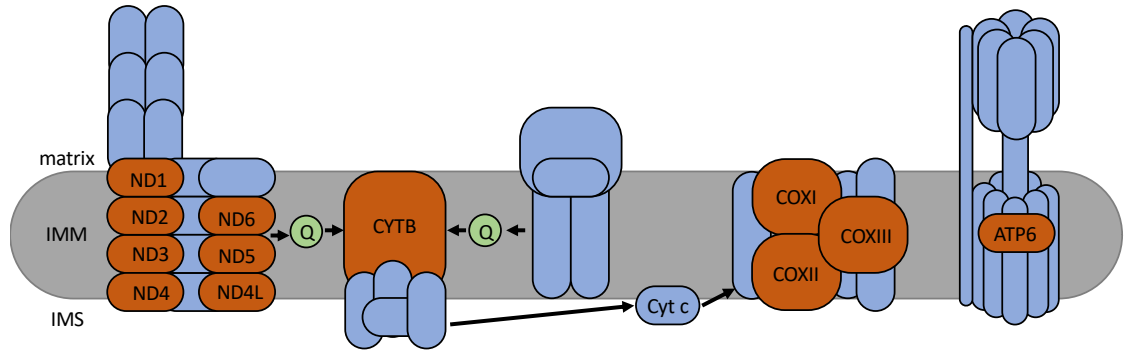

Complex:	I	III	II	IV	V
nDNA-encoded:	~30	~8	4	~6	~13
mtDNA-encoded:	7	1	0	3	1

Figure 1. Human and *C. elegans* mtDNA and the MRC. (A) Diagram of human mtDNA. Blue bars with arrows indicate the locations of genes and direction of transcription. Black bars with letters indicate the locations of tRNAs. Genes and tRNAs

written in black are transcribed in the clockwise direction, and those written in orange are transcribed in the counter-clockwise direction. ATP8, indicated in red, is the only gene present on human mtDNA that is not present *in C. elegans* mtDNA. **(B)** Diagram showing the MRC machinery subunits in humans. Blue indicates nDNA-encoded subunits, orange indicates mtDNA-encoded subunits. Purple indicates the subunit that is present on human mtDNA but not *C. elegans* mtDNA. **(C)** Diagram of *C. elegans* mtDNA. Blue bars with arrows indicate the locations of genes and direction of transcription. Black bars with letters indicate the locations of tRNAs. Green bars show the locations of the *uaDf5* deletion as well as the linked *w47* deletion that I identified via Illumina sequencing. **(D)** Diagram showing the MRC machinery subunits in *C. elegans*. Blue indicates nDNA-encoded subunits, orange indicates mtDNA-encoded subunits

Figure 2

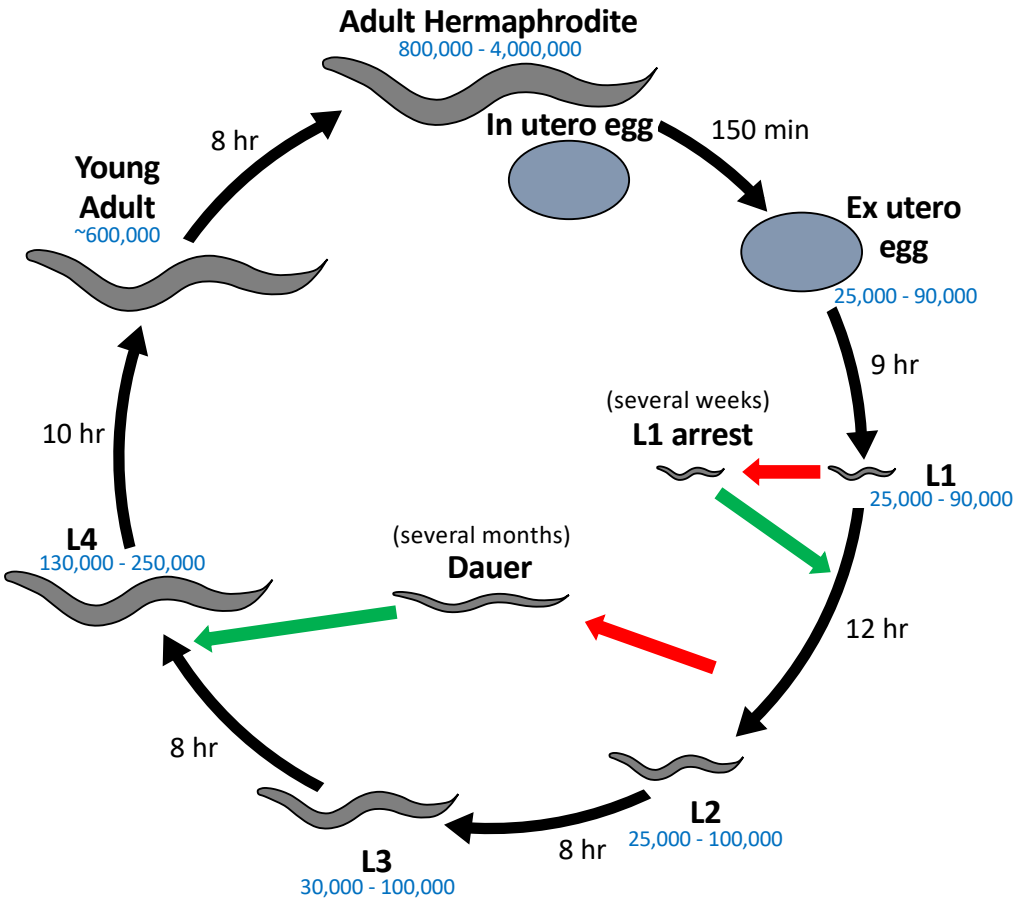

Figure 2. *C. elegans* developmental stages and mtDNA levels. Diagram of the developmental stages of *C. elegans*, including the time it takes between each stage (written in black on the outside of the circle). Estimates for total mtDNA copy number of each stage are indicated in blue. The outer circle shows the stages of development under fed conditions, the red arrows indicate alternative stages of development which *C. elegans* enter if they experience starvation (L1 arrest, dauer), or other forms of stress such as crowding or exposure to dauer pheromone (dauer). Once food is made available, worms can re-enter the normal development pathway via the green arrows. Not shown: adult hermaphrodites lay an average of 300 embryos over the course of about 4 days, then live in a post-gravid state for 10 or more days.

Figure 3

A.

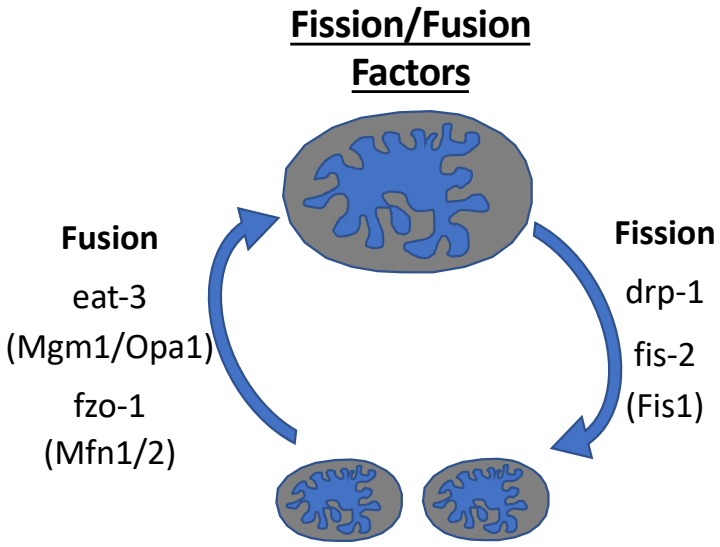

B.

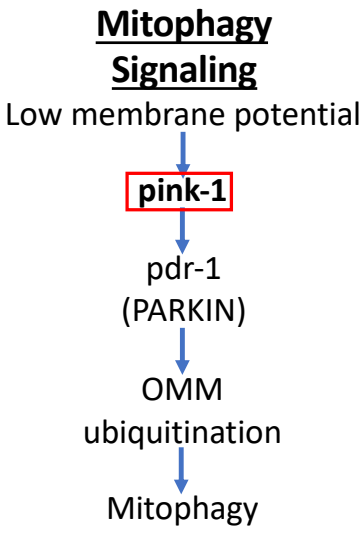

Figure 3. Pathways that act in mtDNA quality control. (A) Diagram of the main *C. elegans* genes involved in mitochondrial fission and fusion. **(B)** Diagram of the main genes involved in mitophagy, with the serine threonine kinase PINK-1 highlighted. Human homologs are indicated in parenthesis.

Figure 4

A.

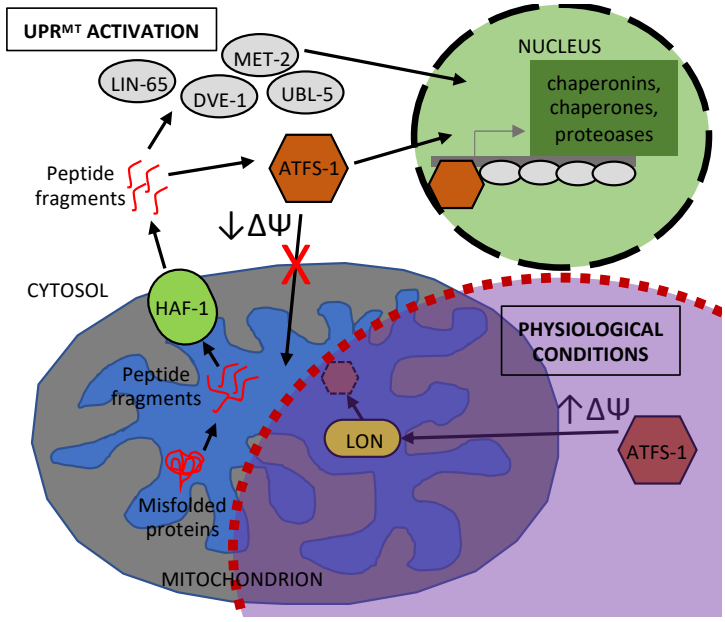

B.

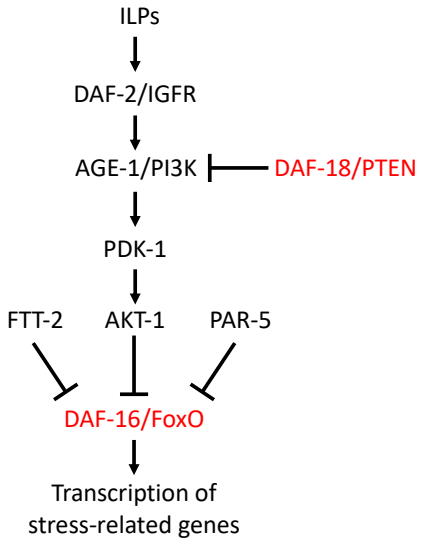

Figure 4. Pathways that protect deleterious mtDNA. (A) Diagram of the main *C. elegans* genes involved in the UPR^{MT}. The purple region indicates how the cell functions under normal physiological conditions with healthy mitochondria. **(B)** Diagram of the main genes involved in the IIS pathway, with the inhibitors indicated in red.

Figure 5

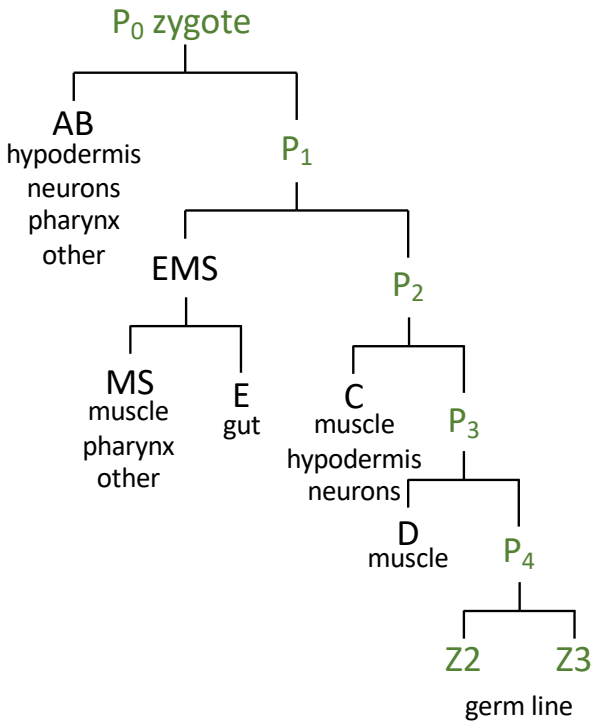

Figure 5. Early embryonic cellular divisions and cell lineages. Diagram outlining the divisions in the early embryo and the resulting cell lineages that each founder cell gives rise to. Green indicates the germline cell lineage up through the end of embryogenesis. After hatching, Z2 and Z3 expand to give rise to the entirety of the germline.

Figure 6

A.

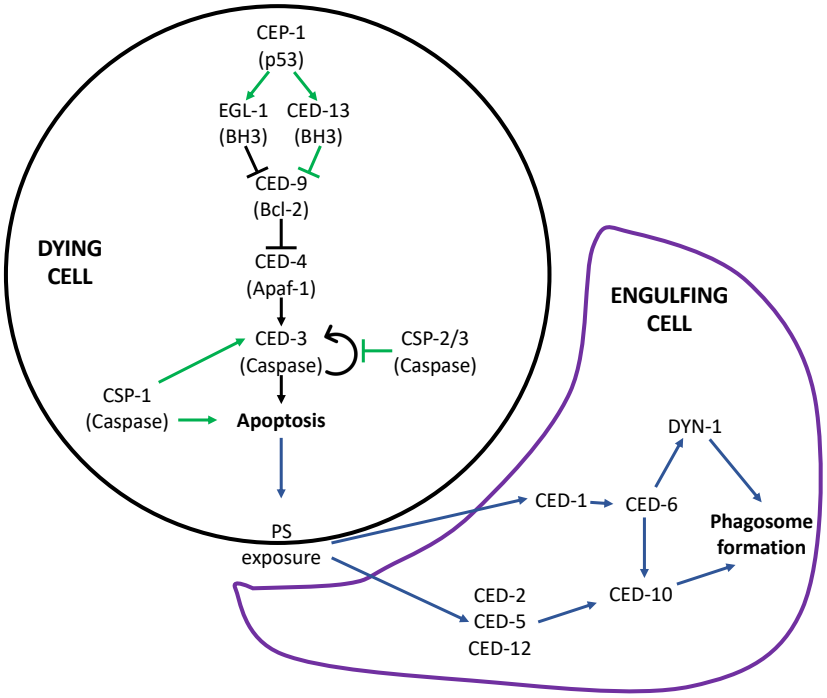

B.

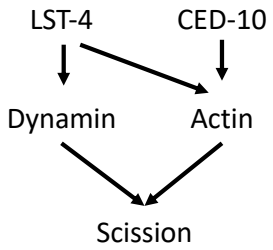

Figure 6. Proposed pathways that may act in mtDNA quality control. (A) Diagram of the main *C. elegans* genes involved in PCD. Black arrows and inhibition symbols indicate the canonical pathway, green indicates non-canonical players. The engulfing cells outlines genes involved in the proper clearance of apoptotic cell corpses following their death. **(B)** Diagram of the main genes involved in endodermal cannibalism, an event that occurs midway through embryogenesis and is an attractive level to investigate for its role in mtDNA quality control.

Chapter Two

Dynamics of Mitochondrial Activity During *C. elegans* Development

SUMMARY

Mitochondria are incredibly dynamic organelles which alter their form and activity continuously throughout development. Control of these dynamics underlie the resulting health of the mitochondrial DNA (mtDNA). Mitochondrial fission allows for the separation of dysfunctional mitochondrial contents from the mitochondrial network, and fusion allows for the mixing of contents to improve health of individual mitochondria. Mitochondrial activity, generally recognized as the membrane potential ($\Delta\Psi$), is an indicator of the health of the organelle. Using mitochondrial-specific dyes (tetramethylrhodamine, ethyl ester: TMRE; $\Delta\Psi$ -dependent, and MitoTracker^{TM} Green FM, $\Delta\Psi$ -independent), I found that mitochondria are sorted immediately following fertilization, resulting in an asymmetric distribution in which the more active mitochondria are concentrated in the posterior side of the zygote, which eventually gives rise to the germline. This suggests that early embryonic segregation is a quality control mechanism that results in a healthier mitochondrial pool to populate the germline lineage. Later in embryogenesis, the nuclei in the germline progenitor cells Z2 and Z3 undergo a DAF-18/PTEN-dependent cellular quiescence with no requirement on DAF-16/FOXO. This cellular quiescence reflects a lowered state of activity that is a likely mechanism for protection of the sacrosanct cell lineage. After hatching, Z2 and Z3 then switch from a quiescent state to an active state in response to food. I found that mitochondrial activity is also depressed in late embryogenesis in Z2 and Z3 and that their activity turns on in response to food after hatching. Similar to nuclear quiescence, I found the mitochondrial quiescence is maintained in a DAF-18/PTEN-dependent manner with no requirement for DAF-16/FOXO, and also observed a dependence on AAK-2/AMPK and DAF-2/IGFR.

INTRODUCTION

Purifying Selection of mtDNA

Mitochondrial DNA (mtDNA) is a highly compact genome that encodes subunits necessary for oxidative phosphorylation. Despite its importance for cellular function, it has been shown that mtDNA has a much higher mutation rate than nuclear DNA, perhaps by as much as a magnitude fold higher [33,48,49]. The possible reasons for this are that the mitochondrial DNA polymerase, DNA polymerase gamma (POLG), is more error prone than the nuclear DNA polymerase [50–52], and the proximity of the mtDNA to the oxidative phosphorylation machinery makes it more likely to be hit with highly damaging reactive oxygen species (ROS; [53]), although this theory has undergone increased scrutiny in recent years [54]. If a cell or organism contains only wildtype mtDNA (WT-mtDNA) it is said to be homoplasmic. However, if there is a mixture of WT-mtDNA and mutated mtDNA then this results in a state known as heteroplasmy [55,56]. Given the high mutation rate of mtDNA, it has become evident that the state of heteroplasmy is extremely common but is generally not tolerated well by the cell [55,56]. In addition to this observation, the mtDNA substitution rate at the long-term phylogenetic scale is much lower than would be extrapolated from the short-term pedigree mutation rate [49], showing that there is a process in which mutations are removed from the germline population (termed purifying selection) or the mutation frequency is specifically reduced in the germline, or some combination of both.

There is evidence for some processes that regulate mtDNA quality control, such as mitochondrial dynamics and mitophagy [67–73] and the mitochondrial unfolded protein response (UPR^{MT}) [74–80]. However, all these processes identified thus far only seem to be part of the story, in that their effects on mtDNA mutation levels are

intermediate. *C. elegans,* a free-living nematode, is an extremely attractive model for the discovery of new mechanisms through which purifying selection operates. In addition to the ease with which one may study genetic questions with this organism, there are also various elements of *C. elegans* development, which show conservation across animals, that are attractive areas to examine for the potential of mitochondrial maintenance. These elements include selective segregation of mitochondria within the early embryo and modulation of mitochondrial activity in the germline during different stages of development to limit production of damaging ROS. Understanding how mtDNA mutations are not only removed from the germline but also how the germline mtDNA mutation rate is reduced is important for the treatment of the subset of mitochondrial diseases that are caused by mtDNA mutations.

The early divisions of embryogenesis

When the *C. elegans* egg is fertilized by the sperm, an entire chain of invariant events is initiated. The establishment of cellular asymmetry is established rapidly, prior to the first cellular division, which is largely dependent on the action of the PAR proteins [147–150]. One of the consequences of this asymmetrical partitioning is the specific movement of P granules into the germline progenitor cell, P1, which undergoes several more divisions to give rise to the entire germline lineage (Fig. 1.5) [151,152]. P granules, also known as germ granules in other organisms, are RNA- and protein - rich spheres that form in the cytoplasm of the germline and are believed to be necessary for the specification of the germ cell fate. Following fertilization, these P granules are segregated into the posterior side of the one cell embryo, which after the first cell division, becomes the P1 cell. The P1 cell then undergoes several more divisions, eventually creating the P4

cell, which gives rise to the entire germline. With each of these divisions, the P granules are segregated into one of the daughters, so that the P4 cell is the only cell in the embryo containing the granules.

Another interesting phenomenon of selective sorting occurs with an intracellular bacterium called *Wolbachia pipientis,* most commonly referred to simply as *Wolbachia*. *Wolbachia* are bacteria in the order Rickettsiales, which interestingly enough, is thought to be the closest living relative to the ancestor of today's eukaryotic mitochondria [153–156]. *Wolbachia* typically infect arthropods and some filarial nematodes, and most of the studies have been done on their relationship with *Drosophila melanogaster* [157–160]. *Wolbachia* must be passed through the fly's maternal germline in order to propagate, very similarly to mitochondria. *Wolbachia* have developed a suite of fascinating strategies for ensuring their transmission, perhaps the most interesting of which is known as "cytoplasmic incompatibility" (CI) which results in inviable embryos if the mother is uninfected. The selective movement of *Wolbachia* into the posterior pole of the mature oocyte (which gives rise to the germline) requires the plus end directed motor kinesin heavy chain, as well as movement along microtubules [157–159].

Perhaps in a mechanism similar to P granule and/or *Wolbachia* sorting, the healthiest mitochondria may be selectively moved to the posterior region of the early embryo. Presumably, mitochondria that contain mutated mtDNA will have impaired oxidative phosphorylation machinery, which will present as a reduced or absent membrane potential. Conversely, mitochondria that contain WT-mtDNA probably have a robust membrane potential. So perhaps the machinery for the selective movement of healthy mitochondria uses a combination of the PAR/P granule-associated proteins and microtubule motor proteins, as well as some sort of membrane potential sensor protein.

As mentioned previously, PINK-1 is a mitochondrial membrane potential sensor, so it is an attractive candidate for this role.

A**lternative development in the starved state: L1 arrest**

C. elegans can enter different developmental programs under cases of extreme stress or starvation (Fig. 1.2). The most studied of these alternate developmental programs is dauer formation, which occurs if L2 larvae experience crowding, starvation, pheromones, or other forms of stress; dauers are able to remain in the dauer stage for several months until conditions improve, upon which they can resume normal development [82,161,162]. This alternate developmental stage results in worms closing up their cuticle and reducing movement in order to conserve energy in the absence of food. The other alternative developmental program is known as L1 arrest/diapause and occurs if L1 larvae hatch in the absence of food, in which they can halt development for up to several weeks until food becomes available [163–165]. There are several genes that are shared between dauer and L1 arrest, all of which are involved in the IIS pathway; *daf-18, age-1, akt-1*, and (likely) *daf-2* [82]. However, unlike the dauer pathway, L1 arrest is not dependent on *daf-16* [165].

L1 arrest is characterized by a developmental arrest in which the germline cells are locked in the G2 phase, and in the absence of DAF-18/PTEN, this G2 arrest is not seen, resulting in inappropriate growth of the germline even in the absence of food [165]. This arrest does not have a requirement for the downstream dauer pathway gene *daf-16*. Thus, the L1 arrest program is actively maintained by *daf-18* by a pathway that differs from longevity and the canonical dauer pathway. In addition to cell cycle arrest, this L1 arrest program may specifically shut down mitochondrial activity in the germline cells in

order to preserve the germline DNA. Mitochondrial activity is associated with increased ROS, which are known to be damaging to DNA [53]. Thus, it would make sense that the immortal, sacrosanct germ cell lineage would have programs in place to limit ROS production during times when cell growth is not happening.

RESULTS

Mitochondria are asymmetrically sorted during early embryonic division

One way the cell may select against deleterious mtDNA from populating the germline is by early embryonic sorting based on mitochondrial membrane potential ($\Delta\Psi$) so that more active mitochondria with a higher $\Delta\Psi$ are moved to the posterior end of the embryo, which gives rise to the germline lineage (Fig. 1.5, 2.1A). In order to determine if mitochondria are sorted based on their $\Delta\Psi$ along the anterior-posterior axis following fertilization, I stained pre-fertilized oocytes and early stage embryos with the $\Delta\Psi$-dependent dye TMRE [188,189] with or without the $\Delta\Psi$-independent dye MitoTracker Green FM which stains all mitochondria regardless of $\Delta\Psi$ [190,191] (Fig. 2.1B). MitoTracker Green FM was used in order to determine the location of all mitochondria within the cell, and the TMRE signal was then used to determine the $\Delta\Psi$ of each mitochondrion. Without normalization to MitoTracker Green FM, there is no way to know if a brighter TMRE signal is due a population of more active mitochondria rather than to more concentrated mitochondria. I then imaged the oocytes and embryos in Z-series every 5 minutes for the first 40 minutes of development, which brings them to the four-cell stage. During these first cellular divisions I quantified the ratio of the TMRE signal in the germline cell lineage, which is the most posterior cell in the early embryo, to the TMRE signal in the rest of the embryo. In our laboratory wildtype strain, N2, I found

that the mitochondria are symmetrically distributed in pre-fertilized oocytes (TMRE: 0.97 ± 0.02; TMRE/MitoTracker Green FM: 0.97 ± 0.0001) but then immediately following fertilization, as the male and female pronuclei are joining, there is a redistribution of mitochondria that results in an asymmetric distribution of mitochondria – resulting in both a higher concentration (TMRE: 1.46 ± 0.03) and in more active mitochondria (TMRE/MitoTracker Green FM: 1.27 ± 0.03) - in the posterior end of the cell (Fig. 2.1C, D). It appears that this movement is linked to the cytoplasmic flow which occurs during early embryogenesis to set up polarity within the cell. The mitochondrial activity in the posterior cell "P1" starts to turn down after the first embryonic division, (TMRE: 1.28 ± 0.01; TMRE/MitoTracker Green FM: 1.18 ± 0.01 in the early two-cell stage), then remains at a constant level through the three-cell stage (TMRE: 1.27 ± 0.02; TMRE/MitoTracker Green FM: 1.16 ± 0.01), and then drops again at the four-cell stage to the point that the activity of the mitochondria in the P2 cell is equivalent to or perhaps even lower than the activity in its sister cell "EMS" (TMRE: 0.88 ± 0.007; TMRE/MitoTracker Green FM: 1.01 ± 0.008).

PAR proteins and SPD-5 play a role in early embryonic mitochondrial sorting

The PAR proteins are the key regulators for setting up polarity within the early embryo and are one of the responsible parties for the downstream movement of P granules into the posterior region of the one cell embryo [83,85,148,150–152,192]. To determine whether the pathways regulating P granule movement also control mitochondrial movement, I did TMRE analysis in mutants for the PAR proteins. To test if mitochondria use the same cellular machinery as *Wolbachia* (which rely largely on

microtubules for maternal germline transmission [157–159]), I also analyzed a mutant for the centrosome coiled-coil domain protein SPD-5 [193]. Additionally I analyzed two mutant alleles for the mitochondrial ΔΨ sensor protein PINK-1 [117,119,120,122], since it is the best candidate for how the cell can differentially tag mitochondria for ΔΨ-based sorting (All mutants used can be found in Table 2.1). Several of the PAR mutants had significantly reduced mitochondrial sorting in early one-cell embryos as measured with TMRE alone (1.18 ± 0.05 in *par-2(e2030ts),* 1.25 ± 0.08 in *par-3(e2074),* 1.19 ± 0.05 in *par-5(it55)*, and 1.14 ± 0.04 in *par-6(zu222)*) (Fig. 2.2B). The PAR mutants *par-1(zu310ts)* and *par-4(it57ts)* did not have any change (1.45 ± 0.09 and 1.42 ± 0.07, respectively), but it is possible that is due to the wildtype activity of the protein reactivating when the embryos were being imaged at room temperature on the microscope.

The mutant *spd-5(or213)* disrupts the normal activity of the centrosomal scaffolding protein SPD-5, resulting in inhibition of both spindle formation and microtubule nucleation [193]. *spd-5* mutants exhibited the strongest effect, with the TMRE ratio dropping all the way to 1.04 ± 0.02, indicating that this mutant exhibits no selective mitochondrial sorting. The trend of reduced sorting in the *par* mutants and *spd-5* remains up through the three-cell stage, at which point both the mutants and wildtype alike all start to approach a ratio of 1 (Fig 2.2C-F), suggesting that neither the PAR proteins nor SPD-5 are involved in the eventual shut down of germline mitochondrial activity after the first cellular division. By the four-cell stage, all strains analyzed had greatly reduced their germline mitochondrial activity. When the germline progenitor cell (P2) was compared to its sister cell, EMS, it had a ratio significantly less than 1 (0.88 ± 0.007), suggesting the P2 cell has less mitochondrial activity than EMS in the 4 cell stage

(Fig. 2.2G), but when the TMRE signal of P2 was measured against the entire rest of the embryo instead of just EMS, it had a ratio closer to 1 (1.03 ± 0.008), suggesting that EMS is the cell with the highest mitochondrial activity starting at the four-cell stage (Fig. 2.2H).

pink-1 mutant embryos exhibit a PAR-like phenotype and the stronger allele has reduced mitochondrial sorting

Although the two alleles of *pink-1* did not give statistically significant results with the TMRE analysis at the early one-cell stage (1.49 ± 0.07 in *pink-1(ok3538)* and 1.37 ± 0.06 in *pink-1(tm1779)*), the stronger of the two alleles, *pink-1(tm1779)* (unpublished data from Julia Dey), did have a reduced ratio value, suggesting that it was approaching significance and may have reached it if more embryos were analyzed. In fact, by the early two-cell stage, *pink-1(tm1779)* did have a significantly lower TMRE ratio (1.2 ± 0.02), supporting its role in mitochondrial sorting.

C. elegans embryogenesis is a highly nonvariant process and the orientation of the cells after each division is highly predictable. However, in PAR mutants, the lack of polarity establishment results in abnormal phenotypes such as equal sized cells at the two-cell stage and various deviations from the typical three-cell division times and orientation along the posterior-anterior axis [148,150]. An observation made while doing the TMRE analysis was that several *pink-1* mutant embryos exhibited a PAR-like morphology in the three-cell stage (Fig 2.3). The lack of functional PINK-1 resulting in a PAR-like embryo suggests that PINK-1 is indeed playing a role in establishing asymmetry during early embryonic development.

Germline mitochondria shut off for the remainder of embryogenesis

A strain containing a GFP reporter driven by the germline-specific *pie-1* promoter [194,195] was utilized to easily identify the germline progenitor cells Z2 and Z3 in later stage embryos (Fig. 2.4A). The germline TMRE signal in bean, comma, 2-fold, and 3-fold stage embryos was analyzed by drawing 7 random ROIs of similar size around the embryo, averaging their mean intensity, and then determining the ratio of the TMRE signal intensity from the germline ROIs to the averaged mean intensity from the rest of the embryo (Fig. 2.4B). Z2 and Z3 in each of these stages had a dimmer TMRE signal than the surrounding cells, suggesting that the germline cells have quiescent mitochondria throughout embryogenesis (Fig. 2.4C). In fact, the germline mitochondria appear to progressively decrease their activity throughout embryogenesis such that the germline mitochondrial is at its lowest at the 3-fold stage of embryogenesis, immediately prior to hatching.

Upon hatching, germline mitochondria remain shut off until food is present

To see if germline mitochondrial activity is differentially regulated upon hatching, I imaged the germline mitochondria in TMRE-stained wildtype L1s hatched in either the presence of absence of food. The Z2 and Z3 cells can be easily identified via DIC because of their large size and unusual morphology compared to the surrounding cells in the L1 stage worm [196,197] (Fig. 2.5A). I found that starved L1s have reduced germline mitochondrial activity, similar to late stage embryos (only 5.4% of worms had active mitochondria). Conversely, if food is present upon hatching, the germline mitochondria switch to a high activity state (65.3% of worms have high activity after 5 hours feeding, 100% after 10 hours on food), presumably surpassing the mitochondrial activity in the

surrounding cells based on the high intensity of the TMRE signal specific to the germline cells (Fig 2.5B). Time lapse studies reveal that the germline mitochondria start increasing their activity within a few hours of exposure to food, with the vast majority of worms (93.33%) having highly active germline mitochondria within 5 hours of feeding (Fig. 2.5C).

Mutant analysis reveals many mutants have delayed response to food

I selected a group of mutants based on their known roles in L1 arrest/diapause, dauer formation, and mitochondrial regulation (Table 2.2). Of these mutants analyzed, I was surprised to find that many of them had a higher percentage with active germline mitochondria after 5 hours of feeding than they did after a longer period of 10 hours of feeding, with the biggest effects seen in the laboratory alternative wildtype liquid culture strain LSJ1 (87.2% highly active after 5 hours down to 0% active after 10 hours). This trend was also observed in *daf-2(e1368)* (47.5% after 5 hours down to 0% after 10 hours), *uaDf5* (65% after 5 hours down to 7.9% after 10 hours), *daf-18(e1375)* (83% after 5 hours down to 10% after 10 hours), *aak-2(gt33)* (90.7% after 5 hours down to 47.5% after 10 hours), *daf-16(mu86)* (64.4% after 5 hours and 45.8% after 10 hours), and *pink-1(tm1779)* (13.6% after 5 hours down to 5% after 10 hours) (Fig. 2.6A). The high frequency with which I observed these dynamics suggests that the extended time protocol itself may have resulted in worms not being able to properly feed.

Of note, I found several mutants that seem to have a general delayed response to food, including *clk-1(qm30)* (2.2% after 5 hours and 82.6% after 10 hours), *ced-3(n717)* (6.3% after 5 hours and 12.8% after 10 hours), *aak-2(rr48)* (29% after 5 hours and 100% after 10 hours), *aak-2(ok524)* (12.1% after 5 hours and 96.7% after 10 hours), *daf-*

18(ok480) (38.5% after 5 hours and 56% after 10 hours), *daf-2(e1370)* (55.1% after 5 hours and 60% after 10 hours), and *daf-2(e1391)* (17.5% after 5 hours, no data for 10 hours). The clearest evidence for the delayed response to food is seen in the *clk-1(qm30), aak-2(rr48),* and *aak-2(ok524)* mutants, which show a marked increase in TMRE signal between the 5-hour and 10-hour timepoints.

Mutant analysis reveals a role for *daf-18, daf-2,* and *aak-2* in mitochondrial quiescence in the starved state

The same analysis was done for improper activation of germline mitochondria in starved L1s which enter the alternative developmental program of L1 arrest (Fig. 1.2). Here, I found that *daf-18, daf-2,* and *aak-2* mutants show improper activation of germline mitochondria in the starved state (Fig. 2.7). This effect was seen in all *daf-18* mutants analyzed (39.5% for *ok480*; 30.9% for *e1375*), all *daf-2* mutants analyzed (36.6% for *e1370*; 33.3% for *e1391*; 25.6% for *e1368*), and two of three *aak-2* mutants analyzed (38.8% for *ok524*; 16.5% for *gt33*). I also found that germline mitochondrial quiescence does not depend on DAF-16/FOXO activity (8.87% for *mu86*), suggesting mitochondrial activity is regulated by the same pathway that keeps the nucleus arrested at the G2 phase during L1 arrest [163–165].

DISCUSSION

Mitochondria are sorted into the germline progenitor cell during early embryogenesis based on their ΔΨ

I present evidence establishing the relationship between germline mitochondrial activity throughout early development in the nematode *C. elegans*. First, I show that

mitochondria are sorted between the posterior and anterior cells of the early embryo such that the mitochondria with a higher ΔΨ are concentrated into the posterior cell which gives rise to the germline. I propose that mitochondria with a higher ΔΨ contain a healthier population of mtDNA, so this sorting is a way of ensuring that the sacrosanct germline is populated with a higher concentration of wildtype mtDNA. I found that the sorting of more active mitochondria into the posterior region of the one-cell embryo is inhibited in mutants involved in polarity establishment of the early embryo, including *par-2, par-3, par-5*, and *par-6* [85,147–150,192]. Polarity establishment is required for the sorting of germline-specific components such as P granules into the germline progenitor cell, suggesting that mitochondrial sorting may use the same machinery as P granules. Further studies need to be done in mutants involved more specifically in P granule sorting, including mutant analysis of the P granule associated proteins: the RGG-domain proteins PGL-1 and PGL-2, and the DEAD-box proteins GLH1-4 [83,84,152,198]. The strongest inhibition of this sorting process was observed in the *spd-5* mutant, which knocks out the function of a centrosomal protein that is involved in microtubule organization and spindle formation [193]. *Wolbachia,* which are an intracellular parasite that are propagated via the maternal germline, rely on microtubules for their movement into the germline progenitor cell [157–159]. This suggests that mitochondria and *Wolbachia* may rely on similar machinery. Further analysis of microtubule-associated proteins and the microtubule motor proteins needs to be done to determine if this is the case.

I also analyzed mutants of the mitochondrial ΔΨ-sensor PINK-1 [117,119,120,122], since I wanted to know if PINK-1 allows for the cell to distinguish the more active mitochondria from the less active ones. *pink-1* mutants had a decreased

posterior enrichment across all stages, although it was not statistically significant until the early two-cell stage. This may be an issue with sample size or may suggest that PINK-1 plays its role later than the other mutants analyzed. In addition to the analysis of mitochondrial sorting, I noted that a fraction of PINK-1 mutant embryos have abnormal morphology that parallels the abnormal embryonic morphologies observed in PAR mutants [150]. This suggests that PINK-1 is indeed playing a role in establishment of asymmetry in the early embryo, and future studies need to be done to examine how loss of PINK-1 affects various parameters of polarity establishment, including TMRE analysis of a stronger *pink-1* allele.

Germline mitochondrial activity shut downs at the four-cell stage and remains shut down for the remainder of embryogenesis

Analysis of the posterior enrichment of active mitochondria through the four-cell stage shows a sudden decrease in mitochondrial activity in the P2 germline progenitor cell such that its activity is lower than the activity in its sister cell "EMS". When the P2 cell activity is compared to the combined average activity in all of the other three cells of the embryo, its activity is shown to be equivalent, inferring that at the four-cell stage, EMS is the cell with the highest activity. It makes sense that the germline mitochondria begin to shut down their activity after their sorting into the posterior cell during the first division since the germline progenitor cell only undergoes a total of 4 divisions during early embryogenesis to make the Z2 and Z3 cells, which then enter a state of quiescence that lasts until the embryo hatches and proceeds with larval development. I examined the mitochondrial activity in the germline progenitor cells Z2 and Z3 throughout the remainder of embryogenesis and found that the mitochondria continue to decrease their

activity as embryogenesis progresses. This makes sense in terms of mtDNA quality control, since a negative consequence of oxidative phosphorylation is that it produces ROS which are mutagenic [53]. Thus, since Z2 and Z3 cells are in a quiescent state throughout embryogenesis [163,164,196], their energy demands are low, and perhaps as a protective mechanism, the germline mitochondria are entirely shut down in order to reduce ROS production.

Germline mitochondria in hatched L1s remain quiescent until food is present in a DAF-18/PTEN, DAF-2/IGFR, and AAK-2/AMPK dependent manner

Upon hatching into the first larval state, L1, normal development proceeds in a food-dependent manner during which both the soma and germline expand [163,164,196]. Analysis shows that the mitochondrial response to food is delayed in several mutants, suggesting this process is controlled by several pathways. If, however, there is no food present upon hatching, the L1 larvae enter an alternative state known as L1 arrest/diapause [163–165,196]. In this state, development is paused for up to two weeks at the L1 state until food becomes available, after which normal development proceeds. This alternative development program shares similarities with dauer development which is dependent on the IIS pathway [82,161,163–165]. The quiescent state observed in the germline cells of L1 arrested worms presents as condensed nuclear chromosomes that are arrested in the G2 phase of the cell cycle. Both L1 arrest and dauer formation are dependent on components of the IIS pathway, most notably, DAF-18/PTEN, although the two processes differ in that L1 arrest has no requirement for DAF-16/FOXO [165]. I found that germline mitochondrial activity also remains quiescent throughout L1 arrest, and that in the presence of food the germline mitochondria activate to levels higher than

the surrounding cells, with most worms exhibiting highly active mitochondria after 5 hours of feeding. Mutant analysis of starved L1s shows that maintenance of germline mitochondrial quiescence throughout L1 arrest is dependent on DAF-2/IGFR, AAK-2/AMPK, and DAF-18/PTEN, with no requirement for DAF-16/FOXO, suggesting the same machinery that acts to keep the nucleus in a quiescent state is also used for the mitochondrial state. Further studies need to be done with mutants known to act in the maintenance of germline cell cycle arrest, including AGE-1/PI-3 and AKT-1/PKB, to see if a common pathway acts on both the mitochondrial state and the nuclear state.

MATERIALS AND METHODS

Strains and culture conditions

Nematode strains were maintained at on NGM plates as previously described at either 20°C or 15°C for the temperature-sensitive strains [199]. Please refer to appendix A1 for a table detailing all strains used in this dissertation. Strains without a JR designation were either provided by the CGC which is funded by NIH Office of Research Infrastructure Programs (P40 OD010440) or were obtained from the Mitani lab (strains with a FX designation or JR strains containing alleles with a tm designation were generated from Mitani lab strains) [200].

Staining of embryos

50 µl of 10 µM tetramethylrhodamine, ethyl ester (TMRE) in DMSO with or without 10 µl of 5 mM MitoTracker™ Green FM was pipetted and spread with a glass spreader onto small 3mm NGM plates and allowed to dry in a dark chamber. ~50 young adults were added to the plates after drying and incubated overnight at 20°C for the non-

temperature sensitive (ts) strains, or at the restrictive temperature of 25°C for the ts strains.

Slide preparation of early embryos

For fluorescent imaging, 3% agarose pads were made. After overnight incubation on the TMRE +/- MitoTracker™ Green FM plates, 10 gravid adults were transferred to a fresh NGM plate for 5 minutes to remove any excess bacteria that were stained with the mitochondrial dyes. After 5 minutes, the adults were picked off and transferred to 8 µl of M9 buffer containing levamisole on a coverslip. Using 25G1½ PrecisionGlide® needles as scissors, the worms were sliced in half at the midline, thus resulting in release of all early stage embryos from the uterus. The agar pad was then lightly placed on top of the liquid droplet to create a seal and imaged.

Staining of L1s

For the starved condition, egg preps were done (as previously described; [199]) on large TMRE plates (made by pipetting and spreading 50 µl of 10 µM TMRE in DMSO onto large 3mm NGM plates and allowed to dry in a dark chamber) containing healthy adult worms. The resulting embryos were pipetted onto a small unseeded TMRE plate (made by pipetting and spreading 50 µl of 10 µM TMRE in DMSO onto small 3mm unseeded plates and allowed to dry in a dark chamber) and incubated overnight before imaging the following morning. For the fed conditions, egg preps were done on large TMRE plates containing healthy adult worms. The resulting embryos were pipetted onto a small unseeded TMRE plate and incubated overnight. The next morning, the L1s were washed off the unseeded plate and transferred to a small seeded TMRE plate for the

amount of time described before imaging (made by pipetting and spreading 50 µl of 10 µM TMRE in DMSO onto small 3mm NGM plates and allowed to dry in a dark chamber).

Slide preparation of L1s

For fluorescent imaging, 3% agarose pads were made. After incubation on the TMRE plates, L1s were picked off and transferred to an 8 µl droplet of M9 containing levamisole on the agar pad. A coverslip was then lightly placed on top of the liquid droplet to create a seal and the worms were imaged.

Imaging

Imaging was done on the Nikon Eclipse Ti. For early embryos, 8-20 slice Z-stacks were performed every 5 minutes for the first 30 minutes of development using DIC, TxRed and/or TRITC, and GFP-YFP channels. For late staged embryos, 8-20 slice Z-stacks were taken using DIC, TxRed and/or TRITC, and GFP-YFP channels. For L1s, 8-slice Z-stacks were performed on each worm using DIC, TxRed and/or TRITC, and GFP-YFP channels.

Image Analysis

For early embryos, the Z slice closest to the center of the embryo was used for analysis. Regions of interest (ROIs) were manually drawn and the average pixel intensity was calculated using the Nikon Elements software. For 1 cell embryos, the posterior and anterior ROIs started at the middle point of the embryo. For 2 cell embryos, the posterior ROI comprised the posterior (P1) cell and the anterior ROI comprised the anterior (AB)

cell. For 3 cell embryos, the posterior ROI comprised the posterior (P1) cell and the anterior ROI comprised both daughters of the AB cell (AB.a and AB.p). For 4 cell embryos, there were two ROI analyses performed. In both, the posterior ROI comprised the posterior (P2) cell. In one analysis, the anterior ROI comprised the sister cell to the P2 cell (EMS), and in the other analysis, the anterior ROI comprised all 3 cells anterior to the P2 cell (EMS, AB.a, and AB.p).

For late stage embryos, the GFP channel was used to determine the Z slice containing the germline progenitor cells Z2 and Z3 to be used for analysis of the TMRE signal in the TRITC channel. Regions of interest (ROIs) were manually drawn around the Z2 and Z3 cells, and 7 additional ROIs of equal size were placed randomly throughout the rest of the embryo. Average pixel intensity of the Z2 and Z3 cells as well as the combined average pixel intensity of the 7 randomly distributed ROIs was calculated using the Nikon Elements software.

For L1 analysis, The DIC channel images were first analyzed to determine the location of the Z2 and Z3 cells. After their location was identified, the TxRed channel was examined to determine if the TMRE signal was brighter or darker in the Z2 and Z3 cells compared to the surrounding gut and muscle cells.

FIGURES

Figure 1

A.

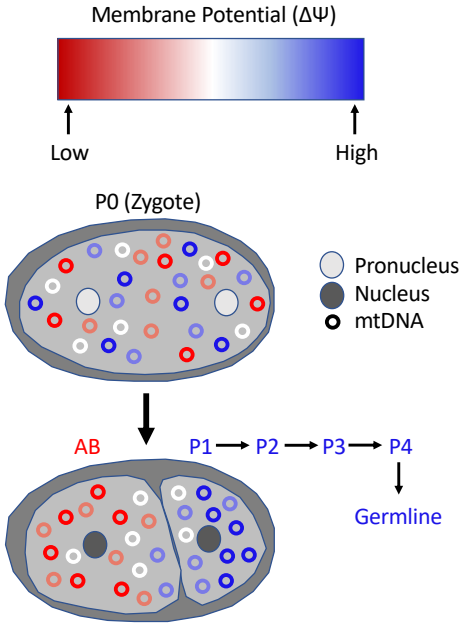

B.

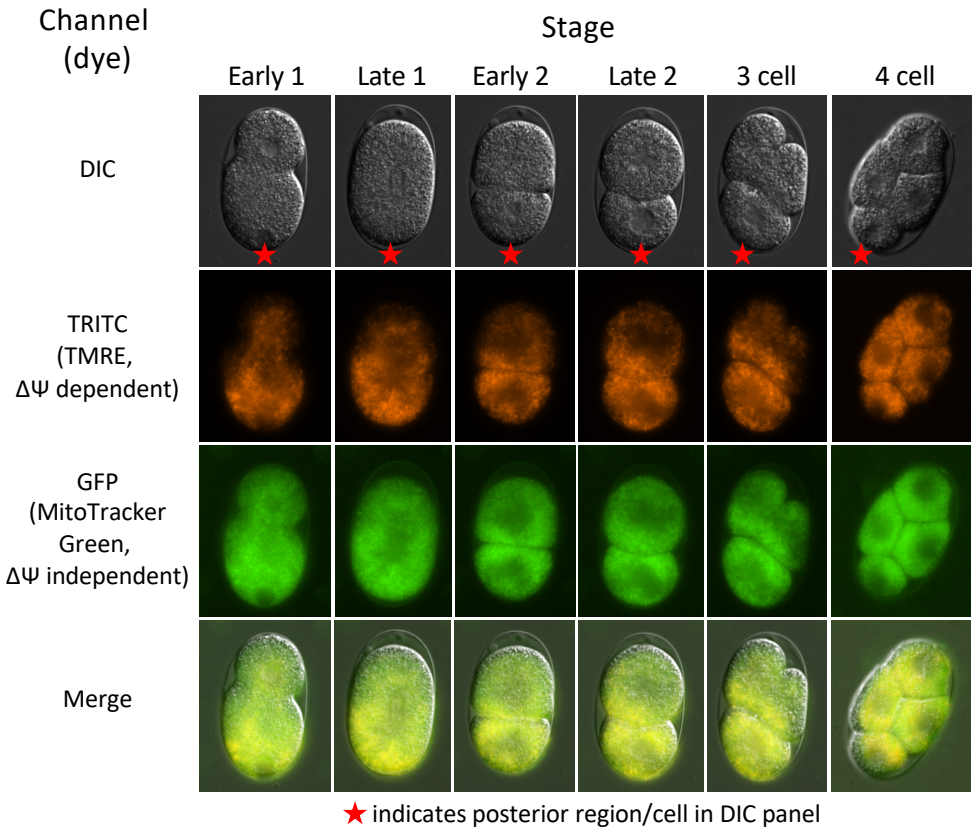

C.

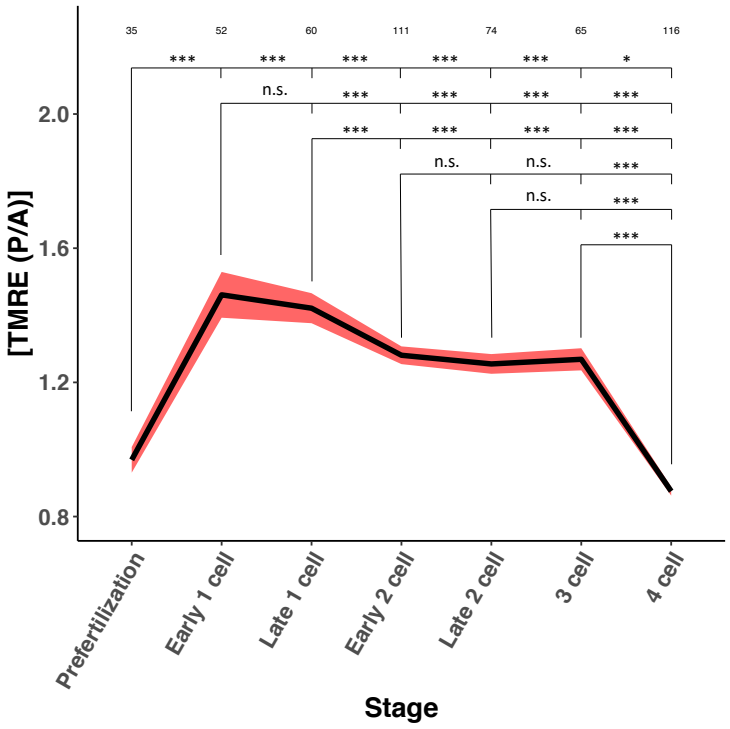
35
52
60
111
74
65
116
[TMRE (P/A)]
2.0
1.6
1.2
0.8
Prefertilization
Early 1 cell
Late 1 cell
Early 2 cell
Late 2 cell
3 cell
4 cell
Stage

D.

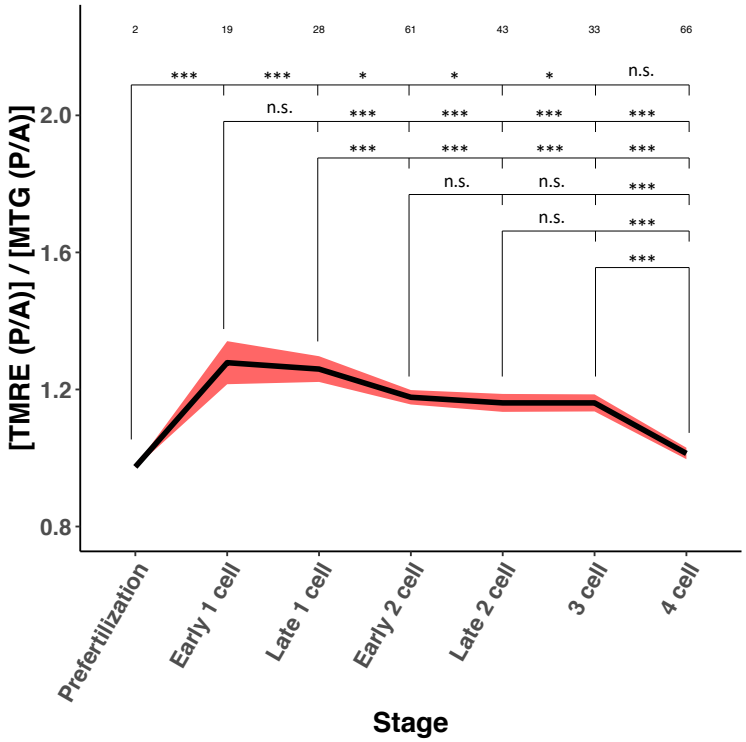
2
19
28
61
43
33
66
[TMRE (P/A)] / [MTG (P/A)]
2.0
1.6
1.2
0.8
Prefertilization
Early 1 cell
Late 1 cell
Early 2 cell
Late 2 cell
3 cell
4 cell
Stage

Figure 1. Mitochondrial sorting during early embryogenesis. (A) Schematic of the expected results from staining early embryos with TMRE and MitoTracker Green FM. If mitochondria are sorted between the germline progenitor cell lineage (P1→P4) based on $\Delta\Psi$, I expect to see a higher TMRE signal (normalized by MitoTracker Green FM, which stains all mitochondria independently of $\Delta\Psi$) on the posterior side of the early embryo. **(B)** Example images of embryos stained with TMRE and MitoTracker Green FM. Early 1 = before pronuclei have joined, Late 1 = immediately before P0 divides, Early 2 = immediately after P0 divides, Late 2 = immediately before AB divides, 3 cell = midway through the 3-cell stage, 4 cell = midway through the 4-cell stage. The posterior side of the embryo/germline progenitor cell is indicated with the red star. **(C)** Quantification of embryonic TMRE staining in N2 (laboratory wild type) animals. **(D)** Quantification of embryonic TMRE normalized to MitoTracker Green FM staining in N2 (laboratory wild type) animals. (*** $p < 0.001$, ** $p < 0.01$, * $p < 0.05$, . $p < 0.1$) For each condition, N is indicated at the top of the graph. Statistical analysis was performed using one-way ANOVA with Tukey correction for multiple comparisons.

Table 1

Gene	Allele	Strain	Protein Effect	Developmental Impact
GFP reporter	axIs1677 [*pie-1p::GFP::histone H2B::pgl-1 3'utr + unc-119(+)]*	JH2320	-	-
par-1	*zu310(ts)*	KK822	Substitution I→N	Polarity defects
par-2	*e2030(ts)*	CB3886	Not curated	Polarity defects
par-3	*e2074*	KK237	Not curated	Polarity defects
par-4	*it57(ts)*	JK1667	Substitution P→S	Polarity defects
par-5	*it55*	KK299	Substitution A→V	Polarity defects
par-6	*zu222*	KK818	Tc1 Transposon insertion	Polarity defects
pink-1	*tm1779*	JR3298	350bp Deletion knocking out start codon	Mitophagy defects, oxidative stress
	ok3538	JR3335	5bp insertion	Mitophagy defects, oxidative stress
spd-5	*or213*	EU856	Substitution R→K	No mitotic spindle assembly or microtubule nucleation

Table 1. Summary of mutants analyzed for early embryonic sorting. Table showing strains tested for early embryonic sorting, outlining the effect on protein for each mutant and the associated phenotype.

Figure 2

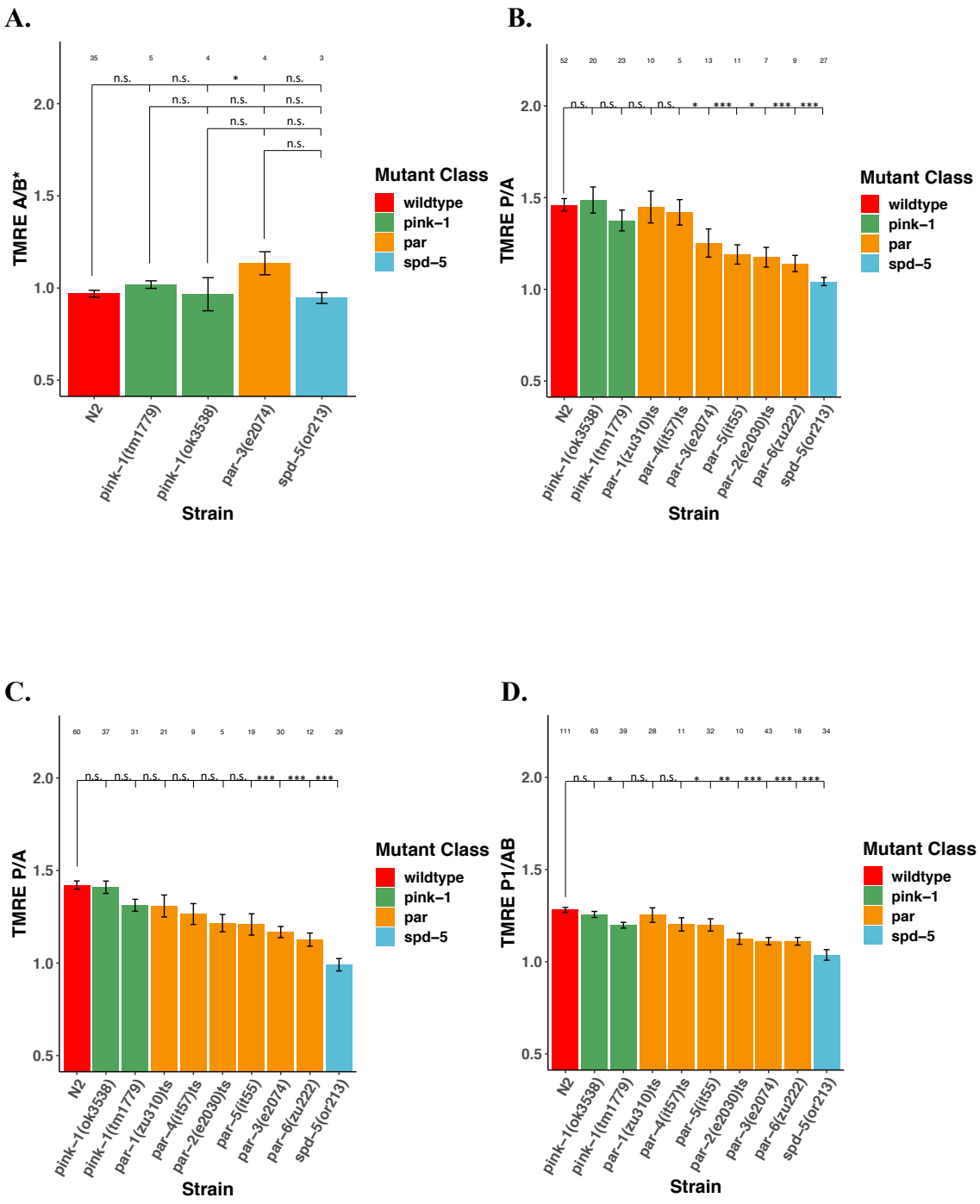
A.
B.
C.
D.
TMRE A/B*
TMRE P/A
TMRE P1/AB
Strain
Mutant Class
wildtype
pink−1
par
spd−5
N2
pink−1(tm1779)
pink−1(ok3538)
par−3(e2074)
spd−5(or213)
pink−1(ok3538)
pink−1(tm1779)
par−1(zu310)ts
par−4(it57)ts
par−3(e2074)
par−5(it55)
par−2(e2030)ts
par−6(zu222)
spd−5(or213)
n.s.
*
**
***

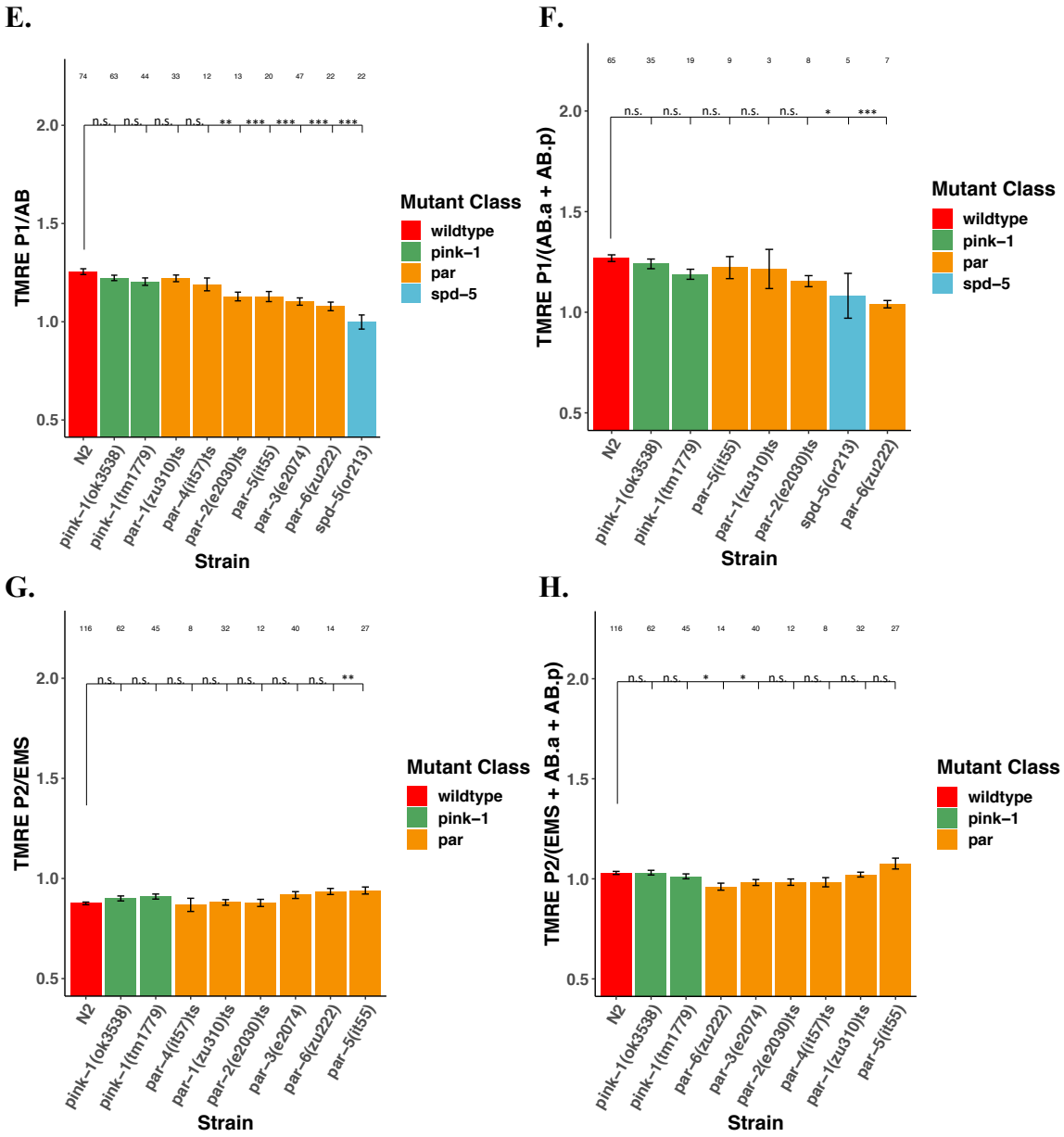

Figure 2. Mitochondrial sorting is altered in *pink-1*, *par*, and *spd-5* mutants. (A) Quantification of TMRE staining of prefertilized oocytes in mutant animals. Oocytes do not have polarity, so the midline was randomly selected. **(B)** Quantification of TMRE staining of early 1-cell embryos in mutant animals. The midline was placed halfway between the posterior and anterior edge of the embryo. **(C** Quantification of TMRE staining of late1-cell embryos in mutant animals. The midline was placed halfway between the posterior and anterior edge of the embryo. **(D)** Quantification of TMRE

staining of early 2-cell embryos in mutant animals. The P1 and AB ROIs were manually drawn around each cell. **(E)** Quantification of TMRE staining of late 2-cell embryos in mutant animals. The P1 and AB ROIs were manually drawn around each cell. **(F)** Quantification of TMRE staining of 3-cell embryos in mutant animals. The P1 ROI was manually drawn around the P1 cell and the AB.a +AB.p ROI was manually drawn around both cells together. **(G)** Quantification of TMRE staining of 4-cell embryos in mutant animals. The P1 and EMS ROIs were manually drawn around each cell. **(H)** Quantification of TMRE staining of 4-cell embryos in mutant animals. The P1 ROI was manually drawn around the P1 cell and the AB.a +AB.p + EMS ROI was manually drawn around all 3 cells together. (*** $p < 0.001$, ** $p < 0.01$, * $p < 0.05$, . $p < 0.1$) For each condition, N is indicated at the top of the graph. Statistical analysis was performed using one-way ANOVA with Dunnett's correction for multiple comparisons.

Figure 3

A.

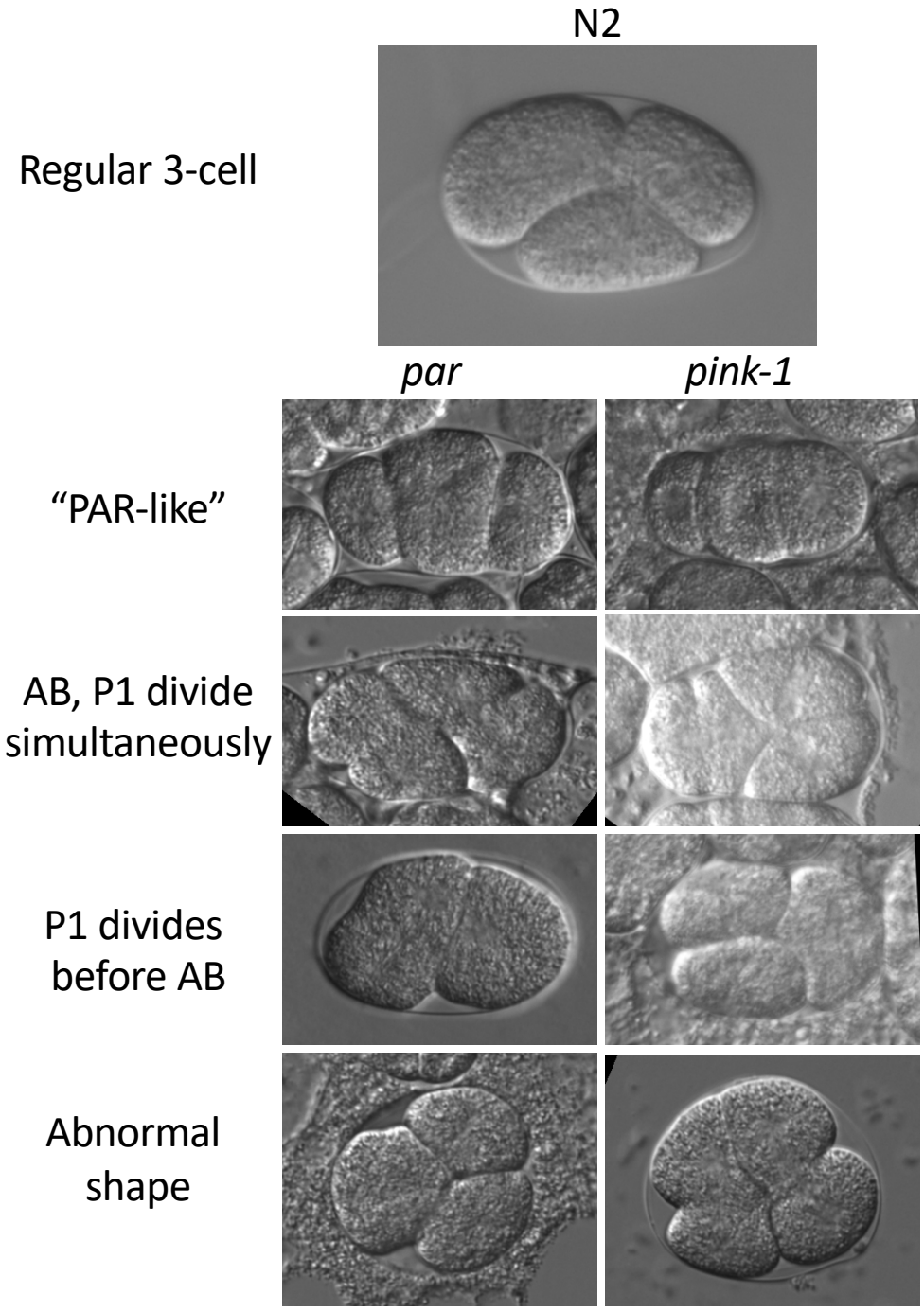
N2
Regular 3-cell
par
pink-1
"PAR-like"
AB, P1 divide simultaneously
P1 divides before AB
Abnormal shape

B.

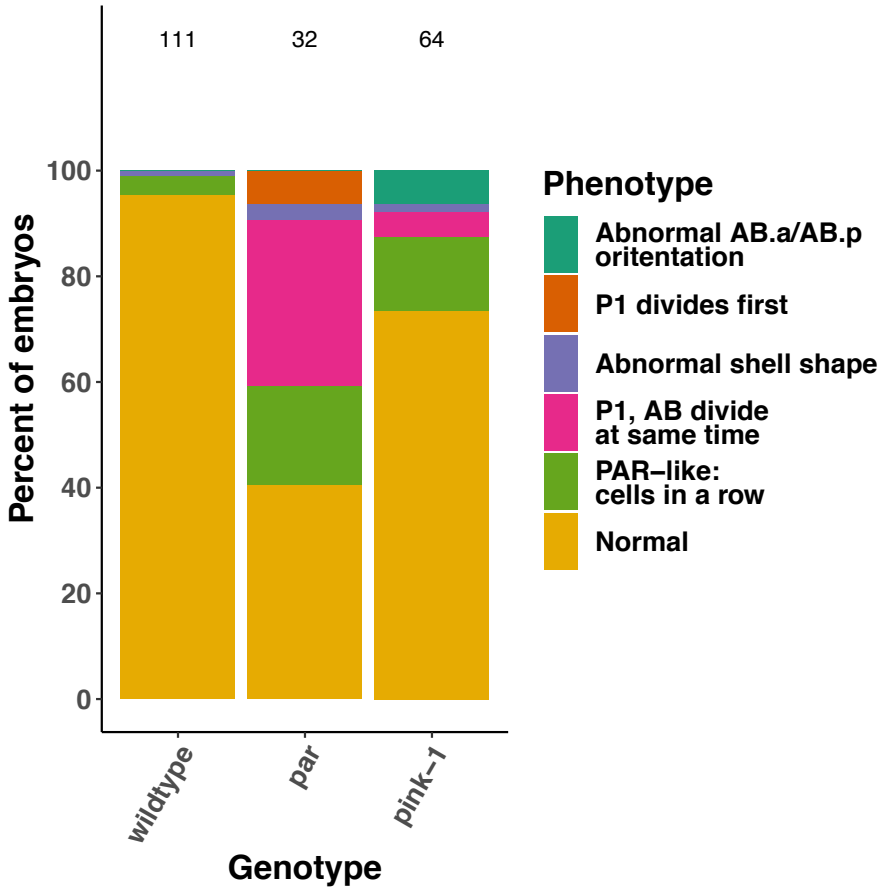

Figure 3. A fraction of *pink-1* mutants have a PAR phenotype. (A) Example images of 3-cell embryos. Normal 3-cell morphology is seen in the laboratory wildtype N2 strain. Phenotypes observed in *par* and *pink-1* mutants are shown. The posterior side of the embryo is on the left in each image. **(B)** Quantification of frequency of PAR-associated phenotypes seen for each class of mutants. For each condition, N is indicated at the top of the graph.

Figure 4

A.

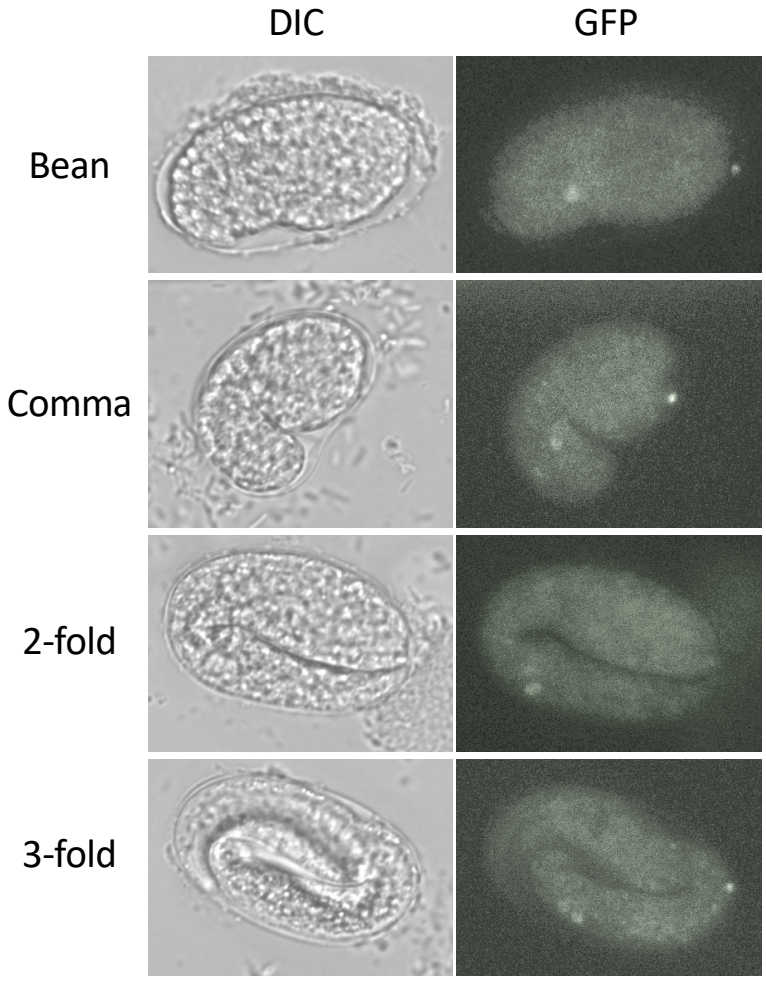
DIC
GFP
Bean
Comma
2-fold
3-fold

B.

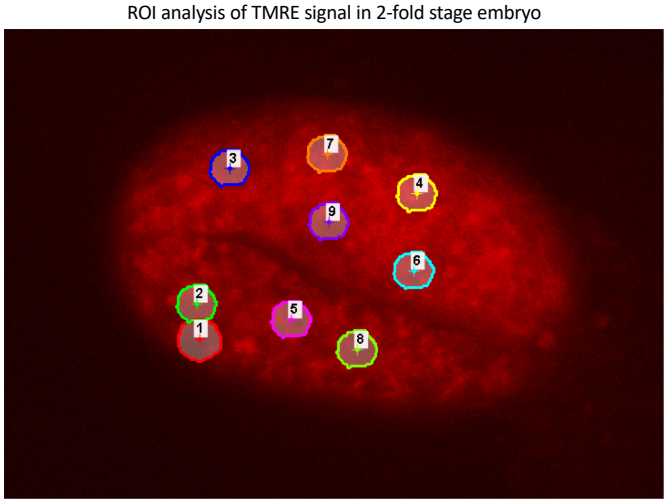
ROI analysis of TMRE signal in 2-fold stage embryo
1
2
3
4
5
6
7
8
9

C.

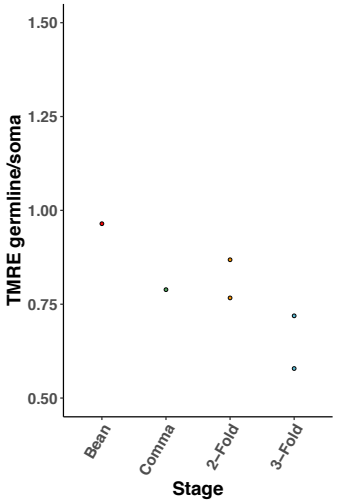
TMRE germline/soma
1.50
1.25
1.00
0.75
0.50
Bean
Comma
2-Fold
3-Fold
Stage

Figure 4. Mitochondrial activity drops for the remainder of embryogenesis. (A) Example images of JH2320 embryos showing the GFP signal indicating the location of the germline progenitor cells Z2 and Z3. Bean = 360 minutes after fertilization, comma = 430 minutes after fertilization, 2-fold = 490 minutes after fertilization, 3-fold = 550 minutes after fertilization. **(B)** ROI analysis of the 2-fold stage embryo shown in figure 2.4A. ROIs #1 and #2 are drawn around the germline progenitor cells Z2 and Z3 based on the GFP signal shown in figure 1.4A. ROIs #3-#9 are of same size as #1 and #2 and are randomly distributed throughout the embryo to get an average of the TMRE signal in the somatic cells. **(C)** Quantification of the ratio of the TMRE signal in Z2 and Z3 compared to the averaged somatic signal shows a progressive decline in mitochondrial activity in the germline progenitor cells throughout embryogenesis.

Figure 5

A.

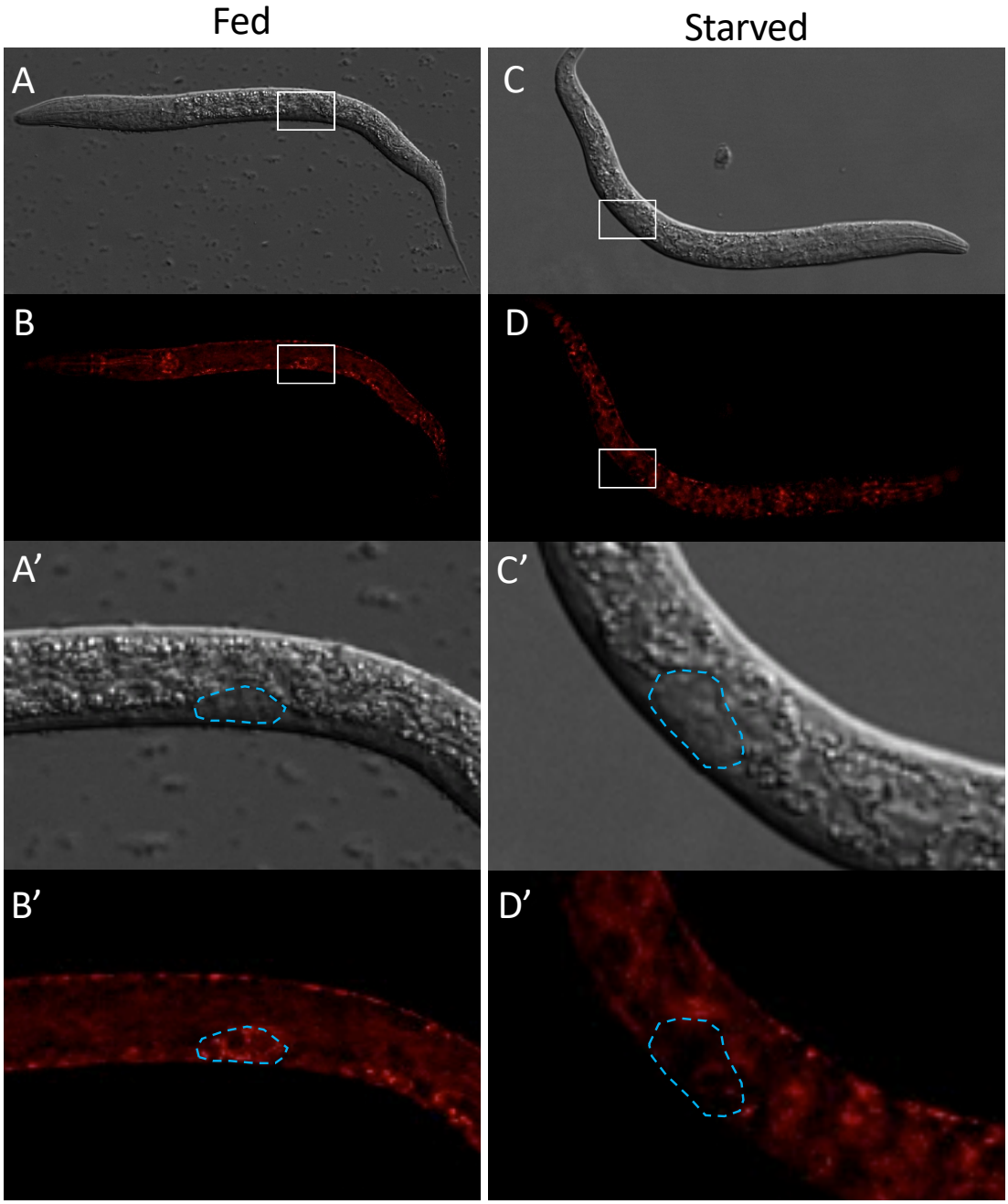

B.

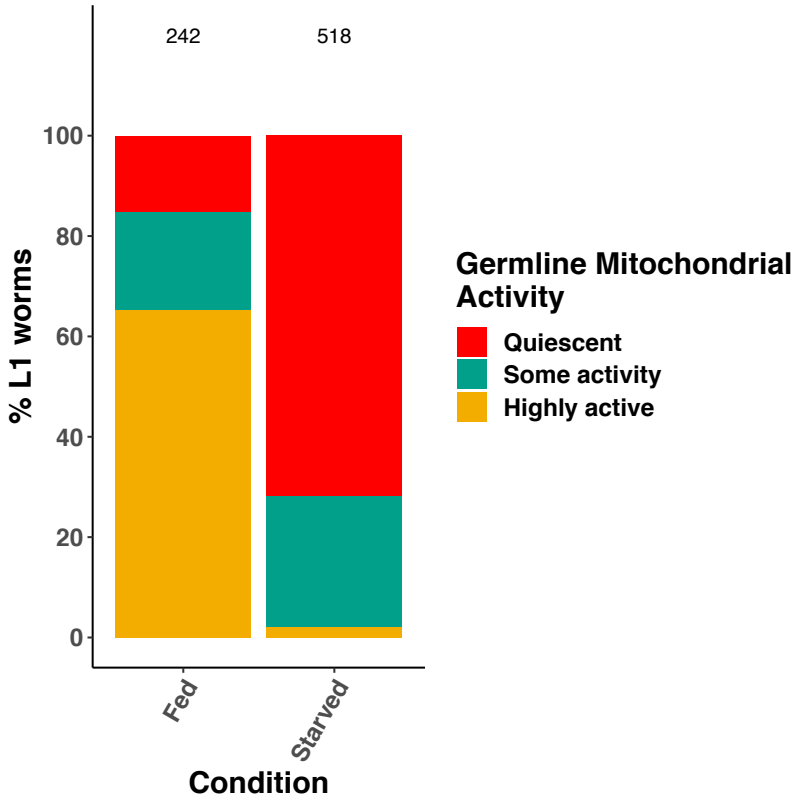
242
518
100
80
60
40
20
0
% L1 worms
Fed
Starved
Condition
Germline Mitochondrial Activity
Quiescent
Some activity
Highly active

C.

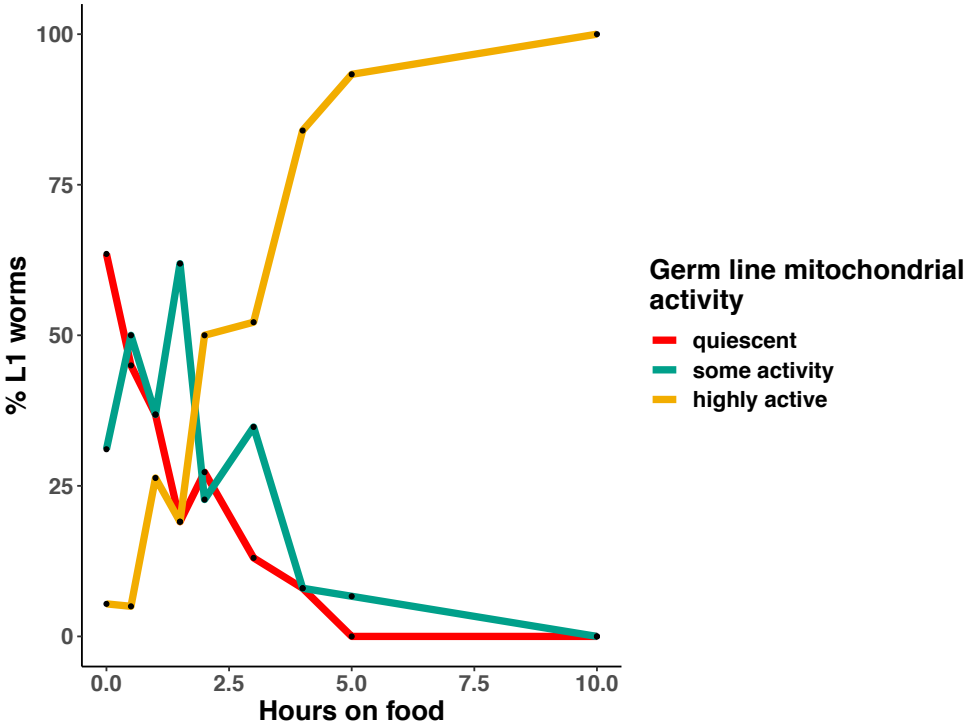
100
75
50
25
0
% L1 worms
0.0
2.5
5.0
7.5
10.0
Hours on food
Germ line mitochondrial activity
quiescent
some activity
highly active

Figure 5. Germline mitochondrial activity is controlled by food availability in L1s. **(A)** Example images of N2 L1 larvae showing the location and morphology of the germline progenitor cells Z2 and Z3 and the corresponding TMRE signal. A', B', C', and D' are zoomed in panels of A, B, C, and respectively. A,C = DIC; B,D = TMRE. **(B)** Quantification of the germline mitochondrial activity in Z2 and Z3 in laboratory wildtype N2 L1s based on the TMRE signal in those cells compared to the signal in the surrounding somatic cells. Quiescent = dimmer TMRE signal intensity in Z2 and Z3, some activity = equal TMRE signal intensity in Z2 and Z3, highly active = brighter TMRE signal intensity in Z2 and Z3. For each condition, N is indicated at the top of the graph. **(C)** Time series of laboratory wildtype N2 L1s showing the increase in germline mitochondrial activity in Z2 and Z3 in response to food based on the TMRE signal in those cells compared to the signal in the surrounding somatic cells. For each condition, N>20.

Table 2

Gene	Allele	Strain	Developmental Impact
-	-	LSJ1	Wildtype; grown in liquid culture
aak-2	*gt33*	TG38	IIS pathway; dauer; lifespan
	ok524	RB754	IIS pathway; dauer; lifespan
	rr48	MR507	IIS pathway; dauer; lifespan
ced-3	*n717*	MT1522	PCD
	n718	MT3002	PCD
clk-1	*qm30*	MQ130	Lifespan; growth rate; metabolism
daf-2	*e1368*	DR1572	IIS pathway; dauer; lifespan
	e1370	CB1370	IIS pathway; dauer; lifespan
	e1391	DR1574	IIS pathway; dauer; lifespan
daf-16	*mu86*	CF1038	IIS pathway; dauer; lifespan
daf-18	*e1375*	CB1375	IIS pathway; dauer; lifespan
	ok480	JR2669	IIS pathway; dauer; lifespan
mir-71	*n4115*	MT12993	Germ line mediated lifespan extension
pink-1	*tm1779*	JR3298	Mitophagy defects, oxidative stress
multiple: *ATP6, CYTB, ND1, ND2*	*uaDf5*	JR3630	mtDNA mutant: general reduced fitness, compromised mitochondrial function

Table 2. Summary of L1 arrest mutants analyzed. Table showing strains tested for L1 germline mitochondrial activity in response to food, outlining the associated pathway each gene is involved in.

Figure 6

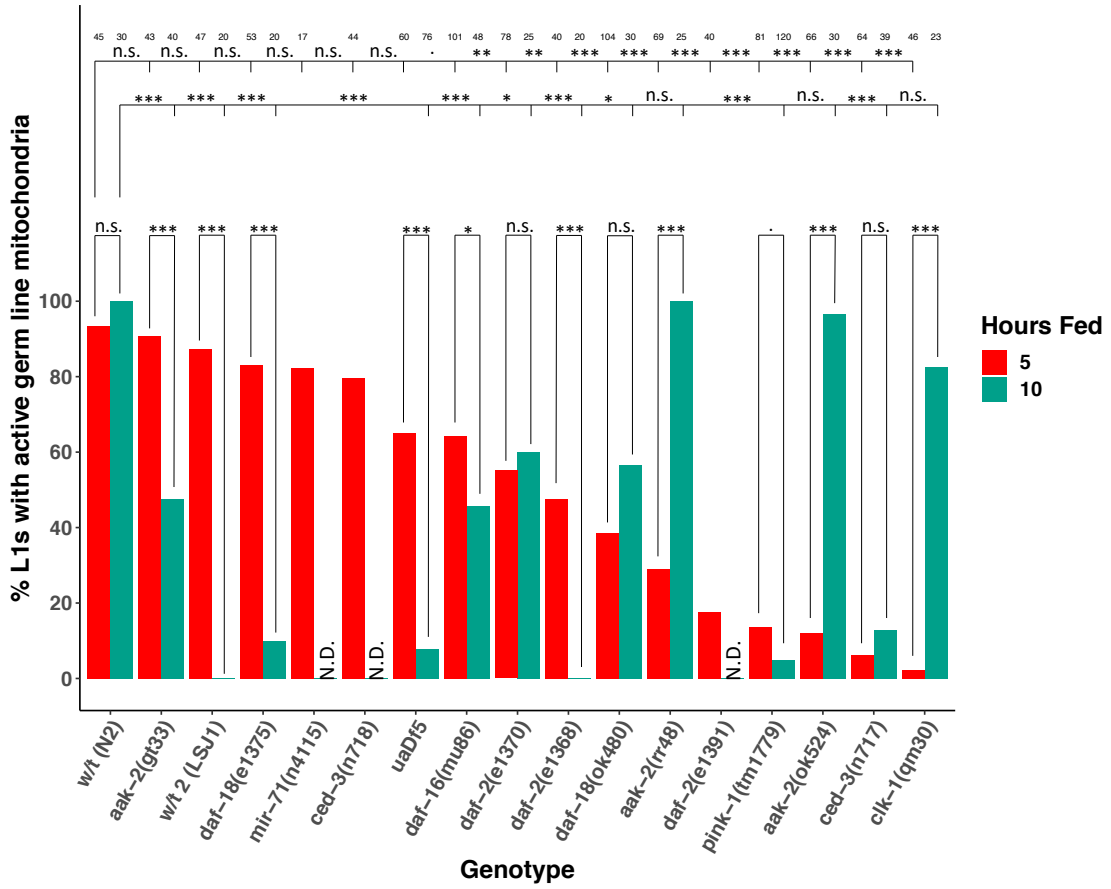

Figure 6. Several mutants have delayed mitochondrial response to food availability. Quantification of the percent of L1 larvae that have highly active germline mitochondria in response to food. Red bars indicate response after 5 hours feeding, green bars indicate response after 10 hours feeding. N.D. = No data collected. For each condition, N is indicated at the top of the graph. Statistical analysis was performed using a pairwise proportion test with Bonferroni correction for multiple comparisons. (*** $p < 0.001$, ** $p < 0.01$, * $p < 0.05$, . $p < 0.1$)

Figure 7

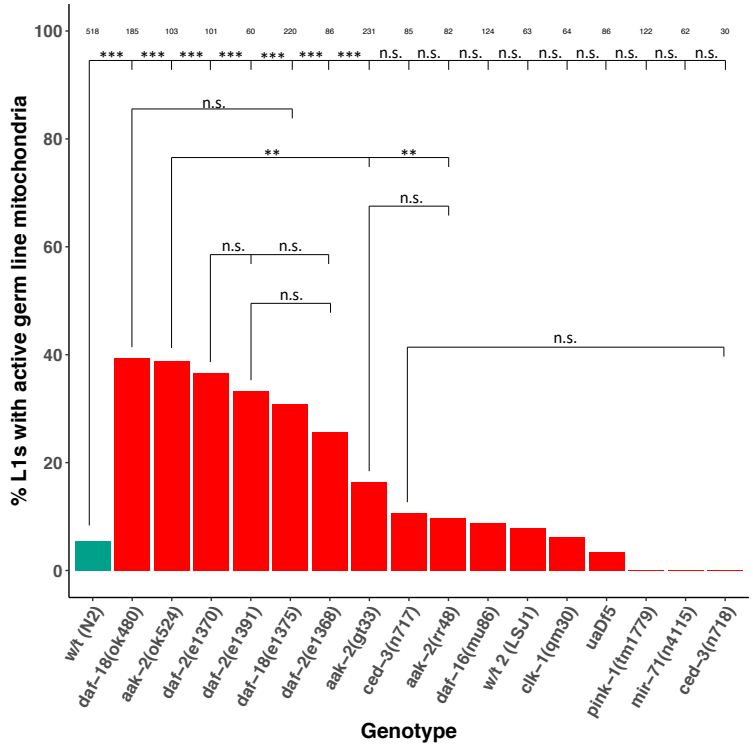

Figure 7. *daf-2, aak-2,* and *daf-18* mutants exhibit improper activation of L1 germline mitochondria. Quantification of the percent of L1 larvae that have highly active germline mitochondria under the starved condition. Red bars indicate mutants, green bar indicates the control laboratory wildtype N2. For each condition, N is indicated at the top of the graph. Statistical analysis was performed using a pairwise proportion test with Bonferroni correction for multiple comparisons. (*** $p < 0.001$, ** $p < 0.01$, * $p < 0.05$, . $p < 0.1$)

Chapter Three

Uncovering the synergistic roles of mitophagy and PCD-related genes in mtDNA quality control using *C. elegans*

SUMMARY

Defective mtDNA accumulates in heteroplasmic animal cells due to replicative advantage. While the removal of such deleterious mitochondrial genomes is critical for cellular function, the precise mechanisms through which these quality control systems act remain poorly understood. The *C. elegans uaDf5* mtDNA mutant is a 3.1kb deletion that is normally stably maintained in a heteroplasmic state with wildtype mtDNA (WT-mtDNA). I found that *uaDf5* mitochondrial levels are elevated in mutants lacking either of two quality control systems: 1) mitophagy (*pink-1(w46)*), or 2) germline programmed cell death (PCD; *ced-13(tm536)*). Unexpectedly, I found that when both *pink-1* and *ced-13* functions are eliminated, the opposite occurs: *uaDf5* mtDNA is rapidly and completely removed, effectively curing the animal of mitochondrial disease. Even more startling, descendants of crosses between *pink-1(w46)* or *ced-13(tm536)* single mutant mothers with males lacking both PINK-1 and CED-13 also show rapid removal of *uaDf5* and this effect occurs irrespective of the differing descendant genotypes. These findings lead us to hypothesize that an initiating genetic event (IGE) from these crosses triggers a potent transgenerational epigenetic process that discriminates and effectively removes defective mtDNA.

INTRODUCTION

Mitochondrial disease and mtDNA purifying selection

Mitochondrial diseases are a group of conditions that affect mitochondrial function and affect as many as 1 in 4,300 people [55,59–64]. They can be due to mutations in either the mtDNA or the nDNA. Generally, these diseases present as dysfunction in the tissues or organs that have the largest energy demands, most

commonly in the muscle and nervous system. Pathogenic mtDNA mutations were first discovered in human patients in the late 1980s [65,66] and since then the body of literature identifying mtDNA-related disease has significantly grown [55]. Mitochondrial diseases also include those disorders in which there is a defect in mitochondrial dynamics, quality control, or communication between the mitochondria and ER [61,62]. Unfortunately, there are few effective treatments for mitochondrial diseases.

Interestingly, mtDNA has a high mutation rate ([33,48,49], and see Chapter 1) and yet, most normal cells can clear mitochondria carrying the mutations in a process called purifying selection. Learning more about the mechanisms that cells normally employ to remove deleterious mtDNA could provide insight into new therapies for mitochondrial diseases. There is evidence for some processes that regulate mtDNA such as mitochondrial fission/fusion dynamics and mitophagy [67–73], the mitochondrial unfolded protein response (UPR^{MT}; [74–80]), and most recently the insulin signaling pathway (IIS; [81,82]). However, all of these processes only seem to be part of the story in that each has only an intermediate effect on mtDNA mutation levels. *C. elegans,* a free-living nematode, is an extremely amenable model for the discovery of new mechanisms through which purifying selection, the process in which defective mtDNA is removed from the germline, operates. In addition to the ease with which one may study genetic questions with this organism, there are also various elements of *C. elegans* development, which show conservation across animals, that are attractive areas to examine for the potential of mitochondrial maintenance. These elements include autophagic removal of dysfunctional mitochondria (mitophagy; [73,115]), endodermal cannibalism [87], and programmed cell death (PCD) in mature female germline [89,170,179].

C. elegans mtDNA and the mtDNA deletion "*uaDf5*"

A somewhat surprising and fascinating observation is that there are many similarities between human and *C. elegans* mtDNA (Fig. 1.1). Human mtDNA has only one extra gene compared to the *C. elegans* counterpart: ATP8, a subunit of complex 5 [3]. There is a high level of homology for all of the genes between species, and the overall size of the mitochondrial genome is roughly equal, with the size of the *C. elegans* mtDNA being 13,794bp (compared to 16,569 bp in humans) [2]. Thus, studying the experimentally tractable nematode is likely to provide insight into human mitochondrial function. A *C. elegans* strain that harbors a 3.1kb mtDNA deletion "*uaDf5*" is a useful tool for studying the mechanisms governing mtDNA quality control. The mutation is maintained indefinitely in a state of stable heteroplasmy, meaning that it is never lost from the mtDNA population even after over 100 generations of propagation [201].

Mechanisms of quality control: mitochondrial dynamics and mitophagy

One of the key processes of mtDNA purifying selection is mitochondrial dynamics. Mitochondria are incredibly dynamic organelles that make up a network within the cell and this filamentous network is constantly undergoing division using a fission process (usually a small portion breaking off the main mitochondrion) and fusion (in which the smaller portions refuse with the main mitochondrial network) [68,70,108]. The main players involved in the fission process are the dynamin 1 like (DNML1) homolog DRP-1 [109] and the fission mitochondrial 1 (FIS1) homolog FIS-2 [110,111]. The main actors involved in fusion are the OPA1 mitochondrial dynamin like GTPase (MGM1/OPA1) homolog EAT-3 [112], and the mitofusin (MFN1/2) homolog FZO-1 [113,114] (Fig. 1.3A).

If a disruption in either fusion or fission occurs, then there is an immediate impairment of the cell's ability to remove mutated mtDNA [69]. It is believed that mitochondrial quality control is tightly linked to fission/fusion due to the necessity of separating the healthy genomes from the mutated genomes prior to mutant mtDNA removal. In order to selectively remove only mutated mtDNA, it makes sense that the mitochondria must fragment so that a mitochondrion with a single genome inside it is the result. Thus, the role of fission is clear.

Once divided, the cell may target a dysfunctional mitochondrion for degradation via a specialized form of autophagy that is specific to mitochondria, known as mitophagy [73,115]. Mitophagy, which works hand in hand with fission and fusion, has been shown to be an important process for selection against deleterious mtDNA [116]. In healthy mitochondria, the PTEN induced kinase 1 (PINK1) homolog, PINK-1, a serine threonine kinase, is imported into the mitochondria and is then cleaved from the mitochondrial surface. However, if the mitochondrion has diminished membrane potential, which is thought to be a general indicator of reduced function, PINK-1 is only imported through the outer membrane and accumulates on the surface. This accumulation of PINK-1 signals to several downstream players, most notably the parkin RBR E3 ubiquitin protein ligase (PARKIN) homolog PDR-1, which is then recruited to the mitochondrion to ubiquitinate proteins on its surface, tagging the organelle for degradation by the liposome (Fig. 1.3B) [71,72,117–122]. In this way, the cell can maintain a population of healthy, functional mitochondria.

Programmed cell death in the mature female germline

Programmed cell death (PCD), also known as cell suicide or apoptosis, is a process in which a cell undergoes a self-destruct program [166,167]. The conditions that influence a cell's decision to do this include excess stress [167,168], immunity [169], and developmentally programmed death of extra cells [91,170]. The process of developmental PCD has been extensively studied in *C. elegans*, where 131 somatic cells are programmed to die, and in fact, it was the work done with *C. elegans* that greatly moved the understanding of apoptosis to where it is today [91]. The core machinery is highly conserved across metazoans [170], which makes it an attractive universal mechanism for maintaining the health of mtDNA.

In *C. elegans*, the genes involved in the canonical cell death pathway are *egl-1*, *ced-9*, *ced-4*, and *ced-3* (Fig.6A) [91,92]. EGL-1, which is homologous to BH3-only (Bcl-1 homology 3) domain proteins, is the upstream activator which acts on the CED-9:CED-4 complex that is present on the mitochondrial surface [171]. When EGL-1/BH3 is activated, it binds to CED-9/BCL2, thereby releasing CED-4/APAF1 to the cytoplasm [172]. Once CED-4/APAF1 is in the cytoplasm, it is free to act on the main executioner caspase CED-3, switching it from the inactive procaspase form (pro-CED-3) to the activated caspase form [173]. Once activated, CED-3 starts a cascade of cellular events which irreversibly result in death of the cell [91,174]. There are other caspase-like genes, including *csp-1*, *csp-2*, and *csp-3*, which seem to play somewhat minor roles in the execution of PCD [91,175]. It's possible that CSP-2 and CSP-3 work together to inhibit improper activation of the cell death pathway by keeping CED-3 from undergoing autocleavage [176,177]. CSP-1, on the other hand, has more direct caspase activity, and seems to act in parallel with CED-3, acting upon different substrates. Importantly, CSP-1

appears to act independently of the canonical pathway players CED-9/BCL2 and CED-4/APAF1 [91,178]. The processes that occur downstream of caspase execution include nuclear DNA fragmentation, elimination of mitochondria, the inhibition of survival signals, and phosphatidylserine (PS) externalization on the outer cell membrane as an "eat me" signal [21,89,91,92,167,170,174,179]. The PS exposure on the cell surface signals to neighboring cells activates an engulfment program which is controlled by multiple redundant pathways, all of which converge on CED-10/RAC [180–182].

In addition to developmental somatic PCD, there is PCD that occurs in the mature female germline, which kills off as many as >95% of the potential oocytes [89,170,179,183]. Germline PCD is of two types: physiological (thought to be stochastic, perhaps as a way of killing off nurse cells for the developing oocytes), and DNA damage-induced [184]. Physiological germline PCD shares many of the same regulators as somatic PCD, except for the lack of requirement on *egl-1* [184,185]. DNA damage-induced PCD requires all of the core PCD machinery and is regulated by CEP-1/p53 in response to DNA damage [186]. In the event of UV-induced DNA image, CEP-1/p53 upregulates EGL-1 and CED-13 (another BH3-only protein), which both then signal the rest of the downstream core pathway [19,89,179,184–187]. Here we investigate the role of PCD in mtDNA quality control in the germline and describe a novel phenomenon whereby an initiating genetic event or "IGE" sets up a condition that results in an incredibly efficient mechanism for removal of deleterious mtDNA.

RESULTS

uaDf5 affects several fitness parameters

Surprisingly, animals containing *uaDf5* appear to be quite healthy at the superficial level, despite its deleterious nature. I wanted to see if *uaDf5* results in any negative consequences on organismal fitness, suggesting its analysis would be useful as a model for mitochondrial disease. To do this I measured brood size, embryonic lethality, unfertilized oocyte production, developmental rate, and lifespan in *uaDf5* and wildtype worms. *uaDf5* animals displayed deficiencies in generation of viable progeny, as seen by measuring brood size (wildtype 304 ± 4.8; *uaDf5* 202 ± 8.6 embryos laid) (Fig. 3.1A), embryonic lethality (wildtype 1.94 ± 0.56%; *uaDf5* 4.18 ± 0.67%) (Fig. 3.1B), and unfertilized oocytes laid (wildtype 30 ± 1.1%; *uaDf5* 20 ± 1.6%) (Fig. 3.1C). *uaDf5* also displayed deficiencies in developmental rate, measured in both the number of hours to reach gravidity (wildtype 63 ± 0.8; *uaDf5* 76 ± 1.4 hours) (Fig. 3.1D) and in the average stage of development after 60 hours of feeding (wildtype: adult; *uaDf5:* mid-L4) (Fig. 3.1E). Lifespan, however, was unaffected (wildtype 14 ± 0.4; *uaDf5* 15 ± 0.5 days) (Fig. 3.1F). This may be only the case in a lab environment, and it would curious to see the effect on lifespan in the wild. Given the significant decline in the majority of fitness parameters tested, I concluded that *uaDf5* is a useful tool for studying mitochondrial disease and mtDNA quality control.

Characterization of the mtDNA deletion "*uaDf5*"

uaDf5 is a 3.1kb deletion that knocks out the function of 4 protein-coding genes and 7 tRNAs (Fig. 3.2A,B) [201]. Given its presumably highly deleterious nature, how is it stably maintained? I first tested the hypothesis that *uaDf5* stability is due to a

complementing allele or secondary mutation. To address this, I did Illumina high-throughput sequencing of mtDNA isolated from the *uaDf5* strain to see if I could detect a secondary mtDNA allele. Instead of finding a secondary allele, I found a secondary mutation, *w47*, which is actually linked to the *uaDf5* deletion. This allele is a single base pair deletion in the *nduo-4* gene which results in a frameshift that causes premature termination of the resulting ND4 protein at position 88 of the 409 amino-acid long wildtype protein (Fig. 3.2C). ND4 is a homolog of the core MT-ND4 transmembrane subunit of complex 1 of the MRC, and transports protons across the inner mitochondrial membrane upon oxidation of NADH [1–3,39,202]. Soon after this finding, papers came out reporting that the UPR^{MT} protects *uaDf5* from removal, in that a loss-of-function mutation in the UPR^{MT} results in a lowered fractional abundance of *uaDf5* [78,80]. Given the nature of the truncated ND4 protein, I propose that accumulation of this truncated protein may be one of the factors that results in this protection of *uaDf5* by the UPR^{MT}.

ddPCR as a tool to study genes involved in mtDNA quality control

If mtDNA quality control pathways are compromised, the level of deleterious mtDNA (such as *uaDf5*) are predicted to increase. Conversely, if the mtDNA quality control machinery is more efficient, deleterious mtDNA levels are predicted to decrease. In order to measure the level of *uaDf5,* I employed droplet digital PCR (ddPCR), a highly quantitative method analogous to qPCR [78,203,204]. This highly sensitive technique makes it possible to measure DNA copy number with extreme accuracy. I first measured the fractional abundance of *uaDf5* (% *uaDf5*) in a wildtype nuclear background in three lines that were grown separately for over five generations to see what kind of natural variation occurs under normal conditions. I measured the fractional abundance of *uaDf5*

in pooled populations of 200 worms in their fourth day of adulthood. I saw very little variation in the three independent lines (trial 1 66.66%, 68.6%, and 73.71%). I repeated this analysis three more times over the span of two years and saw no statistical change in the steady state fractional abundance of *uaDf5* (trial 2 72.94%, 74.58%, and 79.44%; trial 3 69.88%, 73.43%, and 74.36%; and trial 4 75.89%, 76.94%, and 77.90%) displaying the marked stability of *uaDf5* in a wildtype background (Fig. 3.3A). To determine if the fractional abundance of *uaDf5* is changed at a measurable level when mtDNA quality control machinery is modulated, I looked at the fractional abundance of *uaDf5* in mutants of two known pathways to act on mtDNA: the UPR^{MT} and mitophagy (Fig. 1.3B, 1.4A).

Mitophagy is the process by which defective mitochondria (and their associated mtDNA) are eliminated from the cell [71,73,115,120]. As expected, I observed an increase in the fractional abundance of *uaDf5*, in mitophagy mutants (*pink-1* and *pdr-1*). Because the only *pink-1* mutant strains available are alleles that retain part of the *pink-1* gene, we used CRISPR to generate a *pink-1(w46)* null mutant that knocks out the entirety of the *pink-1* locus. In worms in their fourth day of adulthood, both *pink-1(tm1779)* (84.29 ± 0.1%) *and pink-1(w46)* (83.94 ± 0.7%) have a significantly increased fractional abundance of *uaDf5* compared to a nuclear wildtype background (81.66 ± 0.42%) and the *pink-1(w46);pdr-1(gk448)* double mutant increases the fractional abundance of *uaDf5* to an even higher level (85.82 ± 0.29%). *pdr-1(gk448)* is the only allele available for *pdr-1* and does not have an increased fractional abundance of *uaDf5* (82.11 ± 0.7%) (Fig. 3.3B). This may be due to the nature of the allele not making it a complete null, or it may be due to secondary effects of alternate roles of *pdr-1*.

The UPR^{MT} has been shown to protect *uaDf5* [78,80]. The *atfs-1* gene, the main regulator of the UPR^{MT}, has both loss-of-function (lof) and gain-of-function (gof) alleles,

so I tested both [78,80,205]. As expected, the lof allele *atfs-1(tm4525)* results in a decreased fractional abundance of *uaDf5* (76.91 ± 0.45%) and the gof allele *atfs-1(et15)* has an increased fractional abundance of *uaDf5* (84.43 ± 0.38%) (Fig. 3.3B). Given that *uaDf5* levels were observed to change as expected when purifying mechanisms were affected, I conclude that ddPCR is a viable technique for quantitative analysis of mtDNA quality control.

The role of germline PCD in mtDNA quality control

I next investigated whether other pathways might be involved in removal of mtDNA. In *C. elegans*, germline PCD removes as many as 95% of potential oocytes [89,179,183,184] and it is unknown if there is a selection process, mitochondrial or otherwise, for which potential oocytes undergo PCD. Currently the understanding is that the process is entirely stochastic. I hypothesize that, instead of random selection, the oocytes that undergo PCD are associated with higher levels of defective mtDNA. To test this hypothesis, I generated a set of PCD mutant strains that also contain *uaDf5* mtDNA (for a list of mutants analyzed please refer to Table 3.1 and Fig. 1.6A 3.4A). Most of the mutants affect both developmental and germline PCD (*ced-3, ced-4, csp-1*, and the engulfment genes), while some only act in germline-specific PCD (*ced-13* and *cep-1*) [91,92,170,184]. Despite the importance of PCD in development, none of the PCD mutants result in any severe fitness deficits.

To test for the role of germline-specific PCD I analyzed *ced-13* mutants. CED-13/BH3 is a germline-specific activator of PCD [91,185,187]. Both *ced-13* alleles have a significantly higher fractional abundance of *uaDf5* (*sv32*: 80.66 ± 0.7%; *tm536*: 83.5 ± 0.39%) (Fig. 3.4A), supporting the idea that germline PCD removes *uaDf5*. CED-9/BCL2

is an inhibitor of PCD that acts upstream of CED-4/APAF1 [172]. *ced-9(n1950)* is a gof allele which results in inhibition of PCD, although this allele does not have an effect in the germline [89,184]. I observed no changes to the fractional abundance of *uaDf5* with this allele (68.89 ± 0.1%) which supports the hypothesis that PCD is acting on *uaDf5* solely in the germline. CSP-2 has homology to the caspases but it has shown to play no significant role in PCD [175,177] and as expected, no change in the fractional abundance of *uaDf5* was observed (73.97 ± 1.61%) (Fig. 3.4B).

CED-3 is the executioner caspase in the canonical PCD pathway [91,174,184]. Our analysis of four strong *ced-3* mutants [206] gave varying results, with two of the four showing an increased fractional abundance of *uaDf5* in worms in their first day of adulthood (*n717:* 77.76 ± 0.75% and *n1286:* 82.26 ± 0.15%) compared to a wildtype nuclear background (74.73 ± 1.18%), one allele showing no significant change (*n2454:* 74.01 ± 0.58%), and one allele showing a decrease (*n718*: 64.18 ± 0.21%). Analysis of cell corpses in embryos of these mutants reveals that developmental PCD is not occurring, but the inhibition of germline PCD has yet to be assayed. CSP-1 is another caspase which acts in a non-canonical role of PCD [174,175,178] and in combination with *ced-3(n717)* I see an additive effect with a greatly increased fractional abundance of *uaDf5* (82.38 ± 0.7%) (Fig. 3.4C). Analysis of the nature of the alleles does not give any immediate clues as to why I observe different phenotypes, but our results with the *ced-3* alleles *n717* and *n1286* suggest that PCD may be playing a role in mtDNA quality control.

CED-4/APAF1 is the upstream activator of CED-3 in the canonical PCD pathway [172,173] and as such I expected to see an increased fractional abundance of *uaDf5* in

ced-4 mutants. However, I observed no effect in both alleles tested (*n1162*: 74.94 ± 1.51%; *n1894*: 77.05 ± 0.48%) (Fig. 3.4D). This either suggests that PCD is not acting on mtDNA, or it may be reflective of secondary effects from alternative roles that *ced-4* has in development [207,208]. Additionally, analysis of embryonic cell corpses of these mutants reveals that developmental PCD is not occurring, but the inhibition of germline PCD has yet to be assayed.

Cells that undergo PCD must be cleared away by the surrounding cells in a process of engulfment and degradation which is carried out through a set of redundant pathways that converge on CED-10 [92,180–182]. Inhibition of the engulfment pathway actually results in inhibition of PCD, likely through a complex feedback mechanism. Consistent with the observation that PCD is regulating levels of *uaDf5*, analysis of engulfment mutants revealed an increased fractional abundance of *uaDf5* (*ced-10(n3246)* 82.72 ± 0.15%; *ced-1(e1735)* 80.41 ± 0.37%; *ced-2(e1752)* 81.79 ± 0.73%; *ced-1(e1735);ced-2(e1752)* 83.8 ± 0.59%) (Fig. 3.4E).

To confirm that the steady state level of the fractional abundance of *uaDf5* that I observe is indicative of the removal capacity of the cellular machinery, I did a multi-generational experiment in which I tried to selectively remove *uaDf5*. To do this, I measured the fractional abundance of *uaDf5* in ~15 individual worms and then measured ~15 individual progeny from the worm that had the lowest fractional abundance of *uaDf5*. This was repeated over the course of at least 5 generations to determine the lower limit of the fractional abundance of *uaDf5*. Those strains that had increased steady state levels of *uaDf5* (*ced-3(n717)* and *ced-10(n1993)*) were resistant to the selective removal of *uaDf5* (within 8 generations *ced-3(n717)* dropped from 75.09% to 53.28% and *ced-10(n1993)* dropped from 78.24% to 70.38%, compared to wildtype which dropped from

74.61% to 49.85%). Those lines that had lower steady state levels of *uaDf5* (*ced-3(n2454*) and *ced-4(n1162)*) were amenable to *uaDf5* reduction each generation (*ced-3(n2454)* dropped from 74.75% to 15.65% in 8 generations and *ced-4(n1162)* dropped from 72.65% to 32.88% in only 5 generations) (Fig. 3.4G). This supports the original findings in figures 3.4B-G that higher steady state levels of the fractional abundance of *uaDf5* are evidence of a decreased capacity for removal of defective mtDNA.

CEP-1/p53 is an activator of germline PCD in response to nuclear DNA damage [19,186,187]. To test if CEP-1/p53 activates PCD, in not just the case of nuclear DNA damage but also in the event of an excessive fractional abundance of mutant mtDNA, I analyzed *cep-1* mutants. Surprisingly, I found that *cep-1(gk138)* has a greatly reduced fractional abundance of *uaDf5* (50.93 ± 1.76%) (Fig. 3.4F). In addition to its role in germline PCD, CEP-1 has actually been shown to act as an inhibitor of mitophagy [209]. It is interesting to note its dual role and how this may result in differential regulation of mtDNA quality control. This led us to question the interplay between the mitophagy and PCD pathways and to further investigate whether CEP-1 is a common element to both pathways in *C. elegans.*

Combinatorial knock out of *ced-13* with certain genes results in rapid removal of *uaDf5*, with no evidence of compromised organismal fitness

The question of the dual role of CEP-1 in mitophagy and germline PCD led us to generate a set of double mutants comprised of components of both pathways (Fig. 3.5A). If germline PCD is acting on *uaDf5*, I would expect to see double mutants composed of genes from the PCD pathway to have the same fractional abundance of *uaDf5* as the single mutants. The same goes for double mutants of genes involved in mitophagy. If

there is crosstalk between the PCD and mitophagy pathways, I expect to see evidence of epistasis in double mutants composed of genes from both pathways. The *cep-1(gk138);pink-1(w46)* double has a fractional abundance of *uaDf5* similar to the *pink-1(w46)* single mutant *(cep-1(gk138);pink-1(w46):* 82.41 ± 0.29%; *pink-1(w46):* 79.42 ± 1.76%; *cep-1(gk138):* 50.93 ± 1.76%), suggesting that CEP-1 is largely acting on *uaDf5* through its role in mitophagy rather than PCD since PINK-1 is downstream of CEP-1. This same effect was also seen in *cep-1(gk138);pdr-1(gk448)* double mutants (*cep-1(gk138);pdr-1(gk448)*: 73.34 ± 1.14%; *pdr-1(gk448):* 64.22 ± 2.23%). The *cep-1(gk138);ced-3(n1286)* double mutant has levels similar to the *ced-3(n1286)* single mutant (*cep-1(gk138);ced-3(n1286):* 82.36 ± 0.28%; *ced-3(n1286)*: 82.26 ± 0.15%), indicating the possibility that improper activation of mitophagy only results in efficient removal of *uaDf5* if PCD is functional. This suggests possible crosstalk between the activities of both pathways. The *ced-4(n1162);ced-13(tm536)* double mutant more closely resembles the downstream *ced-4(n1162)* single mutant rather than the *ced-13(tm536)* single mutant (*ced-4(n1162);ced-13(tm536)*: 77.62 ± 1.72%; *ced-13(tm536):* 83.5 ± 0.39%; *ced-4(n1162):* 74.94 ± 1.51%).

There were two double mutants analyzed which gave unexpected results, both containing *ced-13(tm536)*. Given the fact that both CED-13 and CED-3 are in the PCD pathway and loss of function in either results in an increased fractional abundance of *uaDf5*, the double mutant was expected to show a similarly high fractional abundance of *uaDf5*. However, I saw a greatly reduced fractional abundance of *uaDf5* in the double mutant (8.62 ± 2.79%) suggesting that one or both genes are acting on mtDNA through novel pathways. Similarly, *ced-13(tm536)* and *pink-1(w46)* single mutants both have a

high fractional abundance of *uaDf5,* but the double mutant exhibits complete removal of *uaDf5* (0 ± 0%). This suggests one of two events; that knocking out both PCD and mitophagy results in a cellular environment which is more efficient at mtDNA quality control, or that one or both of these genes is acting on mtDNA through some unidentified pathway(s) which have yet to be discovered.

We hypothesized that the removal phenotype was due to culling of *uaDf5*-containing worms at the organismal level. We proposed that these genetic backgrounds set up an environment in the cell that is particularly intolerant of mtDNA mutations, resulting in a highly reduced level of production of viable progeny, such that only those worms that contain the lowest fractional abundance of *uaDf5* are the ones that survive. To address this question, I performed sets of genetic crosses which would generate *ced-3(n1286);ced-13(tm536);uaDf5* and *pink-1(w46);ced-13(tm536);uaDf5* double mutants and scored the F2 hermaphrodites for brood size (Fig. 3.5B) and embryonic lethality (Fig. 3.5C). For generating *ced-3(n1286);ced-13(tm536);uaDf5* lines I crossed *ced-3(n1286);ced-13(tm536);uaDf5* males into either *ced-13(tm536);uaDf5* or *ced-3(n1286);uaDf5* hermaphrodites. I found that brood size was decreased following these crosses (*ced-13(tm536);uaDf5* P0 hermaphrodites: 141 ± 14; *ced-3(n1286);uaDf5* P0 hermaphrodites: 98 ± 11; *uaDf5* control 201 ± 9). I also saw that embryonic lethality was increased following these crosses (*ced-13(tm536);uaDf5* P0 hermaphrodites: 6.82 ± 1.59%; *ced-3(n1286);uaDf5* P0 hermaphrodites: 10.45 ± 2.05%; *uaDf5* control 4.18 ± 0.67%). However, these deficits in brood size and embryonic lethality were not high enough to suggest that the sole mechanism of *uaDf5* reduction is due to worms being culled at the organismal level due to an intolerance of *uaDf5*, which I propose would have had to be compromised at much higher levels.

For generating *pink-1(w46);ced-13(tm536);uaDf5* lines I crossed *pink-1(w46);ced-13(tm536);uaDf5* males into either *ced-13(tm536);uaDf5* or *pink-1(w46);uaDf5* hermaphrodites. Following these crosses, I actually found a slight increase in brood size (*ced-13(tm536);uaDf5* P0 hermaphrodites: 238 ± 17; *pink-1(w46);uaDf5* P0 hermaphrodites: 241 ± 18) and a minimal to no increase in embryonic lethality (*ced-13(tm536);uaDf5* P0 hermaphrodites: 5.63 ± 1.1%; *pink-1(w46);uaDf5* P0 hermaphrodites: 4.59 ± 1.14%), indicating that culling at the organismal level is not a factor contributing to the removal phenotype in the *pink-1(w46);ced-13(tm536);uaDf5* lines.

Despite low steady state fractional abundance of *uaDf5* in stable *ced-3(n1286);ced-13(tm536);uaDf5* lines, *uaDf5* removal is not observed in the 4 generations following the generation of the double mutant

How is it that knocking out two genes in the PCD pathway results in an increased capacity of *uaDf5* removal? To understand the mechanism through which *uaDf5* removal occurs, I carried out a generational analysis of the sets of crosses which would result in the *ced-3(n1286);ced-13(tm536);uaDf5* double mutant and measured the fractional abundance of *uaDf5* in the lines resulting from those crosses for four generations to see how quickly the removal of *uaDf5* occurs (Fig. 3.6A,B). To make these lines, I performed the two crosses mentioned previously: *ced-3(n1286);ced-13(tm536);uaDf5* males mated to *ced-13(tm536);uaDf5* hermaphrodites, and *ced-3(n1286);ced-13(tm536);uaDf5* males mated to *ced-3(n1286);uaDf5* hermaphrodites, both of which result in F2 descendants with the *ced-3(n1286);ced-13(tm536);uaDf5* genotype. I measured the fractional abundance of *uaDf5* from the P0 to the F4 generation in 10 lines

resulting from the *ced-3(n1286);ced-13(tm536);uaDf5* males mated to *ced-3(n1286);uaDf5* hermaphrodite cross (Fig. 3.6C,D), and in 7 lines resulting from the *ced-3(n1286);ced-13(tm536);uaDf5* males mated to *ced-13(tm536);uaDf5* hermaphrodite cross (Fig. 3.6E,F). I also did genotyping of the F2 generation (capturing homozygotic segregants) to see if only the *ced-3(n1286);ced-13(tm536);uaDf5* double mutants reconstituted from the cross exhibit the removal phenotype and that the other genotypes do not. Surprisingly, I found that none of the lines generated from either of the two crosses had greatly decreased fractional abundance of *uaDf5* by the F4 generation, although the fractional abundance of *uaDf5* had dropped slightly (the largest drop was by 10.14%; from 80% down to 69.86%).

In the steady state population analysis, the worms had gone through a step of starvation immediately following the F2 generation, so I wondered if starvation was a necessary step for the removal phenotype we observed. I starved the same lines that were used for the generational analysis and measured the fractional abundance of *uaDf5* in the three generations following starvation and found that there was no measurable drop in the fractional abundance of *uaDf5* (data not shown). Perhaps the *ced-3(n1286);ced-13(tm536);uaDf5* double mutant needs more generations before *uaDf5* removal occurs, or perhaps the male used for the cross needs to have the *ced-13(tm536);uaDf5* genotype (which was used for generation of the double mutant lines analyzed for steady state population levels) instead of *ced-3(n1286);ced-13(tm536);uaDf5*. Further analysis of this genetic condition must be done before I can determine more about the removal capacity.

pink-1(w46);ced-13(tm536);uaDf5* males crossed to *ced-13(tm536);uaDf5* or *pink-1(w46);uaDf5* hermaphrodites result in half of the F2 lines rapidly removing *uaDf5

I performed the same experimental analysis for the *pink-1(w46);ced-13(tm536);uaDf5* condition as I did for the *ced-3(n1286);ced-13(tm536);uaDf5* condition outlined in figure 3.6 (Fig. 3.7). I measured the fractional abundance of *uaDf5* from the P0 to the F4 generation in 16 lines resulting from crossing *pink-1(w46);ced-13(tm536);uaDf5* males to *pink-1(w46);uaDf5* hermaphrodites (Fig. 3.7D-G) and in 18 lines resulting from crossing *pink-1(w46);ced-13(tm536);uaDf5* males to *ced-13(tm536);uaDf5* hermaphrodites (Fig. 3.7H-K). 16 of the 34 lines generated exhibited rapid removal of *uaDf5* by the F4 generation (defined as dropping the fractional abundance of *uaDf5* to below 25%, with the lowest dropping to 1.56%) with the remainder of the lines having a moderate level of removal (40-80% by the F4 generation). For the 16 rapid removal lines, the removal starts as early as the F2 generation and drops by an average of 25% each generation thereafter. When *pink-1(w46);ced-13(tm536);uaDf5* males were crossed to *pink-1(w46);uaDf5* hermaphrodites, 6 of the 16 lines had a low level of cleanup by the F4 generation with the fractional abundance of *uaDf5* still above 70%, 3 lines had a moderate level of cleanup with the fractional abundance of *uaDf5* down to 40-50%, and 7 had a high level of cleanup with the fractional abundance of *uaDf5* below 25% representing a tri-modal removal phenotype. Analysis of embryonic lethality in the progeny laid by the F2 hermaphrodites shows a correlation between removal capacity and embryonic lethality (r^2= 0.27) (Fig. 3.7G), suggesting embryonic lethality may play a minor role in the removal capability. When *pink-1(w46);ced-13(tm536);uaDf5* males were crossed to *ced-13(tm536);uaDf5* hermaphrodites, 9 of the 18 lines with a moderate level of cleanup by the F4 generation

with the fractional abundance of *uaDf5* spanning the range of 50-80%, and the other 9 lines had a high level of cleanup with the fractional abundance of *uaDf5* below 20%, representing a bi-modal removal phenotype. Analysis of embryonic lethality in the progeny laid by the F2 hermaphrodites shows no correlation between removal capacity and embryonic lethality (r^2= 0.017) (Fig. 3.7K) suggesting it plays no role when the hermaphrodite is *ced-13(tm536);uaDf5*. Further analysis of the differential dynamics through which *uaDf5* removal occurs in different hermaphrodite genotypes needs to be done to dissect if there are different mechanisms occurring in each case.

Following the "IGE", genotype is not correlated with the *uaDf5* removal capacity

I noticed that half of the F2 lines had a high level of cleanup phenotype, which is much higher than predicted since only 25% of lines should have the double mutant genotype (*pink-1(w46);ced-13(tm536);uaDf5*) following the P0 cross. Perhaps most shockingly, genotyping of the F2 founder hermaphrodites for each set of crosses revealed that the double mutant genotype does not correlate with the removal capacity phenotype (Fig. 3.7). Rather, any of the five possible genotypes resulting from the two sets of crosses are able to efficiently remove *uaDf5*. This suggests that the removal phenotype is due to a heritable transgenerational epigenetic state resulting from the cross, rather than the genetic state of the worms. Thus, I now refer to the initial cross as the initiating genetic event or "IGE" which sets up a condition that results in an incredibly efficient *uaDf5* removal mechanism. Why it is that not all lines resulting from the IGE remove *uaDf5* at the same rate is a question for future studies, and suggests there may be a dosage-dependency factor at play.

The lines resulting from the IGE that have a rapid removal phenotype show a striking amplification of WT-mtDNA in the F3 generation, suggesting there is increased partitioning of *uaDf5* from WT-mtDNA after the IGE

What is the mechanism through which *uaDf5* is removed in these IGE lines? In order to get a better idea of what dynamics are at play, I analyzed mtDNA copy number dynamics in the generations following the IGE (Fig. 3.8A,B). I found that there is a 3-step process that is common to the lines that rapidly remove *uaDf5* (Fig. 3.8A): i) a preliminary decrease in both WT-mtDNA and *uaDf5* copy number, followed by ii) a specific amplification of WT-mtDNA, and then lastly iii) a specific removal of *uaDf5*. For all lines, including those that do not rapidly remove *uaDf5,* I observed a global reduction in total mtDNA levels between the P0 (time of the cross) and F2 generations with a slight bias toward removal of *uaDf5* (data not shown). For the lines that have a rapid removal phenotype, I found that between the F2 and F3 generations WT-mtDNA is specifically amplified to levels above what is normally seen (WT-mtDNA copy number is typically extremely non-variable in a stage-specific manner, even in the presence of *uaDf5* [78,106,107,201]). This amplification is less prominent and less specific to WT-mtDNA in the lines that do not exhibit a rapid removal phenotype (Fig 3.8B). In the lines that rapidly remove *uaDf5*, the WT-mtDNA-specific amplification precedes a secondary wave of *uaDf5* removal (this time unaccompanied by removal of WT-mtDNA, unlike the first wave of removal seen in the P0 to F2 generation) between the F3 and F4 generations. These dynamics give insight into a potential mechanism through which *uaDf5* is removed following the IGE. The specific amplification of WT-mtDNA followed by the specific elimination of *uaDf5* suggests that *uaDf5* is separated from WT-mtDNA in a way in which the cell can properly act differentially on the two mtDNA populations.

I propose that there may be a global mitochondrial fission event that happens soon after the IGE, thus allowing for a distinct separation of the alleles into individual mitochondria (Fig. 3.8C). Further analysis of the IGE in a fission-deficient background must be done to determine if this is a crucial element of the IGE-associated removal phenotype.

DISCUSSION

I present several lines of evidence indicating that germline PCD is a mechanism through which deleterious mtDNA is removed from the germline, and the startling discovery of a heritable transgenerational epigenetic mechanism of greatly increased mtDNA quality control following an initiating genetic event, or "IGE".

uaDf5 has negative consequences on fitness, making it a good model for mitochondrial disease

The 3.1kb mtDNA deletion mutant *uaDf5* exhibits stable heteroplasmy despite its highly deleterious nature [201]. Why is *uaDf5* maintained in a heteroplasmic state despite its presumably negative effect on cellular and organismal health? One possibility is that there is no WT-mtDNA in this strain, and instead there are two deleterious mtDNA alleles that complement each other. To answer this question, I used high throughput sequencing to determine the sequence of the presumed WT-mtDNA to see if it in fact contains a mutation that the *uaDf5* allele complements. Instead, I found that the second mtDNA allele is indeed wildtype. However, our high throughput analysis led to the discovery of a secondary mutation that is linked to the *uaDf5* deletion. This secondary mutation, "*w47*", is a single base pair deletion in the ND4 gene which results in a frameshift leading to premature truncation of the protein such that only the first 88 amino

acids of the 409 amino acid long protein is produced. This tells us that the *uaDf5* allele not only knocks out 7 tRNAs and the ATP6, ND1, ND2, and CYTB genes, but also knocks out a fifth gene, ND4. The nature of the allele presumably results in at least two truncated proteins that are necessary transmembrane subunits of complex 1 (ND1 and ND4) in addition to reduced capacity for making proteins due to the loss of several necessary tRNAs. Thus, *uaDf5* mutants are anticipated to have heightened mitochondrial stress which would activate the mitochondrial UPR (UPR^{MT}). In line with these discoveries, it was recently discovered that the UPR^{MT} is increased in *uaDf5* mutants and actually acts to protect *uaDf5* from mtDNA quality control machinery [78,80].

To investigate whether there are detectable health consequences of this mutant mtDNA, I measured various fitness parameters in *uaDf5* mutants. Surprisingly lifespan was unaffected, but there are observable negative consequences on brood size, embryonic lethality, and developmental rate showing that *uaDf5* is a good model for mtDNA disease and that analysis of its regulation is a good tool for studying mechanisms of mtDNA quality control.

Using the highly sensitive technique of droplet digital PCR (ddPCR; [203,204]) I was able to accurately measure the fractional abundance of *uaDf5* in both individual worms and populations of worms. I first measured the fractional abundance of *uaDf5* in pooled 200-worm-populations with a wildtype nuclear background in three biological replicates grown independently for over 8 generations. I found that there was very little variation between the replicates showing a marked stability of the steady state level of the fractional abundance of *uaDf5*. I repeated this experiment two more times, separated by many months, and found that the fractional abundance of *uaDf5* remains constant. This tells us that the measurement of the fractional abundance of *uaDf5* is a highly stable

value and that our control serves as a robust parameter for comparing mutants to. To see if modulation of mtDNA quality control results in a measurable change in the fractional abundance of *uaDf5*, I analyzed mutants in the mitophagy and the UPR^{MT} pathways. As expected, inhibition of mitophagy results in an increase in the fractional abundance of *uaDf5*. Inhibition of the UPR^{MT} results in a lowered fractional abundance of *uaDf5*, while overactivation results in an increase in the fractional abundance of *uaDf5*, which follows with the UPR^{MT} being a protector of *uaDf5*.

PCD mutants have increased fractional abundance of *uaDf5*

Is germline PCD, which kills off upwards of 95% of potential oocytes [183], a mechanism through which mtDNA quality control operates? To answer this, I analyzed the steady state fractional abundance of *uaDf5* in populations of worms containing mutations in various PCD-related genes. Our analysis gave differing results, with most mutants exhibiting an effect, however there were several mutants which did not such as *ced-4* and two of the *ced-3* alleles analyzed. Why *ced-4* mutants do not have an increased fractional abundance of *uaDf5* may be explained by the fact that it has roles outside of PCD [207,208] and those alternative roles may act to reduce mtDNA quality control. Why certain alleles of *ced-3 (n718* and *n2454*) do not show increased fractional abundance of *uaDf5* is unclear since the nature of the mutations and their presumed impact on CED-3 function do not distinguish them from the two alleles (*n717* and *n1286*) that did increase the fractional abundance of *uaDf5* [206]. Further molecular analysis of the nature of the alleles needs to be done to determine the reason behind this. Curiously, analysis of a *csp-1* mutant (CSP-1 is a non-canonical caspase that has largely been seen to play a minor role in PCD [175,178]) greatly increases the fractional abundance of

uaDf5 in a *ced-3(n717)* background, suggesting that CSP-1 may play a larger role in mutant mtDNA-induced germline PCD. Analysis of the *csp-1* single mutant needs to be done to clarify the extent of its role. Mutations in the *ced-13* gene result in a large increase in the fractional abundance of *uaDf5* supporting the claim that it is germline-specific PCD, and not developmental PCD, that acts in mtDNA quality control. To further bolster this claim, *egl-1* mutants need to be analyzed which are expected to have no effect on the fractional abundance of *uaDf5*.

Although the increased fractional abundance of *uaDf5* seen in the engulfment mutants supports the idea that PCD is acting in mitochondrial quality control, these results could also be reflective of the potential role of a recently discovered process called "endodermal cannibalism" [87]. This discovery was made in *C. elegans* embryos and details an event in which the germline progenitor cells (PGCs) pinch off a decent-sized lobe - packed with mitochondria - which then undergoes scission and is degraded by the surrounding endodermal cells. This endodermal cannibalism process happens about midway through embryogenesis after the P4 cell has further divided to produce the 2 primordial germ cells (PGCs) Z2 and Z3 [196]. This cannibalism event is dependent on the dual actions of LST4/SNX9 and CED-10/RAC, which has mostly been recognized as a major downstream player in cell corpse engulfment following apoptosis [92,180–182]. LST4 and CED-10 regulate dynamin and actin dynamics for the successful constriction and scission of the lobe (Fig. 1.6B). There are several things that are removed in these excised lobes, including P granules, but it seems that the majority of the material is actually mitochondria. This is a likely quality control step for the developing organism to remove any deleterious genomes from the germline, since it occurs immediately after the bottleneck when there is a reduced population of mitochondria, and precedes the massive

uptick in replication that is due to happen [106,107]. Our *ced-10* results may therefore be the result of inhibition of endodermal cannibalism rather than cell corpse engulfment. Further studies using temperature sensitive mutants need to be done to narrow down the developmental time window at which CED-10/RAC is acting in mtDNA quality control.

The interplay between mitophagy and PCD

Our *ced-13* results led us to question if the upstream activator of CED-13/BH3 in response to genotoxic stress, CEP-1/p53 [184,186,187,210], activates the cell death pathway in response to mtDNA disease. This would be a fascinating result if true since CEP-1/p53 is largely thought to activate germline PCD in response to genotoxic stress in the nucleus. If it also responds to mitochondrial genotoxic stress, that would make it a crucial element for general DNA health in the germline. However, I found that knocking out CEP-1/p53 actually results in increased mtDNA quality control, seen as greatly reduced fractional abundance of *uaDf5*. This confounding result may be explained by the largely unexplored role of CEP-1/p53 in inhibition of mitophagy. CEP-1/p53 has been shown to directly inhibit PDR-1/PARKIN [209], the ubiquitin ligase that is activated by PINK-1 in the mitophagy pathway. Perhaps I have shown further evidence for its role in mitophagy and these results reveal potential crosstalk that may occur between the mitophagy and PCD pathways. It raises interesting questions about how players that are involved in both pathways may differentially regulate the levels of each pathway in response to mutant mtDNA.

In order to further understand the possible crosstalk occurring between the pathways, I generated a set of double mutants composed of genes from each pathway to see what levels of epistasis occur. A *cep-1(gk138);ced-3(n1286)* double mutant has

increased fractional abundance of *uaDf5*, suggesting that even with increased mitophagy the lack of PCD results in an accumulation of *uaDf5*, further suggesting that PCD is a larger contributor to mtDNA quality control. Similar results were seen in the *ced-13(tm536);ced-4(n1162)* double mutant. As expected, if you knock out both pathways, which was done in the *cep-1(gk138);pink-1(w46), cep-1(gk138);pdr-1(gk448),* and *pdr-1(gk448);ced-13(tm536)* double mutants, you see increased fractional abundance of *uaDf5*.

However, there were two double mutants which gave unexpected results. The *ced-3(n1286);ced-13(tm536)* double mutant, which is presumed to only inhibit PCD, shows an extreme decline in the fractional abundance of *uaDf5*. Fitness analysis of lines resulting from crossing *ced-3(n1286);ced-13(tm536);uaDf5* males into either *ced-13(tm536);uaDf5* or *ced-3(n1286);uaDf5* hermaphrodites show negative effects on brood size and embryonic lethality. This suggests that at least part of the reason for the removal of *uaDf5* is due to a decreased tolerance of *uaDf5* such that worms containing high levels of *uaDf5* do not survive, resulting in culling at the organismal level. However, the effects on fitness are not as extreme as one would expect if organismal culling is the only factor resulting in *uaDf5* removal, so there may be another element to the removal phenotype that has yet to be understood. In order to better understand how *uaDf5* is being removed from the population in a *ced-3(n1286);ced-13(tm536)* background, I crossed *ced-3(n1286);ced-13(tm536);uaDf5* males into either *ced-13(tm536);uaDf5* or *ced-3(n1286);uaDf5* hermaphrodites and then measured the fractional abundance of *uaDf5* in the resulting lines up through the F4 generation following the cross. None of the lines analyzed had dropped their fractional abundance of *uaDf5* below 70% within four generations, suggesting that the removal process may take more generations or may

require a certain environmental factor. Putting those lines through a round of starvation did not result in removal, so starvation is unlikely to be a necessary step. The reason that a *ced-3(n1286);ced-13(tm536)* double mutant is less tolerant to *uaDf5* than any of the single mutants of the PCD pathway suggests that one or both genes are acting in roles outside of PCD.

The other double mutant that gave a shocking result was the *pink-1(w46);ced-13(tm536)* double, which is presumed to knock out both mitophagy and PCD. Surprisingly, this double mutant results in complete removal of *uaDf5* within the 8 generations it was grown before analysis. It is unlikely that CED-13 and/or PINK-1 are acting on mtDNA through their canonical pathways, seeing as how much the level of *uaDf5* removal under this genetic condition differs from the results seen in other double mutants that knock out both mitophagy and PCD. Fitness analysis of lines resulting from crossing *pink-1(w46);ced-13(tm536);uaDf5* males into either *ced-13(tm536);uaDf5* or *pink-1(w46);uaDf5* hermaphrodites show no deficits in brood size or embryonic lethality and the superficial appearance of the worms appears to be very healthy, suggesting the removal phenotype is not caused by decreased tolerance of *uaDf5* resulting in culling at the organismal level.

The "IGE": *pink-1(w46);ced-13(tm536);uaDf5* mutants show a striking *uaDf5* removal phenotype that is epigenetic in nature

In order to better understand how *uaDf5* is being removed from the population in a *pink-1(w46);ced-13(tm536)* background, I crossed *pink-1(w46);ced-13(tm536);uaDf5* males into either *ced-13(tm536);uaDf5* or *pink-1(w46);uaDf5* hermaphrodites and then measured the fractional abundance of *uaDf5* in the resulting lines up through the F4

generation following the cross. I observed immediate removal of *uaDf5* in roughly half of the lines (16/34) generated from these crosses, with the fractional abundance dropping to below 50% as early as the F2 generation. By the F4 generation, one of the lines had already reduced the fractional abundance of *uaDf5* down to 1.56%. Following the cross outlined above, there is a segregation of genotypes in the F2 generation such that only 25% of the lines should have the reconstituted *pink-1(w46);ced-13(tm536);uaDf5* genotype. Genotyping of the F2 "line founder hermaphrodites" revealed that the double mutant genotype was not necessary for the rapid removal phenotype. In fact, any of the segregating genotypes are capable of the rapid removal phenotype, unlinking a genetic requirement from the transgenerational rapid removal of *uaDf5*. I suggest that this heritable, transgenerational phenotype is epigenetic in nature, and is the result of the event of the original P0 cross in which I crossed double mutant males into single mutant mothers, hereby referred to as the initiating genetic event, or "IGE". The genotype of the P0 mother used in the IGE does not appear to be of consequence, as rapid removal is observed in lines when using either *ced-13(tm536);uaDf5* or *pink-1(w46);uaDf5* hermaphrodites in the original cross. This raises the possibility that the only requirement for the IGE is that the male be a *pink-1(w46);ced-13(tm536);uaDf5* double mutant which results in an epigenetic environment that is enormously efficient at removing mutant mtDNA with no expense to organismal health.

How is this IGE-associated removal of mutant mtDNA occurring? One possibility is that the paternal mitochondria are licensed to survive following the IGE, instead of being rapidly degraded as is the case during normal fertilization [45,47,211]. It is unlikely that the males used in the IGE still contain *uaDf5* since the *pink-1(w46);ced-13(tm536)* nuclear background has been shown to result in rapid removal of *uaDf5*. If this is true,

then the males used in the IGE only contain WT-mtDNA, and perhaps something about the *pink-1(w46);ced-13(tm536)* background marks the male mitochondria in a way that their degradation does not occur after fertilization and they end up repopulating the resulting progeny in a transgenerational manner. Further studies need to be done to determine both the paternal and maternal requirements for the IGE-associated removal phenotype. Additionally, the generality of the phenomenon needs to be investigated. Is this removal phenotype specific to *uaDf5*, or does it act on all mtDNA mutants? Does the size of the deletion matter, or influence the rate of removal? Does the location of the deletion or the nature of the resulting truncated proteins matter, suggesting the UPR^{MT} may play a crucial role in the IGE process? There are a set of mtDNA point mutation strains, deletion strains that vary in size and location around the genome, and a mtDNA duplication strain that is larger than WT-mtDNA, and studies of the IGE in those strains will give insight into the mtDNA requirements for the removal phenotype [212].

Mitochondrial fission as a likely mechanism of *uaDf5* removal following the IGE

In order to get a more thorough understanding of possible mechanisms through which the IGE results in *uaDf5* removal, I analyzed the total copy number of both WT-mtDNA and *uaDf5* mtDNA in the generations following the IGE. I found that all of the lines exhibit a precipitous decrease in total mtDNA copy number between the P0 and F2 generations, such that F2 worms have much lower mtDNA copy number than is normally seen. This decline in mtDNA has a slight bias toward *uaDf5*, though it is insignificant. Between the F2 and F3 generation, I saw that only those lines that exhibit the rapid removal phenotype have a specific amplification of WT-mtDNA to supranormal levels, considerably higher than is ever seen (WT-mtDNA copy number is highly invariable

even in the presence of *uaDf5* [78,106,107,201]), with little to no amplification of *uaDf5*. This increase in WT-mtDNA copy number between the F2 and F3 generations is then followed by a specific decrease in *uaDf5* copy number, with no decrease in WT-mtDNA copy number, between the F3 and F4 generations. The copy number dynamics observed in the rapid removal lines in the F2-F4 generations are not observed in those lines that maintain *uaDf5* at a higher level through the F4 generation.

The specific amplification of WT-mtDNA followed by the selective removal of *uaDf5* suggests that the cell is more capable of discerning between *uaDf5* and WT-mtDNA by the F2 generation. A possible mechanism for better discrimination is that of mitochondrial fission (Fig. 3.8C,D) [68,108,115]. If the mitochondrial network undergoes global fission, the mtDNA molecules are then divided up into individual mitochondria which would better allow the cellular machinery to differentially act on the different alleles. Mitochondria containing WT-mtDNA would presumably have a robust membrane potential and wouldn't be leaky due to intact MRC machinery, and those mitochondria would be the only ones taking up replication machinery resulting in increased WT-mtDNA copy number. Mitochondria containing *uaDf5* mtDNA would have diminished membrane potential (please refer to chapter 2) and may be leaky due to dysfunctional MRC machinery, which could inhibit the import of replication machinery. The mitophagic removal of mitochondria with a low membrane potential would normally happen in a PINK-1-dependent manner, but seeing as there is no functional PINK-1 in a fraction of the lines that have the rapid removal phenotype, the removal of *uaDf5*-containing mitochondria must occur through some other mechanism. Further studies need to be done to elucidate if mitochondrial fission is indeed a mechanism through which the

IGE results in removal of *uaDf5*, and to uncover how a PINK-1-independent removal process proceeds.

Another question that is raised is why do only a fraction of the lines exhibit the removal phenotype following the IGE? Is there a dosage dependency, perhaps of a cytoplasmic component, or is there a threshold effect in which the rapid removal is observed as soon as either the fractional abundance of *uaDf5*, or the copy number of *uaDf5*, gets below a certain level? Further analysis of the lines that do not exhibit the rapid removal phenotype will give some insight here. Perhaps if given a few more generations, all of the lines following the IGE will eventually eliminate *uaDf5*.

MATERIALS AND METHODS

Culturing of nematodes

Nematode strains were maintained at on NGM plates as previously described at either 20°C or 15°C for the temperature-sensitive strains [199]. Please refer to appendix A1 for a table detailing all strains used in this dissertation. Strains without a JR designation were either provided by the CGC which is funded by NIH Office of Research Infrastructure Programs (P40 OD010440) or were obtained from the Mitani lab (strains with a FX designation or JR strains containing alleles with a tm designation were generated from Mitani lab strains) [200].

Population collection by age

Upon retrieval of a stock plate for a given strain, three chunks were taken from the stock plate and placed onto three separate large NGM plates to create three biological replicate “lines”. Each of these lines was chunked approximately each generation to fresh

large NGM plates (every three days if maintained at 20°C or 25°C, or every four days if maintained at 15°C, being careful to not let the worms starve between chunks). After four generations of chunks, an egg prep was performed on each line (as described previously) and left to spin in M9 overnight to synchronize the hatched L1s. The next day, each egg prep was plated onto three large seeded plates at an equal density and the worms were left to grow to day 2 adults (second day of egg laying). The day two adult worms were egg prepped for synchronization and left to spin in M9 overnight. The next day, each egg prep was plated onto five large NGM plates at equal density. Once the worms reached day one of adulthood (first day egg-laying), one of the plates was used to collect 200 adult worms by picking into 400 µl of lysis buffer, and the remaining adults on the plate were egg prepped for the collection of hatched L1 larvae in 400 µl lysis buffer the following day. The worms on the four remaining plates were transferred to a 40 µm nylon mesh filter in order to separate the adults from the progeny, and the resulting adults were resuspended in M9 and pipetted onto fresh large NGM plates. This process was repeated for the following three days (day two - day four of adulthood). Day 5-10 adults were moved to fresh NGM plates every 2nd day using a 40 µm nylon mesh filter, and the resulting day 10 adults were collected in lysis buffer.

ddPCR

The worm lysates were incubated at 65°C for 1.5-4 hours and then 95°C for 30 minutes to deactivate the proteinase K. Each lysate was diluted; 100-fold for 200 worm adult population lyses, 2-fold for 200 worm L1 population lyses, and 25-fold for individual adult lyses. 2 µl of the diluted lysate was then added to 23µl of the ddPCR

reaction mixture, which contained a primer/probe mixture and the ddPCR probe supermix with no dUTP. The primers used were:

WTF: 5'-GAGGGCCAACTATTGTTAC-3'

WTR: 5'-TGGAACAATATGAACTGGC-3'

UADF5F: 5'-CAACTTTAATTAGCGGTATCG-3'

UADF5R: 5'-TTCTACAGTGCATTGACCTA-3'

The probes used were:

WT: 5'-HEX-TTGCCGTGAGCTATTCTAGTTATTG-Iowa Black→ FQ-3'

UADF5: 5'-FAM-CCATCCGTGCTAGAAGACAAAG- Iowa Black→ FQ-3'

The ddPCR reactions were put on the BioRad droplet generator and the resulting droplet-containing ddPCR mixtures were run on a BioRad thermocycler with the following cycle parameters, with a ramp rate of 2°C/sec for each step:

1. 95°C for 5 minutes
2. 95°C for 30 seconds
3. 60°C for 1 minute
4. Repeat steps 2 and 3 40x
5. 4°C for 5 minutes
6. 90°C for 5 minutes

After thermocycling, the ddPCR reaction plate was transferred to the BioRad droplet reader and the Quantasoft software was used to calculate the concentration of *uaDf5* (FAM/HEX? positive droplets) and WT-mtDNA (FAM/HEX? positive droplets) in each well.

Selective *uaDf5* removal experiment

15 individual L4 worms were singled out onto small plates and allowed to lay eggs for one day before being lysed (as day one adults). After lysis, the fractional abundance of *uaDf5* in each worm was quantified using ddPCR. The worm with the lowest fractional abundance of *uaDf5* was selected, and 15 of its progeny were singled out onto small plates and were allowed to lay eggs for one day before being lysed as day one adults. Once again, the fractional abundance of *uaDf5* was measured and the worm with the lowest % *uaDf5* was selected for the next generation. This process was continued for as many as 12 generations.

Lifespan analysis

Confluent large plates were egg prepped and left to spin in M9 overnight for synchronization. The hatched L1s were plated onto large thick plates and allowed to grow to day two adults before being egg prepped a second time and left to spin in M9 overnight. The next morning, referred to as day one for lifespan determination, L1s were singled out onto small plates. Once the worms started laying eggs, they were transferred each day to a fresh small plate until egg laying ceased, after which the worms remained on the same plate unless bacterial contamination required transfer to a fresh plate. Worms were considered dead if there was no movement after being lightly prodded with a worm pick.

Brood size, embryonic lethality, and unfertilized oocytes analysis

Confluent large plates were egg prepped and left to spin in M9 overnight for synchronization. The hatched L1s were plated onto large thick plates and allowed to grow

to day two adults before being egg prepped a second time and left to spin in M9 overnight. The next morning, L1s were singled out onto small plates. Once the worms started laying eggs, they were transferred each day to a fresh small plate until egg laying ceased. The day after transfer to a fresh plate, unfertilized oocytes, unhatched embryos, and hatched larvae on the plate from the previous day were counted. This was done for each of the days of laying and the total of unhatched embryos and hatched larvae from all plates from a single worm were tabulated to determine total brood size. To determine embryonic lethality, the total number of unhatched embryos was divided by the total brood size. To determine unfertilized oocyte percentage, the total number of unfertilized oocytes was divided by the total brood size.

Developmental time analysis

Confluent large plates were egg prepped and left to spin in M9 overnight for synchronization as has been previously described [199]. The hatched L1s were plated onto large thick plates and allowed to grow to day two adults before being egg prepped a second time and left to spin in M9 overnight. The next morning, L1s were singled out onto small plates. The stage of the worms was assayed every 12 hours for the first 72 hours after plating.

Illumina identification of *w47*

WT-mtDNA (N2) and *uaDf5*-containing strains (LB138, JR3630, and JR3688) were used for Illumina analysis. 20 large confluent plates were used for each strain. Worms were collected off the plates and a mitochondrial isolation followed by a DNA extraction was performed. The resulting DNA sample was prepped using the Nextera

library kit and was then run on the Illumina NextSeq 500 using the 300 cycle Mid-output kit with paired end reads (2x150). The corresponding reads were mapped to the *C. elegans* assembly reference sequence WBcel235. The reads were first trimmed using Trimmomatic before being mapped to the reference sequence using BWA. Picard Tools was used to sort the sam files giving a bam file output and then to mark and remove duplicates. The resulting bam files were merged, indexed and then converted to mpileup files using SamTools. SNP calling was done with the program VarScan, with a minimum coverage of 100 and a minimum variant frequency call of 0.01.

Creation and analysis of IGE lines

One mating plate contained ~30 *pink-1(w46);ced-13(tm536);uaDf5/+* P0 males with ~10 *pink-1(w46);uaDf5/+* P0 hermaphrodites, and another mating plate had ~30 *pink-1(w46);ced-13(tm536);uaDf5/+* P0 males with ~10 *ced-13(tm536);uaDf5/+* P0 hermaphrodites. Mating was allowed to continue overnight. The next morning, the P0 hermaphrodites were singled out onto small plates. Three days later, one F1 hermaphrodite was singled to a fresh plate from each plate containing ~50% male F1 progeny, and the P0 hermaphrodite was lysed. On the first day of egg laying by the F1 hermaphrodite, F2 embryos were singled out onto new plates, creating ~20 F2 lines from each original P0 mating plate, and the F1 hermaphrodite was lysed. F2 adults were lysed on the first day that they started laying eggs. Once the resulting F3 generation reached adulthood, 10 F3 adults were lysed together for each F2 line. Once the resulting F4 generation reached adulthood, 20 F4 adults were lysed together for each F2 line. The resulting P0, F1, F2, F3, and F4 lysates were then used for genotyping via PCR and *uaDf5* quantification via ddPCR.

FIGURES

Figure 1

A.

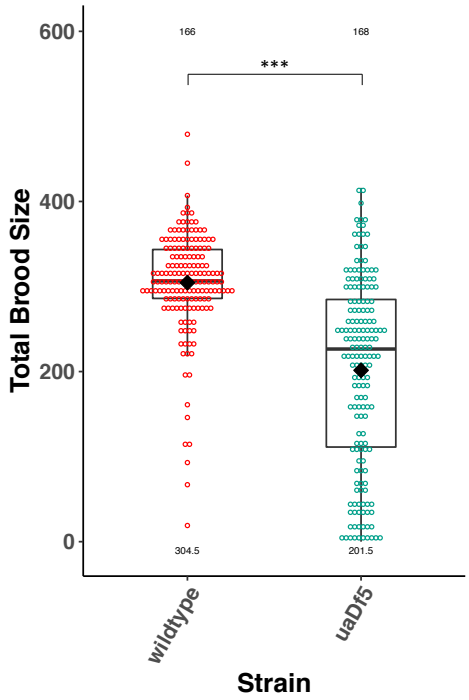

B.

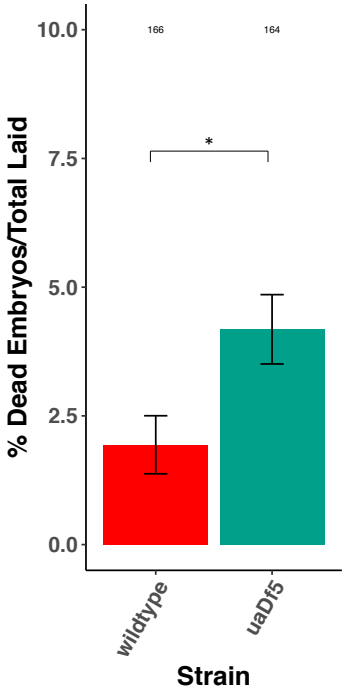

C.

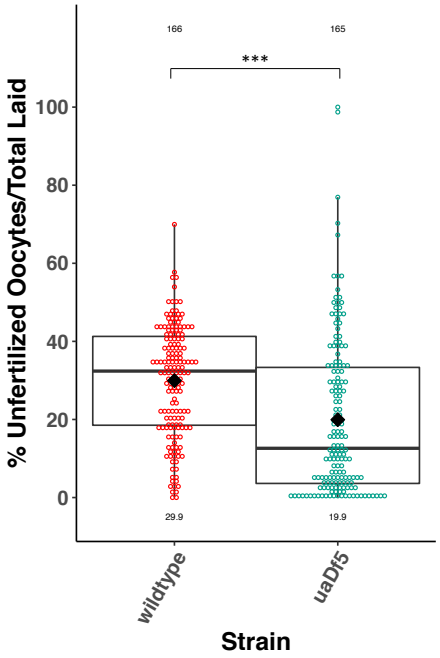

D.

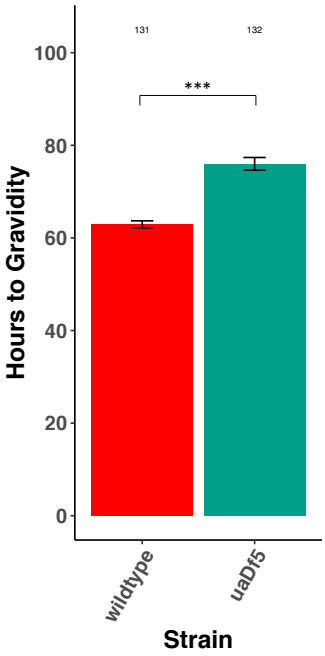

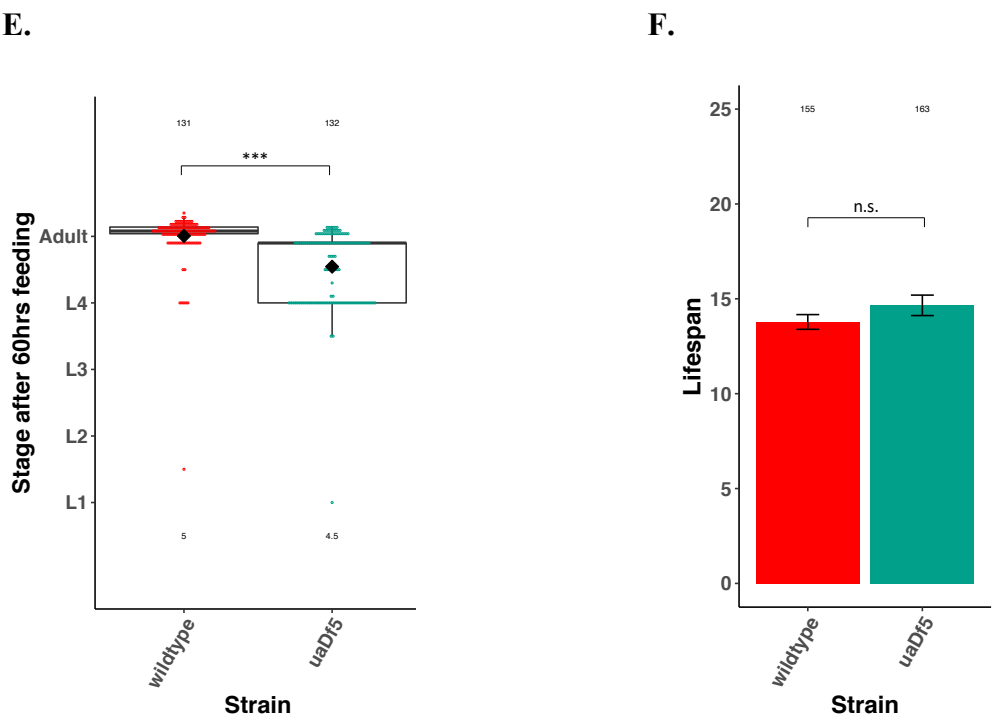

Figure 1. Analysis of the impact of *uaDf5* on fitness parameters. (A) Brood size analysis of *uaDf5* compared to laboratory wild type N2. Box plot shows median and IQR, number at the bottom indicates mean. **(B)** Embryonic lethality analysis of *uaDf5* compared to laboratory wild type N2. **(C)** Unfertilized oocyte analysis of *uaDf5* compared to laboratory wild type N2. Box plot shows median and IQR, number at the bottom indicates mean. **(D)** Developmental rate analysis of *uaDf5* compared to laboratory wild type N2, counting how many hours it takes for starved L1s to reach gravidity once plated on food. **(E)** Developmental rate analysis of *uaDf5* compared to laboratory wild type N2, staging worms 60 hours after starved L1s are plated on food. Box plot shows median and IQR, number at the bottom indicates mean. **(F)** Lifespan analysis of *uaDf5* compared to laboratory wild type N2, day 1 is defined as the day starved L1s are plated on food. (*** $p < 0.001$, ** $p < 0.01$, * $p < 0.05$, . $p < 0.1$) For each condition, N is indicated at the top of the graph. Statistical analysis was performed using the Mann-Whitney Wilcoxon test.

Figure 2

A.

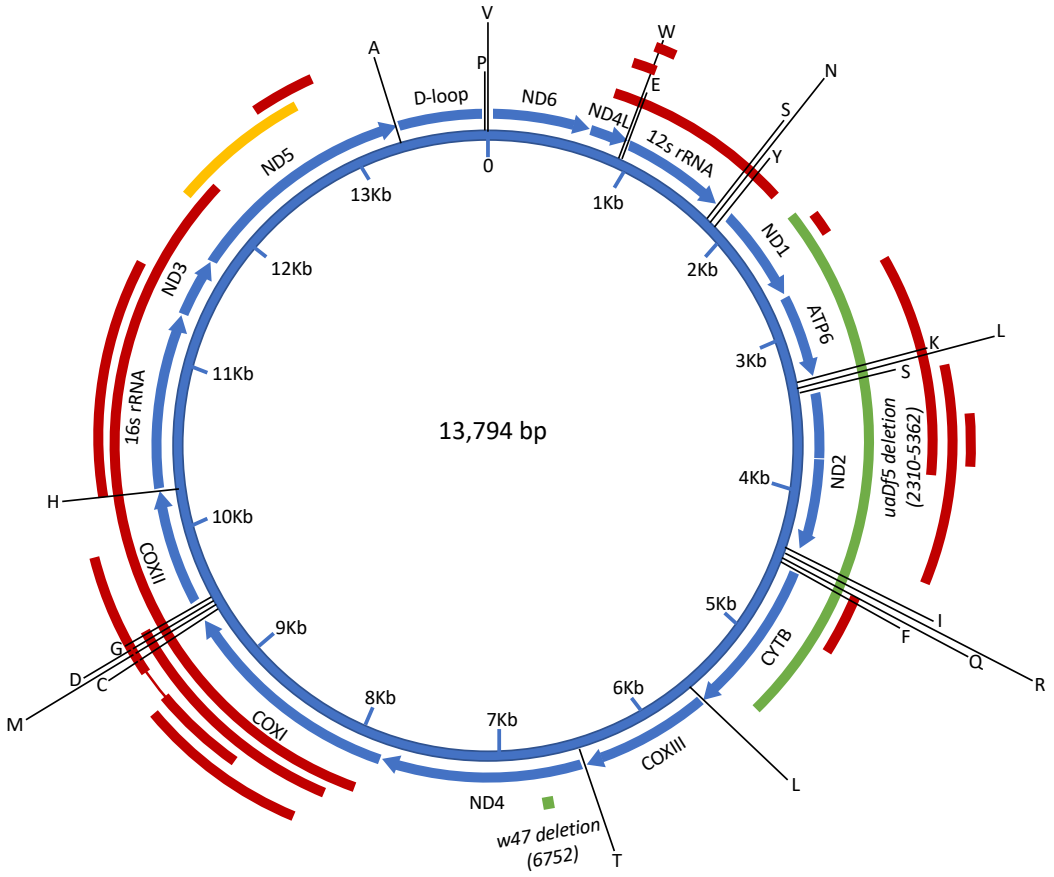

B.

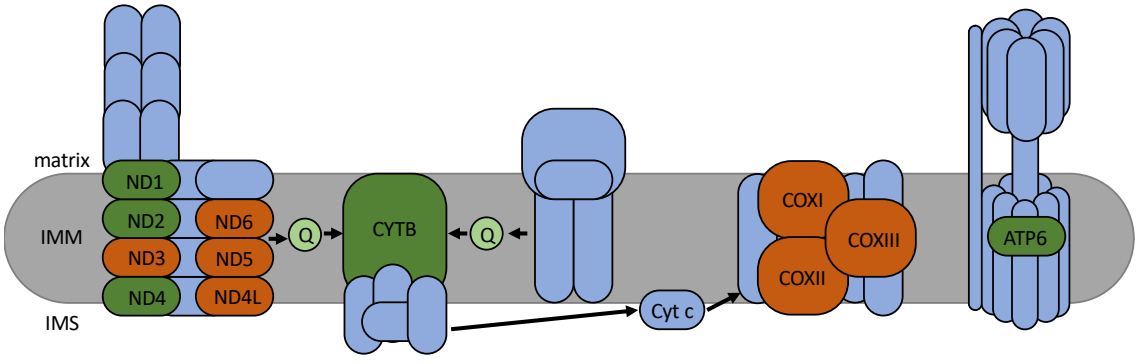

Complex:	I	III	II	IV	V
nDNA-encoded:	~30	~8	4	~6	~13
mtDNA-encoded:	7	1	0	3	1

C.

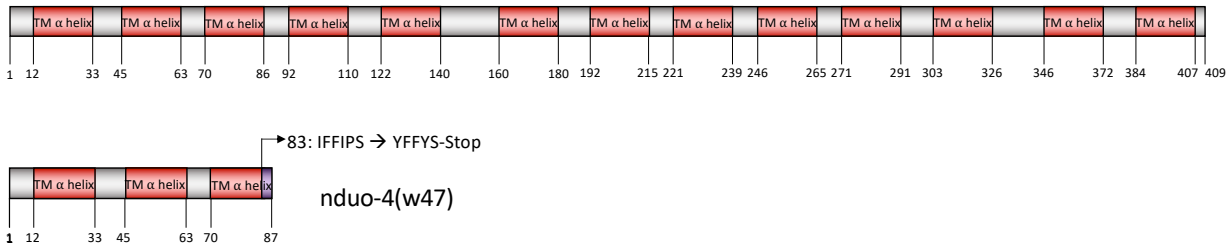

Figure 2. Characterization of the *uaDf5* allele. (A) Diagram of *C. elegans* mtDNA. Blue bars with arrows indicate the locations of genes and direction of transcription. Black bars with letters indicate the locations of tRNAs. Green bars show the locations of the *uaDf5* deletion as well as the linked *w47* deletion that I identified via Illumina sequencing. Red bars indicate other deletions that have been identified in the mtDNA that are available for analysis. The yellow bar indicates a duplication that is available for analysis. **(B)** Diagram showing the mitochondrial respiratory chain (MRC) machinery subunits. Blue indicates nDNA-encoded subunits, orange and green indicate mtDNA-encoded subunits. Green indicates those subunits that are knocked out in the *uaDf5* allele (including ND4 which is knocked out by the linked *w47* mutation). **(C)** Diagram showing the likely effect of the *w47* mutation on ND4 protein translation. ND4 is a 409-aa long transmembrane subunit that spans the inner mitochondrial membrane 13 times. The *w47* mutation results in a premature stop codon at position 89, eliminating 10 of the 13 alpha-helix membrane domains.

Figure 3

A.

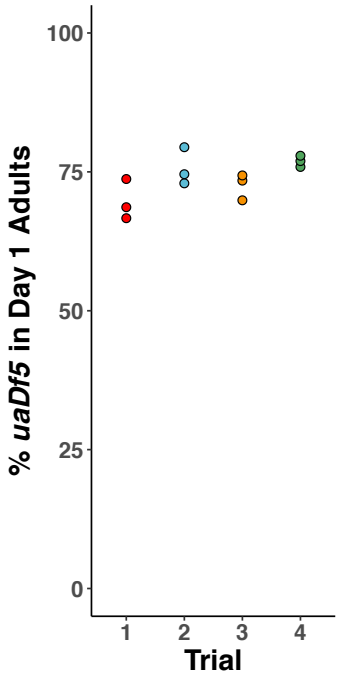
100
75
50
25
0
% uaDf5 in Day 1 Adults
1
2
3
4
Trial

B.

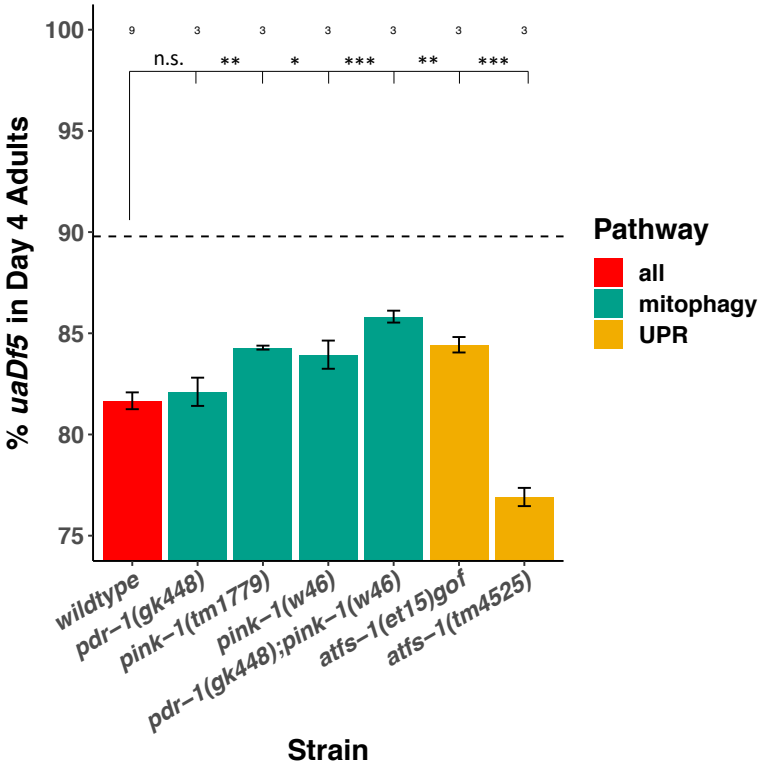
100
95
90
85
80
75
% uaDf5 in Day 4 Adults
9
3
3
3
3
3
3
n.s.
**
*
***
**
***
Pathway
all
mitophagy
UPR
wildtype
pdr−1(gk448)
pink−1(tm1779)
pink−1(w46)
pdr−1(gk448);pink−1(w46)
atfs−1(et15)gof
atfs−1(tm4525)
Strain

Figure 3. ddPCR as a technique for studying mtDNA quality control. (A) Testing for reproducibility in measuring *uaDf5* with ddPCR. Trials are each composed of 3 lines grown independently for at least 5 generations, trials were collected months or even years apart. **(B)** ddPCR analysis of *uaDf5* levels in UPR^{MT} and mitophagy mutants. For each strain, N is indicated at the top of the graph and represents the number of 200-worm populations analyzed. (*** $p < 0.001$, ** $p < 0.01$, * $p < 0.05$, . $p < 0.1$) Statistical analysis was performed using one-way ANOVA with Dunnett's correction for multiple comparisons.

Table 1

Gene	Homolog	Core Machinery	Role in apoptosis	Allele	Parental Strain	Molecular Nature of allele	Protein Change
ced-1	SCARF2	N	Pro (engulfment)	*e1735*	CB3203	Substitution	Nonsense Q→Ochre
ced-2	CRK	N	Pro (engulfment)	*e1752*	CB3257	Substitution	Nonsense W→Opal
ced-3	CASPASE	Y	Pro (executor caspase)	*n717*	MT1522	Substitution	Splice Site C to T
				n1286	MT3002	Substitution	Nonsense W→Opal
				n718	MT1743	Substitution	Missense G→R
				n2454	MT8354	Substitution	Missense A→T
ced-4	APAF1	Y	Pro (apoptosome)	*n1162*	MT2547	Substitution	Nonsense Q→Ochre
				n1894	MT5287	Not Curated	Unknown
ced-5	DOCK	N	Pro (engulfment)	*n1812*	MT4434	Substitution	Nonsense E→Ochre
ced-9	BCL2	Y	Anti	*n1950gf*	MT4770	Substitution	Missense G→E
ced-10	RAC	N	Pro (engulfment)	*n1993*	MT5013	Substitution	Missense V→G
				n3246	MT9958	Substitution	Missense G→R
ced-13	BH3	N	Pro	*tm536*	FX536	523bp Deletion	Only first 17 bp remain
				sv32	MD792	1304bp Deletion	Complete knockout, also inx-5
cep-1	p53	N	Pro (DNA damage response)	*gk138*	VC172	1660bp Deletion	Starts at position 1989, deletes part of exons 8 and 10 and all of exon 9
				ep347	CE1255	1827bp Deletion	Starts at position 2545, removes part of exon 9 through most of exon 13 (the last exon)
csp-1	CASPASE	N	Pro (caspase)	*tm917*	JR3196	751bp Deletion	Only first 59 bp remain
csp-2	CASPASE	N	Unknown	*tm3077*	JR3397	319bp Deletion	Starts at position 7317, deletes part of exon 13 and all of 14

Table 1. Summary of PCD-associated mutants analyzed. A summary of all mutants analyzed in the PCD pathway, including their known homologs, whether they are part of the core PCD machinery, if they are pro-apoptotic or anti-apoptotic, and molecular details of the alleles analyzed.

Figure 4

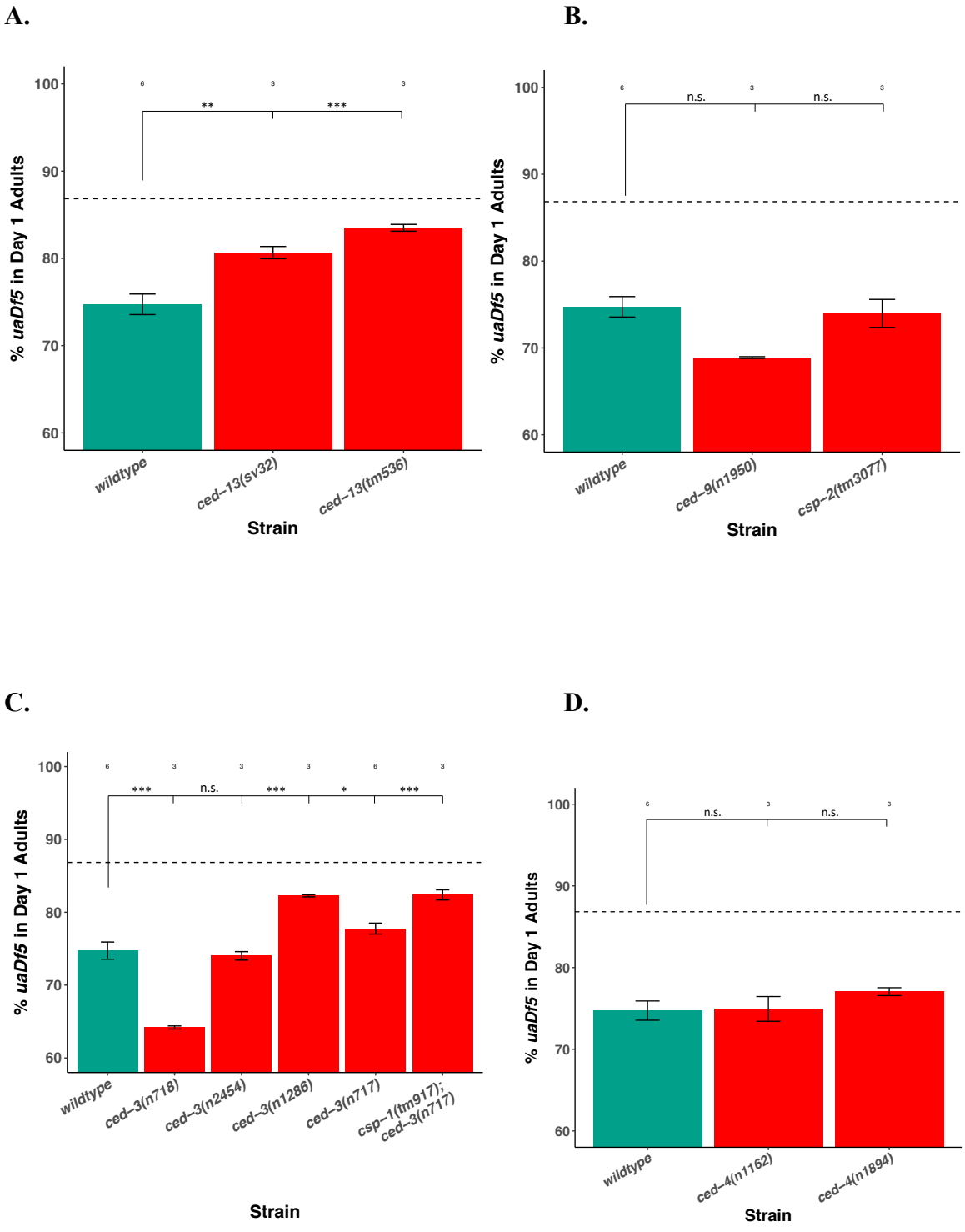
A.
B.
C.
D.
% uaDf5 in Day 1 Adults
Strain
wildtype
ced-13(sv32)
ced-13(tm536)
ced-9(n1950)
csp-2(tm3077)
ced-3(n718)
ced-3(n2454)
ced-3(n1286)
ced-3(n717)
csp-1(tm917); ced-3(n717)
ced-4(n1162)
ced-4(n1894)
n.s.
**
***
*

E.

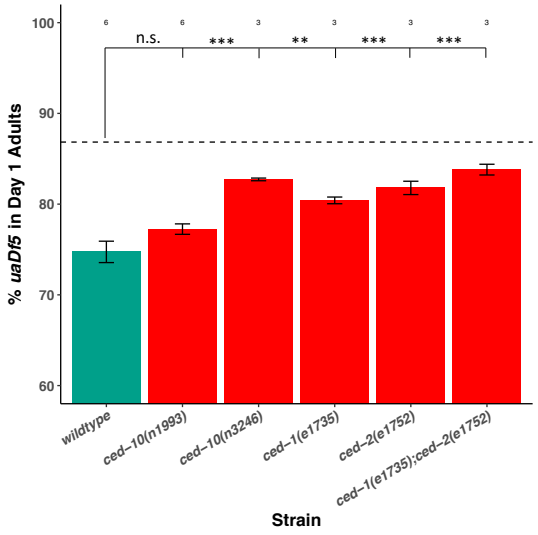
% uaDf5 in Day 1 Adults
100
90
80
70
60
n.s.
***
**
***
***
wildtype
ced−10(n1993)
ced−10(n3246)
ced−1(e1735)
ced−2(e1752)
ced−1(e1735);ced−2(e1752)
Strain

F.

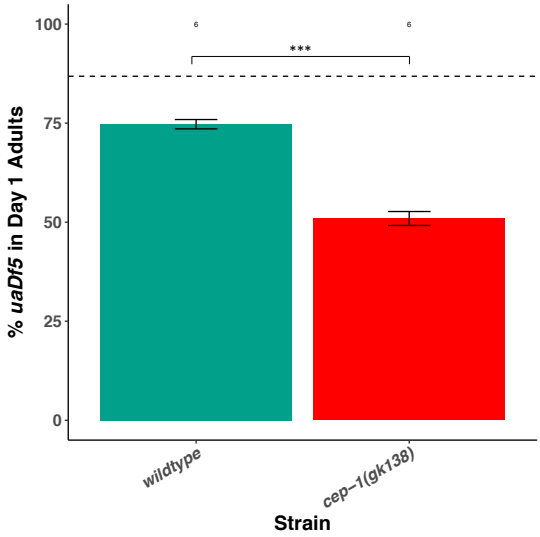
% uaDf5 in Day 1 Adults
100
75
50
25
0
***
wildtype
cep−1(gk138)
Strain

G.

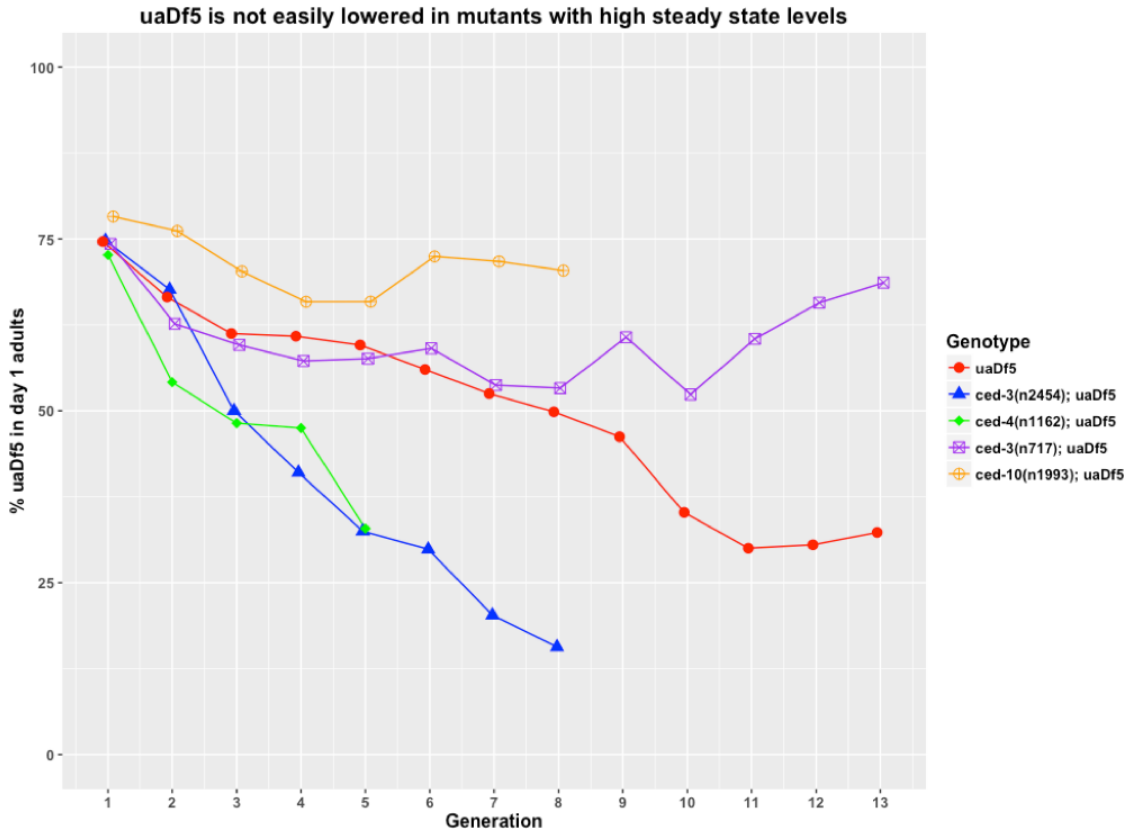
uaDf5 is not easily lowered in mutants with high steady state levels
% uaDf5 in day 1 adults
100
75
50
25
0
1
2
3
4
5
6
7
8
9
10
11
12
13
Generation
Genotype
uaDf5
ced-3(n2454); uaDf5
ced-4(n1162); uaDf5
ced-3(n717); uaDf5
ced-10(n1993); uaDf5

Figure 4. PCD mutant results show that germline PCD is likely acting on mtDNA maintenance. (A) ddPCR results of the *ced-13* alleles. **(B)** ddPCR results of the *ced-9* and c*sp-2* alleles. **(C)** ddPCR results of the *ced-3* and *csp-1* alleles. **(D)** ddPCR results of the *ced-4* alleles. **(E)** ddPCR results of the engulfment genes. **(F)** ddPCR results of the *cep-1* allele. **(G)** *uaDf5* removal experiment showing the average % *uaDf5* between 15 sibling worms each generation. The sibling with the lowest % *uaDf5* was used as the parent for the following generation. **(A-F)** For each strain, N is indicated at the top of the graph and represents the number of 200-worm populations analyzed. (*** $p < 0.001$, ** $p < 0.01$, * $p < 0.05$, . $p < 0.1$) Statistical analysis was performed using one-way ANOVA with Dunnett's correction for multiple comparisons.

Figure 5

A.

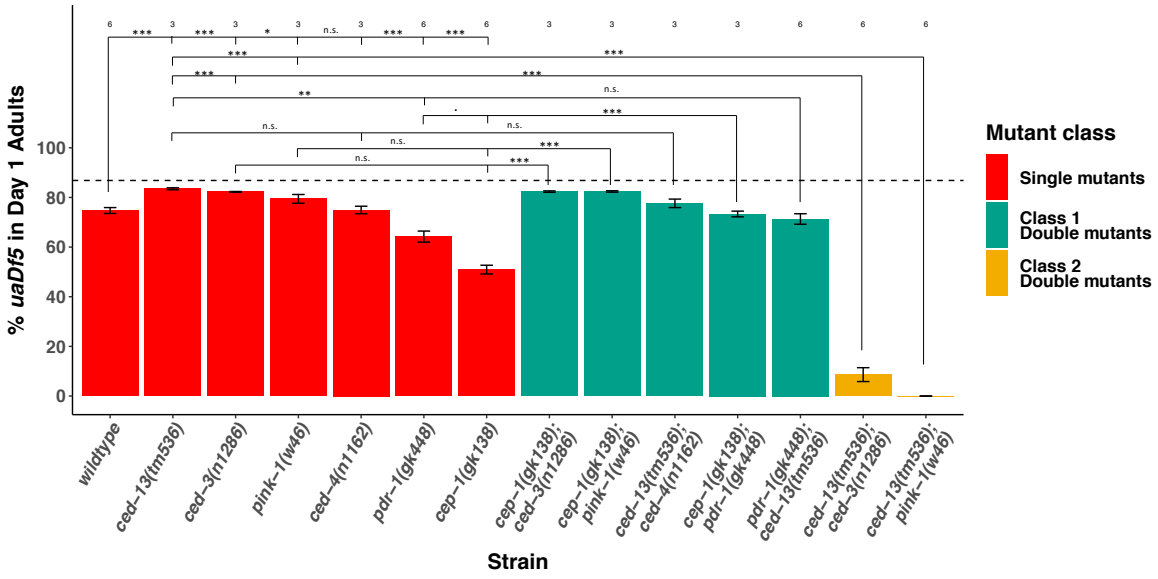
% uaDf5 in Day 1 Adults
Strain
wildtype
ced−13(tm536)
ced−3(n1286)
pink−1(w46)
ced−4(n1162)
pdr−1(gk448)
cep−1(gk138)
cep−1(gk138); ced−3(n1286)
cep−1(gk138); pink−1(w46)
ced−13(tm536); ced−4(n1162)
cep−1(gk138); pdr−1(gk448)
pdr−1(gk448); ced−13(tm536)
ced−13(tm536); ced−3(n1286)
ced−13(tm536); pink−1(w46)
Mutant class
Single mutants
Class 1 Double mutants
Class 2 Double mutants

B.

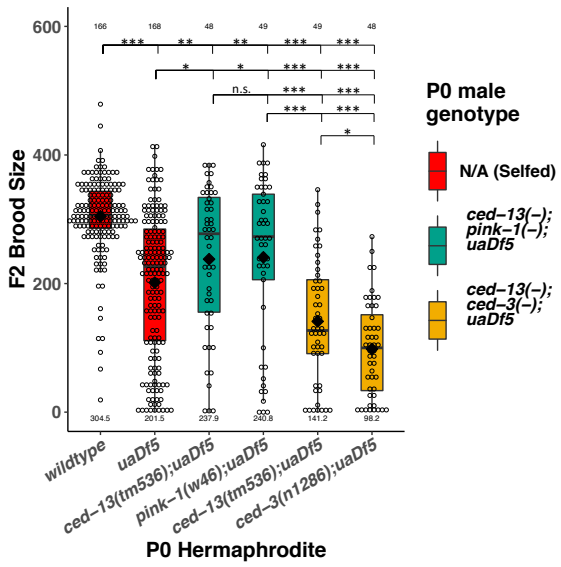
F2 Brood Size
P0 Hermaphrodite
wildtype
uaDf5
ced−13(tm536);uaDf5
pink−1(w46);uaDf5
ced−13(tm536);uaDf5
ced−3(n1286);uaDf5
P0 male genotype
N/A (Selfed)
ced−13(−); pink−1(−); uaDf5
ced−13(−); ced−3(−); uaDf5

C.

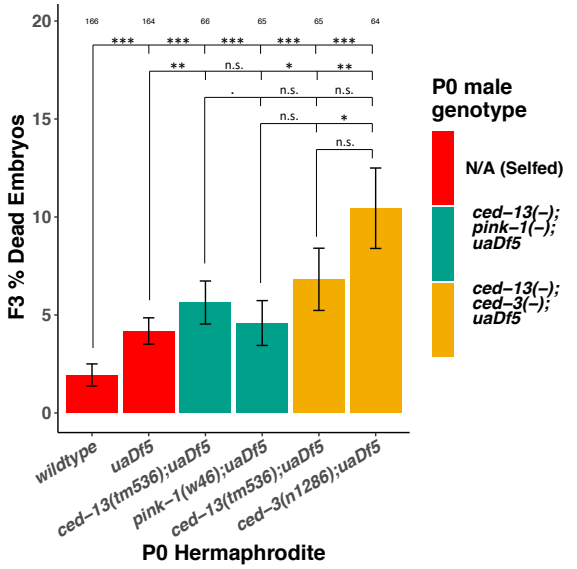
F3 % Dead Embryos
P0 Hermaphrodite
wildtype
uaDf5
ced−13(tm536);uaDf5
pink−1(w46);uaDf5
ced−13(tm536);uaDf5
ced−3(n1286);uaDf5
P0 male genotype
N/A (Selfed)
ced−13(−); pink−1(−); uaDf5
ced−13(−); ced−3(−); uaDf5

Figure 5. Double mutant analysis shows a shocking synergistic removal effect between *ced-13* and either *pink-1* or *ced-3*, with no evidence of *uaDf5* removal at the organismal level. (A) ddPCR analysis of double mutants. **(B)** Brood size analysis of F2 lines generated from the crosses indicated. For each condition, N>50. Statistical analysis was performed using the Kruskal-Wallis test. **(C)** Embryonic lethality analysis of F2 lines generated from the crosses indicated. For each condition, N is indicated at the top of the graph. Statistical analysis was performed using the Kruskal-Wallis test. (*** $p < 0.001$, ** $p < 0.01$, * $p < 0.05$, . $p < 0.1$)

Figure 6

A.

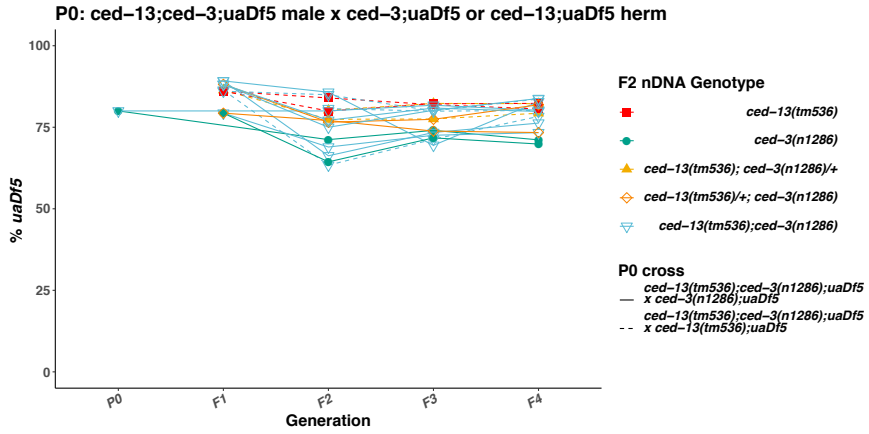

B.

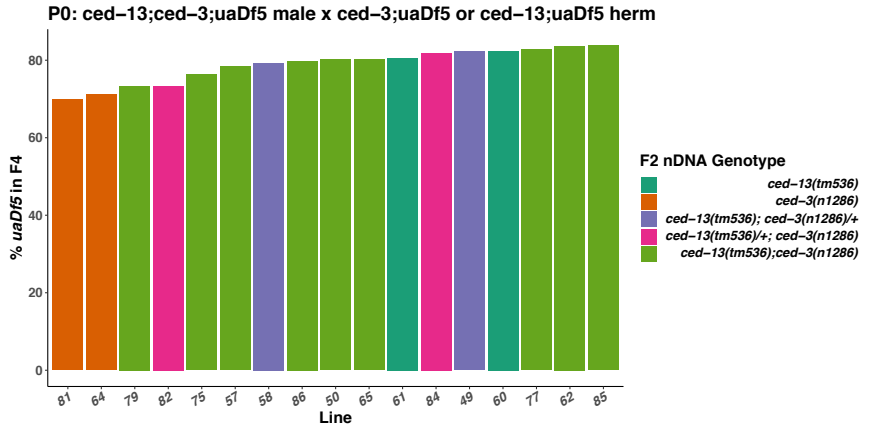

C.

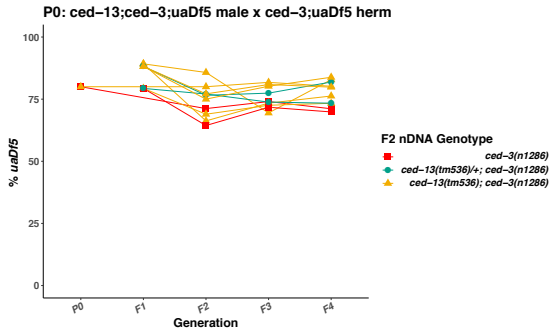

D.

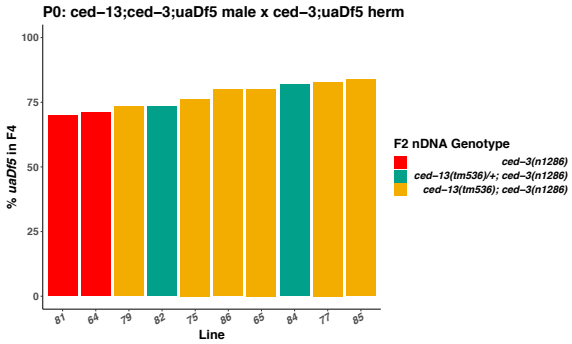

E. **F.**

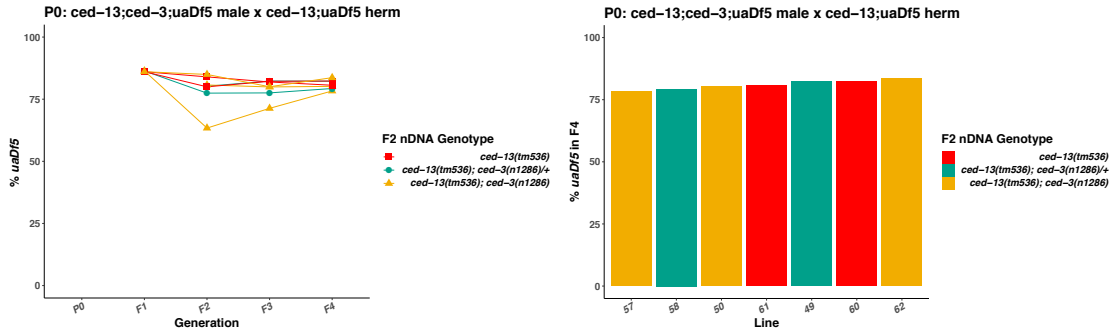

Figure 6. *ced-3;ced-13* lines do not show *uaDf5* removal within the first 4 generations following the cross. (A) Multigenerational ddPCR analysis of lines following the crosses of *ced-3(n1286);ced-13(tm536);uaDf5* males into *ced-13(tm536);uaDf5* (dashed lines) and *ced-3(n1286);uaDf5* (solid lines) hermaphrodites. **(B)** Bar plot showing the relationship between % *uaDf5* in F4 and F2 genotype for both crosses combined *(ced-3(n1286);ced-13(tm536);uaDf5* males crossed to both *ced-13(tm536);uaDf5* hermaphrodites and *ced-3(n1286);uaDf5* hermaphrodites). **(C)** Multigenerational ddPCR analysis of lines following the cross of *ced-3(n1286);ced-13(tm536);uaDf5* males into *ced-3(n1286);uaDf5* hermaphrodites. **(D)** Bar plot showing the relationship between % *uaDf5* in F4 and F2 genotype for crossing *ced-3(n1286);ced-13(tm536);uaDf5* males to *ced-3(n1286);uaDf5* hermaphrodites. **(E)** Multigenerational ddPCR analysis of lines following the cross of *ced-3(n1286);ced-13(tm536);uaDf5* males into *ced-13(tm536);uaDf5* hermaphrodites. **(F)** Bar plot showing the relationship between % *uaDf5* in F4 and F2 genotype for crossing *ced-3(n1286);ced-13(tm536);uaDf5* males to *ced-13(tm536);uaDf5* hermaphrodites. For all graphs, P0 and F2 both represent single worms, F1and F3 represent 10 worms pooled, and F4 is 20 worms pooled. P0 worms were older adults of unknown age, F1-F4 worms were day one adults. The F2 genotype is indicated by color.

Figure 7

A.

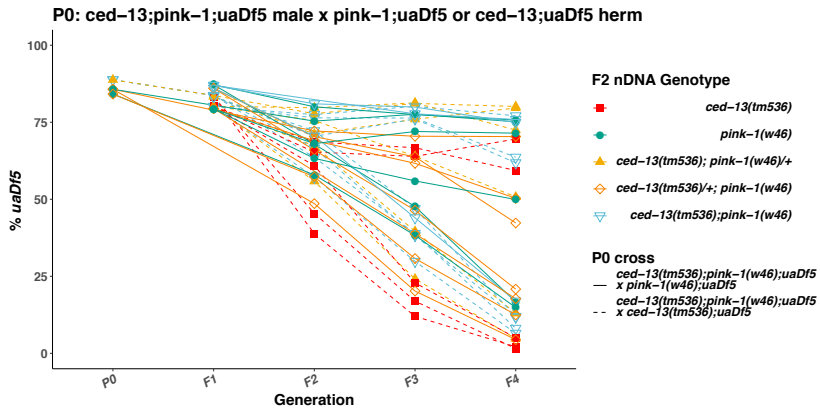

B.

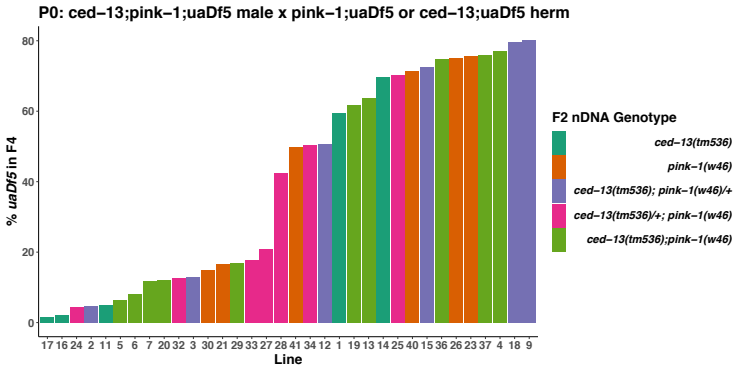

C.

F2 genotype	Number of lines with uaDf5 < 25% in F4
ced-13	3/5 (60%)
pink-1	2/6 (33%)
ced-13;pink-1/+	2/6 (33%)
ced-13/+;pink-1	4/7 (57%)
ced-13;pink-1	5/10 (50%)
All	**16/34 (47%)**

D.

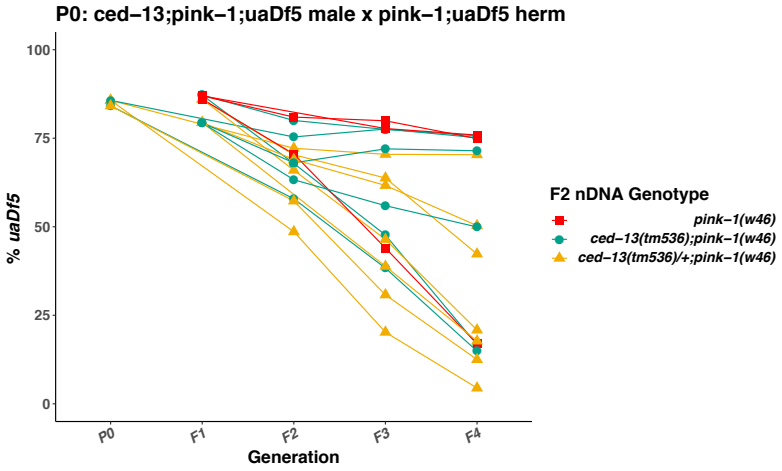

E.

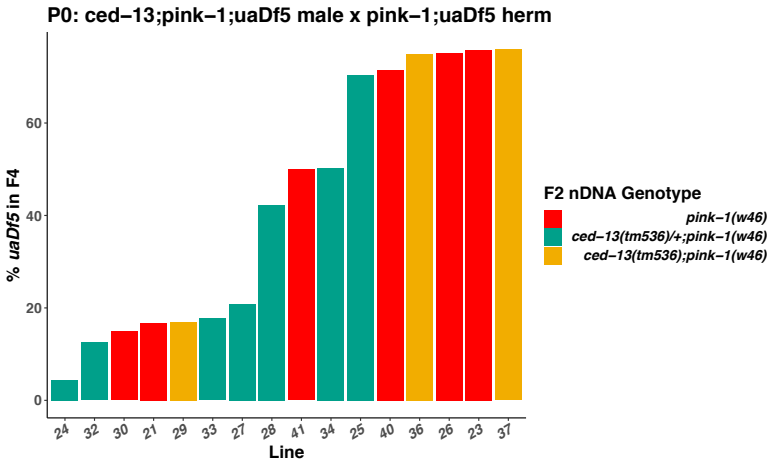

F.

F2 genotype	Number of lines with uaDf5 < 25% in F4
pink-1	2/6 (33%)
ced-13/+;pink-1	4/7 (57%)
ced-13;pink-1	1/3 (33%)
All	**7/16 (44%)**

G.

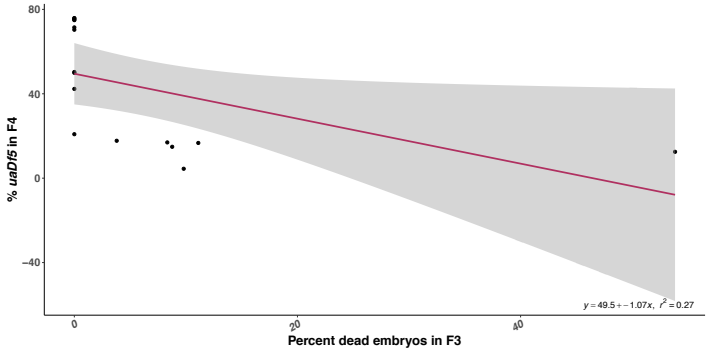

H.

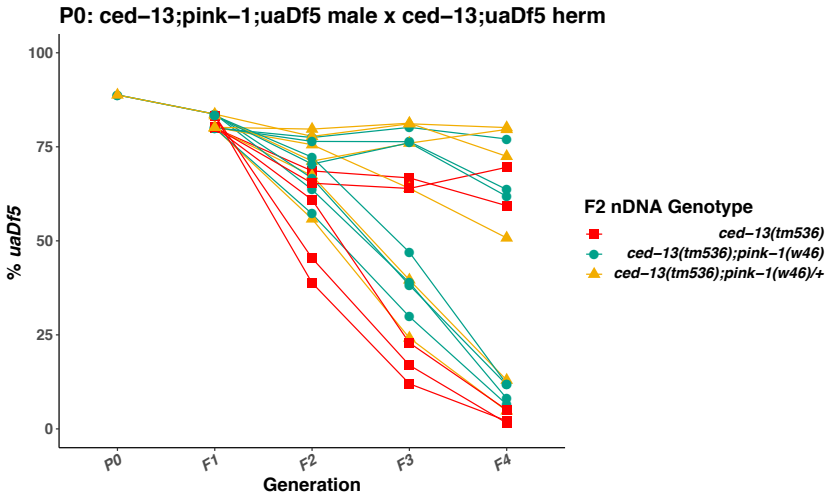

I.

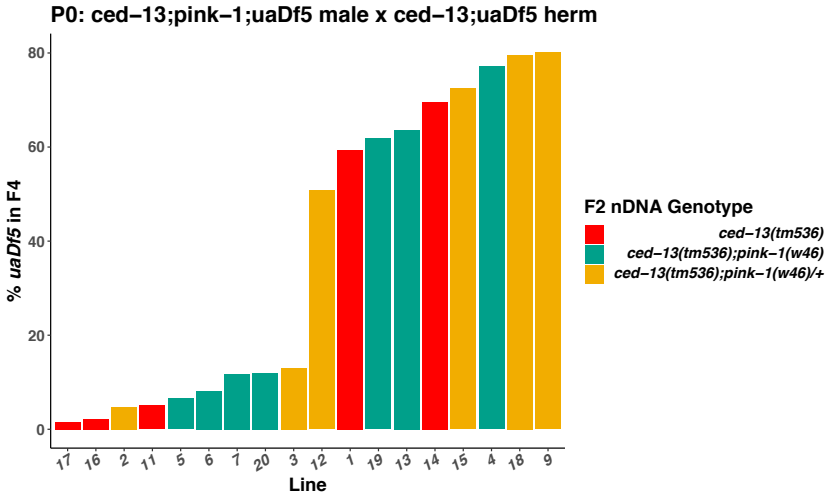

J.

F2 genotype	Number of lines with uaDf5 < 25% in F4
ced-13	3/5 (60%)
ced-13;pink-1/+	2/6 (33%)
ced-13;pink-1	4/7 (57%)
All	**9/18 (50%)**

K.

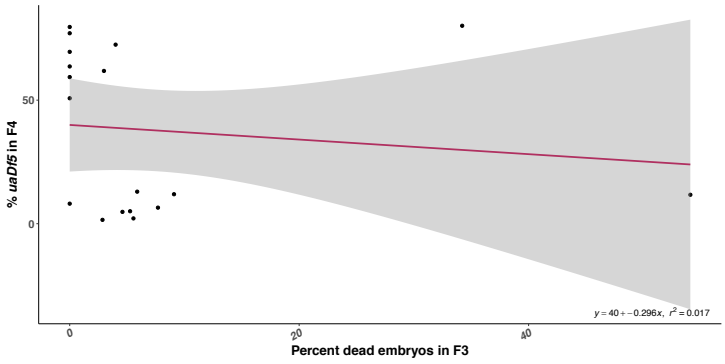

Figure 7. Following the IGE, lines show a striking and rapid removal of *uaDf5* within the first 4 generations following the cross that is not dependent on F2 genotype. (A) Multigenerational ddPCR analysis of lines following the crosses of *pink-1(w46);ced-13(tm536);uaDf5* males into *ced-13(tm536);uaDf5* (dashed lines) and *pink-1(w46);uaDf5* (solid lines) hermaphrodites. **(B)** Bar plot showing the relationship between % *uaDf5* in F4 and F2 genotype for both crosses combined *(pink-1(w46);ced-13(tm536);uaDf5* males crossed to *both ced-13(tm536);uaDf5* hermaphrodites and *pink-1(w46);uaDf5* hermaphrodites). **(C)** Table summarizing the number/percentage of lines resulting from both sets of crosses that have the rapid removal phenotype. (**D)** Multigenerational ddPCR analysis of lines following the cross of *pink-1(w46);ced-13(tm536);uaDf5* males into *pink-1(w46);uaDf5* hermaphrodites. **(E)** Bar plot showing the relationship between % *uaDf5* in F4 and F2 genotype for crossing *pink-1(w46);ced-13(tm536);uaDf5* males to *pink-1(w46);uaDf5* hermaphrodites. **(F)** Table summarizing the number/percentage of lines resulting from crossing *pink-1(w46);ced-13(tm536);uaDf5* males to *pink-1(w46);uaDf5* hermaphrodites that have the rapid removal phenotype. **(G)** Dot plot with a linear regression model showing the correlation between embryonic lethality and removal capacity of *uaDf5* following crossing *pink-1(w46);ced-13(tm536);uaDf5* males to *pink-1(w46);uaDf5* hermaphrodites. (**E)** Multigenerational ddPCR analysis of lines following the cross of *pink-1(w46);ced-13(tm536);uaDf5* males into *ced-13(tm536);uaDf5* hermaphrodites. **(F)** Bar plot showing the relationship between % *uaDf5* in F4 and F2 genotype for crossing *pink-1(w46);ced-13(tm536);uaDf5* males to *ced-13(tm536);uaDf5* hermaphrodites. **(G)** Table summarizing the number/percentage of lines resulting from crossing *pink-1(w46);ced-13(tm536);uaDf5* males to *ced-13(tm536);uaDf5* hermaphrodites that have the rapid

removal phenotype. **(H)** Dot plot with a linear regression model showing the correlation between embryonic lethality and removal capacity of *uaDf5* following crossing *pink-1(w46);ced-13(tm536);uaDf5* males to *ced-13(tm536);uaDf5* hermaphrodites. For all graphs, P0 and F2 both represent single worms, F1and F3 represent 10 worms pooled, and F4 is 20 worms pooled. P0 worms were older adults of unknown age, F1-F4 worms were day one adults. The F2 genotype is indicated by color.

Figure 8

A.

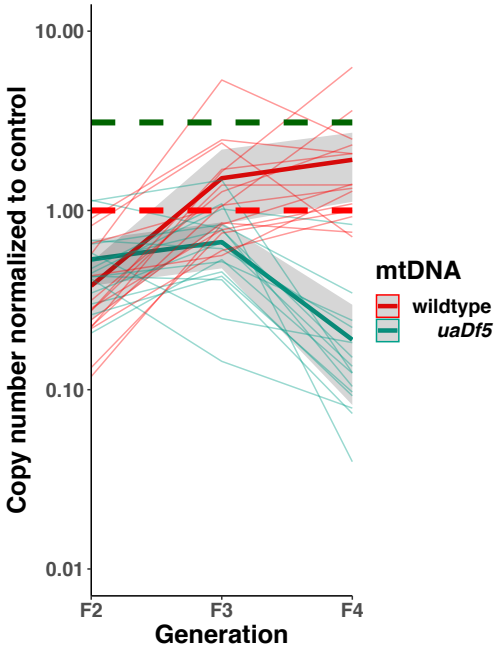
10.00
1.00
0.10
0.01
Copy number normalized to control
F2
F3
F4
Generation
mtDNA
wildtype
uaDf5

B.

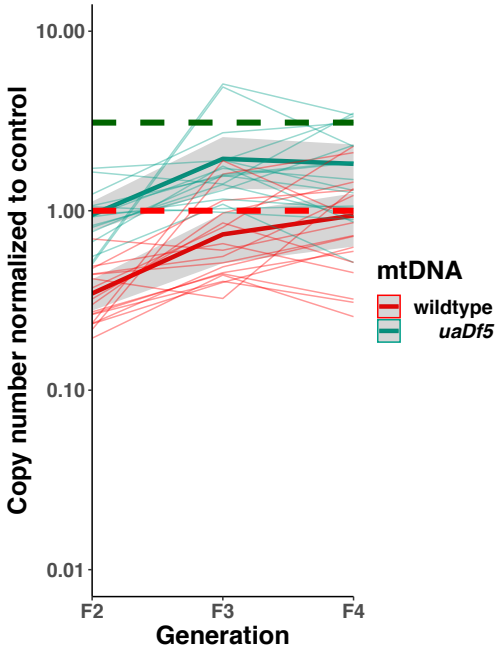
10.00
1.00
0.10
0.01
Copy number normalized to control
F2
F3
F4
Generation
mtDNA
wildtype
uaDf5

C.

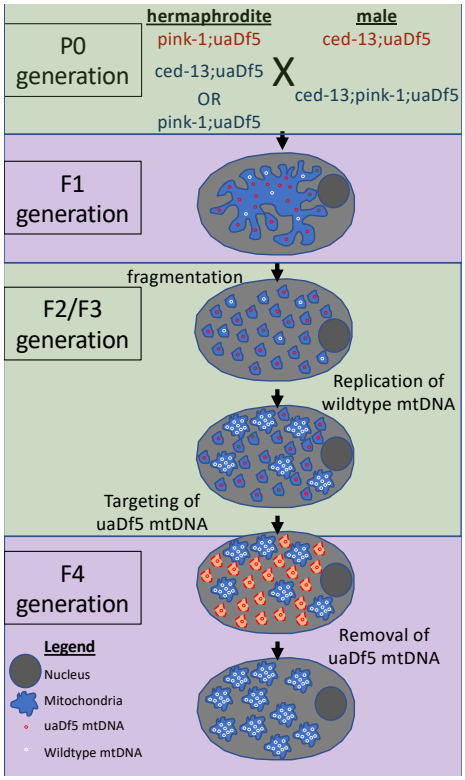
P0 generation
hermaphrodite
pink-1;uaDf5
ced-13;uaDf5
OR
pink-1;uaDf5
X
male
ced-13;uaDf5
ced-13;pink-1;uaDf5
F1 generation
fragmentation
F2/F3 generation
Replication of wildtype mtDNA
Targeting of uaDf5 mtDNA
F4 generation
Removal of uaDf5 mtDNA
Legend
Nucleus
Mitochondria
uaDf5 mtDNA
Wildtype mtDNA

Figure 8. WT-mtDNA is amplified to supranormal levels before subsequent *uaDf5* removal, suggesting global mitochondrial fission is crucial for the IGE phenotype. **(A)** Copy number analysis of WT-mtDNA (red) and *uaDf5* mtDNA (green) in lines exhibiting the rapid removal phenotype in the F2-F4 generation after the IGE. Dashed horizontal lines indicate the average *uaDf5* and WT-mtDNA levels seen in a wildtype nuclear background. Thick solid lines indicate the average copy number values of all the individual lines (thin solid), shaded regions indicate the confidence intervals. *uaDf5* copy number is normalized to WT-mtDNA copy number. Everything has been normalized to the same amount of input nDNA. **(B)** Copy number analysis of WT-mtDNA (red) and *uaDf5* mtDNA (green) in lines that do not exhibit the rapid removal phenotype in the F2-F4 generation after the IGE. Dashed horizontal lines indicate the average *uaDf5* and WT-mtDNA levels seen in a wildtype nuclear background. Thick solid lines indicate the average copy number values of all the individual lines (thin solid), shaded regions indicate the confidence intervals. *uaDf5* copy number is normalized to WT-mtDNA copy number. Everything has been normalized to the same amount of input nDNA. **(C)** Proposed model in which the IGE results in global mitochondrial fission, thus allowing for mitochondria containing WT-mtDNA to import replication machinery, followed by mitochondria containing *uaDf5*-mtDNA to be selectively degraded in a PINK-1-independent manner.

Chapter Four

mtDNA dynamics and mitochondrial function in the context of aging

SUMMARY

Mitochondrial DNA (mtDNA) mutations have been shown to accumulate in aging organisms and have been proposed to be a major contributor to the aging phenotype. In *C. elegans*, the occurrence of mitochondria carrying a 3.1 kb mtDNA deletion mutant, *uaDf5*, reproducibly increases in the germline with adult age, consistent with accumulation of mtDNA mutations in aging mammals. The fractional abundance of *uaDf5* is reduced in L1 stage larval progeny of these adults, suggesting the deployment of a mitochondrial quality control system between oocyte production and larval hatching. However, we found that maternal age correlates with *uaDf5* abundance in progeny: offspring of older mothers show a higher fractional abundance of *uaDf5*. We found that both the steady state, fractional abundance and age-related accumulation rate of *uaDf5* in adults is lowered in long-lived mutants (*clk-1, daf-2,* and *cep-1*) and increased in short-lived mutants (*daf-16* and *aak-2*). We also see that various fitness phenotypes are affected by the presence of *uaDf5* differentially in several lifespan mutants. Thus, the fractional abundance of *uaDf5* is a consistent marker of aging, and, in offspring, is indicative of the age of their mother.

INTRODUCTION

Mitochondrial disease and mtDNA mutations

Mitochondrial diseases are a group of conditions that affect mitochondrial function and affect as many as 1 in 4,300 people [55,59–64]. They can be due to mutations in either the mtDNA or the nDNA. Generally, these diseases present as dysfunction in the tissues or organs that have the largest energy demands, most commonly in the muscle and nervous system. Pathogenic mtDNA mutations were first

discovered in human patients in the late 1980s [65,66] and since then the body of literature identifying mtDNA-related disease has significantly grown [55]. Mitochondrial diseases also include those disorders in which there is a defect in mitochondrial dynamics, quality control, or communication between the mitochondria and ER [61,62]. One common trait among mitochondrial diseases is that they tend to be progressive in nature, due to the age-related accumulation of mutant mtDNA [60,63,67].

In order to progress toward mitochondrial disease therapy, we must learn more about the mechanisms that cells employ to remove deleterious mtDNA. There is evidence that some processes regulate mtDNA maintenance, such as mitochondrial fission/fusion dynamics and mitophagy [67–73], the mitochondrial unfolded protein response (UPR^{MT}; [74–80]), and most recently the insulin signaling pathway (IIS; [81,82]). However, all of these processes only seem to be part of the story in that their effects on mtDNA mutation levels are intermediate. Understanding how mtDNA mutations are removed is not only important for the treatment of the subset of mitochondrial diseases that are caused by mtDNA mutations, but also for the prevention of aging.

Mitochondria in aging

The problem of aging has been one that has confounded scientists over the years [93]. Many theories that try to give a molecular basis of aging have been proposed, but there has been limited experimental evidence. However, the most widely accepted idea in the field of aging, the “free radical theory”, places mitochondria front and center [94–97].

The free radical theory of aging was first proposed by Denham Harman in 1956 [96]. This theory states that increased mitochondrial respiration will lead to an increase in reactive oxygen species (ROS) levels, which in turn results in an accumulation of

oxidative damage to nucleic acids, proteins, and lipids. This oxidative damage is thought to be the driving force behind aging.

Evidence supporting this theory includes mutations that affect ROS levels, mitochondrial function, and metabolism shifts [51,53,54,98]. Mutations that increase lifespan are associated with decreased oxygen consumption (isp-1; Rieske iron sulfur protein of complex III in the electron transport chain [99]), a shift from respiration to other metabolic pathways that don't require mitochondria (the insulin/IGF-1 receptor (IGFR) homolog DAF-2 [100] and the leucyl-tRNA synthetase 2 (LARS2) homolog LARS-2 [101]), and loss of mitochondrial function (the mitochondrial hydroxylase (MCLK1) homolog CLK-1 [102]) [2] . If animals are treated with mitochondrial inhibitors, such as antimycin A, there is a notable increase in lifespan. Additionally, increased expression of ROS scavengers via treatment with superoxide dismutase mimetics such as EUK-8 and EUK-134 result in an increased lifespan [2]. Mutations that are associated with increased ROS levels (such as the succinate dehydrogenase complex subunit C (SDHC) homolog MEV-1 [103]), as well as sensitivity to oxidative damage and hyperoxia (such as the NADH:ubiquinone oxidoreductase core subunit S2 (NDUFS2) homolog GAS-1 [104]), are associated with decreased lifespan [2].

The insulin/IGF-1 signaling (IIS) pathway in mitochondrial surveillance

The highly conserved insulin/IGF-1 (insulin-like growth factor-1) pathway (IIS) has been studied for years in regard to its central role in aging [131–133]. In *C. elegans*, the IIS pathway is regulated by the binding of insulin-like peptides (ILPs) to the insulin/IGF-1 receptor (IGFR) homolog DAF-2, which ultimately results in inhibition of DAF-16/FoxO (a member of the FoxO family of transcription factors) from entering the

nucleus to activate transcription of a set of genes that fight various forms of cellular stress [82,100] (Fig. 1.4B). Once bound by ILPs, DAF-2/IGFR activates AGE-1/PI3K, a phosphoinositide 3-kinase [134], which in turn activates a set of serine/threonine kinases including PDK-1/PDK (phosphoinositide-dependent kinase [135]) and Akt/Protein Kinase B (PKB) family members AKT-1 and AKT-2 [136]. Their activation then causes phosphorylation of DAF-16/FoxO, which then interacts with PAR-5 and FTT-2, a set of 14-3-3 proteins, thus inhibiting DAF-16/FoxO from translocating to the nucleus to regulate transcription and interact with other nuclear factors including SIR-2.1/SIRT1 (in the sirtuin family of NAD^+-dependent deacetylases; [137]), HCF-1/HCFC2 (host cell factor; [138]), HSF-1 (a heat shock transcription factor; [139]) and SKN-1/Nrf (a Nrf family transcription factor; [140]). DAF-18/PTEN (phosphatase and tensin homolog, a lipid phosphatase; [141,142]) counteracts AGE-1/PI3K signaling, and PPTR-1/PP2A (a serine-threonine phosphatase; [143]) counteracts AKT-1 signaling, thus acting as inhibitors of DAF-2/IGFR [82].

The IIS pathway is not only associated with regulation of lifespan and aging but is also implicated in a large set of processes, including dauer arrest, L1 arrest, germline proliferation, stress resistance, fat metabolism, and neuronal/behavioral programs [82]. Given the part that mitochondria play in aging and metabolism, it may not be surprising that researchers recently discovered that the IIS pathway is a crucial regulator of mtDNA quality control; they found that inhibition of the IIS pathway results in a rescue of various fitness parameters in a mtDNA mutator strain [81]. We further explore the role of the IIS pathway and other non-IIS dependent lifespan-regulating genes (including the coenzyme Q7 hydroxylase (COQ7) homolog CLK-1/MCLK1 [144], the genotoxic stress response activator CEP-1/p53 [145], and the von Hippel-Lindau tumor suppressor (VHL) homolog

VHL-1 [146]) on mtDNA maintenance. Given the likely central role that mitochondria play in the process of aging, examination of how deleterious mitochondrial mutations behave as the organism ages will give crucial insight into potential strategies for slowing the aging process.

C. elegans mtDNA and the mtDNA deletion "*uaDf5*"

Although separated by hundreds of million years of evolution, there are many similarities between human and *C. elegans* mtDNA (Fig. 1.1). Human mtDNA has only one more gene than the *C. elegans* counterpart, ATP8, a subunit of complex 5 [3], and the overall size of the mitochondrial genome is roughly equal, with the size of the *C. elegans* mtDNA being 13,794 bp (compared to 16,569 bp in humans) [2]. Interestingly, a strain of *C. elegans* harbors a 3.1kb mtDNA deletion "*uaDf5*" that is maintained indefinitely in a state of stable heteroplasmy, meaning that it is never lost from the mtDNA population even after over 100 generations of propagation, even though it is presumably deleterious [201]. *uaDf5* thus serves as a valuable tool for studying the mechanisms governing mtDNA quality control throughout development (see Chapter 3).

The life cycle of the worm includes embryogenesis within an eggshell and once it hatches it is in the first larval stage, L1, where it has 558 somatic cells. The worm then goes through 3 more larval stages, L2, L3, and L4, before going through its final molt to become an adult hermaphrodite which has 959 somatic cells and can make up to 300 self-progeny [105] (Fig. 1.2). The total time between fertilization and becoming a gravid adult takes about 3 days at 20° C. Estimates of the mtDNA copy number *in C. elegans* range from 25,000 [106] to 90,000 [107] in the single-cell embryo, which remains largely unchanged through the L3 stage of larval development, suggesting that the mitochondrial

genomes are roughly equally divided amongst the cells up until the L3 stage. The copy number then undergoes two incremental increases, concurrent with the growth of the germline. The L3-L4 transition sees an increase to 130,000 (5x) - 250,000 (3x), followed by a secondary increase in the L4-adult transition, resulting in a total of 800,000 (6x) - 4,000,000 (16x) copies. This results in an overall 30-40 fold increase in mtDNA in the animal between the embryo and adult, and the majority of this replication is specific to the oocytes (Fig. 1.2) [106,107].

RESULTS

Adults accumulate *uaDf5* as they age, and progeny from older mothers have a higher fractional abundance of *uaDf5*

mtDNA mutations have been shown to accumulate in tissues as organisms age, and this accumulation has been suggested to be one of the main contributors to aging [54,213,214]. We wanted to know if the mtDNA deletion *uaDf5* accumulates in aging worms. To do this, we measured the fractional abundance of *uaDf5* in adults at different ages: day 1 (defined as the first day egg laying begins), day 2, day 3, day 4, and day 10 (Fig. 4.1A). Day 1 through day 4 of adulthood spans the time in which the vast majority of progeny are laid. After day 4, adults transition into a post-gravid state due to the depletion of sperm [196,215,216]. Day 10 adults represent very old worms and is close to the average lifespan of a wildtype worm. Analysis of fractional abundance of *uaDf5* in aging adult worm populations reveals an accumulation of *uaDf5* by ~8% throughout gravidity (day 1: 72.56 ± 1.36%; day 2: 78.5 ± 0.43%; day 3: 80.48 ± 0.38%; day 4: 80.91 ± 0.59%), followed by another increase of about 4% over the 6 days post-egg laying (84.55 ± 0.14% for day 10 adults). Analysis of the fractional abundance of *uaDf5* was

measured in 40 different mutant backgrounds and the trend was consistent across all strains (Fig. 4.1C). This age-related accumulation of *uaDf5* in adult worms mirrors the accumulation of mtDNA mutants seen in aging mammals and suggests that investigation of *uaDf5* in *C. elegans* could be a useful tool for studying the role that mtDNA mutations play in aging.

The measurable increase in the fractional abundance of *uaDf5* in aging gravid adults led us to question if progeny from younger adults inherit a lower load of *uaDf5* than progeny from older adults. Therefore, we measured the fractional abundance of *uaDf5* in populations of L1 larvae from day 1 – day 4 adults (Fig. 4.1A). We found that there is a reduction in *uaDf5* load between mother and offspring (decrease of 1.03% from day 1 adults to offspring, 3.41% from day 2 adults, 2.3% from day 3 adults, and 0.61% from day 4 adults), and that offspring from older mothers have a higher fractional abundance of *uaDf5* than the offspring of younger mothers (71.53% in L1 progeny from day 1 adults compared to 80.3% in L1 progeny from day 4 adults, showing an 8.77% increase). We measured the transmission of *uaDf*5 from mother to offspring in six other strains and found this trend to be consistent, with a noticeable increased level of removal between mother and offspring from day 4 adults in strains that have a higher steady state fractional abundance of *uaDf5* (reduction of 8.2% in *atfs-1(et15)*, 10.07% in *ced-10(n1993),* and 9.55% in *ced-13(sv32))* compared to strains that have a lower steady state fractional abundance of *uaDf5* (reduction of 5.58% in *atfs-1(tm4525),* 6.14% in *ced-3(n2454),* and 3.59% in *daf-2(m41))* (Fig. 4.1B). This indicates that there is a level of mtDNA quality control that occurs sometime between oocyte production and L1 hatching.

Age-related accumulation of *uaDf5* occurs predominantly in the germline

We next wondered if the age-related accumulation of *uaDf5* is occurring predominantly in the maternal germline or in the soma. To answer this, we measured *uaDf5* accumulation in aging adults of temperature sensitive mutants that lack germline development when put at the restrictive temperature of 25C (but have normal germline development at the permissive temperature of 15C) (Fig. 4.2). The FEM proteins are required for spermatogenesis and a gain-of-function mutant in the *fem-3* gene, *fem-3(q20),* results in masculinization of the germline so that the hermaphrodites only produce excess sperm and no oocytes [89,106,217]. GLP-1 is a Notch family receptor that is necessary for the maintenance and proliferation of germline stem cells [218]. *glp-1(q231)* is a temperature sensitive mutant that results in the production of only 4-8 germline cells, compared to the ~1500 that are produced in wildtype worms, with no impact on somatic gonad development [106]. GLP-4 is another protein responsible for the proliferation of the germline, although its function at the molecular level is unknown [219]. The *glp-4(bn2)* mutant, similar to *glp-1(q231),* only produces a handful of germline cells (~12) compared to wildtype with no effect on somatic gonad development [106]. All three mutants showed a reduction of the accumulation of *uaDf5* in aging adults, although *glp-1* had a mild reduction which was not statistically significant (an increase of 2.8% by day 4 at the permissive temperature dropped to 1.28% by day 4 at the restrictive temperature). The *fem-3(q20)* mutant exhibited the strongest effect with a large decrease in *uaDf5* levels as the worms aged (an increase of 6.56% by day 4 at the permissive temperature dropped to and actual decrease by 3.13% by day 4 at the restrictive temperature). *glp-4(bn2)* exhibited a strong effect with an overall decrease by day 4 of adulthood (an increase of 8.49% by day 4 at the permissive temperature dropped

to a slight decrease by 1.43% by day 4 at the restrictive temperature). These results support a model whereby the accumulation of *uaDf5* is largely happening in the germline. Analysis of *uaDf5* levels in these mutants in day 10 adults grown at the restrictive temperature shows a marked increase of *uaDf5* (up by 7.44% from day 1 levels in *fem-3(q20),* 0.87% in *glp-1(q231),* and 8.84% in *glp-4(bn2))* suggesting that accumulation does occur in the soma after egg laying ceases.

Long-lived mutants have lower steady state fractional abundance of *uaDf5*, short-lived mutants have a higher steady state fractional abundance

The link between accumulation of mtDNA mutations and aging led us to question if long-lived mutants have lower steady state levels of *uaDf5,* since presumably these long-lived mutants should have more effective mtDNA quality control machinery. To answer this, we measured steady state population levels of *uaDf5* in a set of long-lived mutants (see Table 4.1 for a list of lifespan mutants used in the analyses). The mutants analyzed are from the IIS pathway, the main pathway known to influence lifespan in *C. elegans (daf-2, age-1)* [82,100,144,220], the mitochondrial ubiquinone pathway (*clk-1)* [102,132,144,220,221], response to hypoxia *(vhl-1)* [146], and the DNA damage response system *(cep-1)* [19,145,186,210]. The majority of long-lived mutants had significantly lower steady levels of the fractional abundance of *uaDf5*, including three alleles of *daf-2 (e1391*: 21.59 ± 1.31%; *e1370*: 42.86 ± 1.57%; *m41:* 56.86 ± 2.31%), *clk-1(qm30)* (23.18 ± 0.76%), and *cep-1(gk138)* (50.93 ± 1.76%). Mutants for *age-1* and *vhl-1* did not show a decrease in the fractional abundance of *uaDf5* (Fig. 4.3A). Repeated studies need to be done on those three mutants to confirm that the results are not due to experimental error.

We also investigated if the converse is true: if short-lived mutants have higher steady state levels of the fractional abundance of *uaDf5*. To do this, we analyzed two genes involved in the IIS pathway that act downstream of *daf-2: daf-16* and *aak-2* (Fig. 4.3B) [82]. Mutants in these genes result in a decreased lifespan. All mutants analyzed showed an increase in the fractional abundance of *uaDf5* (*daf-16(mu86)* 76.93 ± 0.84%; *daf-16(mgDf50)* 77.56 ± 0.44%; *aak-2(ok524)* 79.28 ± 0.74%; *aak-2(gt33)* 81.6 ± 0.41%), although only the *aak-2* alleles were significant. These results suggest a link between mtDNA cleanup capacity and aging.

Long-lived mutants accumulate *uaDf5* at a slower rate, short-lived mutants accumulate *uaDf5* at a faster rate

The association between the steady state levels of the fractional abundance of *uaDf5* and rate of aging led us to question if long-lived mutants accumulate *uaDf5* at a slower rate. To test this, we measured the accumulation rate of *uaDf5* in a set of long-lived mutants (Fig. 4.4A). Several of the mutants are in the IIS pathway (*daf-2* and *age-1*) which is the main lifespan-regulating pathway studied in *C. elegans.* Other long-lived mutants analyzed act in pathways independent of the IIS pathway and include *clk-1, cep-1,* and *vhl-1.* Linear regression analysis reveals that most of the long-lived mutants accumulate *uaDf5* at a slower rate than is observed in a wildtype background, as seen with a lower slope value on the linear regression model (Fig. 4.4B). The outlier that accumulates *uaDf5* at a much higher rate than wildtype, *daf-1(m41),* may be the result of experimental error and more studies need to be done to see if the effect is real. Both the *age-1* and *vhl-1* mutants have a rate of accumulation similar to the *uaDf5* control, but

their impact on lifespan extension is not as strong as *daf-2, clk-1,* or *cep-1,* so these results may be reflective of that fact (data not shown).

We next wanted to see if short-lived mutants have a higher rate of accumulation of *uaDf5*, which would support the theory that mtDNA mutant accumulation is causal of the aging phenotype. To confirm this, we measured *uaDf5* accumulation in short-lived mutants involved in the IIS pathway (Fig. 4.4C). We analyzed *daf-16* and *aak-2* mutants, which act as downstream inhibitors of DAF-2/IGFR-dependent lifespan extension [82]. We also analyzed *daf-16;daf-2* double mutants to see if the reduced accumulation of *uaDf5* in *daf-2* mutants is due to activity of the IIS pathway. While the *aak-2(gt33)* and *daf-16(mgDf50)* mutants did not have an increased accumulation rate, most of the short-lived mutants analyzed, including the *daf-16;daf-2* doubles, exhibit an increased rate of *uaDf5* accumulation as seen with linear regression analysis (Fig. 4.4D) suggesting that mtDNA mutant accumulation is a predictor of aging.

daf-16 **partially rescues the** ***daf-2*** **phenotype**

The *daf-2* and *daf-16* results suggest that the IIS pathway may be acting directly on mtDNA quality control. In order to confirm this, we crossed *daf-16(mu86)* males into *daf-2;uaDf5* mutant hermaphrodites to see if *daf-16*, which acts downstream of *daf-2*, rescues the *daf-2* phenotype of a low fractional abundance of *uaDf5*. We observed a partial rescue in each of the double mutants analyzed (*daf-2(e1391);uaDf5* 21.59 ± 1.31% compared to *daf-2(e1391);daf-16(mu86);uaDf5* 51 ± 0.39%; *daf-2(e1370);uaDf5* 36.64 ± 1.31% compared *to daf-2(e1370);daf-16(mu86);uaDf5* 64.91 ± 1.95%; *daf-2(m41);uaDf5* 56.86 ± 2.31% compared *to daf-2(m41);daf-16(mu86);uaDf5* 68.8 ± 1.06%), suggesting that *daf-2* and *daf-16* are indeed acting on *uaDf5* via the IIS pathway

(Fig. 4.5). It is possible that the rescue was only partial because the double mutants were not grown for enough generations to get a full recovery of *uaDf5* to its wildtype level. In order to determine if this is the case, further studies need to be done in which the double mutants are grown out for more generations to see if the fractional abundance of *uaDf5* continues to increase.

There is an additive effect on the fractional abundance of *uaDf5* in double mutants composed of long-lived mutants, suggesting they act on *uaDf5* through independent pathways

The long-lived mutants analyzed are known to act on lifespan via independent pathways, but it is a formal possibility that they act on mtDNA via a common pathway. To investigate this, we generated double mutants comprised of long-lived mutants from the various pathways and measured the fractional abundance of *uaDf5* in those double mutants to see if there is an additive effect, which would suggest there are multiple pathways that act on both lifespan regulation and mtDNA. Analysis of *daf-2(e1391);cep-1(gk138);uaDf5* (1.48 ± 0.85*%), daf-2(e1391);clk-1(qm30);uaDf5* (0 ± 0%) and *cep-1(gk138);clk-1(qm30);uaDf5* (0.0074 ± 0.007%) double mutants show an additive effect in which the double mutants have an extremely low fractional abundance or even complete removal of *uaDf5*, suggesting all three long-lived mutants are acting on mtDNA through entirely independent pathways (Fig. 4.6A,B).

Fitness parameters are differentially affected by *uaDf5* in lifespan mutants

Does the presence of a mtDNA mutant impact organismal fitness in lifespan mutants? We tested various fitness parameters, including lifespan, brood size, embryonic

lethality, and unfertilized oocyte production (see also Chapter 3) in lifespan mutant backgrounds from different pathways both with and without *uaDf5* to see if these independently acting lifespan mutants tolerate *uaDf5* differentially from wildtype (Fig. 4.7). We tested fitness parameters in two long-lived mutants, *clk-1(qm30)* and *cep-1(gk138)*, and one short-lived mutant, *daf-16(mu86)*. We found that lifespan was not affected by the presence of *uaDf5* in all three mutants analyzed (wildtype 14 ± 0.7 days compared to *uaDf5* 15 ± 1.1 days; *clk-1(qm30)* 21 ± 1.2 days compared to *clk-1(qm30);uaDf5* 22 ± 1.4 days; *cep-1(gk138)* 18 ± 1.1 days compared to *cep-1(gk138);uaDf5* 16 ± 1 days; *daf-16(mu86)* 13 ± 0.6 days compared to *daf-16(mu86);uaDf5* 12 ± 0.7 days) (Fig. 4.7A). Analysis of the effect of *uaDf5* on fitness in a *cep-1(gk138)* background gave the most shocking results, with a significant increase in brood size (*cep-1(gk138)* 240 ± 16 compared to *cep-1(gk138);uaDf5* 311 ± 10) (Fig. 4.7B) and a marked decline in embryonic lethality (*cep-1(gk138)* 12.76 ± 3.94% compared to *cep-1(gk138);uaDf5* 5.71 ± 2.41%) (Fig. 4.7C), suggesting that the presence of *uaDf5* actually increases fitness in a *cep-1(gk138*) background (see Discussion). The *clk-1(qm30)* mutant had a moderate reduction in brood size (*clk-1(qm30)* 163 ± 10 compared to *clk-1(qm30);uaDf5* 151 ± 10) and a moderate increase in embryonic lethality (*clk-1(qm30)* 4.04 ± 0.57% compared to *clk-1(qm30);uaDf5* 5.65 ± 0.88%), both much less prominent than what is seen in a wildtype background (brood size: wildtype 308 ± 6 compared to *uaDf5* 203 ± 17; and embryonic lethality: wildtype 1.79 ± 0.36% compared to *uaDf5* 4.44 ± 1.19%), suggesting that *clk-1(qm30)* is more tolerant of *uaDf5*. The *daf-16(mu86)* mutant on the other hand had a reduction in brood size (*daf-16(mu86)* 286 ± 8

compared to *daf-16(mu86);uaDf5* 168 ± 16) and an increase in embryonic lethality (*daf-16(mu86)* 1.9 ± 0.44% compared to *daf-16(mu86);uaDf5* 4.86 ± 1.24%) which both strongly resemble the trends seen in a wildtype background, suggesting its toleration of *uaDf5* is unaltered. Lastly, analysis of unfertilized oocyte production shows a slight increase in the long-lived mutants, while the short-lived mutant *daf-16(mu86)* has a decrease that mirrors the wildtype background (wildtype 23.06 ± 1.91% compared to *uaDf5* 18.14 ± 2.39%; *clk-1(qm30)* 20.68 ± 2.76% compared to *clk-1(qm30);uaDf5* 28.58 ± 3.65%; *cep-1(gk138)* 26.86 ± 2.83% compared to *cep-1(gk138);uaDf5* 34.81 ± 2.43%; *daf-16(mu86)* 23.58 ± 2% compared to d*af-16(mu86);uaDf5* 12.38 ± 1.87%) (Fig. 4.7D). Thus, the long-lived mutants show an improvement in several fitness parameters in the response to *uaDf5*, while the short-lived mutant shows no observable deviation from wildtype. This suggests that mtDNA mutations in long-lived mutants may actually activate programs that improve overall health of the organism, though the mechanisms are unknown.

DISCUSSION

We present several lines of evidence showing an association between aging and the accumulation of mutant mtDNA in *C. elegans*, using the mtDNA deletion strain *uaDf5.* We show that *uaDf5* accumulates in the germline of aging adults, that offspring from older mothers inherit a larger load of *uaDf5* than their siblings from younger mothers, and that mtDNA quality control is improved in long-lived mutants.

The fractional abundance of *uaDf5* increases during adulthood, and is largely occurring in the germline

Analysis of the fractional abundance of *uaDf5* in aging adults with a wild type nuclear background shows an accumulation of *uaDf5* in aging worms that occurs throughout gravidity and beyond. To determine if the accumulation is occurring in the germline, we analyzed three temperature sensitive mutants that inhibit female germline development. The gof mutant *fem-3(q20)* produce excess sperm and no oocytes, while the *glp-1(q231)* and *glp-4(bn2)* mutants both result in the production of only a handful of oocytes [106]. When oocyte production is inhibited in *fem-3(q20), glp-1(q231),* and *glp-4(bn2)* backgrounds, we see a reduction of the accumulation rate during gravidity, showing that the majority of the age-related accumulation occurs in the germline. Analysis of the accumulation beyond gravidity [196], in day 10 of adulthood, shows an increase in the fractional abundance of *uaDf5* demonstrating that accumulation is also occurring in the somatic tissues throughout the aging process. This demonstrates that *uaDf5* dynamics during aging mirror those of mutant mtDNAs studied in other organisms. Does the accumulation specific to the germline result in the aging phenotype? Removal of the germline via ablation or mutations results in an extended lifespans [222,223], but it is unclear how much increased lifespan is due to the accumulation of mutant mtDNA since the lack of germline results in a plethora of cellular responses, any of which could be the main cause of the associated lifespan extension. Why is aging associated with accumulation of mutant mtDNA? Does aging cause the accumulation, or does the accumulation cause aging? These results do not give direct answers to these questions, and more studies need to be done to determine the causality linking these aging and mutant mtDNA accumulation.

uaDf5 is transmitted from mother to offspring with a moderate process of cleanup, and progeny from older mothers inherit a larger fractional abundance of _uaDf5_ than progeny from young mothers

Analysis of L1 progeny from different aged-mothers reveals that the load of *uaDf5* is transmitted from mother to offspring such that progeny from older mothers inherit a larger mutant mtDNA burden than their siblings from younger mothers, with evidence of a cleanup mechanism. This tells us that there is a level of mtDNA quality control that happens sometime between oocyte maturation and L1 hatching. This window spans many potential areas in development in which mtDNA quality control could be occurring, including germline PCD, oocyte maturation, and the entirety of embryogenesis. Narrowing down the window in which this cleanup occurs will lead to a better understanding of which processes are involved in the cleanup of mtDNA that we have observed between mother and offspring. Analysis of the transmission from mother to offspring in mutants in germline PCD, including *ced-13(sv32)* [19,89,179,183–186] and *ced-10(n1993)* [180–182], shows that the transmission-associated cleanup is slightly reduced in younger mothers but increased in old mothers, suggesting that germline PCD may play a larger role in mtDNA quality control in young mothers versus old mothers. This may indicate a switch from germline PCD to some other cleanup process that is inhibited by germline PCD as mothers get older, possibly due to increased stress associated with aging making the germline PCD pathway less efficient. To determine the level of cleanup occurring during the process of embryogenesis, analysis of different staged embryos needs to be done. Analysis of the fractional abundance in dead embryos will reveal how much of the decrease observed between mother and offspring is due to culling at the organismal level.

Mutants that regulate lifespan via independent pathways, including the IIS pathway, regulate the control of both the steady state fractional abundance and accumulation rate of *uaDf5*

The consistent rate of age-related *uaDf5* accumulation observed in various genetic backgrounds led us to question if mutants that affect lifespan have a lower rate of accumulation of *uaDf5*. We found that not only is the rate of accumulation lowered in long-lived mutants (*daf-2* (IIS pathway; [82]), *clk-1* (mitochondrial function; [102,221]), and *cep-1* (genotoxic stress-response; [19,145,186]), but also the steady state level of the fractional abundance of *uaDf5* is drastically lowered. This was a common phenotype observed in long-lived mutants that act on lifespan through independent pathways. However, there were two long-lived mutants analyzed that did not have lowered steady state abundance or accumulation rate, *vhl-1* (involved in hypoxia response [146]) and *age-1* (in the IIS pathway [82]). Further analysis of these strains needs to be done to see if this is an allele-specific effect, or if some long-lived mutants do not act on mtDNA quality control, suggesting the link between lifespan and mtDNA quality control is not as global as our other results suggest.

Overall, our results show a link between the ability to remove deleterious mtDNA and lifespan extension, supporting the idea that mutant mtDNA plays a central role in the aging phenotype. Further bolstering this link is our analysis of short-lived mutants (*daf-16* and *aak-2,* both involved in the IIS pathway [82]) which reveals that the converse is true; a reduction in lifespan is associated with an increased rate of accumulation of *uaDf5* in addition to higher steady state levels of the fractional abundance of *uaDf5.* Thus, we have shown that there is indeed a dependency on mtDNA quality control for regulation of lifespan. How it is that the independent lifespan regulation pathways act on mutant

mtDNA has yet to be determined. Perhaps the pathways all converge on a global mitochondrial stress response pathway such as mitophagy. Double mutant analysis of lifespan-extension mutants from the different pathways reveals that there is an additive effect on the mtDNA quality control machinery suggesting that the lifespan-regulating pathways converge on a common system for mutant mtDNA removal. Further studies need to be done to determine what the common mtDNA quality control system is. Likely candidates include mitochondrial fission/fusion [68,70,108], mitophagy [71,72,115], and the mitochondrial unfolded protein response (UPR^{MT}; [75–80]) which are known to act in mtDNA quality control.

uaDf5 has differential effects on fitness parameters in long-lived and short-lived mutants

Analysis of how the presence of mutant mtDNA affects fitness in lifespan-associated mutants reveals that long-lived mutants have fewer negative consequences on health than short-lived mutants. Of particular note, *cep-1(gk138)* mutants actually exhibit increased fitness parameters (lifespan, brood size, and embryonic lethality) when *uaDf5* is present. How it is that a mutant mtDNA results in an improvement in organismal health is a question of great interest. Perhaps, in a *cep-1* background, the presence of mutant mtDNA activates stress response pathways in a way that increases general quality control pathways to a level that is actually beneficial to the organism. Further analysis needs to be done to dissect how mutant mtDNA triggers various quality control pathways in lifespan-associated mutants in order to more thoroughly understand these dynamics of stress-response pathways and developmental fidelity.

MATERIALS AND METHODS

Culturing of nematodes

Nematode strains were maintained at on NGM plates as previously described at either 20°C or 15°C for the temperature-sensitive strains [199]. Please refer to appendix A1 for a table detailing all strains used in this dissertation. Strains without a JR designation were either provided by the CGC which is funded by NIH Office of Research Infrastructure Programs (P40 OD010440) or were obtained from the Mitani lab (strains with a FX designation or JR strains containing alleles with a tm designation were generated from Mitani lab strains) [200].

Population collection by age

Upon retrieval of a stock plate for a given strain, 3 chunks were taken from the stock plate and placed onto 3 separate large NGM plates to create 3 biological replicate "lines". Each of these lines was chunked approximately each generation to fresh large NGM plates (every 3 days if maintained at 20°C or 25°C, or every 4 days if maintained at 15°C, being careful to not let the worms starve between chunks). After 4 generations of chunks, an egg prep was performed on each line (as described previously; [199]) and left to spin in M9 overnight to synchronize the hatched L1s. The next day, each egg prep was plated onto 3 large seeded plates at an equal density and the worms were left to grow to day 2 adults (second day of egg laying). The day 2 adult worms were egg prepped for synchronization and left to spin in M9 overnight. The next day, each egg prep was plated onto 5 large NGM plates at equal density. Once the worms reached day 1 of adulthood (first day egg-laying), one of the plates was used to collect 200 adult worms by picking into 400 µl of lysis buffer, and the remaining adults on the plate were egg prepped for the

collection of hatched L1 larvae in 400 µl lysis buffer the following day. The worms on the four remaining plates were transferred to a 40 µm nylon mesh filter in order to separate the adults from the progeny, and the resulting adults were resuspended in M9 and pipetted onto fresh large NGM plates. This process was repeated for the following three days (day 2 - day 4 of adulthood). Day 5-10 adults were moved to fresh NGM plates every 2nd day using a 40 µm nylon mesh filter, and the resulting day 10 adults were collected in lysis buffer.

ddPCR

The worm lysates were incubated at 65°C for 1.5-4 hours and then 95°C for 30 minutes to deactivate the proteinase K. Each lysate was diluted; 100-fold for 200 worm adult population lyses, 2-fold for 200 worm L1 population lyses, and 25-fold for individual adult lyses. 2 µl of the diluted lysate was then added to 23µl of the ddPCR reaction mixture, which contained a primer/probe mixture and the ddPCR probe supermix with no dUTP. The primers used were:

WTF: 5'-GAGGGCCAACTATTGTTAC-3'

WTR: 5'-TGGAACAATATGAACTGGC-3'

UADF5F: 5'-CAACTTTAATTAGCGGTATCG-3'

UADF5R: 5'-TTCTACAGTGCATTGACCTA-3'

The probes used were:

WT: 5'-HEX-TTGCCGTGAGCTATTCTAGTTATTG-Iowa Black→ FQ-3'

UADF5: 5'-FAM-CCATCCGTGCTAGAAGACAAAG- Iowa Black→ FQ-3'

The ddPCR reactions were put on the BioRad droplet generator and the resulting droplet-containing ddPCR mixtures were run on a BioRad thermocycler with the following cycle parameters, with a ramp rate of 2°C/sec for each step:

1. 95°C for 5 minutes
2. 95°C for 30 seconds
3. 60°C for 1 minute
4. Repeat steps 2 and 3 40x
5. 4°C for 5 minutes
6. 90°C for 5 minutes

After thermocycling, the ddPCR reaction plate was transferred to the BioRad droplet reader and the Quantasoft software was used to calculate the concentration of *uaDf5* (FAM/HEX? positive droplets) and WT-mtDNA (FAM/HEX? positive droplets) in each well.

Lifespan analysis

Confluent large plates were egg prepped and left to spin in M9 overnight for synchronization. The hatched L1s were plated onto large thick plates and allowed to grow to day 2 adults before being egg prepped a second time and left to spin in M9 overnight. The next morning, referred to as day 1 for lifespan determination, L1s were singled out onto small plates. Once the worms started laying eggs, they were transferred each day to a fresh small plate until egg laying ceased, after which the worms remained on the same plate unless bacterial contamination required transfer to a fresh plate. Worms were considered dead if there was no movement after being lightly prodded with a worm pick.

Brood size, embryonic lethality, and unfertilized oocytes analysis

Confluent large plates were egg prepped and left to spin in M9 overnight for synchronization. The hatched L1s were plated onto large thick plates and allowed to grow to day 2 adults before being egg prepped a second time and left to spin in M9 overnight. The next morning, L1s were singled out onto small plates. Once the worms started laying eggs, they were transferred each day to a fresh small plate until egg laying ceased. The day after transfer to a fresh plate, unfertilized oocytes, unhatched embryos, and hatched larvae on the plate from the previous day were counted. This was done for each of the days of laying and the total of unhatched embryos and hatched larvae from all plates from a single worm were tabulated to determine total brood size. To determine embryonic lethality, the total number of unhatched embryos was divided by the total brood size. To determine unfertilized oocyte percentage, the total number of unfertilized oocytes was divided by the total brood size.

Developmental time analysis

Confluent large plates were egg prepped and left to spin in M9 overnight for synchronization. The hatched L1s were plated onto large thick plates and allowed to grow to day 2 adults before being egg prepped a second time and left to spin in M9 overnight. The next morning, L1s were singled out onto small plates. The stage of the worms was assayed every 12 hours for the first 72 hours after plating.

FIGURES

Figure 1:

A.

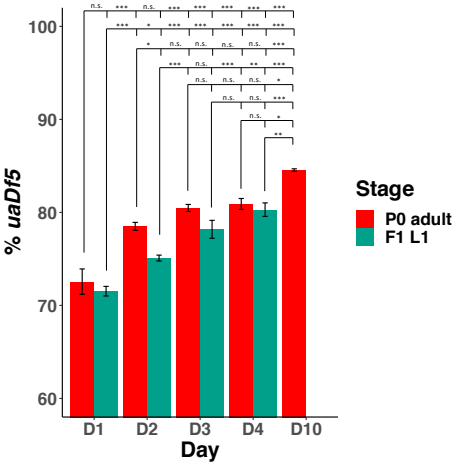

B.

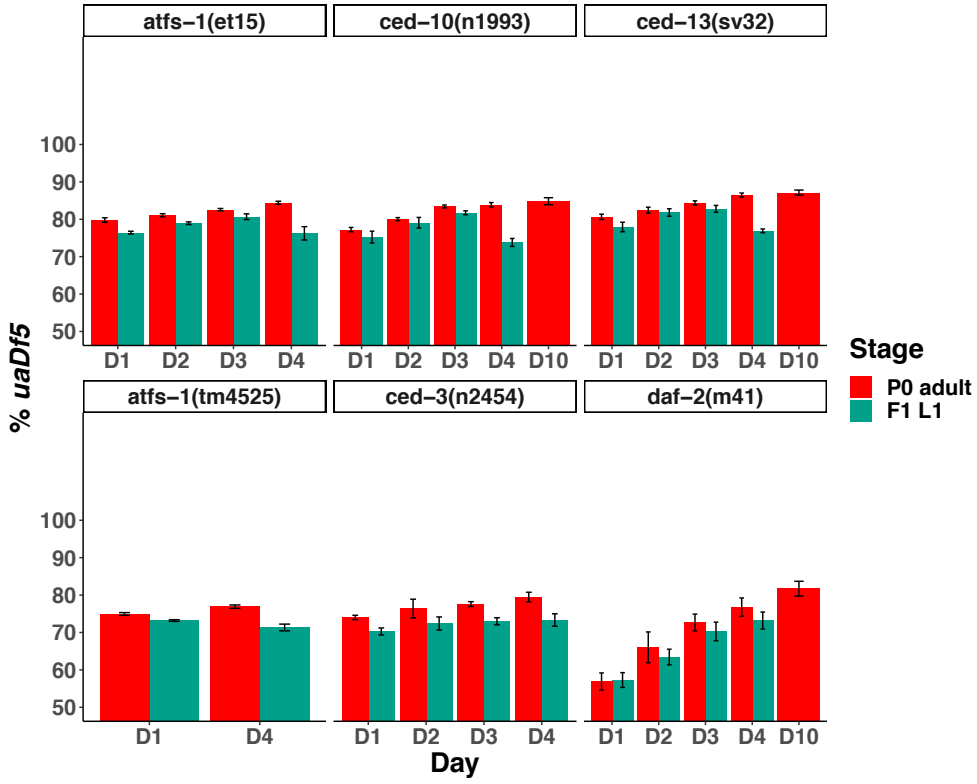

C.

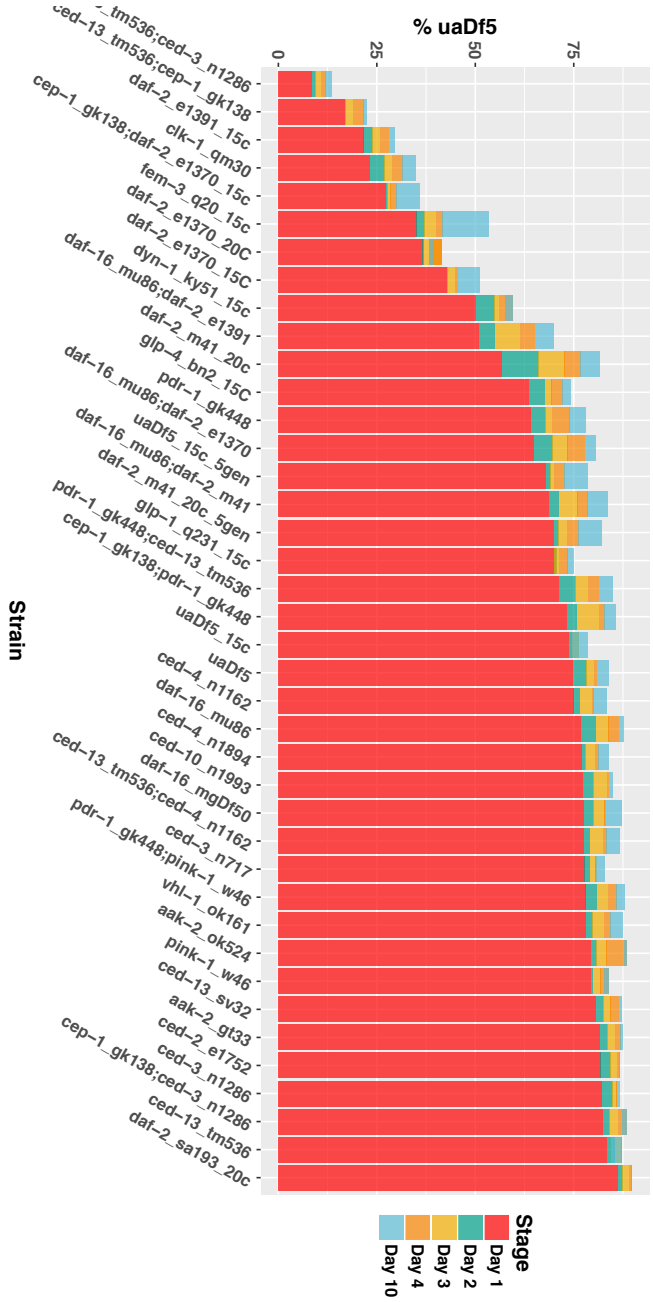

Figure 1. *uaDf5* accumulates in aging adults, and there is a moderate clean up that happens between mother and offspring. (A) ddPCR analysis of different aged adults and their L1 progeny in a wildtype nuclear background. D1 = day 1 adults (first day of egg laying), D2 = day 2 adults, D3 = day 3 adults, D4 = day 4 adults, D10 = day 10

adults. L1 progeny were not collected from day 10 adults because they are no longer gravid at that age. N=3 replicates of 200 worm populations per condition. Statistical analysis was performed using a one way ANOVA with Dunnett's correction for multiple comparisons. (*** $p < 0.001$, ** $p < 0.01$, * $p < 0.05$, . $p < 0.1$). **(B)** ddPCR analysis of different aged adults and their L1 progeny in various mutant nuclear backgrounds. *atfs-1(et15), ced-10(n1993),* and *ced-13(sv32)* have high steady state % *uaDf5*; *atfs-1(tm4525), ced-3(n2454),* and *daf-2(m41)* have low steady state % *uaDf5.* D1 = day 1 adults (first day of egg laying), D2 = day 2 adults, D3 = day 3 adults, D4 = day 4 adults, D10 = day 10 adults. L1 progeny were not collected from day 10 adults because they are no longer gravid at that age. N=3 replicates of 200 worm populations per condition. **(C)** ddPCR analysis of the accumulation of *uaDf5* in 40 backgrounds, rank ordered by the % *uaDf5* in day 1 adults.

Figure 2

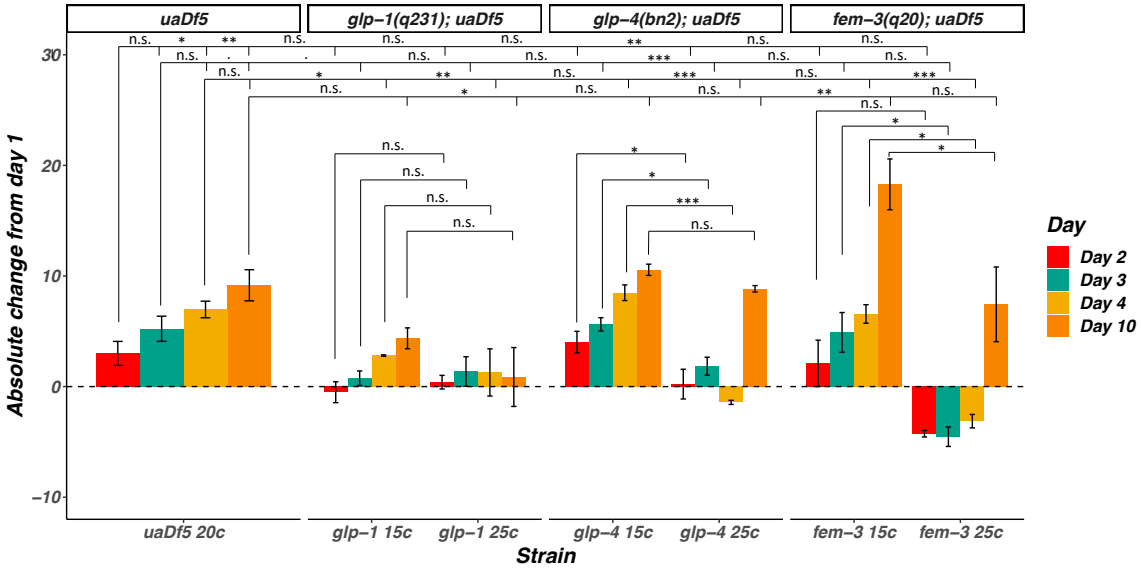

Figure 2. Accumulation of *uaDf5* occurs predominantly in the germline. ddPCR analysis of the absolute change of % *uaDf5* from day 1 (Y axis = % *uaDf5* day x -% *uaDf5* day 1). For *uaDf5*, 20C is the normal growth temperature. For *glp-1(q231ts), fem-3(q20ts),* and *glp-4(bn2ts),* 15C is the permissive temperature (germline development occurs) and 25C is the restrictive temperature (female germline development is inhibited). N=3 replicates of 200 worm populations per condition. Statistical analysis was performed using a one way ANOVA with Tukey correction for multiple comparisons. (*** $p < 0.001$, ** $p < 0.01$, * $p < 0.05$, . $p < 0.1$)

Table 1

Gene	Homologs	Pathway	Allele	Parental Strain	Molecular Nature of allele	Protein Change	Mutant increase or decrease lifespan	Note
aak-2	AMPK	**IIS pathway**, adult lifespan, peptidyl-serine phosphorylation, regulation of establishment of protein localization	*gt33*	TG38	606 bp deletion	Starts at position 3979, deletes exon 3	decrease	
			ok524	RB754	408 bp deletion	Starts at position 4136, deletes part of exon 3	decrease	
			rr48	MR507	Substitution	Missense H→Y	decrease	
age-1	PI3K	**IIS pathway**, cellular response to salt, chemosensory behavior and chemotaxis	*hx546*	TJ1052	Substitution	Missense P→S	increase	
cep-1	p53	Adult lifespan, intracellular signal transduction, response to hypoxia	*gk138*	VC172	1660 bp deletion	Starts at position 1989, deletes part of exon 8, 9, 10	increase	
clk-1	COQ7	Adult behavior, regulation of cellular metabolism	*qm30*	MQ130	590 bp deletion	Starts at position 1044, deletes part of exon 4 and 5	increase	
daf-2	IGFR	**IIS pathway**, cellular response to salt, negative regulation of macromolecule metabolic process, positive regulation of developmental growth	*e1391*	DR1574	Substitution	Missense P→L	increase	ts
			e1370	CB1370	Substitution	Missense P→S	increase	ts
			m41	DR1564	Substitution	Missense G→E	increase	ts
			sa193	JT193	Not Curated	-	increase	ts
daf-16	FOXO	**IIS pathway,** defense response to bacterium, regulation of cellular biosynthetic process, regulation of post-embryonic development	*mu86*	CF1038	10980 bp Deletion	Deletes 5 exons	decrease	
			mgDf50	GR1307	20193 bp Deletion with TCTTCATTTTCAG insertion	Deletes 7 exons	decrease	
fem-3	novel	Male somatic sex determination, masculinization of hermaphrodite germline, positive regulation of macromolecule metabolic process	*q20*	JK816	Not Curated	-	increase	Gof and ts; female germ line dev'ment inhibited
glp-1	NOTCH	Cell fate specification, embryonic pattern specification, positive regulation of cell population proliferation	*q231*	JK509	Substitution	Missense G→E	increase	ts; germ line dev'ment inhibited
glp-4	VARS	Determination of adult lifespan	*bn2*	SS104	Substitution	Missense G→D	increase	ts; germ line dev'ment inhibited
vhl-1	VHL	Hypoxia response	*ok161*	CB5602	1302 bp deletion	Ends at position 570, deletes exons 1 and 2	increase	

Table 1. Summary of lifespan mutants. A summary of all lifespan mutants analyzed, including their known homologs, cellular pathways they are known to act in, whether the mutant extends or reduces lifespan, and molecular details of the alleles analyzed.

Figure 3

A.

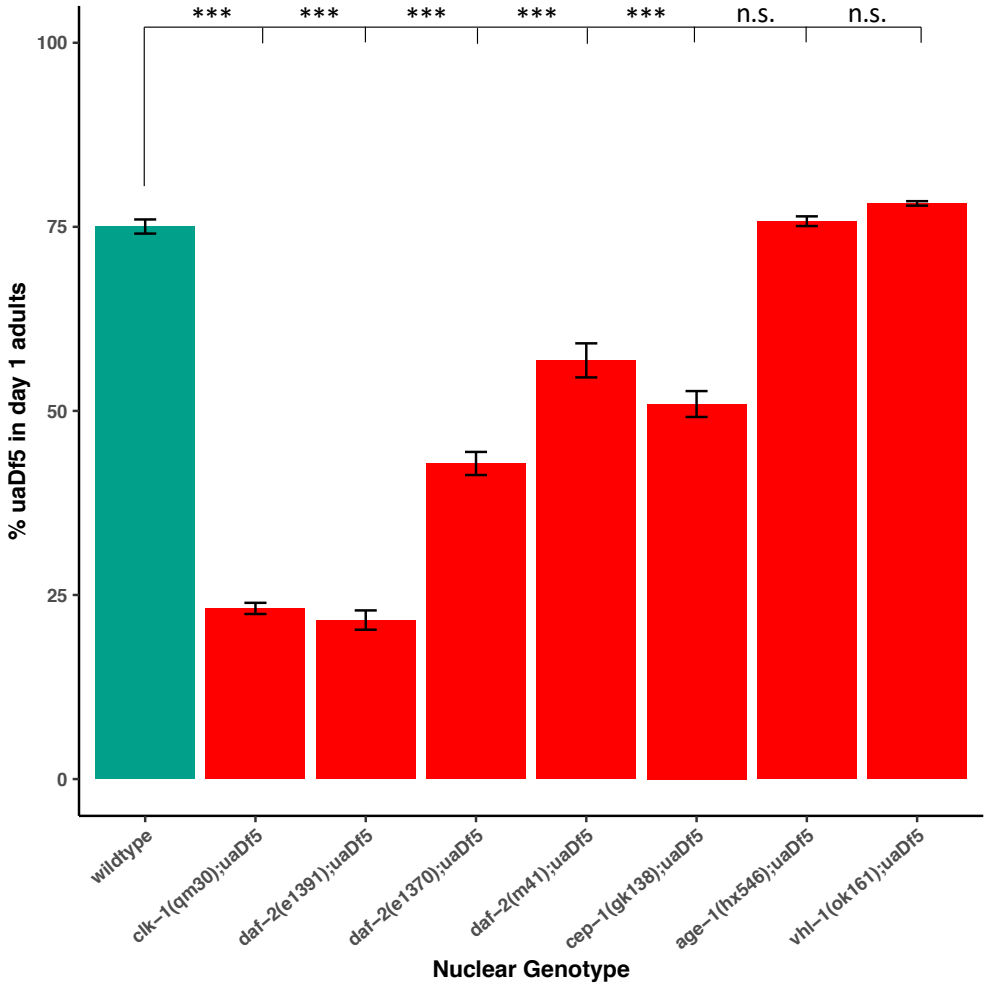
***
***
***
***
***
n.s.
n.s.
100
75
50
25
0
% uaDf5 in day 1 adults
wildtype
clk−1(qm30);uaDf5
daf−2(e1391);uaDf5
daf−2(e1370);uaDf5
daf−2(m41);uaDf5
cep−1(gk138);uaDf5
age−1(hx546);uaDf5
vhl−1(ok161);uaDf5
Nuclear Genotype

B.

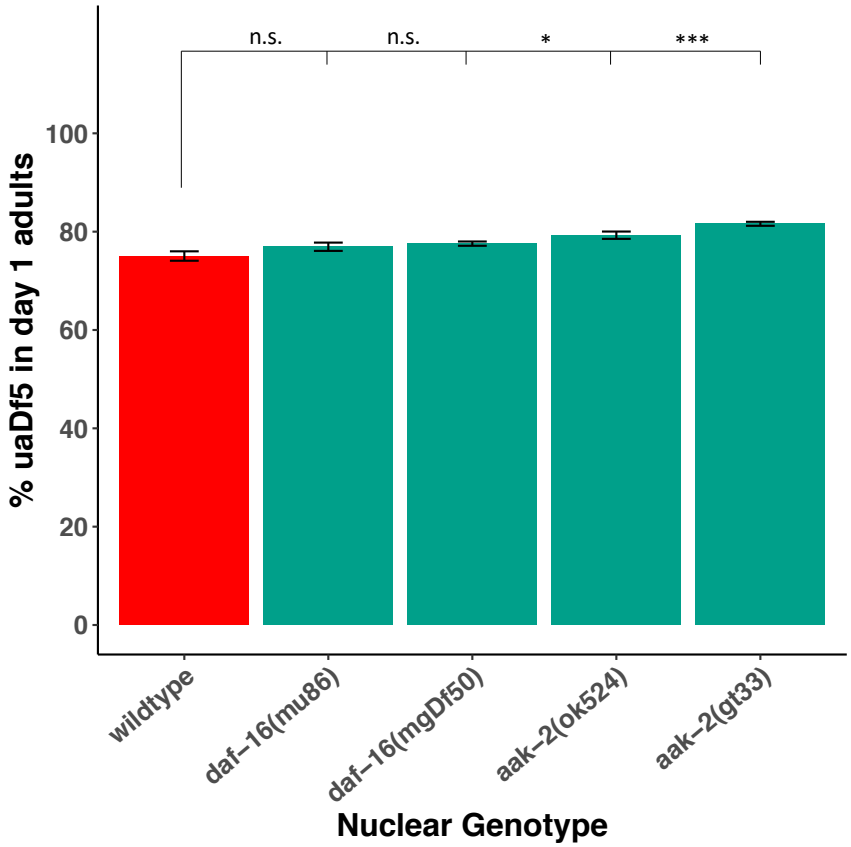

Figure 3. Steady state levels of *uaDf5* are lower in long-lived mutants, higher in short-lived mutants. (A) ddPCR analysis of fractional abundance *uaDf5* in steady state populations of long-lived mutants, with mutants rank ordered by the % *uaDf5*. **(B)** ddPCR analysis of fractional abundance *uaDf5* in steady state populations of short-lived mutants, with mutants rank ordered by the % *uaDf5*. N=3 replicates of 200 worm populations per condition. Statistical analysis was performed using a one way ANOVA with Dunnett's correction for multiple comparisons. (*** $p < 0.001$, ** $p < 0.01$, * $p < 0.05$, . $p < 0.1$).

Figure 4

A.

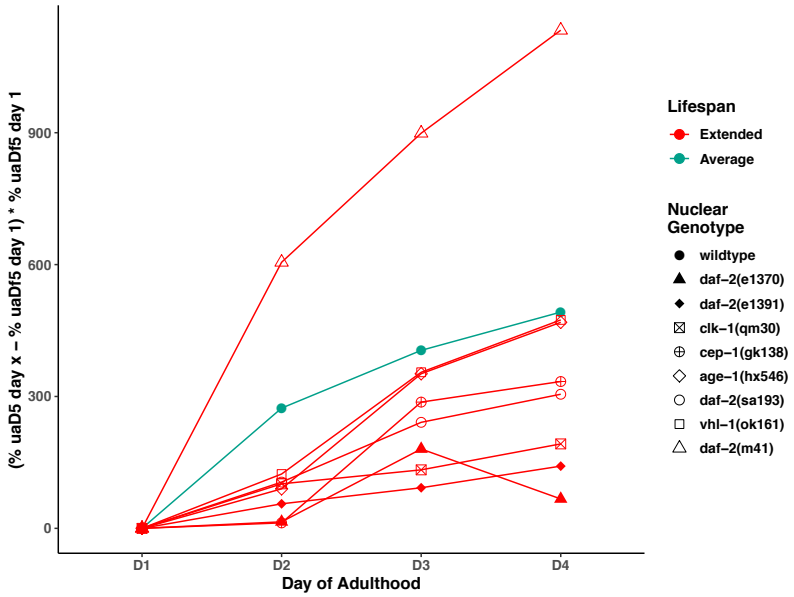
(% uaD5 day x – % uaDf5 day 1) * % uaDf5 day 1
900
600
300
0
D1
D2
D3
D4
Day of Adulthood
Lifespan
Extended
Average
Nuclear Genotype
wildtype
daf–2(e1370)
daf–2(e1391)
clk–1(qm30)
cep–1(gk138)
age–1(hx546)
daf–2(sa193)
vhl–1(ok161)
daf–2(m41)

B.

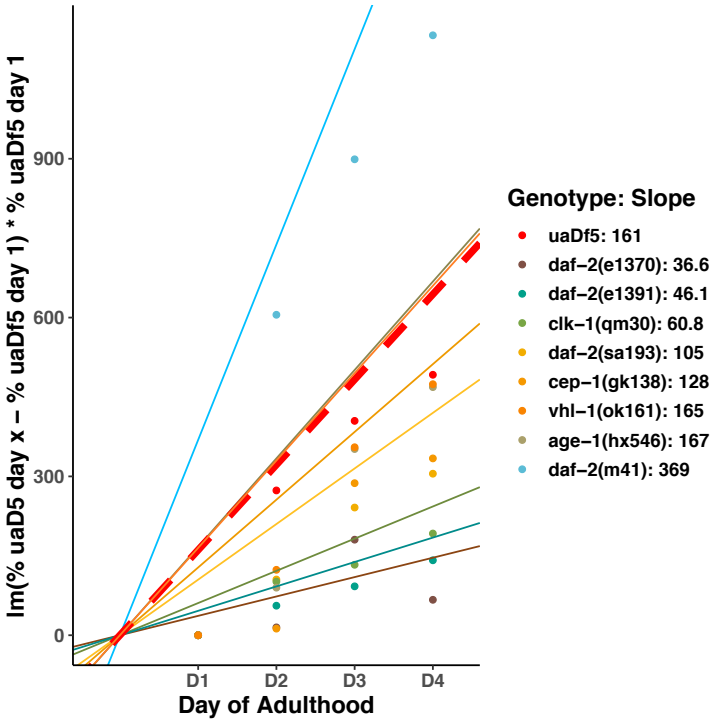
lm(% uaD5 day x – % uaDf5 day 1) * % uaDf5 day 1
900
600
300
0
D1
D2
D3
D4
Day of Adulthood
Genotype: Slope
uaDf5: 161
daf–2(e1370): 36.6
daf–2(e1391): 46.1
clk–1(qm30): 60.8
daf–2(sa193): 105
cep–1(gk138): 128
vhl–1(ok161): 165
age–1(hx546): 167
daf–2(m41): 369

C.

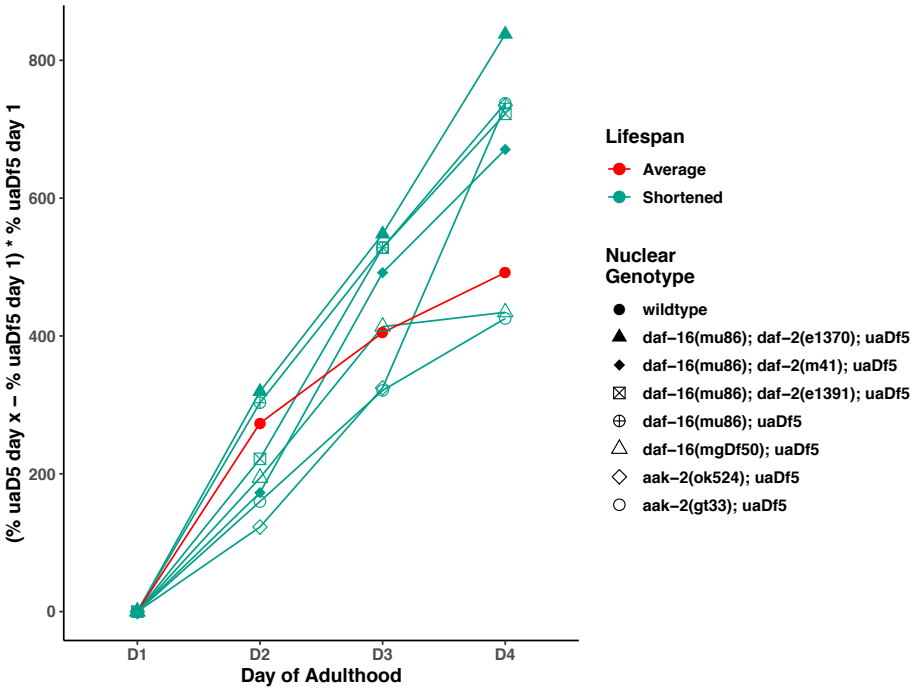
(% uaD5 day x – % uaDf5 day 1) * % uaDf5 day 1
800
600
400
200
0
D1
D2
D3
D4
Day of Adulthood
Lifespan
Average
Shortened
Nuclear Genotype
wildtype
daf–16(mu86); daf–2(e1370); uaDf5
daf–16(mu86); daf–2(m41); uaDf5
daf–16(mu86); daf–2(e1391); uaDf5
daf–16(mu86); uaDf5
daf–16(mgDf50); uaDf5
aak–2(ok524); uaDf5
aak–2(gt33); uaDf5

D.

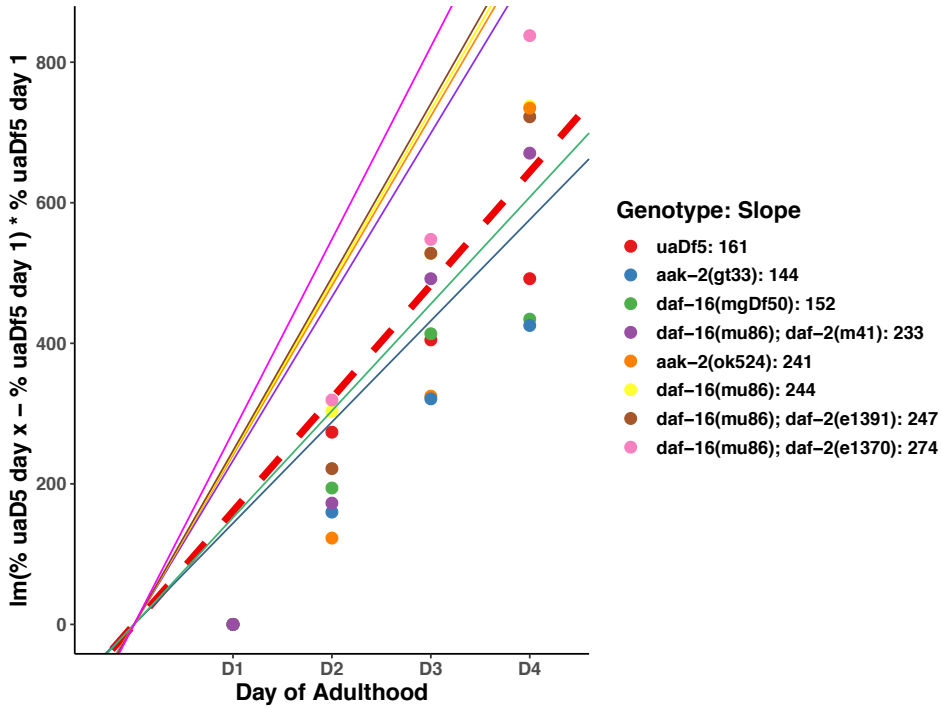
lm(% uaD5 day x – % uaDf5 day 1) * % uaDf5 day 1
800
600
400
200
0
D1
D2
D3
D4
Day of Adulthood
Genotype: Slope
uaDf5: 161
aak–2(gt33): 144
daf–16(mgDf50): 152
daf–16(mu86); daf–2(m41): 233
aak–2(ok524): 241
daf–16(mu86): 244
daf–16(mu86); daf–2(e1391): 247
daf–16(mu86); daf–2(e1370): 274

Figure 4. *uaDf5* accumulates more slowly in long-lived mutants, more quickly in short-lived mutants. (A) ddPCR analysis of the normalized fractional abundance *uaDf5* in steady state populations of long-lived mutants, showing the accumulation of *uaDf5* as worms age. **(B)** Linear regression analysis of the normalized fractional abundance *uaDf5* in steady state populations of long-lived mutants, showing the accumulation of *uaDf5* as worms age. **(C)** ddPCR analysis of the normalized fractional abundance *uaDf5* in steady state populations of short-lived mutants, showing the accumulation of *uaDf5* as worms age. **(D)** Linear regression analysis of the normalized fractional abundance *uaDf5* in steady state populations of short-lived mutants, showing the accumulation of *uaDf5* as worms age. For **A** and **C** the percent change from day x to day 1 was normalized to the day 1 steady state value. For **B** and **D** the percent change from day x to day 1 was normalized to the day 1 steady state value and a best fit linear regression model was then applied. The slope of the resulting line was maintained while the y intercept was adjusted to "0" for the purpose of data presentation. The slope for each line is indicated in the legend (higher slope means a higher rate of accumulation). N=3 replicates of 200 worm populations per condition.

Figure 5

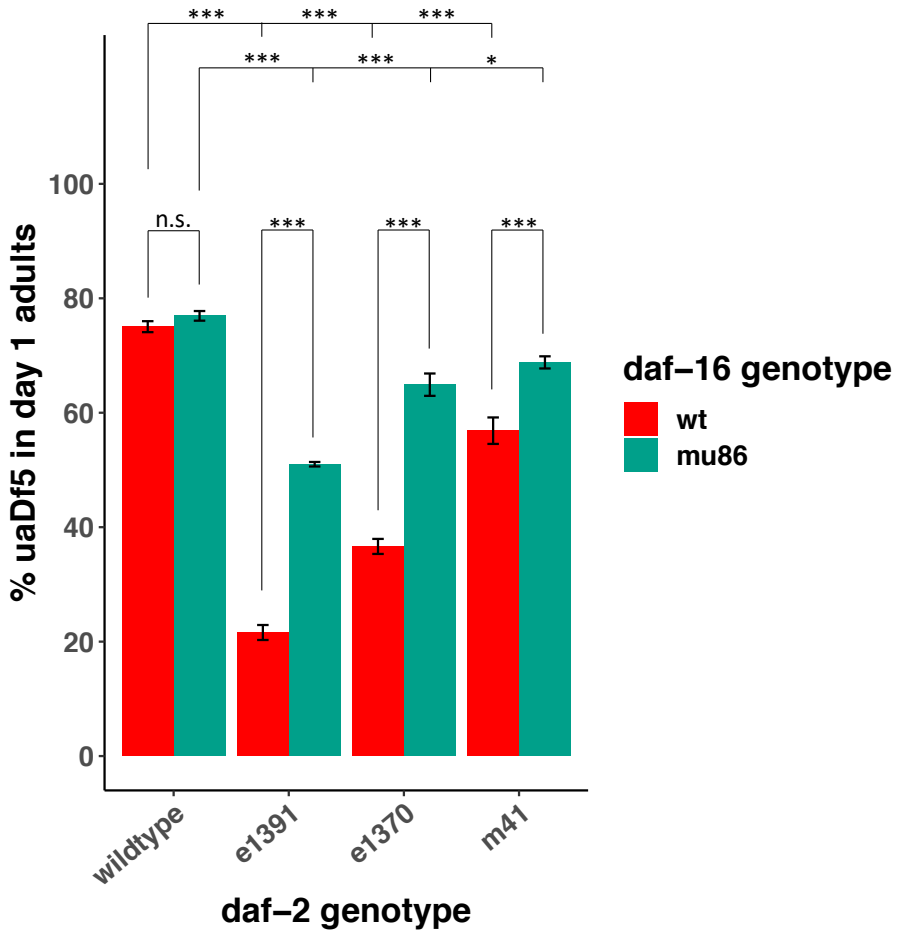

Figure 5. *daf-16* partially rescues *daf-2*, suggesting that the IIS pathway is acting directly on mutant mtDNA. ddPCR analysis of fractional abundance *uaDf5* in steady state populations of *daf-16;daf-2* double mutants, showing a partial rescue of *daf-2* by *daf-16.* Statistical analysis was performed using a one way ANOVA with Tukey correction for multiple comparisons. (*** $p < 0.001$, ** $p < 0.01$, * $p < 0.05$, . $p < 0.1$).

Figure 6

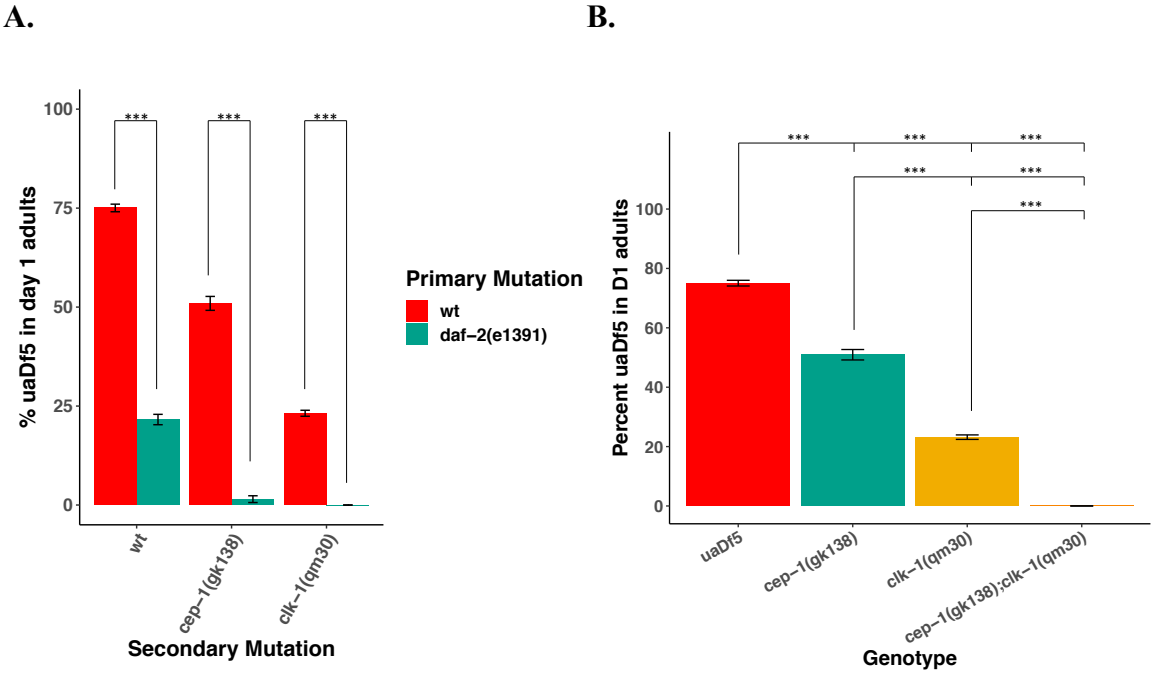

Figure 6. Double mutant analysis shows an additive effect between lifespan extension genes, suggesting they act on mtDNA via different pathways. (A) ddPCR analysis of fractional abundance *uaDf5* in steady state populations of double mutants composed of *daf-2(e1391)* in combination with long-lived mutants from independent pathways, showing an additive effect on *uaDf5* removal capacity. **(A)** ddPCR analysis of fractional abundance *uaDf5* in steady state populations of double mutants composed of the long-lived mutants *cep-1(gk138)* and *clk-1(qm30),* showing an additive effect on *uaDf5* removal capacity. Statistical analysis was performed using a one way ANOVA with Tukey correction for multiple comparisons. (*** $p < 0.001$, ** $p < 0.01$, * $p < 0.05$, . $p < 0.1$).

Figure 7

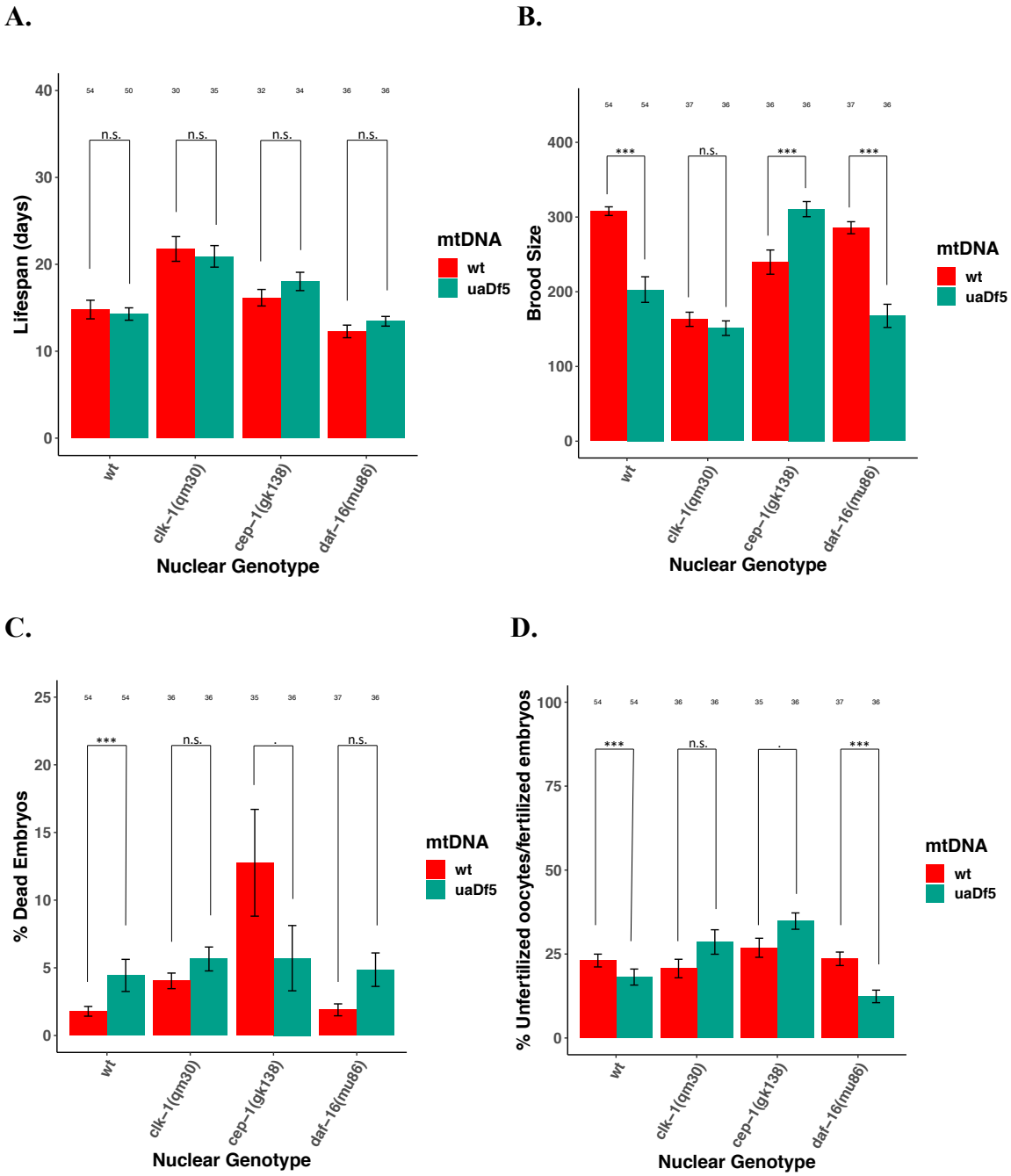

Figure 7. *uaDf5* differentially impacts various fitness parameters in the lifespan regulating genes. (A) Analysis of the effect of *uaDf5* on lifespan in lifespan-associated mutants. Day 1 is the day starved L1s are plated onto food. **(B)** Analysis of the effect of *uaDf5* on brood size in lifespan-associated mutants. **(C)** Analysis of the effect of *uaDf5*

on embryonic lethality in lifespan-associated mutants. Embryonic lethality was calculated by dividing the total number of dead embryos by the total number of embryos laid. **(D)** Analysis of the effect of *uaDf5* on unfertilized oocyte production in lifespan-associated mutants. % unfertilized oocytes was calculated by dividing the total number of unfertilized oocytes laid by the total number of embryos laid. *clk-1* and *cep-1* mutants extend lifespan, and the *daf-16* mutant reduces lifespan. For each condition, N is indicated at the top of the graph. Statistical analysis was performed using the Kruskal-Wallis test. (*** $p < 0.001$, ** $p < 0.01$, * $p < 0.05$, . $p < 0.1$)

Chapter Five

Conclusions and future directions

CONCLUSIONS

This thesis describes a suite of experimental investigations into the relationship between mitochondrial health, mutation, and fitness of the individual, including ageing. Using the genetically tractable nematode *C. elegans* and the mtDNA deletion mutant *uaDf5*, I describe foundational work to characterize mitochondrial dynamics and maintenance of mtDNA over the lifespan of the animal, focused primarily on the germline. Our data shows that there are three mechanisms through which purifying selection is operating: asymmetric segregation in early embryonic divisions, PCD in the mature female germline, and insulin signaling. In addition to the discovery of these mechanisms, I also characterized the dynamics of mtDNA selection during development and aging, as well as the dynamics of mitochondrial activity in response to the environment. Lastly, I discovered a potent epigenetically activated mtDNA quality control mechanism that is activated in response to an initiating genetic event, or "IGE". Altogether, my work shows how *C. elegans* is an extremely useful system for examining mtDNA dynamics and for the further elucidation of the various ways in which the mtDNA population is maintained.

MITOCHONDRIAL DYNAMICS FROM FERTILIZATION TO L1 HATCHING

In chapter two of this dissertation I present evidence establishing the relationship between germline mitochondrial activity throughout early development in the nematode *C. elegans* (Fig. 5.1).

Mitochondria undergo a sorting event based on membrane potential (ΔΨ) immediately after fertilization that is dependent on genes involved in polarity establishment and microtubule organization

First, I show that mitochondria are sorted between the posterior and anterior cells of the early embryo such that the mitochondria with a higher ΔΨ are concentrated into the posterior cell which gives rise to the germline [151]. I found that the sorting of more active mitochondria into the posterior region of the one-cell embryo is inhibited in mutants involved in polarity establishment of the early embryo, including *par-2, par-3, par-5*, and *par-6*, which also control the movement of P granules into the germline [147,148,150–152]. The strongest inhibition of this sorting process was observed in the *spd-5* mutant, which knocks out the function of a centrosomal protein that is involved in microtubule organization and spindle formation [193], showing the role of microtubules in mitochondrial movement in the early embryo.

The membrane potential sensor PINK-1 appears to play a role in mitochondrial sorting

I also analyzed mutants of the mitochondrial ΔΨ-sensor PINK-1 [117,118,120,122], since I wanted to know if PINK-1 allows for the cell to distinguish the more active mitochondria from the less active ones. *pink-1* mutants had a decreased posterior enrichment across all stages, although it was not statistically significant until the early two-cell stage. In addition to the analysis of mitochondrial sorting, I noted that a fraction of PINK-1 mutant embryos have abnormal morphology that parallels the abnormal embryonic morphologies observed in PAR mutants [147,148]. This suggests that PINK-1 is indeed playing a role in establishment of asymmetry in the early embryo.

Germline mitochondria shut down their activity by the four-cell stage and remain shut down throughout embryogenesis

Analysis of the posterior enrichment of active mitochondria through the four-cell stage shows a sudden decrease in mitochondrial activity in the P2 germline progenitor cell such that its activity is lower than the activity in its sister cell "EMS" [224]. When the P2 cell activity is compared to the combined average activity in all of the other three cells of the embryo, its activity is shown to be equivalent. I examined the mitochondrial activity in the germline progenitor cells Z2 and Z3 throughout the remainder of embryogenesis and found that the mitochondria continue to decrease their activity as embryogenesis progresses. This makes sense in terms of mtDNA quality control, since a negative consequence of oxidative phosphorylation is that it produces ROS which are mutagenic [53]. Thus, since Z2 and Z3 cells are in a quiescent state throughout embryogenesis, their energy demands are low, and perhaps as a protective mechanism, the germline mitochondria are entirely shut down in order to reduce ROS production.

After hatching, the germline mitochondria activate in response to food in a DAF-2, DAF-18, and AAK-2 – dependent manner

Upon hatching into the first larval state, L1, normal development proceeds in a food-dependent manner during which both the soma and germline expand [163,164,196]. If, however, there is no food present upon hatching, the L1 larvae enter an alternative state known as L1 arrest/diapause [163,164,196]. This alternative development program shares many similarities with dauer development which is dependent on the IIS pathway [82,161,163–165]. The quiescent state observed in the germline cells of L1 arrested worms presents as condensed nuclear chromosomes that are arrested in the G2 phase of

the cell cycle. Both L1 arrest and dauer formation are dependent on components of the IIS pathway, most notably, DAF-18/PTEN, although the two processes differ in that L1 arrest has no requirement for DAF-16/FOXO [165]. I found that germline mitochondrial activity remains quiescent throughout L1 arrest, and that in the presence of food the germline mitochondria activate to levels higher than the surrounding cells, with most worms exhibiting highly active mitochondria after 5 hours of feeding. Mutant analysis of starved L1s shows that maintenance of germline mitochondrial quiescence throughout L1 arrest is dependent on DAF-2/IGFR, AAK-2/AMPK, and DAF-18/PTEN, with no requirement for DAF-16/FOXO, suggesting the same machinery that acts to keep the nucleus in a quiescent state is also used for the mitochondrial state.

ESTABLISHMENT OF A MODEL FOR MITOCHONDRIAL DISEASE IN THE NEMATODE *C. ELEGANS*

The 3.1kb mtDNA deletion mutant *uaDf5* exhibits stable heteroplasmy despite its highly deleterious nature [201]. Why is *uaDf5* maintained in a heteroplasmic state despite its unavoidable negative effect on organismal health? Our investigation of the *uaDf5* allele led to the discovery of a secondary mutation that is linked to the *uaDf5* deletion. This secondary mutation, "*w47*", is a single base pair deletion in the ND4 gene which results in a frameshift leading to premature truncation of the protein such that only the first 88 amino acids of the 409 amino acid long protein is produced [1–3,39,202]. . This tells us that the *uaDf5* allele not only knocks out 7 tRNAs and the ATP6, ND1, ND2, and CYTB genes, but also knocks out a fifth gene, ND4. The nature of the allele presumably results in at least two truncated proteins (ND1 and ND4) in addition to reduced capacity for making proteins due to the loss of several necessary tRNAs. Thus, *uaDf5* mutants are

anticipated to have heightened mitochondrial stress which would activate the mitochondrial UPR.

To uncover the consequences on organismal health of this mutant mtDNA, I measured various fitness parameters in *uaDf5* mutants. Surprisingly, lifespan was unaffected, but there are observable negative consequences on brood size, embryonic lethality, and developmental rate, showing that *uaDf5* is a good model for mtDNA disease, and that analysis of its regulation is a good tool for studying mechanisms of mtDNA quality control.

MTDNA MAINTENANCE DURING AGING

In chapter four of this dissertation I present several lines of evidence showing the link between aging and the accumulation of mutant mtDNA using the *C. elegans* mtDNA deletion strain *uaDf5.* I show that *uaDf5* accumulates in the germline of aging adults, that offspring from older mothers inherit a larger load of *uaDf5* than their siblings from younger mothers, and that mtDNA quality control is improved in long-lived mutants.

uaDf5 accumulates in aging adults predominantly in the germline, though there is evidence that there is also somatic accumulation as is seen in post-gravid adults

Analysis of the fractional abundance of *uaDf5* in aging adults with a wildtype nuclear background shows an accumulation of *uaDf5* as the worms get older that occurs throughout gravidity and beyond. To determine if the accumulation is occurring in the germline I analyzed three temperature sensitive mutants that inhibit female germline development and saw a reduction of the accumulation rate during gravidity, showing that the majority of the age-related accumulation occurs in the female germline. Analysis of

the accumulation beyond gravidity, in day 10 of adulthood [196,215,216], shows an increase in the fractional abundance of *uaDf5,* demonstrating that accumulation is also occurring in the somatic tissues throughout the aging process. This demonstrates that *uaDf5* dynamics during aging mirror those of mutant mtDNAs studied in other organisms [54,213,214].

The load of mutant mtDNA is transmitted from mother to offspring with evidence of a level of mtDNA quality control

Analysis of L1 progeny from different aged-mothers reveals that the load of *uaDf5* is transmitted from mother to offspring such that progeny from older mothers inherit a larger mutant mtDNA burden than their siblings from younger mothers, with evidence of a cleanup mechanism. This tells us that there is a level of mtDNA quality control that happens sometime between oocyte maturation and L1 hatching. Analysis of the transmission from mother to offspring in mutants in germline PCD, including *ced-13(sv32)* [19,89,179,184–187] and *ced-10(n1993)* [180–182], shows that the transmission-associated cleanup is slightly reduced in younger mothers, but actually increased in old mothers, suggesting that germline PCD may play a larger role in mtDNA quality control in young mothers than in old mothers. This may indicate a switch from germline PCD to some other cleanup process that is inhibited by germline PCD as mothers get older, possibly due to increased stress associated with aging making the germline PCD pathway less efficient.

Lifespan-associated mutants alter the capacity of mtDNA quality control, with evidence of the IIS pathway acting directly on mutant mtDNA

The consistent rate of age-related *uaDf5* accumulation I observed in various genetic backgrounds led us to question if mutants that affect lifespan have a lower rate of accumulation of *uaDf5*. I found that not only is the rate of accumulation lowered in long-lived mutants (*daf-2* (IIS pathway; [82,100,144,220]), *clk-1* (mitochondrial function; [102,132,144,220,221]), and *cep-1* (genotoxic stress-response; [19,145,186,210])), but also the steady state level of the fractional abundance of *uaDf5* is drastically lowered. This was a common phenotype observed in long-lived mutants that act on lifespan through independent pathways. However, there were two long-lived mutants analyzed did not have lowered steady state abundance or accumulation rate, *vhl-1* (involved in hypoxia response [146]) and *age-1* (in the IIS pathway [82]). It is possible that this is showing allele-specific effects; the alleles analyzed may have activity in regulation of lifespan but not on mtDNA quality control. Further analysis with more alleles of *vhl-1* and *age-1* need to be analyzed to determine if this is the case. If no alleles of *age-1* show a role in mtDNA quality control, it is possible that a non-canonical version of the insulin signaling pathway acts on mtDNA quality control.

Overall, our results show a link between the ability to remove deleterious mtDNA and lifespan extension, supporting the idea that mutant mtDNA plays a central role in the aging phenotype. Further bolstering this link is our analysis of short-lived mutants (*daf-16* and *aak-2,* both involved in the IIS pathway [82]) which reveals that the converse is true; a reduction in lifespan is associated with an increased rate of accumulation of *uaDf5* in addition to higher steady state levels of the fractional abundance of *uaDf5.* Thus, I have shown that there is indeed a dependency on mtDNA quality control for regulation of

lifespan. Double mutant analysis of lifespan-extension mutants from the different pathways reveals that there is an additive effect on the mtDNA quality control machinery, suggesting that the lifespan-regulating pathways converge on a common system for mutant mtDNA removal, which is something that has not been reported previously and is of great interest to look into going forward.

Analysis of how the presence of mutant mtDNA affects fitness in lifespan-associated mutants reveals that long-lived mutants have fewer negative consequences on health than short-lived mutants. Of particular note, *cep-1(gk138)* mutants actually exhibit increased fitness parameters (lifespan, brood size, and embryonic lethality) when *uaDf5* is present.

SYNERGISM OF PINK-1 AND CED-13 ON MUTANT MTDNA

In chapter three of this dissertation I present several lines of evidence indicating that germline PCD is a mechanism through which deleterious mtDNA is removed from the germline, and the startling discovery of a heritable transgenerational epigenetic mechanism of greatly increased mtDNA quality control following an initiating genetic event, or "IGE".

Analysis of PCD mutants suggests a role in mtDNA quality control

To investigate whether germline PCD is involved in mtDNA quality control I analyzed the steady state fractional abundance of *uaDf5* in populations of worms containing mutations in various PCD-related genes [89,179,183,184]. Our analysis gave differing results, with most mutants exhibiting an effect (including two *ced-3* alleles and the engulfment-related *genes ced-1, ced-2,* and *ced-10*), however there were several

mutants which did not, such as *ced-4* and two of the *ced-3* alleles analyzed. Curiously, analysis of a *csp-1* mutant (CSP-1 is a non-canonical caspase that has largely been seen to play a minor role in PCD [174,175,178]) greatly increases the fractional abundance of *uaDf5* in a *ced-3(n717)* background, suggesting that CSP-1 may play a larger role in mutant mtDNA-induced germline PCD. Mutations in the *ced-13* gene result in a large increase in the fractional abundance of *uaDf5*, supporting the model that it is germline-specific PCD, and not developmental PCD, that acts in mtDNA quality control.

The reduction in the fractional abundance of *uaDf5* in a *cep-1* mutant suggests there is crosstalk occurring between mitophagy and PCD

Our *ced-13* results led us to question if the upstream activator of CED-13/BH3, CEP-1/p53 [19,186,187], activates the cell death pathway in response to mtDNA disease. However, I found that knocking out CEP-1/p53 actually results in increased mtDNA quality control, seen a greatly reduced fractional abundance of *uaDf5*. This confounding result may be explained by the largely unexplored role of CEP-1/p53 in inhibition of mitophagy [209]. These results may represent further evidence for its role in mitophagy and reveal potential crosstalk that could be occurring between the mitophagy and PCD pathways. It raises interesting questions about how players that are involved in both pathways may differentially regulate the levels of each pathway in response to mutant mtDNA.

In order to further understand the possible crosstalk occurring between both pathways, I generated a set of double mutants composed of genes from both pathways to see what levels of epistasis occur. A *cep-1(gk138);ced-3(n1286)* double mutant has increased fractional abundance of *uaDf5*, suggesting that PCD is a larger contributor to

mtDNA quality control. Similar results were seen in the *ced-13(tm536);ced-4(n1162)* double mutant. As expected, if you knock out both pathways, which was done in the *cep-1(gk138);pink-1(w46), cep-1(gk138);pdr-1(gk448),* and *pdr-1(gk448);ced-13(tm536)* double mutants, you see increased fractional abundance of *uaDf5*.

However, there were two double mutants which gave unexpected results. The *ced-3(n1286);ced-13(tm536)* double mutant, which is presumed to only inhibit PCD, shows an extreme decline in the fractional abundance of *uaDf5*. Further analysis of the fitness of this double mutant shows negative effects on brood size and embryonic lethality, which suggests that at least part of the reason for the removal of *uaDf5* is due to a decreased tolerance of *uaDf5* such that worms containing high levels of *uaDf5* do not survive, resulting in culling at the organismal level. However, the effects on fitness are not as extreme as one would expect, so there may be another element to the removal phenotype that has yet to be understood. Further analysis of the *ced-3(n1286);ced-13(tm536)* double mutant needs to be done to determine when and where *uaDf5* removal occurs and the conditions necessary to initiate the removal process. This includes first replicating the removal outcome initially observed via experimental crosses and testing different conditions after those crosses to see what results in removal. After the precise conditions that result in removal are determined, we need to take a closer look at the details underlying the removal process, such as examination of fitness parameters, cellular and mitochondrial morphology, and mutant analysis to determine which pathways are necessary for *uaDf5* removal.

The other double mutant that gave a shocking result was the *pink-1(w46);ced-13(tm536)* double, which is presumed to knock out both mitophagy and PCD. Surprisingly, this double mutant results in complete removal of *uaDf5* within the 8

generations it was grown before analysis. It is unlikely that CED-13 and/or PINK-1 are acting on mtDNA through their canonical pathways, seeing as how much this genetic condition differs from the results seen in other double mutants that knock out both mitophagy and PCD. Fitness analysis of lines resulting from crossing *pink-1(w46);ced-13(tm536);uaDf5* males into either *ced-13(tm536);uaDf5* or *pink-1(w46);uaDf5* hermaphrodites show no deficits in brood size or embryonic lethality, and the superficial appearance of the worms appears to be very healthy, suggesting the removal phenotype is not due decreased tolerance of *uaDf5* resulting in culling at the organismal level.

The removal capacity following the IGE is not dependent on the double mutant genotype, suggesting the cross itself may result in an epigenetic state that is propagated transgenerationally

In order to better understand how *uaDf5* is being removed from the population in a *pink-1(w46);ced-13(tm536)* background, I crossed *pink-1(w46);ced-13(tm536);uaDf5* males into either *ced-13(tm536);uaDf5* or *pink-1(w46);uaDf5* hermaphrodites and observed immediate removal of *uaDf5* in roughly half of the lines (16/34) generated from these crosses, with the fractional abundance dropping to below 50% as early as the F2 generation. Genotyping of the F2 “line founder hermaphrodites” revealed that the double mutant genotype was not necessary for the rapid removal phenotype. In fact, any of the segregating genotypes are capable of the rapid removal phenotype, unlinking a genetic requirement from the transgenerational rapid removal of *uaDf5*. I thus suggest that this heritable, transgenerational phenotype is epigenetic in nature, and is the result of the event of the original P0 cross in which I crossed double mutant males into single mutant mothers, hereby referred to as the initiating genetic event, or “IGE”. The genotype of the

P0 mother used in the IGE does not appear to be of consequence either, as you get rapid removal lines when using either *ced-13(tm536);uaDf5* or *pink-1(w46);uaDf5* hermaphrodites in the original cross. This raises the possibility that the only requirement for the IGE is that the male be a *pink-1(w46);ced-13(tm536);uaDf5* double mutant, and that results in an epigenetic environment that is enormously efficient at removing mutant mtDNA with no expense to organismal health.

Specific amplification of WT-mtDNA to supranormal levels in the generation preceding the subsequent removal of *uaDf5*

In order to get a more thorough understanding of possible mechanisms through which the IGE results in *uaDf5* removal, I analyzed the total copy number of both WT-mtDNA and *uaDf5* in the generations following the IGE. Between the F2 and F3 generation, I saw that only those lines that exhibit the rapid removal phenotype have a specific amplification of WT-mtDNA to supranormal levels, considerably higher than is ever seen (WT-mtDNA copy number is highly invariable even in the presence of *uaDf5* [78,106,107,201]), with little to no amplification of *uaDf5*. This increase in WT-mtDNA copy number between the F2 and F3 generations is then followed by a specific decrease in *uaDf5* copy number, with no decrease in WT-mtDNA copy number, between the F3 and F4 generations. The copy number dynamics observed in the rapid removal lines in the F2-F4 generations are not observed in those lines that maintain *uaDf5* at a higher level through the F4 generation.

FUTURE DIRECTIONS

EMBRYONIC SEGREGATION

How do the polarity establishment, microtubule organization, and membrane-potential sensing genes work together to regulate mitochondrial movement during early embryogenesis?

Are proteins associated with P granules players in mitochondrial sorting? Further studies need to be done in mutants involved more specifically in P granule sorting, including mutant analysis of the P granule associated proteins: the RGG-domain proteins PGL-1 and PGL-2, and the DEAD-box proteins GLH1-4 [83,84,152,198]. Do other alleles of pink-1 have a stronger effect? Future studies need to be done to examine how loss of PINK-1 affects various parameters of polarity establishment, including TMRE analysis of a stronger *pink-1* allele.

L1 DIAPAUSE

What is responsible for turning off mitochondria during embryogenesis?

What players are involved in the shutting down of mitochondria in the PGC starting at the four-cell stage? Are those same players responsible for the maintenance of mitochondrial quiescence throughout embryogenesis? The IIS pathway, which shows a role for the maintenance of nuclear quiescence during L1 arrest [82,161,163–165], is likely to be involved in this process and should be studied.

Do AAK-2, DAF-2, and DAF-18 all regulate germline mitochondrial activity through a common pathway?

Analysis of cell cycle arrest in the PGCs during L1 arrest show a requirement for DAF-2 and DAF-18 with no dependence on DAF-16 [165], similarly to our results for regulation of mitochondrial quiescence during L1 arrest. Double mutant analysis needs to be done to determine if the genes responsible for mitochondrial quiescence are acting in a common pathway that is known to regulate L1-diapause associated cell cycle arrest in the germline.

MTDNA QUALITY CONTROL IN AGING

Why is aging associated with accumulation of mutant mtDNA and how are mutant mtDNA differently regulated in long-lived mutants?

Does aging cause the accumulation, or does the accumulation cause aging? These results do not give direct answers to these questions, and more studies need to be done to determine the causality linking these aging and mutant mtDNA accumulation. Further analysis of the *age-1* and *vhl-1* genes needs to be done to see if their lack of control on the fractional abundance of *uaDf5* is an allele-specific effect, or if some long-lived mutants do not act on mtDNA quality control, suggesting the link between lifespan and mtDNA quality control is not as global as our other results suggest.

How it is that the independent lifespan regulation pathways act on mutant mtDNA has yet to be determined. Perhaps the pathways all converge on a global mitochondrial stress response pathway such as mitophagy. Further studies need to be done to determine what this common mtDNA quality control system, and likely candidates include mitochondrial fission/fusion [68,70,108], mitophagy [71,72,115], and the mitochondrial

unfolded protein response (UPR^{MT}; [75–80]) which are known to act in mtDNA quality control.

How mutant mtDNA results in an improvement in organismal health is a question of great interest. Perhaps in a *cep-1* background, the presence of mutant mtDNA activates stress response pathways in a way that increases general quality control pathways to a level that is actually beneficial to the organism. Further analysis needs to be done to dissect how it is that mutant mtDNA triggers various quality control pathways in lifespan-associated mutants in order to more thoroughly understand these dynamics of stress-response pathways and developmental fidelity.

What mechanisms results in mutant mtDNA removal between mother and offspring?

Narrowing down the window in which this cleanup occurs will lead to a better understanding of which processes are involved in the cleanup of mtDNA that I have observed between mother and offspring. To determine the level of cleanup occurring during the process of embryogenesis, analysis of different staged embryos needs to be done. Additionally, analysis of the fractional abundance in dead embryos will reveal how much of the decrease observed between mother and offspring is due to culling at the organismal level.

THE ROLE OF GERMLINE PCD IN MTDNA QUALITY CONTROL

Is germline PCD indeed acting in mtDNA quality control?

Why *ced-4* mutants do not have an increased fractional abundance of *uaDf5* may be explained by the fact that it has roles outside of PCD [207,208], and those alternative

roles may act to reduce mtDNA quality control. Why certain alleles of *ced-3 (n718* and *n2454*) do not show increased fractional abundance of *uaDf5* is immediately unclear, since the nature of the mutations and their presumed impact on CED-3 function do not distinguish them from the two alleles (*n717* and *n1286*) that did increase the fractional abundance of *uaDf5* [206]. Further molecular analysis of the nature of the alleles needs to be done to determine the reason behind this. Analysis of the *csp-1* single mutant needs to be done to clarify the extent of its role. Mutations in the *ced-13* gene result in a large increase in the fractional abundance of *uaDf5*, supporting the claim that it is germline-specific PCD, and not developmental PCD, that acts in mtDNA quality control. To further bolster this claim, *egl-1* mutants need to be analyzed, and are expected to have no effect on the fractional abundance of *uaDf5*.

Although the increased fractional abundance of *uaDf5* seen in the engulfment mutants supports the idea that PCD is acting in mitochondrial quality control, these results could also be reflective of the potential role of a recently discovered process called "endodermal cannibalism" [87]. This discovery was made in *C. elegans* embryos and details an event in which the germline progenitor cells (PGCs) pinch off a lobe that is roughly half the size of the cell - notably composed majorly of mitochondria - and that lobe then undergoes scission and is degraded by the surrounding endodermal cells. This endodermal cannibalism process happens about midway through embryogenesis, after the P4 cell has further divided to produce the 2 primordial germ cells (PGCs) Z2 and Z3 [196]. This cannibalism event is dependent on the dual actions of LST4/SNX9 and CED-10/RAC, which has mostly been recognized as a major downstream player in cell corpse engulfment following apoptosis [92,180–182]. LST4 and CED10 regulate dynamin and actin dynamics for the successful constriction and scission of the lobe. There are several

things that are removed in these excised lobes, including P granules, but it seems that the majority of the material is actually mitochondria. This seems like a likely quality control step for the developing organism to remove any deleterious genomes from the germline, since it occurs right after the bottleneck, when there is a reduced population of mitochondria, and right before the massive uptick in replication that is due to happen [106,107]. Our *ced-10* results may therefore be the result of inhibition of endodermal cannibalism rather than cell corpse engulfment, and further studies using temperature sensitive mutants need to be done to narrow down the developmental time window at which CED-10/RAC is acting in mtDNA quality control.

INVESTIGATION OF THE IGE

What is the developmental time, tissue, and age-dependence of uaDf5 removal after the IGE?

In order to determine the precise mechanisms through which the IGE is occurring, investigation of the developmental time in which the removal is occurring must be done. Is the process only occurring during embryogenesis, larval development, or adulthood, or is it happening continuously throughout development? Answering this question will narrow down the list of possible mechanisms. Additionally, examination of the rate of removal in individual tissues will help elucidate the removal process.

What is the generality of the IGE response?

The impressive removal of *uaDf5* has huge implications in the field of mitochondrial disease research, and the generality of the phenomenon needs to be investigated. Is this removal phenotype specific to *uaDf5*, or does it act on all mtDNA

mutants? Does the size of the deletion matter, or influence the rate of removal? Does the location of the deletion or the nature of the resulting truncated proteins matter, suggesting the UPR^{MT} may play a crucial role in the IGE process? There are a set of mtDNA point mutation strains, deletion strains that vary in size and location around the genome, and a mtDNA duplication strain that is larger than WT-mtDNA, and studies of the IGE in those strains will give insight into the mtDNA requirements for the removal phenotype [212]. Additionally, it is of probing interest as to whether the IGE is an allele-specific phenomenon, and to answer this, analysis needs to be done with alternate alleles of *pink-1* and *ced-13*.

Is the IGE triggered by loss of mitophagy and PCD, or are we uncovering noncanonical actions of PINK-1 and CED-13 in the paternal lineage?

How is this IGE-associated removal of mutant mtDNA occurring? One possibility is that the paternal mitochondria are licensed to survive following the IGE, instead of being rapidly degraded as is the case during normal fertilization [45,47,211]. It is unlikely that the males used in the IGE still contain *uaDf5* since the *pink-1(w46);ced-13(tm536)* nuclear background has been shown to result in rapid removal of *uaDf5*. If this is true, then the males used in the IGE only contain WT-mtDNA, and perhaps something about the *pink-1(w46);ced-13(tm536)* background marks the male mitochondria in a way that they are not degraded after fertilization and end up repopulating the resulting progeny in a transgenerational manner.

Another interesting hypothesis is that the males need to be "primed" with *uaDf5* in order to observe the IGE. Perhaps even after *uaDf5* is completely removed, there is a memory of *uaDf5* left in the paternal epigenetic landscape which makes it highly efficient

at removal if *uaDf5* is encountered again, similarly to an immune response. If the male line has never "seen" *uaDf5*, will the IGE still occur? Further studies need to be done to determine both the paternal and maternal requirements for the IGE-associated removal phenotype. Additionally, transcription profiling will offer insights into which pathways are modulated in response to the IGE.

Does the IGE require mitochondrial fission for the removal phenotype?

The specific amplification of WT-mtDNA followed by the selective removal of *uaDf5* suggests that the cell is more capable of discriminating between *uaDf5* and WT-mtDNA by the F2 generation. A possible mechanism for better discrimination is that of mitochondrial fission (Fig. 5.2) [68,108,115]. If the mitochondrial network undergoes global fission, the mtDNA molecules are then divided up into individual mitochondria, which would better allow the cellular machinery to differentially act on the different alleles. Mitochondria containing WT-mtDNA would presumably have a robust membrane potential and wouldn't be leaky due to intact MRC machinery, and those mitochondria would be the only ones taking up replication machinery, resulting in increased WT-mtDNA copy number. Mitochondria containing *uaDf5* mtDNA would have diminished membrane potential and may be leaky due to dysfunctional MRC machinery, which could inhibit the import of replication machinery. The mitophagic removal of mitochondria exhibiting a low membrane potential would normally happen in a PINK-1-dependent manner, but seeing as there is no functional PINK-1 in a fraction of the lines that have the rapid removal phenotype, the removal of *uaDf5*-containing mitochondria must occur through some other mechanism. Further studies need to be done to elucidate if mitochondrial fission is indeed a mechanism through which the IGE results

in removal of *uaDf5*, and to uncover how a PINK-1-independent removal process proceeds.

Is WT-mtDNA amplification a necessary step for the IGE to remove defective mtDNA?

What happens to the removal capacity of the IGE if WT-mtDNA amplification is inhibited? Would the inhibition affect the rate or completely inhibit the removal of *uaDf5*? To answer this question, the dynamics of *uaDf5* removal need to be analyzed in animals treated with ethidium bromide (EtBr; [225]) or RNAi against POLG (the mtDNA polymerase [1,226]), which both inhibit mtDNA replication [107,227–230]. It would be curious to find that WT-mtDNA replication is necessary and suggests that the IGE process is more dependent on clonal expansion of specific mtDNA rather than selective removal of *uaDf5*.

Does the IGE antagonize the UPR^{MT}?

The stability of *uaDf5* has been associated with the activity of the UPR^{MT} [78,80], and thus it would be of interest to see if the UPR^{MT} is actually inhibited after the IGE. Analysis of the removal capacity after the IGE in the *atfs-1* gain-of-function mutant, which results in constitutive activity of the UPR^{MT}, will give insights into whether the activity of the UPR^{MT} is a crucial component of the IGE-associated removal phenotype.

Is the transgenerational removal of *uaDf5* following the IGE transmitted through the nucleus, the mitochondrion, or the cytoplasm?

Have I indeed found an epigenetic state that results in increased mtDNA quality control? If so, at what level in the cell are the epigenetics occurring? Is this a case of traditional nuclear epigenetics [231–235], or have I found epigenetic control at the mitochondrial level [236–239], or even the cytoplasmic level? Epigenetic analysis of the chromatin structure needs to be performed, as well as mutational analysis of epigenetic regulators. Another question that is raised is why do only a fraction of the lines exhibit the removal phenotype following the IGE? Is there a dosage dependency, perhaps of a cytoplasmic component, or is there a threshold effect in which the rapid removal is observed as soon as either the fractional abundance of *uaDf5*, or the copy number of *uaDf5*, gets below a certain level? Further analysis of the lines that do not exhibit the rapid removal phenotype will give some insight here. Perhaps if given a few more generations, all of the lines following the IGE will eventually eliminate *uaDf5*.

FIGURES

Figure 1

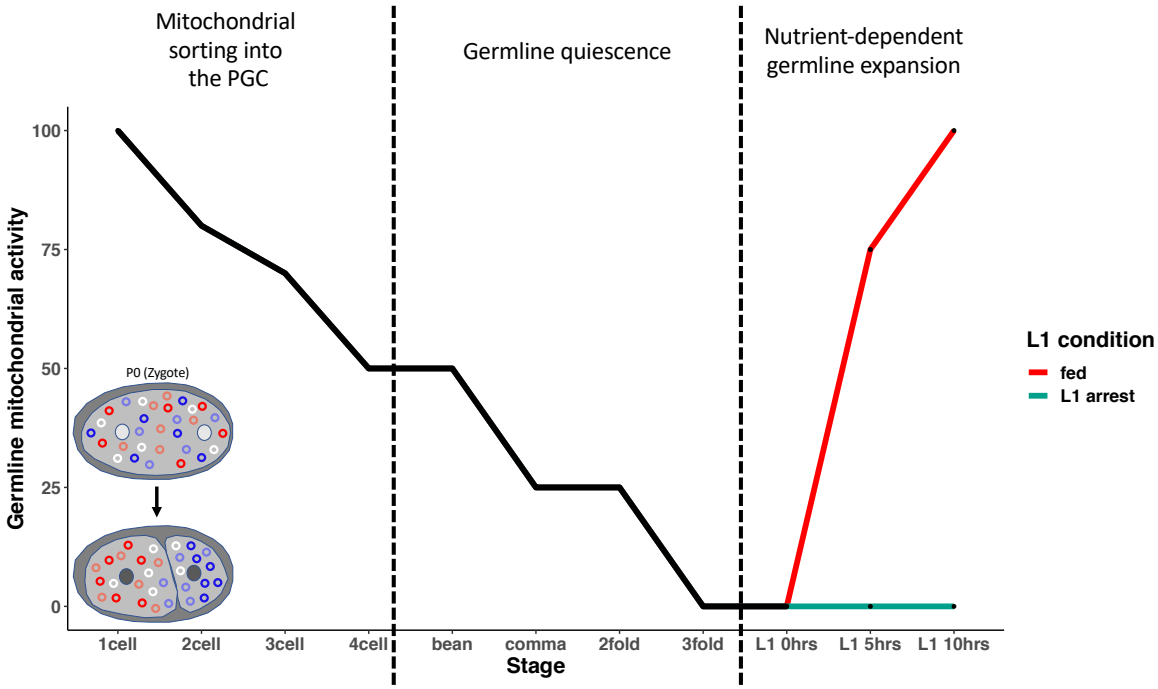

Figure 1. Mitochondrial dynamics during early development. Diagram outlining the dynamics of the regulation of mitochondrial activity throughout early development, starting at the one-cell embryo and extending through to the first larval state L1. Mitochondrial activity is high at the one-cell stage such that mitochondria can be sorted between the PGC and soma, then they enter a state of quiescence at the four-cell stage that lasts throughout embryogenesis. Upon hatching, mitochondria remain quiescent in a DAF-18, DAF-2, and AAK-2 dependent manner until food is available, after which they turn on their activity.

Figure 2:

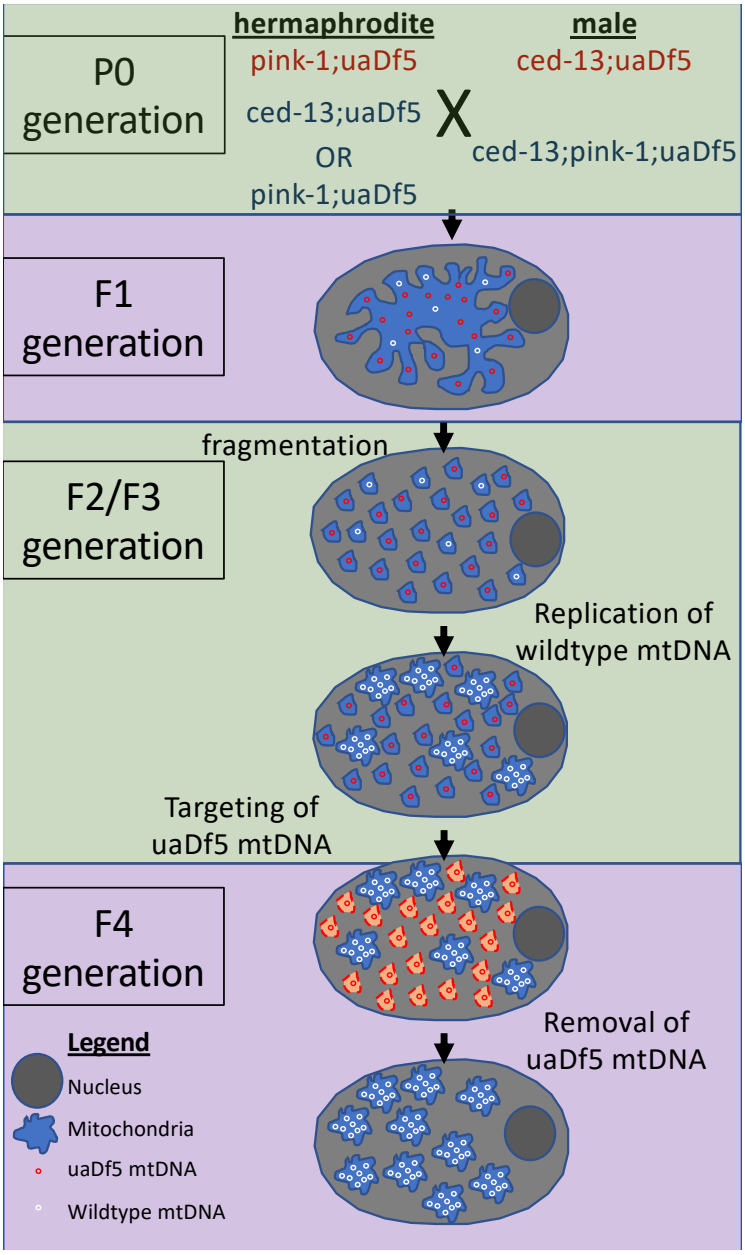

Figure 2. Proposed model of the IGE-associated removal mechanism. Diagram of our proposed model in which the IGE results in global mitochondrial fission, thus allowing for mitochondria containing WT-mtDNA to import replication machinery, followed by mitochondria containing *uaDf5*-mtDNA to be selectively degraded in a PINK-1-independent manner.

APPENDIX

Additional studies in C. elegans: mtDNA quality control

A1. Strain Table

Strain	Genotype	Paternal		Maternal		Ch.
		Strain	Genotype	Strain	Genotype	
CB1370	*daf-2(e1370)*	-	-	-	-	2, 4
CB1375	*daf-18(e1375)*	-	-	-	-	2, 4
CB3886	*par-2(e2030ts)*	-	-	-	-	2
CF1038	*daf-16(mu86)*	-	-	-	-	2, 4
DR1572	*daf-2(e1368)*	-	-	-	-	2, 4
DR1574	*daf-2(e1391)*	-	-	-	-	2, 4
EU856	*spd-5(or213)*	-	-	-	-	2
FX536	*ced-13(tm536)*	-	-	-	-	
JH2320	*axIs1677 [pie-1p::GFP::histone H2B::pgl-1 3'UTR +unc-119(+)]*	-	-	-	-	2
JK1667	*par-4(it57)ts*	-	-	-	-	2
JR2669	*daf-18(ok480)*	N2 (2x)	*wildtype*	RB712	*daf-18(ok480)*	2, 4
JR3298	*pink-1(tm1779)*	N2 (5x)	*wildtype*	FX01779	*pink-1(tm1779)*	2
JR3335	*pink-1(ok3538)*	N2 (3x)	*wildtype*	RB2547	*pink-1(ok3538)*	2
JR3487	*uaDf5*	N2	*wildtype*	LB138	*him-8(e1489); uaDf5*	
JR3630	*uaDf5*	N2 (8x)	*wildtype*	JR3487	*uaDf5*	all
JR3634	*ced-3(n717); uaDf5*	MT1522	*ced-3(n717)*	JR3630	*uaDf5*	
JR3648	*edIs20[F25B3.3::GFP; pRF4]; him-8(e1489); uaDf5*	JR797	*edIs20[F25B3.3::GFP; pRF4]; him-8(e1489)*	JR3630	*uaDf5*	
JR3680	*myo-3p::TOM20::mRFP; uaDf5*	PS6192	*myo-3p::TOM20::mRFP*	JR3630	*uaDf5*	
JR3688	*pink-1(tm1779); uaDf5*	JR3298	*pink-1(tm1779)*	JR3630	*uaDf5*	3
JR3880	*ced-3(n717); uaDf5*	MT1522	*ced-3(n717)*	JR3630	*uaDf5*	3
JR3925	*ced-4(n1162); uaDf5*	MT2547	*ced-4(n1162)*	JR3630	*uaDf5*	3
JR3926	*ced-10(n1993); uaDf5*	MT5013	*ced-10(n1993)*	JR3630	*uaDf5*	3
JR3927	*ced-10(n1993); uaDf5*	MT5013	*ced-10(n1993)*	JR3630	*uaDf5*	3
JR3928	*ced-10(n1993); uaDf5*	MT5013	*ced-10(n1993)*	JR3630	*uaDf5*	3

JR3929	*atfs-1(tm4525); uaDf5*	TM4525	*atfs-1(tm4525)*	JR3630	*uaDf5*	3
JR3930	*atfs-1(tm4525); uaDf5*	TM4525	*atfs-1(tm4525)*	JR3630	*uaDf5*	3
JR3931	*ced-4(n1162); uaDf5*	MT2547	*ced-4(n1162)*	JR3630	*uaDf5*	3
JR3932	*ced-4(n1162); uaDf5*	MT2547	*ced-4(n1162)*	JR3630	*uaDf5*	3
JR3937	*atfs-1(et15); uaDf5*	QC115	*atfs-1(et15)*	JR3630	*uaDf5*	3
JR3938	*ced-3(n2454); uaDf5*	MT8354	*ced-3(n2454)*	JR3630	*uaDf5*	3
JR3941	*glp-1(q231ts); uaDf5*	JK530	*glp-1(q231ts)*	JR3630	*uaDf5*	4
JR3942	*glp-1(q231ts); uaDf5*	JK530	*glp-1(q231ts)*	JR3630	*uaDf5*	4
JR3948	*daf-2(m41); uaDf5*	DR1564	*daf-2(m41)*	JR3630	*uaDf5*	4
JR3949	*fem-3(q20ts); uaDf5*	JK816	*fem-3(q20ts)*	JR3630	*uaDf5*	4
JR3950	*fem-3(q96ts); uaDf5*	JK1973	*fem-3(q96ts)*	JR3630	*uaDf5*	4
JR3955	*ced-13(sv32); uaDf5*	MD792	*ced-13(sv32)*	JR3630	*uaDf5*	3
JR3956	*ced-13(sv32); uaDf5*	MD792	*ced-13(sv32)*	JR3630	*uaDf5*	3
JR3957	*pink-1(w46); uaDf5*	JR3879	*pink-1(w46)*	JR3630	*uaDf5*	3
JR3958	*pink-1(w46); uaDf5*	JR3879	*pink-1(w46)*	JR3630	*uaDf5*	3
JR3959	*daf-2(e1370); uaDf5*	CB1370	*daf-2(e1370)*	JR3630	*uaDf5*	4
JR3960	*daf-2(e1370); uaDf5*	CB1370	*daf-2(e1370)*	JR3630	*uaDf5*	4
JR3961	*dyn-1(ky51ts); uaDf5*	CX51	*dyn-1(ky51ts)*	JR3630	*uaDf5*	
JR3962	*dyn-1(ky51ts); uaDf5*	CX51	*dyn-1(ky51ts)*	JR3630	*uaDf5*	
JR3963	*daf-2(e1391); uaDf5*	DR1574	*daf-2(e1391)*	JR3630	*uaDf5*	4
JR3964	*daf-2(e1391); uaDf5*	DR1574	*daf-2(e1391)*	JR3630	*uaDf5*	4
JR3965	*glp-4(bn2ts); uaDf5*	SS104	*glp-4(bn2ts)*	JR3630	*uaDf5*	4
JR3966	*glp-4(bn2ts); uaDf5*	SS104	*glp-4(bn2ts)*	JR3630	*uaDf5*	4
JR3972	*ced-1(e1735); uaDf5*	CB3203	*ced-1(e1735)*	JR3630	*uaDf5*	3
JR3973	*ced-1(e1735); uaDf5*	CB3203	*ced-1(e1735)*	JR3630	*uaDf5*	3
JR3974	*ced-5(n1812); uaDf5*	MT4434	*ced-5(n1812)*	JR3630	*uaDf5*	3

JR3975	*ced-5(n1812); uaDf5*	MT4434	*ced-5(n1812)*	JR3630	*uaDf5*	3
JR3976	*ced-13(tm536); uaDf5*	FX536	*ced-13(tm536)*	JR3630	*uaDf5*	3
JR3977	*ced-3(n1286); uaDf5*	MT3002	*ced-3(n1286)*	JR3630	*uaDf5*	3
JR3978	*ced-2(e1752); uaDf5*	CB3257	*ced-2(e1752)*	JR3630	*uaDf5*	3
JR3979	*cep-1(gk138); uaDf5*	VC172	*cep-1(gk138)*	JR3630	*uaDf5*	3, 4
JR3980	*cep-1(gk138); uaDf5*	VC172	*cep-1(gk138)*	JR3630	*uaDf5*	3, 4
JR3981	*csp-1(tm917); ced-3(n717); uaDf5*	JR3196	*csp-1(tm917); ced-3(n717)*	JR3880	*ced-3(n717); uaDf5*	3
JR3982	*csp-1(tm917); ced-3(n717); uaDf5*	JR3196	*csp-1(tm917); ced-3(n717)*	JR3880	*ced-3(n717); uaDf5*	3
JR3983	*ced-3(n718); uaDf5*	MT1743	*ced-3(n718)*	JR3630	*uaDf5*	3
JR3984	*ced-3(n718); uaDf5*	MT1743	*ced-3(n718)*	JR3630	*uaDf5*	3
JR3986	*csp-2(tm3077); uaDf5*	JR3397	*csp-2(tm3077)*	JR3630	*uaDf5*	3
JR3987	*csp-2(tm3077); uaDf5*	JR3397	*csp-2(tm3077)*	JR3630	*uaDf5*	3
JR3992	*clk-1(qm30); uaDf5*	MQ130	*clk-1(qm30)*	JR3630	*uaDf5*	3, 4
JR3993	*clk-1(qm30); uaDf5*	MQ130	*clk-1(qm30)*	JR3630	*uaDf5*	3, 4
JR3995	*daf-16(mu86); uaDf5*	CF1038	*daf-16(mu86)*	JR3630	*uaDf5*	4
JR3996	*daf-16(mu86); uaDf5*	CF1038	*daf-16(mu86)*	JR3630	*uaDf5*	4
JR3997	*daf-16(mgDf50); uaDf5*	GR1307	*daf-16(mgDf50)*	JR3630	*uaDf5*	4
JR3998	*daf-16(mgDf50); uaDf5*	GR1307	*daf-16(mgDf50)*	JR3630	*uaDf5*	4
JR4001	*ced-10(n3246); uaDf5*	MT9958	*ced-10(n3246)*	JR3630	*uaDf5*	3
JR4002	*ced-10(n3246); uaDf5*	MT9958	*ced-10(n3246)*	JR3630	*uaDf5*	3
JR4003	*age-1(hx546); uaDf5*	TJ1052	*age-1(hx546)*	JR3630	*uaDf5*	4
JR4004	*age-1(hx546); uaDf5*	TJ1052	*age-1(hx546)*	JR3630	*uaDf5*	4
JR4005	*daf-16(mu86); daf-2(e1370); uaDf5*	CF1038	*daf-16(mu86)*	JR3960	*daf-2(e1370); uaDf5*	4

JR4006	*daf-16(mu86); daf-2(e1370); uaDf5*	CF1038	*daf-16(mu86)*	JR3960	*daf-2(e1370); uaDf5*	4
JR4007	*daf-16(mu86); daf-2(e1391); uaDf5*	CF1038	*daf-16(mu86)*	JR3963	*daf-2(e1391); uaDf5*	4
JR4008	*daf-16(mu86); daf-2(e1391); uaDf5*	CF1038	*daf-16(mu86)*	JR3963	*daf-2(e1391); uaDf5*	4
JR4010	*ced-1(e1735); ced-2(e1752); uaDf5*	JR3972	*ced-1(e1735); uaDf5*	JR3978	*ced-2(e1752); uaDf5*	3
JR4011	*aak-2(ok524); uaDf5*	RB754	*aak-2(ok524)*	JR3630	*uaDf5*	4
JR4012	*aak-2(gt33); uaDf5*	TG38	*aak-2(gt33)*	JR3630	*uaDf5*	4
JR4013	*aak-2(gt33); uaDf5*	TG38	*aak-2(gt33)*	JR3630	*uaDf5*	4
JR4014	*vhl-1(ok161); uaDf5*	CB5602	*vhl-1(ok161)*	JR3630	*uaDf5*	4
JR4015	*vhl-1(ok161); uaDf5*	CB5602	*vhl-1(ok161)*	JR3630	*uaDf5*	4
JR4016	*cep-1(gk138); ced-3(n1286); uaDf5*	JR3979	*cep-1(gk138); uaDf5*	JR3977	*ced-3(n1286); uaDf5*	3
JR4017	*ced-4(n1894); uaDf5*	MT5287	*ced-4(n1894)*	JR3630	*uaDf5*	3
JR4024	*daf-16(mu86); daf-2(m41); uaDf5*	CF1038	*daf-16(mu86)*	JR3948	*daf-2(m41); uaDf5*	4
JR4025	*daf-16(mu86); daf-2(m41); uaDf5*	CF1038	*daf-16(mu86)*	JR3948	*daf-2(m41); uaDf5*	4
	ced-9(n1950); uaDf5	MT4770	*ced-9(n1950)*	JR3630	*uaDf5*	3
JR4027	*ced-9(n1950); uaDf5*	MT4770	*ced-9(n1950)*	JR3630	*uaDf5*	3
JR4029	*pdr-1(gk448); uaDf5*	VC1024	*pdr-1(gk448)*	JR3630	*uaDf5*	3
JR4030	*pdr-1(gk448); uaDf5*	VC1024	*pdr-1(gk448)*	JR3630	*uaDf5*	3
	cep-1(gk138); pink-1(w46); uaDf5	JR3979	*cep-1(gk138); uaDf5*	JR3957	*pink-1(w46); uaDf5*	3
JR4035	*cep-1(gk138); pink-1(w46); uaDf5*	JR3979	*cep-1(gk138); uaDf5*	JR3957	*pink-1(w46); uaDf5*	3
JR4042	*cep-1(ep347); uaDf5*	CE1255	*cep-1(ep347)*	JR3630	*uaDf5*	3
JR4043	*cep-1(ep347); uaDf5*	CE1255	*cep-1(ep347)*	JR3630	*uaDf5*	3

JR4048	*pdr-1(gk448); ced-13(tm536); uaDf5*	VC1024	*pdr-1(gk448)*	JR3976	*ced-13(tm536); uaDf5*	3
JR4049	*pdr-1(gk448); ced-13(tm536); uaDf5*	JR3976	*ced-13(tm536); uaDf5*	JR4029	*pdr-1(gk448); uaDf5*	3
JR4053	*cep-1(gk138); daf-2(e1370); uaDf5*	JR3979	*cep-1(gk138); uaDf5*	JR3960	*daf-2(e1370); uaDf5*	4
JR4054	*cep-1(gk138); daf-2(e1370); uaDf5*	JR3979	*cep-1(gk138); uaDf5*	JR3960	*daf-2(e1370); uaDf5*	4
JR4055	*ced-13(tm536); ced-4(n1126); uaDf5*	JR3976	*ced-13(tm536); uaDf5*	JR3925	*ced-4(n1162); uaDf5*	3
JR4056	*ced-13(tm536); ced-4(n1126); uaDf5*	JR3976	*ced-13(tm536); uaDf5*	JR3925	*ced-4(n1162); uaDf5*	3
JR4057	*ced-13(tm536); ced-3(n1286); uaDf5*	JR3976	*ced-13(tm536); uaDf5*	JR3977	*ced-3(n1286); uaDf5*	3
JR4058	*ced-13(tm536); ced-3(n1286); uaDf5*	JR3976	*ced-13(tm536); uaDf5*	JR3977	*ced-3(n1286); uaDf5*	3
JR4059	*clk-1(qm30); daf-2(e1391); uaDf5*	MQ130	*clk-1(qm30)*	JR3963	*daf-2(e1391); uaDf5*	4
JR4060	*clk-1(qm30); daf-2(e1391); uaDf5*	JR3963	*daf-2(e1391); uaDf5*	JR3993	*clk-1(qm30); uaDf5*	4
JR4061	*cep-1(gk138); pdr-1(gk448); uaDf5*	JR3979	*cep-1(gk138); uaDf5*	JR4029	*pdr-1(gk448); uaDf5*	3
JR4062	*cep-1(gk138); pdr-1(gk448); uaDf5*	JR3979	*cep-1(gk138); uaDf5*	JR4029	*pdr-1(gk448); uaDf5*	3
JR4065	*pdr-1(gk448); pink-1(w46); uaDf5*	VC1024	*pdr-1(gk448)*	JR3957	*pink-1(w46); uaDf5*	3
JR4066	*pdr-1(gk448); pink-1(w46); uaDf5*	VC1024	*pdr-1(gk448)*	JR3957	*pink-1(w46); uaDf5*	3
JR4067	*ced-13(tm536); pink-1(w46); uaDf5*	JR3976	*ced-13(tm536); uaDf5*	JR3957	*pink-1(w46); uaDf5*	3
JR4068	*ced-13(tm536); pink-1(w46); uaDf5*	JR3976	*ced-13(tm536); uaDf5*	JR3957	*pink-1(w46); uaDf5*	3

JR4069	*ced-13(tm536); cep-1(gk138); uaDf5*	JR3976	*ced-13(tm536); uaDf5*	JR3979	*cep-1(gk138); uaDf5*	3
JR4070	*ced-13(tm536); cep-1(gk138); uaDf5*	JR3976	*ced-13(tm536); uaDf5*	JR3979	*cep-1(gk138); uaDf5*	3
JR4071	*cep-1(gk138); clk-1(qm30); uaDf5*	JR3979	*cep-1(gk138); uaDf5*	JR3993	*clk-1(qm30); uaDf5*	4
JR4073	*cep-1(gk138); clk-1(qm30); uaDf5*	JR3979	*cep-1(gk138); uaDf5*	JR3993	*clk-1(qm30); uaDf5*	4
JR4074	*cep-1(gk138); daf-2(e1391); uaDf5*	JR3979	*cep-1(gk138); uaDf5*	JR3963	*daf-2(e1391); uaDf5*	4
JR4075	*cep-1(gk138); daf-2(e1391); uaDf5*	JR3963	*daf-2(e1391); uaDf5*	JR3979	*cep-1(gk138); uaDf5*	4
JR4076	*daf-2(e1391); ced-3(n1286); uaDf5*	JR3963	*daf-2(e1391); uaDf5*	JR3977	*ced-3(n1286); uaDf5*	4
KK237	*par-3(e2074)*	-	-	-	-	2
KK299	*par-5(it55)*	-	-	-	-	2
KK818	*par-6(zu222)*	-	-	-	-	2
KK822	*par-1(zu310ts)*	-	-	-	-	2
LSJ1	*wildtype*	-	-	-	-	2
MQ130	*clk-1(qm30)*	-	-	-	-	2, 4
MR507	*aak-2(rr48)*	-	-	-	-	2, 4
MT12993	*mir-71(n4115)*	-	-	-	-	2
MT1522	*ced-3(n717)*	-	-	-	-	2
MT3002	*ced-3(n718)*	-	-	-	-	2
RB754	*aak-2(ok524)*	-	-	-	-	2, 4
TG38	*aak-2(gt33)*	-	-	-	-	2, 4
VC172	*cep-1(gk138)*	-	-	-	-	4

A2. Illumina as a technique to measure mtDNA heteroplasmy

INTRODUCTION

In order to better characterize the consequences of *uaDf5*, we wanted to determine if the *uaDf5* strain has excess levels of general heteroplasmy (increased number of SNPs across the mtDNA genome). To do this we utilized Illumina sequencing to quantify heteroplasmies. We did 3 separate runs and got varying results from all runs. However, our third run revealed that the strain containing *uaDf5* has a 1 base pair deletion at position 6752 in the *nduo-4* gene, which results in premature truncation of the ND4 protein.

RESULTS AND FIGURES

A. Initial Illumina run reveals that *uaDf5* (green) has greatly increased frequency of SNPs across the entire mtDNA genome as compared to wildtype (red). Frequency of each SNP is represented on the y axis, location along the mtDNA genome is indicated on the x axis.

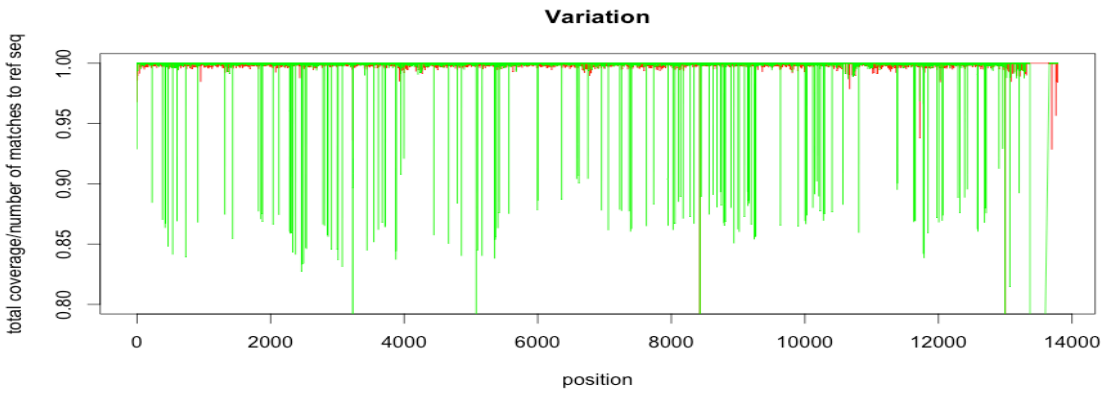

B. The second run shows that *uaDf5* strain only has an increased number of SNPs as compared to wildtype (red) if grown for 12 generations with no starvation (green), suggesting starvation results in cleanup of mtDNA SNPs. showed higher numbers of low frequency SNPs across both wildtype (red) and *uaDf5* (1 generation post-starvation = blue; 12 generations post-starvation = green) strains. SNP calling, shown in the second figure, shows that the sample grown for 16 generations has a greatly increased frequency of SNPs (indicated as the black lines along the x axis). The effects of those called SNPs are tabulated in the third image and the table at the end.

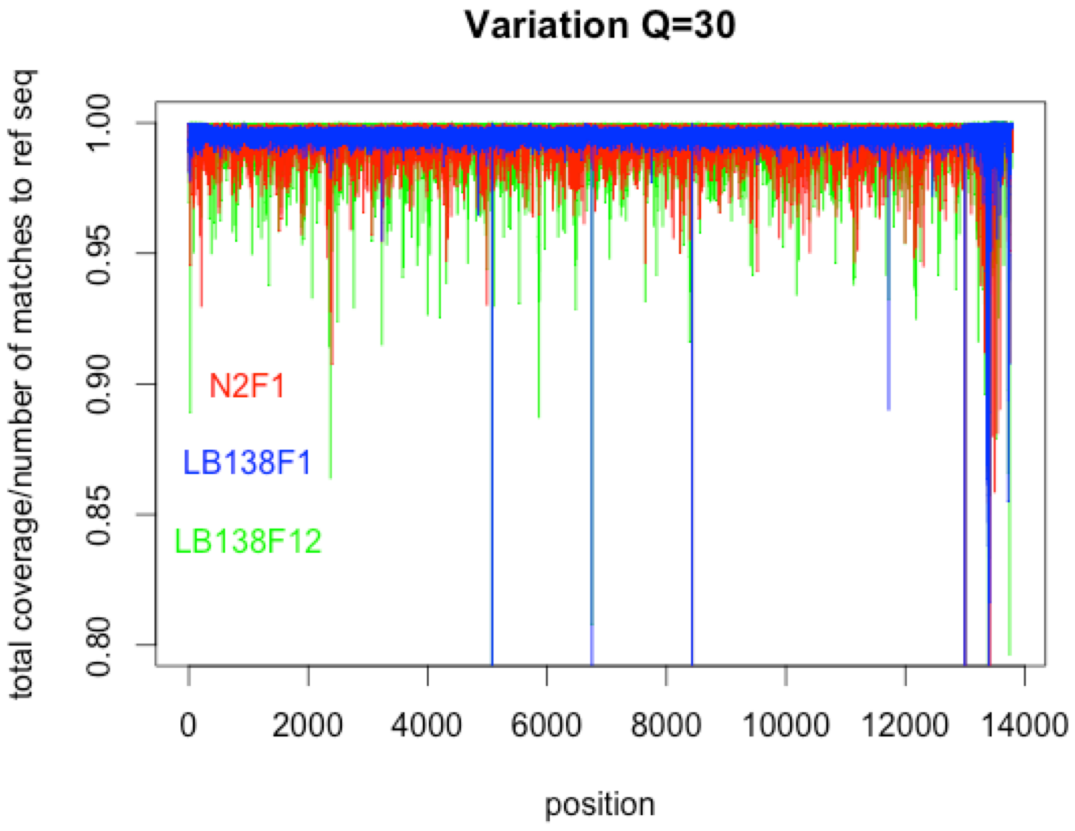

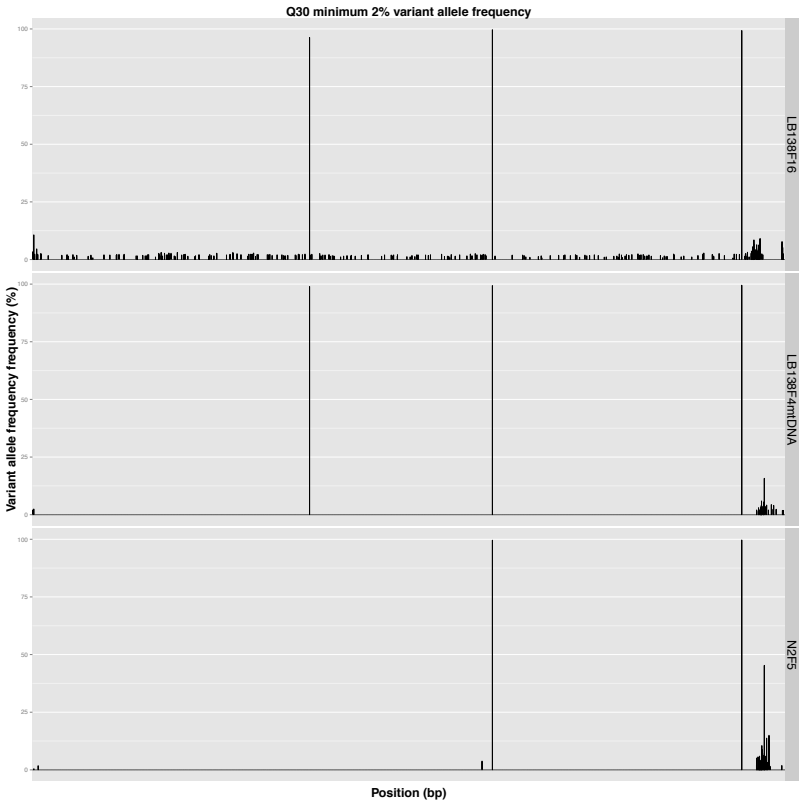

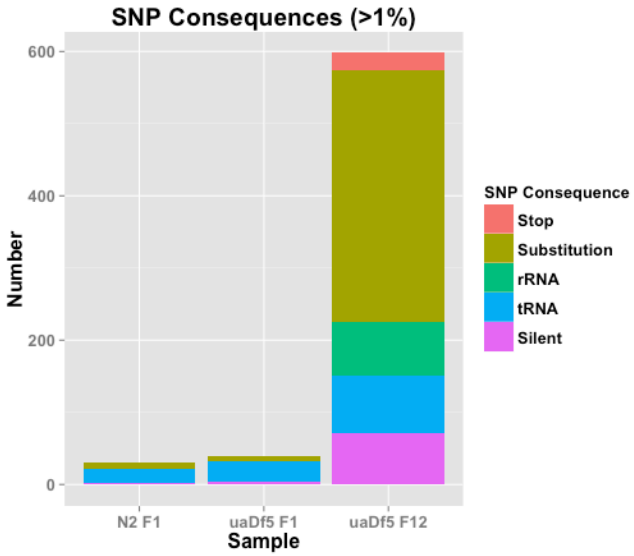

Sample	Total # SNPs	# Silent	# Amino Acid substitution	# tRNA	# rRNA
N2- F1	30	2	9	19	0
uaDf5 – F1	39	4	7	28	0
uaDf5- F12	598	71	349 (24 stop)	79	75

C. Our third run revealed low levels of SNP frequency in all samples analyzed. The first image shows N2 results, with starved samples on top and fed samples on bottom. The second image shows *uaDf5* results, with starved samples on top and fed samples on bottom. The third image shows the called SNPs in all strains analyzed, and these results show no correlation between starvation and heteroplasmy frequencies. However, analysis of a 1 base pair deletion at base position 6752 shows it is specific to *uaDf5* samples (shown in the fourth image). The fifth image shows our analysis of this SNP in a strain containing a *pink-1* mutation (*pink-1(tm1779)*), and shows that both the *uaDf5* deletion and deletion at position 6752 was represented by ~70% of reads, suggesting the two deletions are linked on the same mtDNA chromosome.

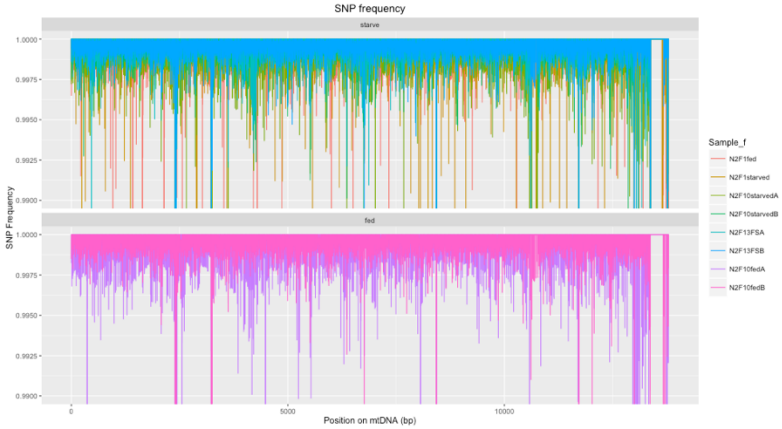

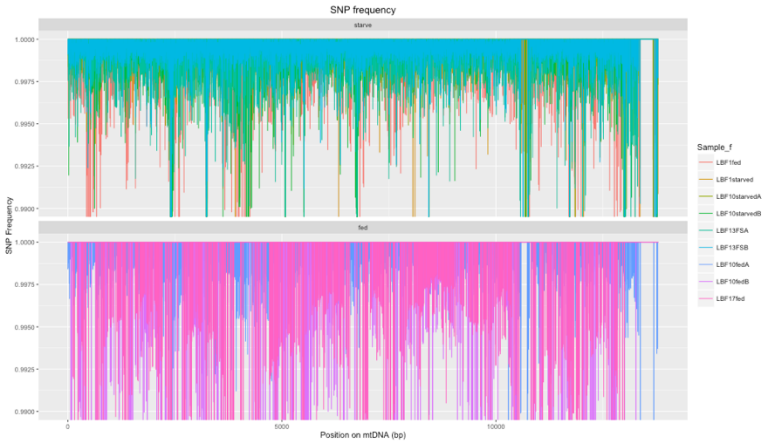

Sample	Total # SNPs	# SNPs before strand bias	# Silent	# Amino Acid substitution	# tRNA	# rRNA
N2-F1 fed A	**2**	**4 (31)**	**2**	**0**	**0**	**0**
N2-F1 starved B	**2**	**5 (45)**	**2**	**0**	**0**	**0**
uaDf5-F1 fed A	**2**	**3 (52)**	**2**	**0**	**0**	**0**
uaDf5-F1 starved B	**3**	**5 (25)**	**3**	**0**	**0**	**0**
N2-F10 starved A	**2**	**4 (20)**	**2**	**0**	**0**	**0**
N2-F10 starved B	**2**	**6 (15)**	**2**	**0**	**0**	**0**
uaDf5-F10 starved A	**3**	**7 (21)**	**3**	**0**	**0**	**0**
uaDf5-F10 starved B	**2**	**3 (34)**	**2**	**0**	**0**	**0**
N2-F13 F->S A	**2**	**5 (19)**	**2**	**0**	**0**	**0**
N2-F13 F->S B	**2**	**6 (13)**	**2**	**0**	**0**	**0**
uaDf5-F13 F->S A	**3**	**3 (26)**	**3**	**0**	**0**	**0**
uaDf5-F13 F->S B	**2**	**6 (18)**	**2**	**0**	**0**	**0**
N2-F10 fed A	**2**	**3 (33)**	**2**	**0**	**0**	**0**
N2-F10 fed B	**2**	**5 (16)**	**2**	**0**	**0**	**0**
uaDf5-F10 fed A	**3**	**3 (20)**	**3**	**0**	**0**	**0**
uaDf5-F10 fed B* **	**2**	**2 (198)**	**2**	**0**	**0**	**0**
uaDf5-F17 fed* **	**2**	**2 (148)**	**2**	**0**	**0**	**0**

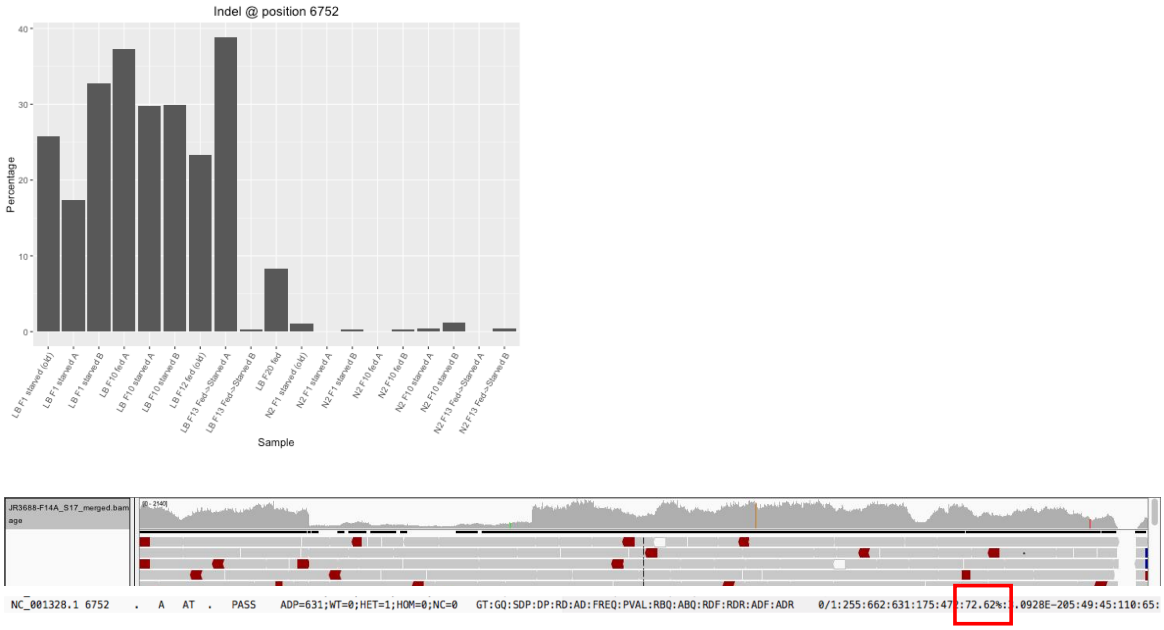

EXPERIMENTAL PROCEDURES

WT-mtDNA (N2) and *uaDf5*-containing strains (LB138, JR3630, and JR3688) were used for Illumina analysis. 20 large confluent plates were used for each strain. Worms were collected off the plates and a mitochondrial isolation followed by a DNA extraction was performed. The resulting DNA sample was prepped using the Nextera library kit and was then run on the Illumina NextSeq 500 using the 300 cycle Mid-output kit with paired end reads (2x150). The corresponding reads were mapped to the *C. elegans* assembly reference sequence WBcel235. The reads were first trimmed using Trimmomatic before being mapped to the reference sequence using BWA. Picard Tools was used to sort the sam files giving a bam file output and then to mark and remove duplicates. The resulting bam files were merged, indexed and then converted to mpileup files using SamTools. SNP calling was done with the program VarScan, with a minimum coverage of 100 and a minimum variant frequency call of 0.01.

A3. Development of a technique for generating heteroplasmic "transmitic" *C. elegans*

INTRODUCTION

In order to determine if *uaDf5* is maintained due to replicative advantage and acts as a true "selfish" DNA element, we generated a technique for making "transmitic" animals. To do this, we purified intact mitochondria from the *uaDf5* strain, labeled them with MitoTracker Red as a co-injection marker, and injected them into adult gonads with wildtype mtDNA in order to introduce *uaDf5* into the germline. We then imaged embryos laid from the injected hermaphrodites to see if any embryos successfully took up the injected *uaDf5* mitochondria. We have shown that embryos do take up the introduced mitochondria, but we have not developed an efficient selection method to determine if any of the resulting lines amplify *uaDf5* via this method.

RESULTS AND FIGURES

A. Our proposed scheme for generating transmitic worms. If *uaDf5* undergoes clonal expansion as a selfish DNA element, one would expect to see a large increase in the fractional abundance of *uaDf5* following the generation of a transmitic worm.

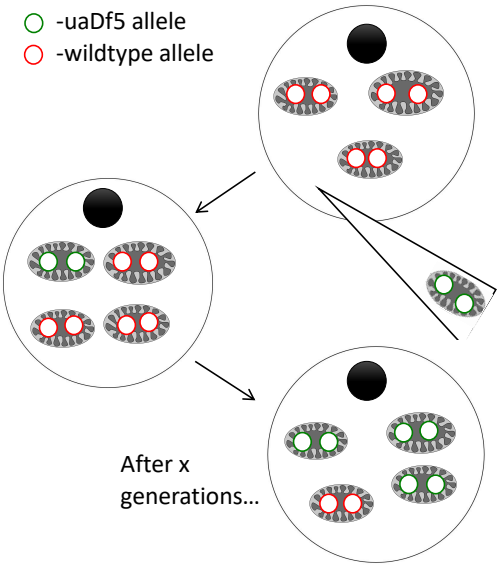

B. Imaging of MitoTracker-labeled injected mitochondria, in both uninjected and injected adult gonads and the resulting F1 embryos shows successful uptake of introduced mitochondria.

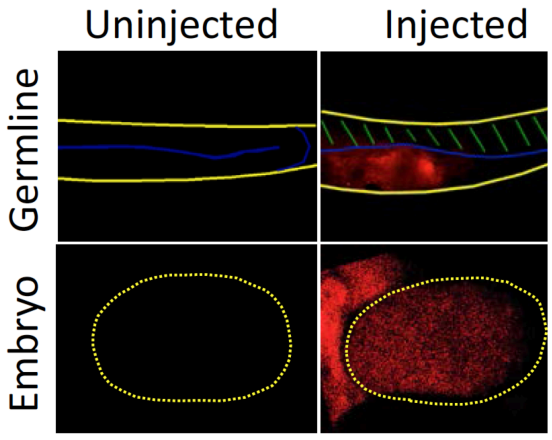

EXPERIMENTAL PROCEDURES

Mitochondrial Isolation

Worms were collected from 20 large plates in M9 and after spinning down were resuspended in 10 ml ice-cold isolation buffer (IB: 210 mM Mannitol, 70 mM Sucrose, 0.1 mM EDTA pH 8.0, 5 mM Tris-HCl pH 7.4) with 1 mM PMSF (phenylmethanesulfonylfluoride). The worms were then homogenized with 30 strokes of a chilled 50 ml homogenizer. The homogenate was transferred to a 50 ml tube and the volume was increased to 20 ml with IB + PMSF. The samples were pelleted for 10 min at 750g. The supernatant was transferred to a fresh 50 ml tube and the pellet was resuspended in 10 ml IB + PMSF and homogenized a second time with 30 more strokes of the homogenizer. The homogenate was transferred to a fresh 50 ml tube and the volume was increased to 20 ml with IB + PMSF and then spun down for 10 min at 750g. The supernatants were spun down for 10 min at 12,000 g at 4C. The resulting pellet was resuspended in 12 ml IB and then centrifuged for 10 min at 750g. The resulting supernatant was then centrifuged a second time at 12,000g for 10 min.

Injections and imaging

10 μM MitoTracker Red was added to the isolated mitochondrial solution and the resulting solution was loaded into a microinjection needle. Young adults were injected with the solution into the gonad and resulting embryos were collected 10 hours after injection for imaging on a Nikon Eclipse Ti.

A4. Fitness parameters of various mutants

INTRODUCTION

In order to determine how *uaDf5* affects various fitness parameters in various mutant backgrounds that we have shown act in mtDNA quality control, we measured brood size, embryonic lethality, unfertilized oocyte production, developmental rate, and lifespan.

RESULTS

A. Analysis of brood size shows that *uaDf5* has no impact on *ced-10* and *ced-13* mutants, with evidence of a small decline in *ced-3* mutants.

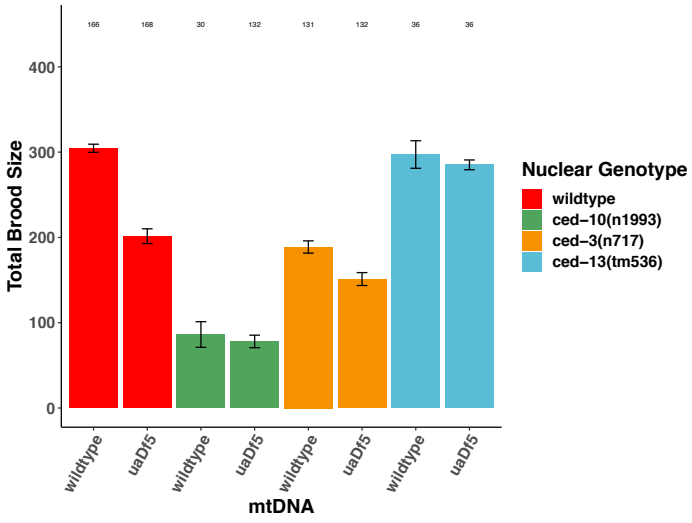

B. Analysis of embryonic lethality shows that *uaDf5* has no impact in *ced-10* mutants, a small increase in *ced-3* mutants, and a large increase in *ced-13* mutants.

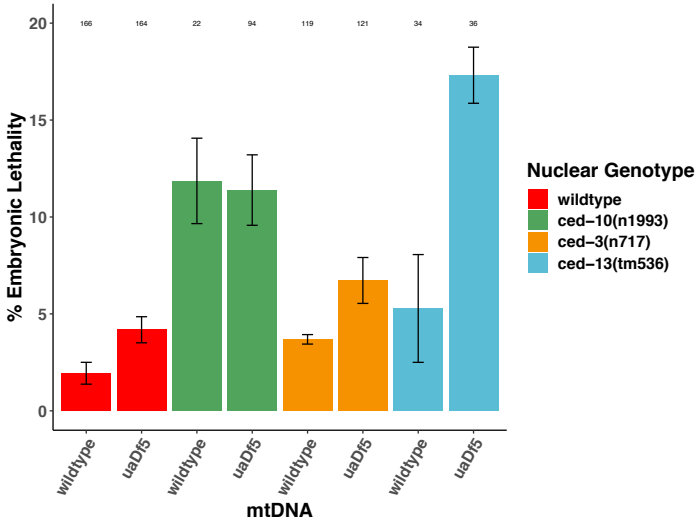

C. Analysis of unfertilized oocyte production shows that *uaDf5* has no impact on *ced-10* and *ced-3* mutants, with evidence of a small increase in *ced-13* mutants.

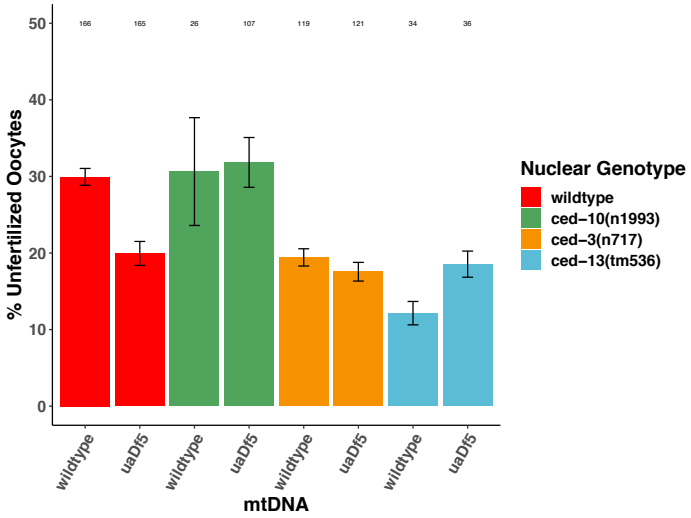

D. Analysis of the number of hours it takes to reach gravidity shows that *uaDf5* slows developmental rate in *ced-10* mutants, with no evidence of an impact in *ced-3* mutants.

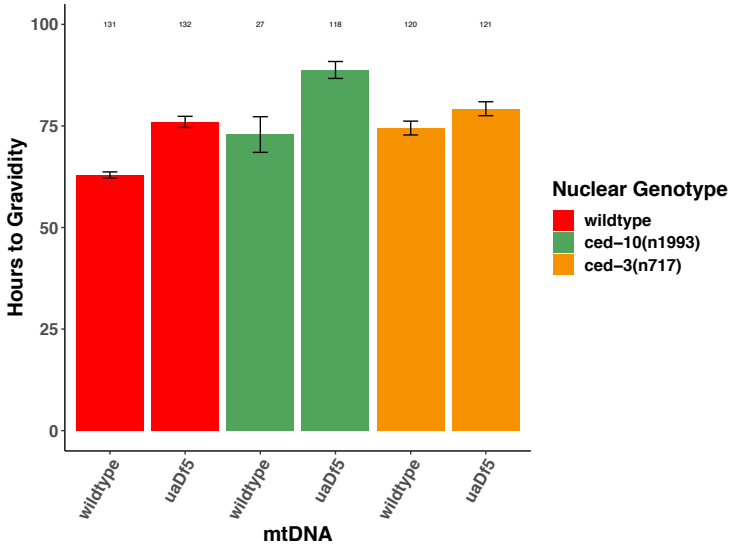

E. Analysis of the developmental stage at 60 hours shows that *uaDf5* has no impact on both *ced-10* and *ced-3* mutants.

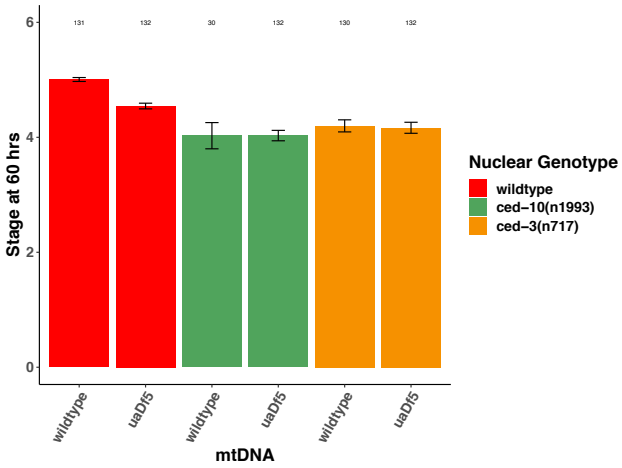

F. Analysis of lifespan shows that *uaDf5* has no impact on *ced-10, ced-3,* and *ced-13* mutants.

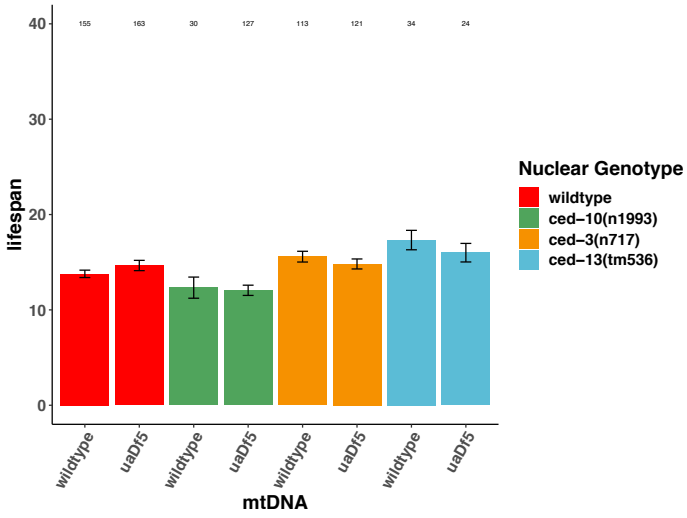

EXPERIMENTAL PROCEDURES

Lifespan analysis

Confluent large plates were egg prepped and left to spin in M9 overnight for synchronization. The hatched L1s were plated onto large thick plates and allowed to grow to day two adults before being egg prepped a second time and left to spin in M9 overnight. The next morning, referred to as day one for lifespan determination, L1s were singled out onto small plates. Once the worms started laying eggs, they were transferred each day to a fresh small plate until egg laying ceased, after which the worms remained on the same plate unless bacterial contamination required transfer to a fresh plate. Worms were considered dead if there was no movement after being lightly prodded with a worm pick.

Brood size, embryonic lethality, and unfertilized oocytes analysis

Confluent large plates were egg prepped and left to spin in M9 overnight for synchronization. The hatched L1s were plated onto large thick plates and allowed to grow to day two adults before being egg prepped a second time and left to spin in M9 overnight. The next morning, L1s were singled out onto small plates. Once the worms started laying eggs, they were transferred each day to a fresh small plate until egg laying ceased. The day after transfer to a fresh plate, unfertilized oocytes, unhatched embryos, and hatched larvae on the plate from the previous day were counted. This was done for each of the days of laying and the total of unhatched embryos and hatched larvae from all plates from a single worm were tabulated to determine total brood size. To determine embryonic lethality, the total number of unhatched embryos was divided by the total brood size. To determine unfertilized oocyte percentage, the total number of unfertilized oocytes was divided by the total brood size.

Developmental time analysis

Confluent large plates were egg prepped and left to spin in M9 overnight for synchronization as has been previously described [199]. The hatched L1s were plated onto large thick plates and allowed to grow to day two adults before being egg prepped a second time and left to spin in M9 overnight. The next morning, L1s were singled out onto small plates. The stage of the worms was assayed every 12 hours for the first 72 hours after plating.

A5. How mother's age affects fitness

INTRODUCTION

Our observation that *uaDf5* increases in the germline as adults age led us to question if *uaDf5*-containing strains have larger fitness deficits in progeny born from older mothers. To answer this we measured brood size, embryonic lethality, unfertilized oocyte production, developmental rate, and lifespan.

RESULTS AND FIGURES

A. Analysis of brood size shows that the there is a decrease in brood size of progeny born from older mothers in strains containing *uaDf5*.

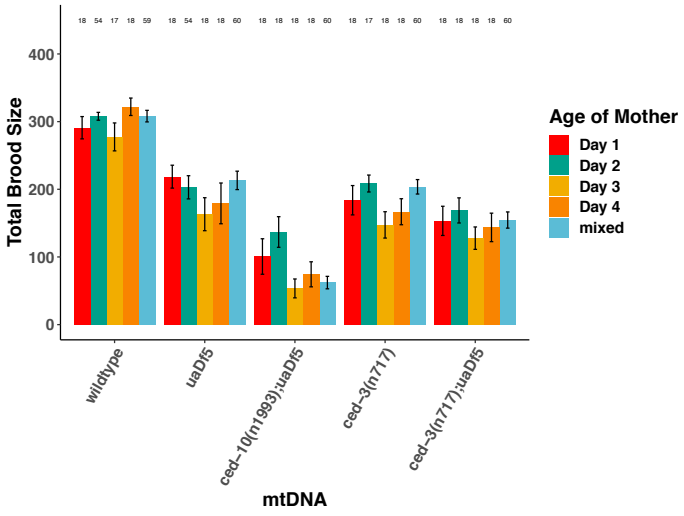

B. Analysis of embryonic lethality shows that the there is an increase in embryonic lethality in progeny born from older mothers in strains containing *uaDf5*.

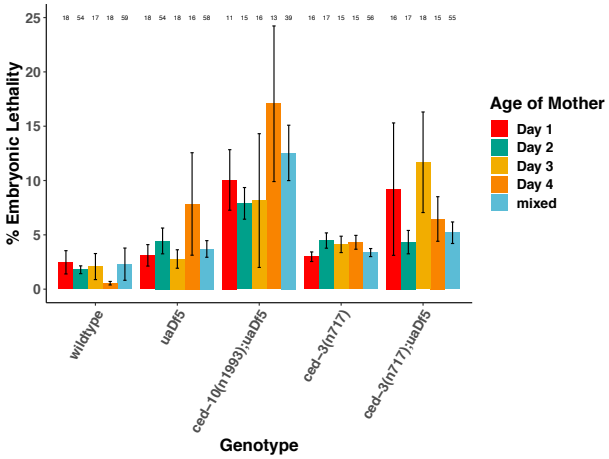

C. Analysis of unfertilized oocyte production shows that the there is a decrease in the production of unfertilized oocytes in progeny born from older mothers in strains containing *uaDf5* as compared to wildtype.

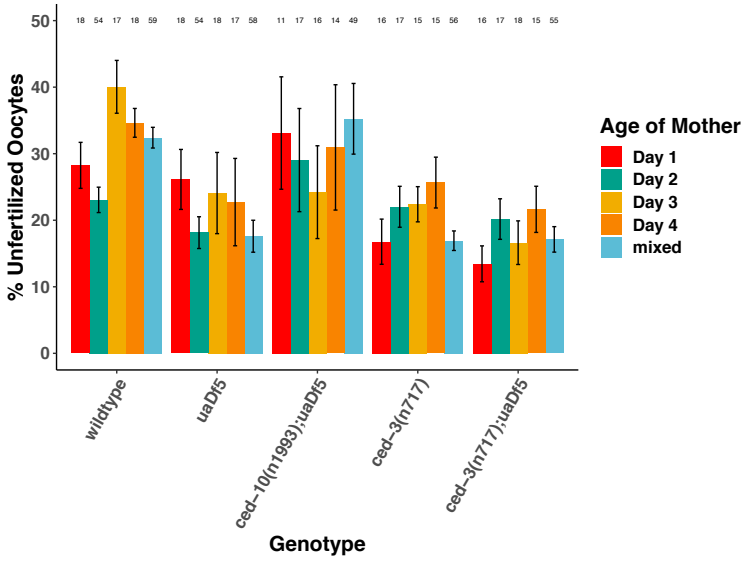

D. Analysis of the hours it takes to reach gravidity shows that the there is a decreased developmental rate in progeny born from older mothers in strains containing *uaDf5*.

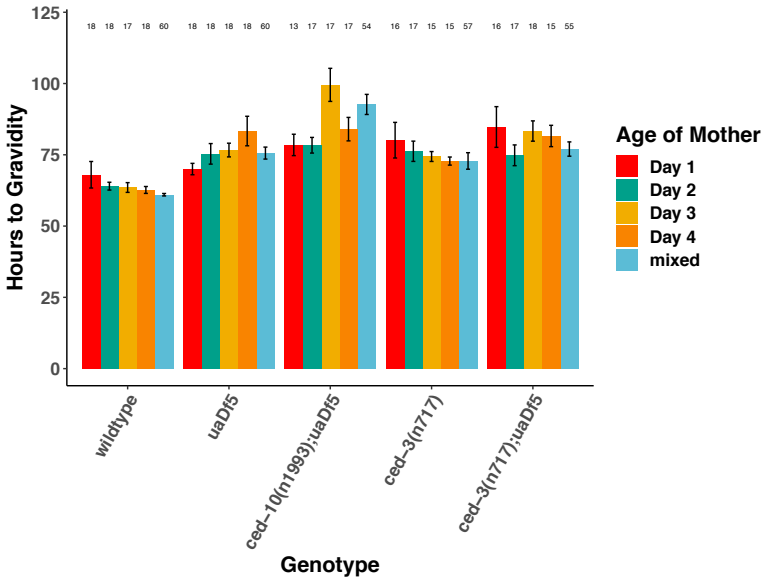

E. Analysis of lifespan shows that the there is no impact on lifespan of progeny born from older mothers in strains containing *uaDf5*.

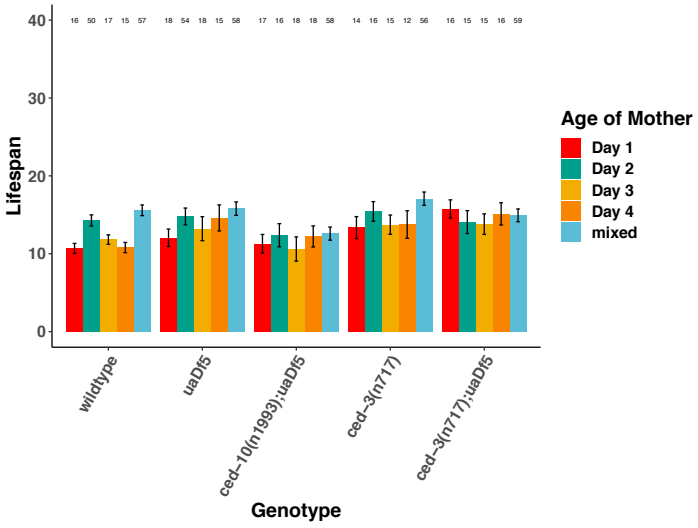

EXPERIMENTAL PROCEDURES

Lifespan analysis

Confluent large plates were egg prepped and left to spin in M9 overnight for synchronization. The hatched L1s were plated onto large thick plates and allowed to grow to the appropriate aged adults (day 1- day 4) before being egg prepped a second time and left to spin in M9 overnight. The next morning, referred to as day one for lifespan determination, L1s were singled out onto small plates. Once the worms started laying eggs, they were transferred each day to a fresh small plate until egg laying ceased, after which the worms remained on the same plate unless bacterial contamination required transfer to a fresh plate. Worms were considered dead if there was no movement after being lightly prodded with a worm pick.

Brood size, embryonic lethality, and unfertilized oocytes analysis

Confluent large plates were egg prepped and left to spin in M9 overnight for synchronization. The hatched L1s were plated onto large thick plates and allowed to grow to the appropriate aged adults (day 1- day 4) before being egg prepped a second time and left to spin in M9 overnight. The next morning, L1s were singled out onto small plates. Once the worms started laying eggs, they were transferred each day to a fresh small plate until egg laying ceased. The day after transfer to a fresh plate, unfertilized oocytes, unhatched embryos, and hatched larvae on the plate from the previous day were counted. This was done for each of the days of laying and the total of unhatched embryos and hatched larvae from all plates from a single worm were tabulated to determine total brood size. To determine embryonic lethality, the total number of unhatched embryos was

divided by the total brood size. To determine unfertilized oocyte percentage, the total number of unfertilized oocytes was divided by the total brood size.

Developmental time analysis

Confluent large plates were egg prepped and left to spin in M9 overnight for synchronization as has been previously described [199]. The hatched L1s were plated onto large thick plates and allowed to grow to the appropriate aged adults (day 1- day 4) before being egg prepped a second time and left to spin in M9 overnight. The next morning, L1s were singled out onto small plates. The stage of the worms was assayed every 12 hours for the first 72 hours after plating.

REFERENCES

1. Van Der Bliek AM, Sedensky MM, Morgan PG. Cell biology of the mitochondrion. Genetics. 2017;207: 843–871. doi:10.1534/genetics.117.300262
2. Tsang WY, Lemire BD. The role of mitochondria in the life of the nematode, Caenorhabditis elegans. Biochimica et Biophysica Acta - Molecular Basis of Disease. Elsevier; 2003. pp. 91–105. doi:10.1016/S0925-4439(03)00079-6
3. Lemire B. Mitochondrial genetics. WormBook. 2005 [cited 11 Oct 2019]. doi:10.1895/wormbook.1.25.1
4. Hederstedt L. Heme A biosynthesis. Biochimica et Biophysica Acta - Bioenergetics. 2012. pp. 920–927. doi:10.1016/j.bbabio.2012.03.025
5. Mühlenhoff U, Hoffmann B, Richter N, Rietzschel N, Spantgar F, Stehling O, et al. Compartmentalization of iron between mitochondria and the cytosol and its regulation. European Journal of Cell Biology. Elsevier GmbH; 2015. pp. 292–308. doi:10.1016/j.ejcb.2015.05.003
6. Paul BT, Manz DH, Torti FM, Torti S V. Mitochondria and Iron: current questions. Expert Review of Hematology. Taylor and Francis Ltd; 2017. pp. 65–79. doi:10.1080/17474086.2016.1268047
7. Houten SM, Violante S, Ventura F V., Wanders RJA. The Biochemistry and Physiology of Mitochondrial Fatty Acid β-Oxidation and Its Genetic Disorders. Annu Rev Physiol. 2016;78: 23–44. doi:10.1146/annurev-physiol-021115-105045
8. Szymański J, Janikiewicz J, Michalska B, Patalas-Krawczyk P, Perrone M, Ziółkowski W, et al. Interaction of mitochondria with the endoplasmic reticulum and plasma membrane in calcium homeostasis, lipid trafficking and mitochondrial structure. International Journal of Molecular Sciences. MDPI AG; 2017. doi:10.3390/ijms18071576
9. Horvath SE, Daum G. Lipids of mitochondria. Progress in Lipid Research. Elsevier Ltd; 2013. pp. 590–614. doi:10.1016/j.plipres.2013.07.002
10. Kastaniotis AJ, Autio KJ, Kerätär JM, Monteuuis G, Mäkelä AM, Nair RR, et al. Mitochondrial fatty acid synthesis, fatty acids and mitochondrial physiology. Biochimica et Biophysica Acta - Molecular and Cell Biology of Lipids. Elsevier B.V.; 2017. pp. 39–48. doi:10.1016/j.bbalip.2016.08.011
11. Daniele T, Schiaffino MV. Lipid transfer and metabolism across the endolysosomal-mitochondrial boundary. Biochim Biophys Acta - Mol Cell Biol Lipids. 2016;1861: 880–894. doi:10.1016/j.bbalip.2016.02.001
12. Fernie AR, Carrari F, Sweetlove LJ. Respiratory metabolism: Glycolysis, the TCA cycle and mitochondrial electron transport. Current Opinion in Plant Biology. 2004. pp. 254–261. doi:10.1016/j.pbi.2004.03.007
13. Nakagawa T, Guarente L. Urea cycle regulation by mitochondrial sirtuin, SIRT5. Aging (Albany NY). 2009;1: 578–581. doi:10.18632/aging.100062
14. Marchi S, Patergnani S, Missiroli S, Morciano G, Rimessi A, Wieckowski MR, et al. Mitochondrial and endoplasmic reticulum calcium homeostasis and cell death. Cell Calcium. Elsevier Ltd; 2018. pp. 62–72. doi:10.1016/j.ceca.2017.05.003
15. Baker ZN, Cobine PA, Leary SC. The mitochondrion: A central architect of copper homeostasis. Metallomics. Royal Society of Chemistry; 2017. pp. 1501–1512. doi:10.1039/c7mt00221a
16. Nam E, Han J, Suh JM, Yi Y, Lim MH. Link of impaired metal ion homeostasis to mitochondrial dysfunction in neurons. Current Opinion in Chemical Biology.

Elsevier Ltd; 2018. pp. 8–14. doi:10.1016/j.cbpa.2017.09.009
17. Bhola PD, Letai A. Mitochondria-Judges and Executioners of Cell Death Sentences. Molecular Cell. Cell Press; 2016. pp. 695–704. doi:10.1016/j.molcel.2016.02.019
18. Estaquier J, Vallette F, Vayssiere JL, Mignotte B. The mitochondrial pathways of apoptosis. Adv Exp Med Biol. 2012;942: 157–183. doi:10.1007/978-94-007-2869-1_7
19. Yamada K, Yoshida K. Mechanical insights into the regulation of programmed cell death by p53 via mitochondria. Biochimica et Biophysica Acta - Molecular Cell Research. Elsevier B.V.; 2019. pp. 839–848. doi:10.1016/j.bbamcr.2019.02.009
20. Matsuyama S, Reed JC. Mitochondria-dependent apoptosis and cellular pH regulation. Cell Death and Differentiation. 2000. pp. 1155–1165. doi:10.1038/sj.cdd.4400779
21. Kaczanowski S. Apoptosis: Its origin, history, maintenance and the medical implications for cancer and aging. Physical Biology. Institute of Physics Publishing; 2016. doi:10.1088/1478-3975/13/3/031001
22. Jeong SY, Seol DW. The role of mitochondria in apoptosis. Journal of Biochemistry and Molecular Biology. 2008. pp. 11–22. doi:10.5483/bmbrep.2008.41.1.011
23. Zimorski V, Ku C, Martin WF, Gould SB. Endosymbiotic theory for organelle origins. Current Opinion in Microbiology. Elsevier Ltd; 2014. pp. 38–48. doi:10.1016/j.mib.2014.09.008
24. Martin WF, Garg S, Zimorski V. Endosymbiotic theories for eukaryote origin. Philosophical Transactions of the Royal Society B: Biological Sciences. Royal Society of London; 2015. doi:10.1098/rstb.2014.0330
25. Roger AJ, Muñoz-Gómez SA, Kamikawa R. The Origin and Diversification of Mitochondria. Current Biology. Cell Press; 2017. pp. R1177–R1192. doi:10.1016/j.cub.2017.09.015
26. Leimbach A, Hacker J, Dobrindt U. E. coli as an all-rounder: The thin line between commensalism and pathogenicity. Curr Top Microbiol Immunol. 2013;358: 3–32. doi:10.1007/82_2012_303
27. Zhou N, Katz M, Knecht W, Compagno C, Piškur J. Genome dynamics and evolution in yeasts: A long-term yeast-bacteria competition experiment. PLoS One. 2018;13. doi:10.1371/journal.pone.0194911
28. Levy A, Salas Gonzalez I, Mittelviefhaus M, Clingenpeel S, Herrera Paredes S, Miao J, et al. Genomic features of bacterial adaptation to plants. Nat Genet. 2018;50: 138–150. doi:10.1038/s41588-017-0012-9
29. Kafsi H El, Gorochov G, Larsen M. Host genetics affect microbial ecosystems via host immunity. Current Opinion in Allergy and Clinical Immunology. Lippincott Williams and Wilkins; 2016. pp. 413–420. doi:10.1097/ACI.0000000000000302
30. Gogna R, Shee K, Moreno E. Cell Competition During Growth and Regeneration. Annu Rev Genet. 2015;49: 697–718. doi:10.1146/annurev-genet-112414-055214
31. Kamada N, Seo SU, Chen GY, Núñez G. Role of the gut microbiota in immunity and inflammatory disease. Nature Reviews Immunology. 2013. pp. 321–335. doi:10.1038/nri3430
32. Elena SF, Lenski RE. Evolution experiments with microorganisms: the dynamics and genetic bases of adaptation. Nat Rev Genet. 2003;4: 457–69.

doi:10.1038/nrg1088
33. Brown WM, George M, Wilson AC. Rapid evolution of animal mitochondrial DNA. Proc Natl Acad Sci U S A. 1979;76: 1967–1971. doi:10.1073/pnas.76.4.1967
34. Anderson S, Bankier AT, Barrell BG, De Bruijn MHL, Coulson AR, Drouin J, et al. Sequence and organization of the human mitochondrial genome. Nature. 1981;290: 457–465. doi:10.1038/290457a0
35. Lardy HA, Ferguson SM. Oxidative Phosphorylation in Mitochondria. Annu Rev Biochem. 1969;38: 991–1034. doi:10.1146/annurev.bi.38.070169.005015
36. Papa S, Martino PL, Capitanio G, Gaballo A, De Rasmo D, Signorile A, et al. The oxidative phosphorylation system in mammalian mitochondria. Adv Exp Med Biol. 2012;942: 1–37. doi:10.1007/978-94-007-2869-1_1
37. Bernardi P, Di Lisa F, Fogolari F, Lippe G. From ATP to PTP and back: A dual function for The mitochondrial ATP synthase. Circulation Research. Lippincott Williams and Wilkins; 2015. pp. 1850–1862. doi:10.1161/CIRCRESAHA.115.306557
38. Song J, Pfanner N, Becker T. Assembling themitochondrial ATP synthase. Proceedings of the National Academy of Sciences of the United States of America. National Academy of Sciences; 2018. pp. 2850–2852. doi:10.1073/pnas.1801697115
39. Sousa JS, D'Imprima E, Vonck J. Mitochondrial respiratory chain complexes. Subcellular Biochemistry. Springer New York; 2018. pp. 167–227. doi:10.1007/978-981-10-7757-9_7
40. Johnston IG, Williams BP. Evolutionary inference across eukaryotes identifies specific pressures favoring mitochondrial gene retention. Cell Syst. 2016;2: 101–111. doi:10.1016/j.cels.2016.01.013
41. Clayton DA. Transcription and replication of mitochondrial DNA. Human Reproduction. Oxford University Press; 2000. pp. 11–17. doi:10.1093/humrep/15.suppl_2.11
42. St. John J. The control of mtDNA replication during differentiation and development. Biochimica et Biophysica Acta - General Subjects. Elsevier; 2014. pp. 1345–1354. doi:10.1016/j.bbagen.2013.10.036
43. Clay Montier LL, Deng JJ, Bai Y. Number matters: control of mammalian mitochondrial DNA copy number. J Genet Genomics. 2009;36: 125–131. doi:10.1016/S1673-8527(08)60099-5
44. Bogenhagen D, Clayton DA. Mouse L cell mitochondrial DNA molecules are selected randomly for replication throughout the cell cycle. Cell. 1977;11: 719–727. doi:10.1016/0092-8674(77)90286-0
45. Schwartz M, Vissing J. Paternal inheritance of mitochondrial DNA. N Engl J Med. 2002;347: 576–580. doi:10.1056/NEJMoa020350
46. Luo S, Valencia CA, Zhang J, Lee NC, Slone J, Gui B, et al. Biparental inheritance of mitochondrial DNA in humans. Proc Natl Acad Sci U S A. 2018;115: 13039–13044. doi:10.1073/pnas.1810946115
47. Sato K, Sato M. Multiple ways to prevent transmission of paternal mitochondrial DNA for maternal inheritance in animals. Journal of Biochemistry. Oxford University Press; 2017. pp. 247–253. doi:10.1093/jb/mvx052
48. Konrad A, Thompson O, Waterston RH, Moerman DG, Keightley PD, Bergthorsson U, et al. Mitochondrial mutation rate, spectrum and heteroplasmy in

Caenorhabditis elegans spontaneous mutation accumulation lines of differing population size. Mol Biol Evol. 2017;34: 1319–1334. doi:10.1093/molbev/msx051
49. Denver DR, Morris K, Lynch M, Vassilieva LL, Thomas WK. High direct estimate of the mutation rate in the mitochondrial genome of Caenorhabditis elegans. Science (80-). 2000;289: 2342–2344. doi:10.1126/science.289.5488.2342
50. Stumpf JD, Saneto RP, Copeland WC. Clinical and molecular features of polg-related mitochondrial disease. Cold Spring Harb Perspect Biol. 2013;5: 1–17. doi:10.1101/cshperspect.a011395
51. DeBalsi KL, Hoff KE, Copeland WC. Role of the mitochondrial DNA replication machinery in mitochondrial DNA mutagenesis, aging and age-related diseases. Ageing Research Reviews. Elsevier Ireland Ltd; 2017. pp. 89–104. doi:10.1016/j.arr.2016.04.006
52. Rahman S, Copeland WC. POLG-related disorders and their neurological manifestations. Nature Reviews Neurology. Nature Publishing Group; 2019. pp. 40–52. doi:10.1038/s41582-018-0101-0
53. Theurey P, Pizzo P. The aging mitochondria. Genes. MDPI AG; 2018. doi:10.3390/genes9010022
54. Kauppila TES, Kauppila JHK, Larsson NG. Mammalian Mitochondria and Aging: An Update. Cell Metabolism. Cell Press; 2017. pp. 57–71. doi:10.1016/j.cmet.2016.09.017
55. Stewart JB, Chinnery PF. The dynamics of mitochondrial DNA heteroplasmy: Implications for human health and disease. Nature Reviews Genetics. Nature Publishing Group; 2015. pp. 530–542. doi:10.1038/nrg3966
56. Burr SP, Pezet M, Chinnery PF. Mitochondrial DNA Heteroplasmy and Purifying Selection in the Mammalian Female Germ Line. Development Growth and Differentiation. Blackwell Publishing; 2018. pp. 21–32. doi:10.1111/dgd.12420
57. Palozzi JM, Jeedigunta SP, Hurd TR. Mitochondrial DNA Purifying Selection in Mammals and Invertebrates. Journal of Molecular Biology. Academic Press; 2018. pp. 4834–4848. doi:10.1016/j.jmb.2018.10.019
58. Stewart JB, Freyer C, Elson JL, Larsson NG. Purifying selection of mtDNA and its implications for understanding evolution and mitochondrial disease. Nature Reviews Genetics. 2008. pp. 657–662. doi:10.1038/nrg2396
59. Wallace DC. A Mitochondrial Paradigm of Metabolic and Degenerative Diseases, Aging, and Cancer: A Dawn for Evolutionary Medicine. Annu Rev Genet. 2005;39: 359–407. doi:10.1146/annurev.genet.39.110304.095751
60. Park CB, Larsson NG. Mitochondrial DNA mutations in disease and aging. Journal of Cell Biology. 2011. pp. 809–818. doi:10.1083/jcb.201010024
61. Area-Gomez E, Schon EA. Mitochondrial genetics and disease. Journal of Child Neurology. SAGE Publications Inc.; 2014. pp. 1208–1215. doi:10.1177/0883073814539561
62. Gorman GS, Schaefer AM, Ng Y, Gomez N, Blakely EL, Alston CL, et al. Prevalence of nuclear and mitochondrial DNA mutations related to adult mitochondrial disease. Ann Neurol. 2015;77: 753–759. doi:10.1002/ana.24362
63. Dhillon VS, Fenech M. Mutations that affect mitochondrial functions and their association with neurodegenerative diseases. Mutation Research - Reviews in Mutation Research. 2014. pp. 1–13. doi:10.1016/j.mrrev.2013.09.001
64. Alston CL, Rocha MC, Lax NZ, Turnbull DM, Taylor RW. The genetics and pathology of mitochondrial disease. Journal of Pathology. John Wiley and Sons

Ltd; 2017. pp. 236–250. doi:10.1002/path.4809
65. Holt IJ, Harding AE, Morgan-Hughes JA. Deletions of muscle mitochondrial DNA in patients with mitochondrial myopathies. Nature. 1988;331: 717–719. doi:10.1038/331717a0
66. Wallace DC, Singh G, Lott MT, Hodge JA, Schurr TG, Lezza AMS, et al. Mitochondrial DNA mutation associated with Leber's hereditary optic neuropathy. Science (80-). 1988;242: 1427–1430. doi:10.1126/science.3201231
67. Burté F, Carelli V, Chinnery PF, Yu-Wai-Man P. Disturbed mitochondrial dynamics and neurodegenerative disorders. Nature Reviews Neurology. Nature Publishing Group; 2015. pp. 11–24. doi:10.1038/nrneurol.2014.228
68. Tilokani L, Nagashima S, Paupe V, Prudent J. Mitochondrial dynamics: Overview of molecular mechanisms. Essays in Biochemistry. Portland Press Ltd; 2018. pp. 341–360. doi:10.1042/EBC20170104
69. Busch KB, Kowald A, Spelbrink JN. Quality matters: How does mitochondrial network dynamics and quality control impact on mtDNA integrity? Philosophical Transactions of the Royal Society B: Biological Sciences. Royal Society of London; 2014. doi:10.1098/rstb.2013.0442
70. Ni HM, Williams JA, Ding WX. Mitochondrial dynamics and mitochondrial quality control. Redox Biology. Elsevier B.V.; 2015. pp. 6–13. doi:10.1016/j.redox.2014.11.006
71. Youle RJ, Narendra DP. Mechanisms of mitophagy. Nat Rev Mol Cell Biol. 2011;12: 9–14. doi:10.1038/nrm3028
72. Ashrafi G, Schwarz TL. The pathways of mitophagy for quality control and clearance of mitochondria. Cell Death and Differentiation. 2013. pp. 31–42. doi:10.1038/cdd.2012.81
73. Twig G, Shirihai OS. The interplay between mitochondrial dynamics and mitophagy. Antioxidants and Redox Signaling. 2011. pp. 1939–1951. doi:10.1089/ars.2010.3779
74. Hernando-Rodríguez B, Artal-Sanz M. Mitochondrial Quality Control Mechanisms and the PHB (Prohibitin) Complex. Cells. 2018;7: 238. doi:10.3390/cells7120238
75. Sté phane Rolland AG, Schneid S, Schwarz M, Mokranjac D, Lambie E, Conradt B. Compromised Mitochondrial Protein Import Acts as a Signal for UPR mt. Cell Rep. 2019;28: 1659–1669. doi:10.1016/j.celrep.2019.07.049
76. Münch C. The different axes of the mammalian mitochondrial unfolded protein response. BMC Biology. BioMed Central Ltd.; 2018. doi:10.1186/s12915-018-0548-x
77. Callegari S, Dennerlein S. Sensing the stress: A role for the UPR mt and UPR am in the quality control of mitochondria. Frontiers in Cell and Developmental Biology. Frontiers Media S.A.; 2018. doi:10.3389/fcell.2018.00031
78. Gitschlag BL, Kirby CS, Samuels DC, Gangula RD, Mallal SA, Patel MR. Homeostatic Responses Regulate Selfish Mitochondrial Genome Dynamics in C. elegans. Cell Metab. 2016;24: 91–103. doi:10.1016/j.cmet.2016.06.008
79. Nargund AM, Pellegrino MW, Fiorese CJ, Baker BM, Haynes CM. Mitochondrial import efficiency of ATFS-1 regulates mitochondrial UPR activation. Science (80-). 2012;337: 587–590. doi:10.1126/science.1223560
80. Lin YF, Schulz AM, Pellegrino MW, Lu Y, Shaham S, Haynes CM. Maintenance and propagation of a deleterious mitochondrial genome by the mitochondrial

unfolded protein response. Nature. 2016;533: 416–419. doi:10.1038/nature17989
81. Haroon S, Li A, Weinert JL, Fritsch C, Ericson NG, Alexander-Floyd J, et al. Multiple Molecular Mechanisms Rescue mtDNA Disease in C. elegans. Cell Rep. 2018;22: 3115–3125. doi:10.1016/j.celrep.2018.02.099
82. Murphy C, Hu P. Insulin/insulin-like growth factor signaling in C. elegans - WormBook - NCBI Bookshelf. In: WormBook [Internet]. 2013 [cited 18 Oct 2019] pp. 1–43. Available: https://www-ncbi-nlm-nih-gov.proxy.library.ucsb.edu:9443/books/NBK179230/
83. Marnik EA, Updike DL. Membraneless organelles: P granules in Caenorhabditis elegans. Traffic. Blackwell Munksgaard; 2019. pp. 373–379. doi:10.1111/tra.12644
84. Gallo CM, Wang JT, Motegi F, Seydoux G. Cytoplasmic partitioning of P granule components is not required to specify the germline in C. elegans. Science (80-). 2010;330: 1685–1689. doi:10.1126/science.1193697
85. Boyd L, Quo S, Levitan D, Stinchcomb DT, Kemphues KJ. PAR-2 is asymmetrically distributed and promotes association of P granules and PAR-1 with the cortex in C. elegans embryos. Development. 1996;122: 3075–3084.
86. Brangwynne CP, Eckmann CR, Courson DS, Rybarska A, Hoege C, Gharakhani J, et al. Germline P granules are liquid droplets that localize by controlled dissolution/condensation. Science (80-). 2009;324: 1729–1732. doi:10.1126/science.1172046
87. Abdu Y, Maniscalco C, Heddleston JM, Chew TL, Nance J. Developmentally programmed germ cell remodelling by endodermal cell cannibalism. Nat Cell Biol. 2016;18: 1302–1310. doi:10.1038/ncb3439
88. Ye AL, Matthew Ragle J, Conradt B, Bhalla N. Differential regulation of germline apoptosis in response to meiotic checkpoint activation. Genetics. 2014;198: 995–1000. doi:10.1534/genetics.114.170241
89. Gumienny TL, Lambie E, Hartwieg E, Horvitz HR, Hengartner MO. Genetic control of programmed cell death in the Caenorhabditis elegans hermaphrodite germline. Development. 1999;126.
90. Salinas LS, Maldonado E, Navarro RE. Stress-induced germ cell apoptosis by a p53 independent pathway in Caenorhabditis elegans. Cell Death Differ. 2006;13: 2129–2139. doi:10.1038/sj.cdd.4401976
91. Conradt B, Wu YC, Xue D. Programmed cell death during Caenorhabditis elegans development. Genetics. 2016;203: 1533–1562. doi:10.1534/genetics.115.186247
92. Wang X, Yang C. Programmed cell death and clearance of cell corpses in Caenorhabditis elegans. Cellular and Molecular Life Sciences. Birkhauser Verlag AG; 2016. pp. 2221–2236. doi:10.1007/s00018-016-2196-z
93. da Costa JP, Vitorino R, Silva GM, Vogel C, Duarte AC, Rocha-Santos T. A synopsis on aging—Theories, mechanisms and future prospects. Ageing Research Reviews. Elsevier Ireland Ltd; 2016. pp. 90–112. doi:10.1016/j.arr.2016.06.005
94. Harman D. Free radical theory of aging. Mutat Res. 1992;275: 257–266. doi:10.1016/0921-8734(92)90030-S
95. Liochev SI. Reactive oxygen species and the free radical theory of aging. Free Radical Biology and Medicine. 2013. pp. 1–4. doi:10.1016/j.freeradbiomed.2013.02.011
96. HARMAN D. Aging: a theory based on free radical and radiation chemistry. J Gerontol. 1956;11: 298–300. doi:10.1093/geronj/11.3.298

97. BECKMAN KB, AMES BN. The Free Radical Theory of Aging Matures. Physiol Rev. 1998;78: 547–581. doi:10.1152/physrev.1998.78.2.547
98. Bratic A, Larsson N-G. The role of mitochondria in aging. J Clin Invest. 2013;123: 951–957. doi:10.1172/JCI64125
99. Dues DJ, Schaar CE, Johnson BK, Bowman MJ, Winn ME, Senchuk MM, et al. Uncoupling of oxidative stress resistance and lifespan in long-lived isp-1 mitochondrial mutants in Caenorhabditis elegans. Free Radic Biol Med. 2017;108: 362–373. doi:10.1016/j.freeradbiomed.2017.04.004
100. Kimura KD, Tissenbaum HA, Liu Y, Ruvkun G. Daf-2, an insulin receptor-like gene that regulates longevity and diapause in Caenorhabditis elegans. Science (80-). 1997;277: 942–946. doi:10.1126/science.277.5328.942
101. Pierce SB, Gersak K, Michaelson-Cohen R, Walsh T, Lee MK, Malach D, et al. Mutations in LARS2, encoding mitochondrial leucyl-tRNA synthetase, lead to premature ovarian failure and hearing loss in Perrault syndrome. Am J Hum Genet. 2013;92: 614–20. doi:10.1016/j.ajhg.2013.03.007
102. Branicky R, Bénard C, Hekimi S. clk-1, mitochondria, and physiological rates. BioEssays. 2000. pp. 48–56. doi:10.1002/(SICI)1521-1878(200001)22:1<48::AID-BIES9>3.0.CO;2-F
103. Adachi H, Fujiwara Y, Ishii N. Effects of oxygen on protein carbonyl and aging in Caenorhabditis elegans mutants with long (age-1) and short (mev-1) life spans. Journals Gerontol - Ser A Biol Sci Med Sci. 1998;53. doi:10.1093/gerona/53A.4.B240
104. Wernick RI, Estes S, Howe DK, Denver DR. Paths of heritable mitochondrial dna mutation and heteroplasmy in reference and gas-1 strains of caenorhabditis elegans. Front Genet. 2016;7. doi:10.3389/fgene.2016.00051
105. Corsi AK, Wightman B, Chalfie M. A transparent window into biology: A primer on Caenorhabditis elegans. Genetics. 2015;200: 387–407. doi:10.1534/genetics.115.176099
106. Tsang WY, Lemire BD. Mitochondrial genome content is regulated during nematode development. Biochem Biophys Res Commun. 2002;291: 8–16. doi:10.1006/bbrc.2002.6394
107. Bratic I, Hench J, Henriksson J, Antebi A, Bürglin TR, Trifunovic A. Mitochondrial DNA level, but not active replicase, is essential for Caenorhabditis elegans development. Nucleic Acids Res. 2009;37: 1817–1828. doi:10.1093/nar/gkp018
108. Youle RJ, Van Der Bliek AM. Mitochondrial fission, fusion, and stress. Science. American Association for the Advancement of Science; 2012. pp. 1062–1065. doi:10.1126/science.1219855
109. Milani M, Byrne DP, Greaves G, Butterworth M, Cohen GM, Eyers PA, et al. DRP-1 is required for BH3 mimetic-mediated mitochondrial fragmentation and apoptosis. Cell Death Dis. 2017;8. doi:10.1038/cddis.2016.485
110. Losó n OC, Song Z, Chen H, Chan DC. Fis1, Mff, MiD49, and MiD51 mediate Drp1 recruitment in mitochondrial fission. Mol Biol Cell. 2013;24: 659–667. doi:10.1091/mbc.E12-10-0721
111. Breckenridge DG, Kang BH, Kokel D, Mitani S, Staehelin LA, Xue D. Caenorhabditis elegans drp-1 and fis-2 Regulate Distinct Cell-Death Execution Pathways Downstream of ced-3 and Independent of ced-9. Mol Cell. 2008;31: 586–597. doi:10.1016/j.molcel.2008.07.015

112. Kanazawa T, Zappaterra MD, Hasegawa A, Wright AP, Newman-Smith ED, Buttle KF, et al. The C. elegans Opa1 homologue EAT-3 is essential for resistance to free radicals. PLoS Genet. 2008;4. doi:10.1371/journal.pgen.1000022
113. Rolland SG, Lu Y, David CN, Conradt B. The BCL-2-like protein CED-9 of C. elegans promotes FZO-1/Mfn1,2- and EAT-3/Opa1-dependent mitochondrial fusion. J Cell Biol. 2009;186: 525–540. doi:10.1083/jcb.200905070
114. Byrne JJ, Soh MS, Chandhok G, Vijayaraghavan T, Teoh JS, Crawford S, et al. Disruption of mitochondrial dynamics affects behaviour and lifespan in Caenorhabditis elegans. Cell Mol Life Sci. 2019;76: 1967–1985. doi:10.1007/s00018-019-03024-5
115. Twig G, Elorza A, Molina AJA, Mohamed H, Wikstrom JD, Walzer G, et al. Fission and selective fusion govern mitochondrial segregation and elimination by autophagy. EMBO J. 2008;27: 433–446. doi:10.1038/sj.emboj.7601963
116. Suen DF, Narendra DP, Tanaka A, Manfredi G, Youle RJ. Parkin overexpression selects against a deleterious mtDNA mutation in heteroplasmic cybrid cells. Proc Natl Acad Sci U S A. 2010;107: 11835–11840. doi:10.1073/pnas.0914569107
117. Poole AC, Thomas RE, Andrews LA, McBride HM, Whitworth AJ, Pallanck LJ. The PINK1/Parkin pathway regulates mitochondrial morphology. Proc Natl Acad Sci U S A. 2008;105: 1638–1643. doi:10.1073/pnas.0709336105
118. Barodia SK, Creed RB, Goldberg MS. Parkin and PINK1 functions in oxidative stress and neurodegeneration. Brain Research Bulletin. Elsevier Inc.; 2017. pp. 51–59. doi:10.1016/j.brainresbull.2016.12.004
119. Koyano F, Okatsu K, Kosako H, Tamura Y, Go E, Kimura M, et al. Ubiquitin is phosphorylated by PINK1 to activate parkin. Nature. 2014;510: 162–166. doi:10.1038/nature13392
120. Eiyama A, Okamoto K. PINK1/Parkin-mediated mitophagy in mammalian cells. Current Opinion in Cell Biology. Elsevier Ltd; 2015. pp. 95–101. doi:10.1016/j.ceb.2015.01.002
121. Wu S, Lei L, Song Y, Liu M, Lu S, Lou D, et al. Mutation of hop-1 and pink-1 attenuates vulnerability of neurotoxicity in C. elegans: the role of mitochondria-associated membrane proteins in Parkinsonism. Exp Neurol. 2018;309: 67–78. doi:10.1016/j.expneurol.2018.07.018
122. Kim Y, Park J, Kim S, Song S, Kwon SK, Lee SH, et al. PINK1 controls mitochondrial localization of Parkin through direct phosphorylation. Biochem Biophys Res Commun. 2008;377: 975–980. doi:10.1016/j.bbrc.2008.10.104
123. Zhang H, Burr SP, Chinnery PF. The mitochondrial DNA genetic bottleneck: Inheritance and beyond. Essays in Biochemistry. Portland Press Ltd; 2018. pp. 225–234. doi:10.1042/EBC20170096
124. Floros VI, Pyle A, DIetmann S, Wei W, Tang WWC, Irie N, et al. Segregation of mitochondrial DNA heteroplasmy through a developmental genetic bottleneck in human embryos. Nat Cell Biol. 2018; 144–151. doi:10.1038/s41556-017-0017-8
125. Johnston IG, Burgstaller JP, Havlicek V, Kolbe T, Rülicke T, Brem G, et al. Stochastic modelling, bayesian inference, and new in vivo measurements elucidate the debated mtDNA bottleneck mechanism. Elife. 2015;4. doi:10.7554/eLife.07464
126. Lynch M. Mutation accumulation in transfer RNAs: Molecular evidence for Muller's ratchet in mitochondrial genomes. Mol Biol Evol. 1996;13: 209–220. doi:10.1093/oxfordjournals.molbev.a025557

127. Gabriel W, Lynch M, Bürger R. MULLER'S RATCHET AND MUTATIONAL MELTDOWNS. Evolution (N Y). 1993;47: 1744–1757. doi:10.1111/j.1558-5646.1993.tb01266.x
128. Howe DK, Denver DR. Muller's Ratchet and compensatory mutation in Caenorhabditis briggsae mitochondrial genome evolution. BMC Evol Biol. 2008;8. doi:10.1186/1471-2148-8-62
129. Loewe L, Cutter AD. On the potential for extinction by Muller's Ratchet in Caenorhabditis elegans. BMC Evol Biol. 2008;8. doi:10.1186/1471-2148-8-125
130. Loewe L. Quantifying the genomic decay paradox due to Muller's ratchet in human mitochondrial DNA. Genet Res. 2006;87: 133–159. doi:10.1017/S0016672306008123
131. Bartke A. Insulin and aging. Cell Cycle. Taylor and Francis Inc.; 2008. pp. 3338–3343. doi:10.4161/cc.7.21.7012
132. Kenyon CJ. The genetics of ageing. Nature. 2010. pp. 504–512. doi:10.1038/nature08980
133. Anisimov VN, Bartke A. The key role of growth hormone-insulin-IGF-1 signaling in aging and cancer. Critical Reviews in Oncology/Hematology. 2013. pp. 201–223. doi:10.1016/j.critrevonc.2013.01.005
134. Friedman DB, Johnson TE. A mutation in the age-1 gene in Caenorhabditis elegans lengthens life and reduces hermaphrodite fertility. Genetics. 1988;118: 75–86.
135. Toker A, Newton AC. Cellular signaling: Pivoting around PDK-1. Cell. Cell Press; 2000. pp. 185–188. doi:10.1016/S0092-8674(00)00110-0
136. Risso G, Blaustein M, Pozzi B, Mammi P, Srebrow A. Akt/PKB: One kinase, many modifications. Biochemical Journal. Portland Press Ltd; 2015. pp. 203–214. doi:10.1042/BJ20150041
137. Tang BL. Sirt1 and the mitochondria. Molecules and Cells. Korean Society for Molecular and Cellular Biology; 2016. pp. 87–95. doi:10.14348/molcells.2016.2318
138. Sun L, Jiang Z, Acosta-Rodriguez VA, Berger M, Du X, Choi JH, et al. HCFC2 is needed for IRF1- and IRF2-dependent Tlr3 transcription and for survival during viral infections. J Exp Med. 2017;214: 3263–3277. doi:10.1084/jem.20161630
139. Baird NA, Douglas PM, Simic MS, Grant AR, Moresco JJ, Wolff SC, et al. HSF-1-mediated cytoskeletal integrity determines thermotolerance and life span. Science (80-). 2014;346: 360–363. doi:10.1126/science.1253168
140. Steinbaugh MJ, Blackwell TK, Ewald CY, Isik M, Hourihan JM. SKN-1/Nrf, stress responses, and aging in Caenorhabditis elegans. Free Radic Biol Med. 2015;88: 290–301.
141. Ogg S, Ruvkun G. The C. elegans PTEN homolog, DAF-18, acts in the insulin receptor-like metabolic signaling pathway. Mol Cell. 1998;2: 887–893. doi:10.1016/S1097-2765(00)80303-2
142. Masse I, Molin L, Billaud M, Solari F. Lifespan and dauer regulation by tissue-specific activities of Caenorhabditis elegans DAF-18. Dev Biol. 2005;286: 91–101. doi:10.1016/j.ydbio.2005.07.010
143. Wlodarchak N, Xing Y. PP2A as a master regulator of the cell cycle. Critical Reviews in Biochemistry and Molecular Biology. Taylor and Francis Ltd; 2016. pp. 162–184. doi:10.3109/10409238.2016.1143913
144. Vanfleteren JR, Braeckman BP. Mechanisms of life span determination in

Caenorhabditis elegans. Neurobiol Aging. 1999;20: 487–502. doi:10.1016/S0197-4580(99)00087-1
145. Yanase S, Suda H, Yasuda K, Ishii N. Impaired p53/CEP-1 is associated with lifespan extension through an age-related imbalance in the energy metabolism of C. elegans. Genes to Cells. 2017;22: 1004–1010. doi:10.1111/gtc.12540
146. Müller RU, Fabretti F, Zank S, Burst V, Benzing T, Schermer B. The von Hippel Lindau tumor suppressor limits longevity. J Am Soc Nephrol. 2009;20: 2513–2517. doi:10.1681/ASN.2009050497
147. Noatynska A, Gotta M. Cell polarity and asymmetric cell division: The C. elegans early embryo. Essays Biochem. 2012;53: 1–14. doi:10.1042/BSE0530001
148. Hoege C, Hyman AA. Principles of PAR polarity in Caenorhabditis elegans embryos. Nature Reviews Molecular Cell Biology. 2013. pp. 315–322. doi:10.1038/nrm3558
149. Griffin EE. Cytoplasmic localization and asymmetric division in the early embryo of Caenorhabditis elegans. Wiley Interdisciplinary Reviews: Developmental Biology. John Wiley and Sons Inc.; 2015. pp. 267–282. doi:10.1002/wdev.177
150. Rose L, Gönczy P. Polarity establishment, asymmetric division and segregation of fate determinants in early C. elegans embryos. WormBook : the online review of C. elegans biology. 2014. pp. 1–43. doi:10.1895/wormbook.1.30.2
151. Strome S. Specification of the germ line. WormBook : the online review of C. elegans biology. 2005. pp. 1–10. doi:10.1895/wormbook.1.9.1
152. Wang JT, Seydoux G. P granules. Current Biology. Cell Press; 2014. doi:10.1016/j.cub.2014.06.018
153. Emelyanov V V. Rickettsiaceae, rickettsia-like endosymbionts, and the origin of mitochondria. Biosci Rep. 2001;21: 1–17. doi:10.1023/a:1010409415723
154. Carvalho DS, Andrade RFS, Pinho STR, Góes-Neto A, Lobão TCP, Bomfim GC, et al. What are the evolutionary origins of mitochondria? A complex network approach. PLoS One. 2015;10. doi:10.1371/journal.pone.0134988
155. Martijn J, Vosseberg J, Guy L, Offre P, Ettema TJG. Deep mitochondrial origin outside the sampled alphaproteobacteria. Nature. 2018;557: 101–105. doi:10.1038/s41586-018-0059-5
156. Wang Z, Wu M. An integrated phylogenomic approach toward pinpointing the origin of mitochondria. Sci Rep. 2015;5. doi:10.1038/srep07949
157. Landmann F. The Wolbachia Endosymbionts. Microbiol Spectr. 2019;7. doi:10.1128/microbiolspec.BAI-0018-2019
158. Russell SL, Lemseffer N, Sullivan WT. Wolbachia and host germline components compete for kinesin-mediated transport to the posterior pole of the Drosophila oocyte. PLoS Pathog. 2018;14. doi:10.1371/journal.ppat.1007216
159. Werren JH, Baldo L, Clark ME. Wolbachia: Master manipulators of invertebrate biology. Nature Reviews Microbiology. 2008. pp. 741–751. doi:10.1038/nrmicro1969
160. Signor S. Population genomics of Wolbachia and mtDNA in Drosophila simulans from California. Sci Rep. 2017;7. doi:10.1038/s41598-017-13901-3
161. Hu PJ. Dauer. WormBook : the online review of C. elegans biology. 2007. pp. 1–19. doi:10.1895/wormbook.1.144.1
162. Ewald CY, Castillo-Quan JI, Blackwell TK. Untangling Longevity, Dauer, and Healthspan in Caenorhabditis elegans Insulin/IGF-1-Signalling. Gerontology. 2017;64: 96–104. doi:10.1159/000480504

163. Baugh LR. To grow or not to grow: Nutritional control of development during Caenorhabditis elegans L1 Arrest. Genetics. 2013. pp. 539–555. doi:10.1534/genetics.113.150847
164. Kaplan REW, Baugh LR. L1 arrest, daf-16 /FoxO and nonautonomous control of post-embryonic development . Worm. 2016;5: e1175196. doi:10.1080/21624054.2016.1175196
165. Fukuyama M, Rougvie AE, Rothman JH. C. elegans DAF-18/PTEN Mediates Nutrient-Dependent Arrest of Cell Cycle and Growth in the Germline. Curr Biol. 2006;16: 773–779. doi:10.1016/j.cub.2006.02.073
166. D'Arcy MS. Cell death: a review of the major forms of apoptosis, necrosis and autophagy. Cell Biology International. Wiley-Blackwell Publishing Ltd; 2019. pp. 582–592. doi:10.1002/cbin.11137
167. Elmore S. Apoptosis: A Review of Programmed Cell Death. Toxicologic Pathology. 2007. pp. 495–516. doi:10.1080/01926230701320337
168. Tower J. Programmed cell death in aging. Ageing Research Reviews. Elsevier Ireland Ltd; 2015. pp. 90–100. doi:10.1016/j.arr.2015.04.002
169. Nagata S, Tanaka M. Programmed cell death and the immune system. Nature Reviews Immunology. Nature Publishing Group; 2017. pp. 333–340. doi:10.1038/nri.2016.153
170. Lord CEN, Gunawardena AHLAN. Programmed cell death in C. elegans, mammals and plants. European Journal of Cell Biology. 2012. pp. 603–613. doi:10.1016/j.ejcb.2012.02.002
171. Nehme R, Conradt B. egl-1: A key activator of apoptotic cell death in C. elegans. Oncogene. 2008. pp. S30–S40. doi:10.1038/onc.2009.41
172. Fairlie WD, Perugini MA, Kvansakul M, Chen L, Huang DCS, Colman PM. CED-4 forms a 2 : 2 heterotetrameric complex with CED-9 until specifically displaced by EGL-1 or CED-13. Cell Death Differ. 2006;13: 426–434. doi:10.1038/sj.cdd.4401762
173. Yang X, Chang HY, Baltimore D. Essential role of CED-4 oligomerization in CED-3 activation and apoptosis. Science (80-). 1998;281: 1355–1357. doi:10.1126/science.281.5381.1355
174. Cohen GM. Caspases: The executioners of apoptosis. Biochemical Journal. Portland Press Ltd; 1997. pp. 1–16. doi:10.1042/bj3260001
175. Shaham S. Identification of multiple Caenorhabditis elegans caspases and their potential roles in proteolytic cascades. J Biol Chem. 1998;273: 35109–35117. doi:10.1074/jbc.273.52.35109
176. Geng X, Shi Y, Nakagawa A, Yoshina S, Mitani S, Shi Y, et al. Inhibition of CED-3 zymogen activation and apoptosis in Caenorhabditis elegans by caspase homolog CSP-3. Nat Struct Mol Biol. 2008;15: 1094–1101. doi:10.1038/nsmb.1488
177. Geng X, Zhou QH, Kage-Nakadai E, Shi Y, Yan N, Mitani S, et al. Caenorhabditis elegans caspase homolog CSP-2 inhibits CED-3 autoactivation and apoptosis in germ cells. Cell Death Differ. 2009;16: 1385–1394. doi:10.1038/cdd.2009.88
178. Denning DP, Hatch V, Horvitz HR. Both the Caspase CSP-1 and a Caspase-Independent Pathway Promote Programmed Cell Death in Parallel to the Canonical Pathway for Apoptosis in Caenorhabditis elegans. PLoS Genet. 2013;9. doi:10.1371/journal.pgen.1003341
179. Baum JS, St. George JP, McCall K. Programmed cell death in the germline.

Seminars in Cell and Developmental Biology. Elsevier Ltd; 2005. pp. 245–259. doi:10.1016/j.semcdb.2004.12.008
180. Hochreiter-Hufford A, Ravichandran KS. Clearing the dead: Apoptotic cell sensing, recognition, engulfment, and digestion. Cold Spring Harb Perspect Biol. 2013;5. doi:10.1101/cshperspect.a008748
181. Wu D, Chai Y, Zhu Z, Li W, Ou G, Li W. CED-10-WASP-Arp2/3 signaling axis regulates apoptotic cell corpse engulfment in C. elegans. Dev Biol. 2017;428: 215–223. doi:10.1016/j.ydbio.2017.06.005
182. Kinchen JM, Cabello J, Kilngele D, Wong K, Felchtinger R, Schnabel H, et al. Two pathways converge at CED-10 to mediate actin rearrangement and corpse removal in C. elegans. Nature. 2005;434: 93–99. doi:10.1038/nature03263
183. Jaramillo-Lambert A, Ellefson M, Villeneuve AM, Engebrecht JA. Differential timing of S phases, X chromosome replication, and meiotic prophase in the C. elegans germ line. Dev Biol. 2007;308: 206–221. doi:10.1016/j.ydbio.2007.05.019
184. Gartner A, Boag PR, Blackwell TK. Germline survival and apoptosis. WormBook : the online review of C. elegans biology. 2008. pp. 1–20. doi:10.1895/wormbook.1.145.1
185. King SD, Gray CF, Song L, Nechushtai R, Gumienny TL, Mittler R, et al. The cisd gene family regulates physiological germline apoptosis through ced-13 and the canonical cell death pathway in Caenorhabditis elegans. Cell Death Differ. 2019;26: 162–178. doi:10.1038/s41418-018-0108-5
186. Derry WB, Putzke AP, Rothman JH. Caenorhabditis elegans p53: Role in apoptosis, meiosis, and stress resistance. Science (80-). 2001;294: 591–595. doi:10.1126/science.1065486
187. Schumacher B, Schertel C, Wittenburg N, Tuck S, Mitani S, Gartner A, et al. C. elegans ced-13 can promote apoptosis and is induced in response to DNA damage. Cell Death Differ. 2005;12: 153–161. doi:10.1038/sj.cdd.4401539
188. Scaduto RC, Grotyohann LW. Measurement of mitochondrial membrane potential using fluorescent rhodamine derivatives. Biophys J. 1999;76: 469–477. doi:10.1016/S0006-3495(99)77214-0
189. Crowley LC, Christensen ME, Waterhouse NJ. Measuring mitochondrial transmembrane potential by TMRE staining. Cold Spring Harb Protoc. 2016;2016: 1092–1096. doi:10.1101/pdb.prot087361
190. Puleston D. Detection of mitochondrial mass, damage, and reactive oxygen species by flow cytometry. Cold Spring Harb Protoc. 2015;2015: 830–834. doi:10.1101/pdb.prot086298
191. Chazotte B. Labeling mitochondria with mitotracker dyes. Cold Spring Harb Protoc. 2011;6: 990–992. doi:10.1101/pdb.prot5648
192. Cheeks RJ, Canman JC, Gabriel WN, Meyer N, Strome S, Goldstein B. C. elegans PAR proteins function by mobilizing and stabilizing asymmetrically localized protein complexes. Curr Biol. 2004;14: 851–862. doi:10.1016/j.cub.2004.05.022
193. Hamill DR, Severson AF, Carter JC, Bowerman B. Centrosome maturation and mitotic spindle assembly in C. elegans require SPD-5, a protein with multiple coiled-coil domains. Dev Cell. 2002;3: 673–684. doi:10.1016/S1534-5807(02)00327-1
194. Tenenhaus C, Schubert C, Seydoux G. Genetic requirements for PIE-1 localization and inhibition of gene expression in the embryonic germ lineage of Caenorhabditis elegans. Dev Biol. 1998;200: 212–224. doi:10.1006/dbio.1998.8940

195. Mello CC, Schubert C, Draper B, Zhang W, Lobel R, Priess JR. The PIE-1 protein and germline specification in C. elegans embryos. Nature. 1996;382: 710–712. doi:10.1038/382710a0
196. Kimble J, Crittenden SL. Germline proliferation and its control. WormBook : the online review of C. elegans biology. 2005. pp. 1–14. doi:10.1895/wormbook.1.13.1
197. Wang JT, Seydoux G. Germ cell specification. Adv Exp Med Biol. 2013;757: 17–39. doi:10.1007/978-1-4614-4015-4-2
198. Seydoux G. The P Granules of C. elegans: A Genetic Model for the Study of RNA–Protein Condensates. Journal of Molecular Biology. Academic Press; 2018. pp. 4702–4710. doi:10.1016/j.jmb.2018.08.007
199. Stiernagle T. Maintenance of C. elegans. WormBook : the online review of C. elegans biology. 2006. pp. 1–11. doi:10.1895/wormbook.1.101.1
200. C. elegans Deletion Mutant Consortium. large-scale screening for targeted knockouts in the Caenorhabditis elegans genome. G3 (Bethesda). 2012;2: 1415–25. doi:10.1534/g3.112.003830
201. Tsang WY, Lemire BD. Stable heteroplasmy but differential inheritance of a large mitochondrial DNA deletion in nematodes. Biochem Cell Biol. 2002;80: 645–654. doi:10.1139/o02-135
202. Okimoto R, Macfarlane JL, Clary DO, Wolstenholme DR. The mitochondrial genomes of two nematodes, Caenorhabditis elegans and Ascaris suum. Genetics. 1992;130: 471–498.
203. Ye W, Tang X, Liu C, Wen C, Li W, Lyu J. Accurate quantitation of circulating cell-free mitochondrial DNA in plasma by droplet digital PCR. Anal Bioanal Chem. 2017;409: 2727–2735. doi:10.1007/s00216-017-0217-x
204. Koepfli C, Nguitragool W, Hofmann NE, Robinson LJ, Ome-Kaius M, Sattabongkot J, et al. Sensitive and accurate quantification of human malaria parasites using droplet digital PCR (ddPCR). Sci Rep. 2016;6. doi:10.1038/srep39183
205. Rauthan M, Ranji P, Aguilera Pradenas N, Pitot C, Pilon M. The mitochondrial unfolded protein response activator ATFS-1 protects cells from inhibition of the mevalonate pathway. Proc Natl Acad Sci U S A. 2013;110: 5981–6. doi:10.1073/pnas.1218778110
206. Shaham S, Reddien PW, Davies B, Horvitz HR. Mutational analysis of the Caenorhabditis elegans cell-death gene ced-3. Genetics. 1999;153: 1655–71. Available: http://www.ncbi.nlm.nih.gov/pubmed/10581274
207. Zermati Y, Mouhamad S, Stergiou L, Besse B, Galluzzi L, Boehrer S, et al. Nonapoptotic Role for Apaf-1 in the DNA Damage Checkpoint. Mol Cell. 2007;28: 624–637. doi:10.1016/j.molcel.2007.09.030
208. Wang G, Sun L, Reina CP, Song I, Gabel C V., Driscoll M. CED-4 CARD domain residues can modulate non-apoptotic neuronal regeneration functions independently from apoptosis. Sci Rep. 2019;9: 13315. doi:10.1038/s41598-019-49633-9
209. Hoshino A, Mita Y, Okawa Y, Ariyoshi M, Iwai-Kanai E, Ueyama T, et al. Cytosolic p53 inhibits Parkin-mediated mitophagy and promotes mitochondrial dysfunction in the mouse heart. Nat Commun. 2013;4. doi:10.1038/ncomms3308
210. Ranjan A, Iwakuma T. Non-canonical cell death induced by p53. International Journal of Molecular Sciences. MDPI AG; 2016. doi:10.3390/ijms17122068

211. Sato M, Sato K. Degradation of paternal mitochondria by fertilization-triggered autophagy in C. elegans embryos. Science (80-). 2011;334: 1141–1144. doi:10.1126/science.1210333
212. Thompson O, Edgley M, Strasbourger P, Flibotte S, Ewing B, Adair R, et al. The million mutation project: A new approach to genetics in Caenorhabditis elegans. Genome Res. 2013;23: 1749–1762. doi:10.1101/gr.157651.113
213. Larsson N-G. Somatic Mitochondrial DNA Mutations in Mammalian Aging. Annu Rev Biochem. 2010;79: 683–706. doi:10.1146/annurev-biochem-060408-093701
214. Payne BAI, Chinnery PF. Mitochondrial dysfunction in aging: Much progress but many unresolved questions. Biochim Biophys Acta. 2015;1847: 1347–53. doi:10.1016/j.bbabio.2015.05.022
215. Yoon DS, Alfhili MA, Friend K, Lee MH. MPK-1/ERK regulatory network controls the number of sperm by regulating timing of sperm-oocyte switch in C. elegans germline. Biochem Biophys Res Commun. 2017;491: 1077–1082. doi:10.1016/j.bbrc.2017.08.014
216. Angeles-Albores D, Leighton DHW, Tsou T, Khaw TH, Antoshechkin I, Sternberg PW. The Caenorhabditis elegans female-like state: Decoupling the transcriptomic effects of aging and sperm status. G3 Genes, Genomes, Genet. 2017;7: 2969–2977. doi:10.1534/g3.117.300080
217. Barton MK, Schedl TB, Kimble J. Gain-of-function mutations of fem-3, a sex-determination gene in Caenorhabditis elegans. Genetics. 1987;115: 107–119.
218. Roy D, Kahler DJ, Yun C, Hubbard EJA. Functional interactions between rsks-1/S6K, glp-1/Notch, and regulators of caenorhabditis elegans fertility and germline stem cell maintenance. G3 Genes, Genomes, Genet. 2018;8: 3293–3309. doi:10.1534/g3.118.200511
219. Tekippe M, Aballay A. C. elegans germline-deficient mutants respond to pathogen infection using shared and distinct mechanisms. PLoS One. 2010;5. doi:10.1371/journal.pone.0011777
220. Mack HID, Heimbucher T, Murphy CT. The nematode Caenorhabditis elegans as a model for aging research. Drug Discovery Today: Disease Models. Elsevier Ltd; 2018. pp. 3–13. doi:10.1016/j.ddmod.2018.11.001
221. Hekimi S, Guarente L. Genetics and the specificity of the aging process. Science. 2003. pp. 1351–1354. doi:10.1126/science.1082358
222. Mack HID, Zhang P, Fonslow BR, Yates JR. The protein kinase MBK-1 contributes to lifespan extension in daf-2 mutant and germline-deficient Caenorhabditis elegans. Aging (Albany NY). 2017;9: 1414–1432. doi:10.18632/aging.101244
223. Libina N, Berman JR, Kenyon C. Tissue-Specific Activities of C. elegans DAF-16 in the Regulation of Lifespan. Cell. 2003;115: 489–502. doi:10.1016/S0092-8674(03)00889-4
224. Gönczy P, Rose LS. Asymmetric cell division and axis formation in the embryo. WormBook : the online review of C. elegans biology. 2005. pp. 1–20. doi:10.1895/wormbook.1.30.1
225. Villa AM, Fusi P, Pastori V, Amicarelli G, Pozzi C, Adlerstein D, et al. Ethidium bromide as a marker of mtDNA replication in living cells. J Biomed Opt. 2012;17: 046001. doi:10.1117/1.JBO.17.4.046001
226. Falkenberg M. Mitochondrial DNA replication in mammalian cells: Overview of the pathway. Essays in Biochemistry. Portland Press Ltd; 2018. pp. 287–296.

doi:10.1042/EBC20170100
227. Addo MG, Cossard R, Pichard D, Obiri-Danso K, Rötig A, Delahodde A. Caenorhabditis elegans, a pluricellular model organism to screen new genes involved in mitochondrial genome maintenance. Biochim Biophys Acta - Mol Basis Dis. 2010;1802: 765–773. doi:10.1016/j.bbadis.2010.05.007
228. Luz AL, Meyer JN. Effects of reduced mitochondrial DNA content on secondary mitochondrial toxicant exposure in Caenorhabditis elegans. Mitochondrion. 2016;30: 255–264. doi:10.1016/j.mito.2016.08.014
229. Moraes CT. What regulates mitochondrial DNA copy number in animal cells? Trends in Genetics. 2001. pp. 199–205. doi:10.1016/S0168-9525(01)02238-7
230. Silva Ramos E, Motori E, Brüser C, Kühl I, Yeroslaviz A, Ruzzenente B, et al. Mitochondrial fusion is required for regulation of mitochondrial DNA replication. PLoS Genet. 2019;15: e1008085. doi:10.1371/journal.pgen.1008085
231. Kalish JM, Jiang C, Bartolomei MS. Epigenetics and imprinting in human disease. Int J Dev Biol. 2014;58: 291–298. doi:10.1387/ijdb.140077mb
232. Gayon J. From Mendel to epigenetics: History of genetics. In: C. R. Biologies [Internet]. 2016 [cited 11 Dec 2019] pp. 225–230. Available: https://www-ncbi-nlm-nih-gov.proxy.library.ucsb.edu:9443/pubmed/27263362
233. Nicoglou A, Merlin F. Epigenetics: A way to bridge the gap between biological fields. Stud Hist Philos Sci Part C Stud Hist Philos Biol Biomed Sci. 2017;66: 73–82. doi:10.1016/j.shpsc.2017.10.002
234. Klosin A, Casas E, Hidalgo-Carcedo C, Vavouri T, Lehner B. Transgenerational transmission of environmental information in C. elegans. Science (80-). 2017;356: 320–323. doi:10.1126/science.aah6412
235. Ladstätter S, Tachibana K. Genomic insights into chromatin reprogramming to totipotency in embryos. Journal of Cell Biology. Rockefeller University Press; 2019. pp. 70–82. doi:10.1083/jcb.201807044
236. Stimpfel M, Jancar N, Virant-Klun I. New Challenge: Mitochondrial Epigenetics? Stem Cell Reviews and Reports. Humana Press Inc.; 2018. pp. 13–26. doi:10.1007/s12015-017-9771-z
237. Matilainen O, Quirós PM, Auwerx J. Mitochondria and Epigenetics – Crosstalk in Homeostasis and Stress. Trends in Cell Biology. Elsevier Ltd; 2017. pp. 453–463. doi:10.1016/j.tcb.2017.02.004
238. Lambertini L, Byun HM. Mitochondrial Epigenetics and Environmental Exposure. Current environmental health reports. 2016. pp. 214–224. doi:10.1007/s40572-016-0103-2
239. van der Wijst MGP, Rots MG. Mitochondrial epigenetics: An overlooked layer of regulation? Trends in Genetics. Elsevier Ltd; 2015. pp. 353–356. doi:10.1016/j.tig.2015.03.009